**Swansea University
Prifysgol Abertawe**

Using Rapid Alloy Prototyping to Investigate the Effects of Residual Elements in Increased Scrap Recycling

Caroline Norrish

Submitted to the Swansea University in fulfilment of the requirements

for the Degree of Doctor of Engineering

Swansea University 2023

ABSTRACT

This work employs a novel, small-scale rapid alloy prototyping (RAP) method, developed throughout the project, to investigate the feasibility of using this research method to investigate the effects of residual elements. The RAP samples vary from 20g to 140g and are quick to produce, allowing an array of unique compositions with synthetic scrap additions, to be tested quickly.

Residual elements are commonly introduced via steel scrap and need to be carefully monitored and controlled throughout the steelmaking process. The impact on product quality resulting from residual elements necessitates strict limits on the percentage of scrap that can be used in the manufacture of new steel products, limiting the environmental and financial benefits that come from increasing scrap use. This highlights the need for research that challenges the stringency of industrially enforced residual limits across different steel grades. There is minimal existing research in this area, predominantly on lower alloy grades, and often published several decades ago. The looming importance of the climate crisis exacerbates the urgency for research focussed on reducing the environmental impact of vital industries such as steel.

This work focusses on two different steels, a DP800 with high levels of alloying content where the impact of residual elements is expected to be less pronounced, and a low carbon steel with far fewer alloying additions and far more industrial concern for the impact of the residual elements.

Results published in this thesis show that the RAP method can be a valuable tool in understanding the impacts of increased scrap use on steel products, demonstrating that environmentally responsible manufacturing does not necessarily require a significant compromise in product quality. Several of the sub-150g lab-scale RAP samples can be produced each week, allowing for far faster alloy research compared to the 30-60kg pilot-scale samples currently used in product development, allowing for rapid investigations into compositional variations in both new and established steel grades.

Declarations

Declaration: This work has not previously been accepted in substance for any degree and is not being concurrently submitted in candidature for any degree.

Signed: Caroline Norrish   Date: 22/12/2023

Statement 1: This thesis is the result of my own investigations, except where otherwise stated. Other sources are acknowledged by footnotes giving explicit references. A bibliography is appended.

Signed: Caroline Norrish   Date: 22/12/2023

Statement 2: I hereby give consent for my thesis, if accepted, to be made available online in the University's Open Access Repository and for inter-library loans.

Signed: Caroline Norrish   Date: 22/12/2023

Acknowledgments

I would first like to thank the funders who have made this project possible. This includes the European Social fund, the Engineering and Physical Sciences Research Council, and Tata Steel. I would also like to thank the M2A for the support over the past few years, and everyone involved in both the Prosperity Partnership and the COMET project for your help, support and difficult question that pushed me to understand more. I am also grateful for those at SaMI who have helped with the sample testing when it wasn't possible in MACH1.

I am especially grateful to everyone, past and present, that I have worked alongside in the MACH1 labs. This includes all the post-docs, fellow EngD's, technicians, and academics. I will avoid mentioning you by name because I will undoubtedly forget someone, but please know I will be forever grateful to all of you for help making any problems seem manageable and for making it so much fun.

The biggest possible thank you needs to go to Nick Lavery, my academic supervisor. Thank you for pushing me to do the best work I can and for taking such an interest in the results I have produced. This thesis wouldn't be half as good without your input. Thank you as well to my industrial supervisor, Richard Underhill. Thank you for your endless knowledge and invaluable support with any questions I sent your way.

Last but not least, thank you to all my friends and family for being there for me, especially to my parents who have always been supportive through my many years of university. I'm very lucky to have such a wonderful network of people around me and I don't doubt this would have been much harder without all of you. I am thankful to those who asked how my thesis was going, and to those who knew better than to ask, I'm even more thankful to you.

TABLE OF CONTENTS

ACRONYMS

BCC – Body Centred Cubic

BOS – Basic Oxygen Steelmaking

Calphad - CALculation of PHAse Diagram

EAF – Electric Arc Furnace

EDX/EDS – Energy Dispersive X-Ray Spectrometry

EPMA – Electron probe microanalyses

FCC – Face Centred Cubic

HCP – Hexagonal Close Packed

OES – Optical Emission Spectroscopy

OM – Optical microscopy

RAP – Rapid Alloy Prototyping

SCE – saturated calomel electrode

SEM – Scanning Electron Microscopy

TEM – Transmission Electron Microscopy

TWIP – Twinning Induced Plasticity

UTS – Ultimate tensile strength

XRD – X-ray diffraction

XRF – X-ray fluorescence

TABLE OF FIGURES

TABLE OF EQUATIONS

TABLE OF TABLES

CHAPTER 1   INTRODUCTION

1.1 OVERVIEW

Stage 1 – The climate crisis is one of the biggest challenges humanity has ever faced, and the necessity for net zero expands to every company in every sector on Earth. Manufacturing, especially the steel industry, is incredibly polluting and needs to dramatically reduce carbon emissions in the next few years if the global temperature rise can be kept below 1.5°C, or even 2°C. Scrap steel has long been incorporated into the steel making process due to lower material costs, but it brings with it disadvantages.

Stage 2 – Increasing the amount of steel scrap used in steelmaking has many benefits. It reduces the environmental impact by reducing the consumption of iron ore and decreases the CO_2 emissions. On the other hand, it can introduce residual elements which often have a detrimental effect on the processing characteristics or performance of the final product.

Stage 3 – There is a lack of research into this topic. A lot of the existing research into residual elements was published pre-2000, and residual elements impact different steel grades in different ways meaning studies such as these need to be repeated for various steels.

Stage 4 – This project has used rapid alloy prototyping to gain a better understanding of residual elements introduced into steel making via scrap steel recycling. The methods used produce samples between 20g and 140g in size and allow alloy synthesis and development to happen faster with fewer time consuming and wasteful full-scale trials.
The main obstacle is getting the smaller samples to accurately represent the properties achieved by a full-scale trial. This involves investigating the manufacturing process and understanding how to replicate it using the equipment available. The industrial

heat treatments and rolling processes produce the desired microstructure and phase distribution which are one of the main influences on the final properties, so accurately simulating this on a smaller scale is vital.

When the trends are fully established, there are opportunities to develop new alloys made with lower quality or increased amounts of scrap steel that allow for higher levels of tramp elements without affecting the necessary properties.

To achieve this, there needs to be a better understanding of the effects that residual elements have on steel alloys which will need a large volume of tests to gain a more well-rounded set of information. Tests will investigate the tensile strength, hardness, corrosion resistance, phase composition and microstructure with the potential to also research other material properties. This will be achieved with the help of methods including SEM, EDX, XRD, OES spectroscopy.

Two steel grades were investigated throughout this work, each with very different levels of alloying additions, to investigate the effects of increasing residual element levels.

1.1.1 DP800

DP800 is a high alloy steel with a dual phase structure, often used in automotive applications. The properties of the steel are achieved by closely controlling the processing parameters such as rolling reductions and processing temperatures. High levels of alloying elements in the original steel grade make it likely that high levels of residual element levels would need to be present before they are disruptive enough to push the material properties outside of the grade specification. The level of complexity and precision required for the processing parameters means that it is a grade that is challenging to replicate, making it difficult to consistently produce lab scale DP800 steel samples that are representative of an industrially produced coil.

1.1.2 3190

3190 is a code referring to a low alloy steel grade with high levels of ductility. This grade has low carbon levels to produce a fairly soft steel which is fairly forgiving of slight variations in the steel processing. Increased levels of residual elements in a low

alloy formable steel allows the effects of the residual elements to be highlighted due to fewer other potential variations in chemistry.

1.2 MAIN OBJECTIVES

The main objective of this work has been to

[OB1] Develop rapid alloying route(s) suitable for the synthesis of two significantly different benchmark alloys, a **low-carbon low-alloy steel** (3190) and a **higher-alloyed Dual Phase** (DP800) steel in sufficient quantities to compare properties, including microstructures, hardness, tensile strength, and corrosion.

[OB2] The routes should include alloying by melting, casting, thermal-deformation (hot-rolling), heat treatments and cold rolling to mimic as closely as possible the processes of the production-scale steels.

[OB3] Try several methods of rapid synthesis at different casting scales, feedstock types (elemental powders, elemental solids, binary and ternary master ferro-alloys).

[OB4] Determine and compare the levels of compositional accuracy and repeatability across these methods, in comparison to the benchmark alloys.

[OB5] Determine and compare the levels of tensile, hardness and corrosion property accuracy and repeatability of the methods compared to the benchmark alloys.

[OB6] Determine and compare microstructures and textures for the synthetic alloys and compare them to actual product material.

[OB7] Once synthetic alloys of both benchmarks have been produced, systematically add residual elements (e.g. Cu, Ni, Sn, …) in levels appropriately identified for each of the two benchmark alloys.

1.3 CONFERENCES AND PUBLICATIONS

In the course of this work, the following paper was published:

[1]   M. A. Yar *et al.*, "Small-Scale Rapid Alloy Prototyping of Extra-Low Carbon Steel to Investigate the Effects of Cu and Cr Residuals," *Miner. Met. Mater. Ser.*, pp. 1202–1213, 2022.
[2] Mehraban, Norrish, Lavery, small scale RAP for the investigation of wide ranges of resisuals in DP800 steel, Ironmaking and Steelmaking, to be submitted 2024.

CHAPTER 2   STEEL MANUFACTURING

2.1   INTRODUCTION

2.1.1   MANUFACTURING METHODS

Approximately two thirds of the global production of steel is done using a blast furnace, also referred to as basic oxygen steel making (BOS). Most of the remaining third is manufactured via an electric arc furnace (EAF) which is well suited to the recycling of scrap steel and can be used with 100% scrap steel input. [2]

Figure 1 shows an overview of the layout of Port Talbot steelworks, and Figure 2 summarises the rolling processes of steel slabs.
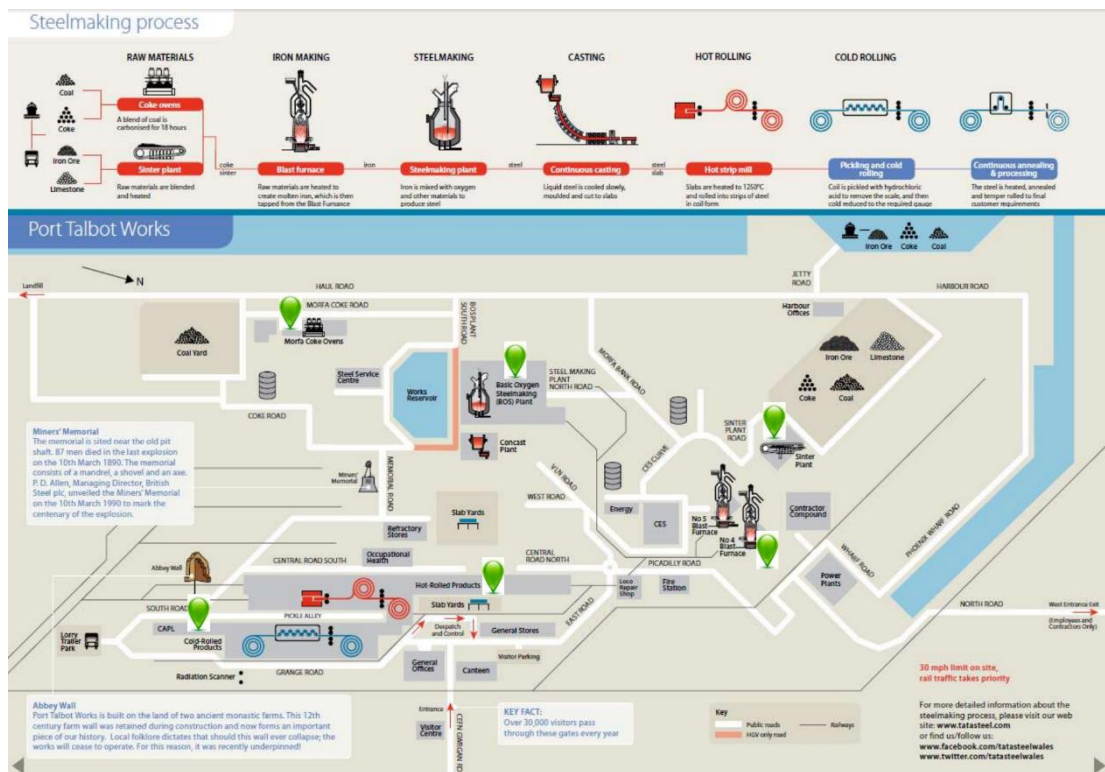
Figure 1 Port Talbot site overview [3]
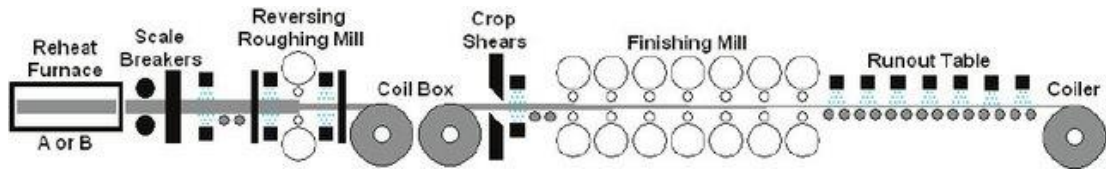
Figure 2 Steel production route [4]

2.1.1.1 BASICS OF THE BLAST FURNACE

The BOS route is the most common method of steel manufacturing and takes place in a large, refractory lined furnace. Iron ore is sintered with coke and heated in the blast furnace. Lime is then added to the furnace and heated air is blown through the mix from the bottom of the furnace.

Oxygen reacts with carbon from the coke and the iron ore to form carbon monoxide and carbon dioxide. As the gases rise, the carbon monoxide reacts with the oxygen in the iron ore, reducing it to pure iron, which can be collected as an iron melt from the bottom of the furnace. The reaction between the iron ore and carbon monoxide is shown in Equation 1.

$$Fe_2O_3 + 3CO \rightarrow 2Fe + 3CO_2$$
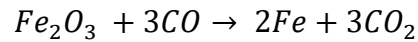
Equation 1 Reduction reaction of iron ore with carbon monoxide

From here, the molten iron is transferred to a BOS furnace where it is poured over scrap steel, making up about 20% of the volume of the new steel. A water-cooled lance is then used to introduce oxygen, allowing the carbon level of the steel to remain low. This method helps to reduce the levels of additional elements that react with oxygen including manganese, silicon, sulphur and phosphorous [5]. Once a steel melt has been formed, it can be poured into a ladle with the volume for over 300 tonnes of steel for the next stage of the process and for additional alloying elements to be added. [2], [5]
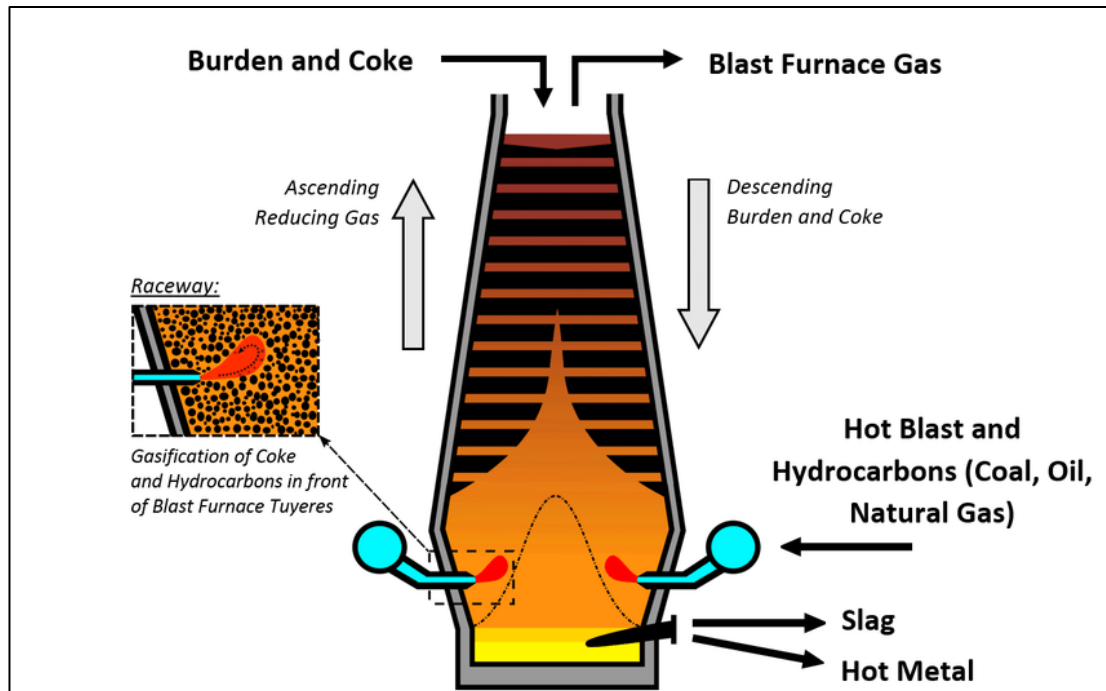
Figure 3 Blast furnace [6]

2.1.1.2 THE ELECTRIC ARC FURNACE (EAF)

The main alternative method to manufacturing steel in a blast furnace is the EAF method. This uses electrodes in a closed container filled with a suitable feedstock, to charge the metal and melt it. The feedstock is generally composed of scrap steel with the addition of direct reduced iron or hot briquetted iron. Scrap can be carefully selected to closely match the composition of the target alloy, reducing the amounts of additional alloying elements that need to be added. This allows better use of resources by halving the energy requirement compared to production from iron ore [7] and can reduce the quantity of alloying elements that need to be added. Once melted, the steel melt can also be transferred to a ladle for the next stage in the steelmaking process. [2]
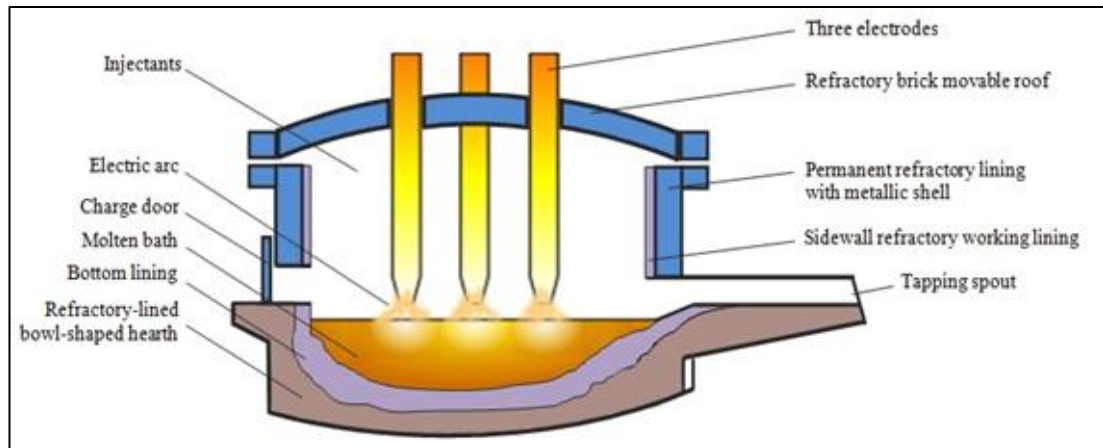
Figure 4 Electric arc furnace [8]

2.1.1.3 FURTHER PROCESSING

Most of the steel produced is continuously cast rather than ingot cast. This involves pouring the molten steel from the ladle and into a tundish where inclusions are removed. The tundish allows for continuous casting of slabs where the tundish always contains a level of molten steel in reserve meaning the melt still flows from the tundish even as the ladles are changed, allowing for more efficient processing. From this, the steel melt is transferred to a water cooled, lubricated copper mould that oscillates to control the rate of solidification. As the steel strip exits the mould, the outer layer has cooled enough to be solid and to keep the slab in shape, but the centre will still be molten. If the solidified layer is not thick enough it can allow the molten steel to flow down leading to a non-uniform thickness or, in extreme cases, the layer can burst, allowing molten metal to flow freely. To ensure the outer layer of the steel cools enough to contain the molten core, it is cooled by a spray of water. Once fully solidified, slabs of specific length are cut using a gas torch. After this, heat treatments and rolling can take place to produce the desired form and properties. [2]

2.1.2 RECYCLING IN STEEL MANUFACTURING

2.1.2.1 WHY SCRAP IS USED

Steel is one of the most recycled materials in the world [7]. Currently, the amount of scrap steel used in steel making is increasing by 12% each year so the importance of

understanding how the use of scrap steel affects quality is getting ever more important [9]. Scrap steel plays a vital role in the production of steel. As iron is heated in a BOS vessel, oxygen is blown into the melt using a lance. This reacts with carbon in the melt to form carbon dioxide and lower the carbon content in the final product. The reaction is an exothermic one and will increase the temperature of the melt without any external heat input. Adding scrap steel acts as a coolant to control the temperature of the melt [10]. It has additional environmental benefits as the energy requirement is reduced. Only the bare minimum amount of iron or steel is melted, the remaining heat needed comes from the oxidising reaction of the carbon which provides the necessary heat to melt the coolant when it is added.

2.1.2.2   RESIDUAL ELEMENTS IN SCRAP STEEL

A <u>residual element</u>, also known as a tramp element, can be defined as one present in steel that is not intended to be there. These elements can be introduced into the new steel from scrap through coatings or alloy elements present in the steel scrap, or through metal attached to the scrap, such as copper wires in electrical components.

Some of these elements such as silicon, titanium and aluminium can easily be completely removed from scrap and some such as manganese can be partially removed due to how easily they oxidise, although some residue will remain [9], [11]. Other elements such as copper, molybdenum, nickel and tin are difficult to remove from the steel and will remain in a melt, increasing in concentration over time and may have undesirable effects on the properties [9], [12]. There is also an issue with other tramp elements which may amplify the effects, such as tin increasing the effects of copper residuals [12].

Figure 5 below shows the expected location of various elements that may be present in a steel melt. Elements that "totally" reside in one location after melting are ones that either completely react with oxygen and rise to the top of the melt as slag (such as aluminium), or will not react with the oxygen at all and remain solely in the melt (such as tin). Those which are listed as being "mostly" in one location will be found in multiple locations, such as chromium which will oxidise slightly and form part of the

slag mixture, but most would be expected to remain in the melt. Elements listed as "partially" in a location will also be expected to be found in multiple sites and the location listed as a partial residence of the element is where the minority of that element will be, such as the amount of chromium found in slag. This demonstrates the tendency of many common residual elements to reside in the molten steel bath and ultimately end up in the final steel product whilst other elements separate into the slag or vaporise. This can be a source of material waste that brings with it other problems, but this does at least reduce the element concentration in the melt, reducing the presence of the element as a residual in the new steel.

To Bath			To Slag		To Gases	
Sb	Cr	B	Al	B	Ca	Pb
As	Pb	Cb	Be	Cr	Zn	
Bi		P	Ca	Cb		
Co		Se	Hf	P		
Cu		S	Mg	Se		
Mo		Te	Si	S		
Ni		V	Ti	Te		
Ag		Zn	Zr	V		
Ta						
Sn						
W						

Totally   **Mostly**   **Partially**

Figure 5 Resulting location of tramp elements after EAF melting [7]

Residual elements can also be introduced if lower quality alloying elements are used. For example, a low-quality manganese will contain a higher quantity of carbon than a high quality manganese but will generally be cheaper [5]. The inclusion of lower quality alloying elements would reduce the cost of production especially if the residuals being introduced are useful to the steel grade being produced.

Currently, much of the information on residual elements focusses on the effects of the elements but not on the levels at which they are acceptable as this will vary depending on the specific alloy. Introducing alloying elements can help reduce the influence of interstitial elements but the inclusion of these additional elements can add an extra cost to the process [5]. The presence of residual elements has a greater impact on low alloyed steels, whereas steels with a high level of alloying elements, the influence of tramp elements can be negligible [13]. The effects of specific alloying elements is discussed in more detail in section 2.2.2 Common tramp elements and effects.

2.1.2.3 TYPES OF SCRAP

Scrap steel can vary in quality depending on the source of the scrap [14]. This can vary from obsolete scrap from end of life products, to home scrap from steel waste within the facility and process or industrial scrap from other steel industrial processes which have fewer unknown levels of alloying elements [12], [14].

Obsolete scrap *encompasses any post-consumer steel from cars and construction steel to electrical components and food cans [12]. This scrap source contains the highest residual levels and accounts for 40-55% of the total scrap steel [9].*

When the metal is recycled it is shredded and the steel is separated from the other metal but there is still some contamination from other elements which gradually increases the concentration of residual elements over time [12].

Home scrap *has very low levels of impurities and residual elements and this makes up 20-30% of scrap steel [7], [9]. It generally will not have any coatings or other attached components meaning it can be used in higher quantities without having such a detrimental effect on properties as other scrap sources [7].*

Industrial scrap *will have known compositions so the residual elements are more predictable and this makes up 15-25% of the scrap [9].*

Types of scrap available are classified as shown in Table 1 and indicate the limits of various residual limits in different scrap sources. This enables steel manufacturers to estimate the residual levels going into the new steel when the scrap is used in the steel making process.

Table 1 Residual levels in different types of steel scrap measured in wt% [15]

Category	Specification	Aimed Analytical Contents (residuals) in %				
		Cu	Sn	Cr, Ni, Mo	S	P
OLD SCRAP	E3	≤0.250	≤0.010	Σ≤0.250		
	E1	≤0.400	≤0.020	Σ≤0.300		
NEW SCRAP Low Residuals, Uncoated (2)	E2	Σ≤0.300				
	E8	Σ≤0.300				
	E6	Σ≤0.300				
SHREDDED	E40	Σ≤0.250	Σ≤0.020			
STEEL TURNINGS (3)	E5H	Prior chemical analysis could be required				
	E5M	≤0.400	≤0.030	Σ≤1	≤0.100	
HIGH RESIDUAL SCRAP	EHRB	≤0.450	≤0.030	Σ≤0.350		
	EHRM	≤0.400	≤0.030	Σ≤1.0		
FRAGMEN-TIZED SCRAP FROM INCINERATION	E46	≤0.500	≤0.070			

2.1.2.4 SCRAP PREDICTIONS FOR THE FUTURE

Current predictions for the future of scrap are that the levels of residual elements such as copper and tin that cannot feasibly be removed will be a limiting factor [16] and low grade scrap will increasingly be used in the steelmaking process [17]. It is estimated that the amount of copper in steel scrap will increase rapidly over time, reaching 4Mt in 2090, more than five times that of the amount of copper in circulation in 2000 [16]. Currently, there is enough demand for steel with a high tolerance for copper that the scrap with a high copper concentration is still expected to be usable until 2050, beyond this, the copper content could reduce the steel quality to a point where it can no longer be used [16].

A major consideration that comes with secondary steel making is that the demand for steel outweighs the supply of scrap steel [18]. Steel products last many years, with an

average lifetime of decades, ranging from 19 years to 40 years in various sources, so will not immediately be reintroduced back into the waste stream [9], [19]. Based on the findings of the US Geological Society, the remaining sources of iron ore are enough to sustain the current level of production for about 65 years although the exact life expectancy varies from country to country [20], [21].

Daehn, Serrenho and Allwood have collated a significant amount of research into the residual content of scrap steel and the current and future end use of steel products, from which, potential realistic future steel grades can be decided [22].
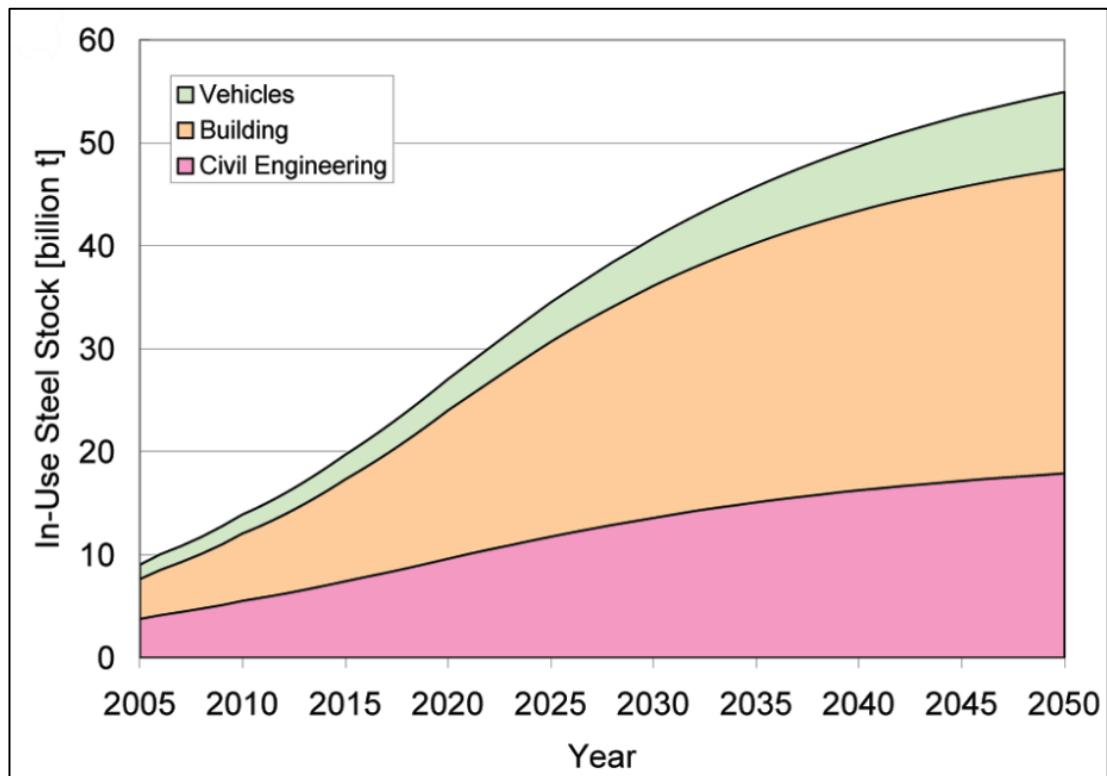
Figure 6 Forecasted end use of steel products [23]

	Cr	Ni	Cu	Sn
DI	0.086	0.075	0.222	0.020
home or prompt scrap from integrated Works	0.024	0.023	0.017	0.003
33	0.230	0.089	0.295	0.020
pig iron	0.000	0.000	0.003	0.002
DRI	0.000	0.000	0.000	0.001

Table IV.   Typical compositions in metallic tramp elements of scrap and other sources of iron found on the French market in 1993 (in weight %).

	DI	low-R	33	iron	DRI	Cu	Cr	Ni	Sn
scrap mix # 1	0	0	0	50	50	0.002	0.000	0.000	0.002
scrap mix # 2	0	50	0	25	25	0.009	0.008	0.012	0.002
scrap mix # 3	25	25	0	25	25	0.061	0.019	0.025	0.007
scrap mix # 4	12.5	25	12.5	25	25	0.070	0.032	0.026	0.007
scrap mix # 5	12.5	25	12.5	50	0	0.070	0.032	0.026	0.007
scrap mix # 6	40	50	0	10	0	0.098	0.032	0.042	0.010
scrap mix # 7	25	25	25	25	0	0.134	0.060	0.047	0.011
scrap mix # 8	25	25	40	10	0	0.178	0.084	0.060	0.014

Table V.   Theoretical composition of liquid steel obtained from various mixes of scrap and other iron sources (each iron source composition is in % of the total charge; composition is in weight %). The table is organised as a function of increasing Cu content, which turns out to be also increasing Cr and Ni contents (DI : industrial demolition; low-R : low-residual scrap, either home or prompt scrap from integrated works; 33 : shredded; iron : pig iron or liquid hot metal).

Figure 7 Tables from [17] showing typical chemistry of scrap mixes where "33" is shredded scrap

Figure 7 demonstrates that scrap can come in different forms, and it is not realistic to assume every batch of scrap steel will be the same. Over time, different types of scrap may change in composition due to the changing grades of steel used in products and the availability of each source of scrap may also change as iron production plants change their manufacturing methods.

2.1.3   ENVIRONMENTAL IMPACTS OF STEELMAKING

The difficulty in removing some elements means that steel must often be diluted with virgin iron to keep the concentration at an acceptable level. If the current limits of common residual elements remain the same, it restricts the amount of recycled steel that can be used in steel making processes.

2.1.3.1 RELEVANT REGULATIONS

Due to environmental regulations, the UK as a whole needs to drastically reduce emissions of CO_2 and other greenhouse gases [9] therefore, the steel industry has a responsibility to cut down on emissions. Increasing the rate of steel recycling will help reduce the emissions of the process. Of the UK nations, Wales has the highest recycling rate with more than half of waste being recycled [24]. There is a goal for Wales to be produce at least 65% less waste compared to the 2010 level by 2050 [24].

2.1.3.2 RESOURCE SAVINGS POTENTIAL

The recycling of steel saves valuable resources. One tonne of steel scrap can save 500 litres of water, 1.5 tonnes of iron ore and more than a tonne of solid waste when compared to using virgin iron [24]. Depending on the production method, each tonne of scrap steel used in the place of virgin iron can save more than 15Gj/tcs (gigajoules per tonne of crude steel), 54 kg of lime, 500-635 kg of coal and 1134 kg of iron ore [7], [18], [24], [25]. This will help contribute to these targets in addition to the reduction in water use and CO_2 emissions. The energy requirement is 75% less than using raw materials to produce steel and the air and water emissions are 86% and 76% respectively [24]. Most of the energy used in the manufacture of steel goes towards the blast furnace which accounts for 60% of the energy use [26].

2.1.3.3 GREEN STEEL

<u>Green steel</u> is term typically applied to steel that is produced in a way that is as sustainable possible, with the aim of producing zero emissions.

There are no current legal restrictions on what can be labelled green steel, but it is a term that is used aspirationally to describe the kind of steel that will be made in the future. Muslemani et al. describes green steel as "steel produced by less carbon-intensive production processes" in a paper that outlines in detail the environmental impact of the steel industry, highlighting the potential for technology to reduce the CO_2 outputs, and the key industries best placed to cope with the cost increases associated with the new steel [27]. A strategy by Liberty Steel includes reducing the

steel scrap exported, instead choosing to use the most readily available scrap in their steel making using renewable energy powered EAFs (known as GREENSTEEL) [27], [28]. Griffin and Hammond have done extensive research in ways to bring the UK to net-zero and in a paper focussed on the opportunities of green steel, they explain that steel produces more greenhouse gas emissions than any other UK industry at 25%[29]–[33]. Not only are the emissions of the steel industry large, they are not evenly spread throughout the country, they are instead concentrated in industrial regions, contributing to ill health in local residents [30], [34], [35]. A lot of research discussing green steel highlights the importance of planning new projects in a way that is ambitious and aligns with, or even go beyond, climate goals [36].

2.1.4 ECONOMIC BENEFITS

There is an economic advantage to an increase in scrap use. As previously discussed, the quality of scrap can vary. Lower quality scrap has a higher level of tramp elements and is therefore cheaper than scrap of a much higher quality [10]. Whilst the price of both iron ore and steel scrap has been rising each year, the percentage cost increase of iron ore is nearly double that of scrap [9]. The raw materials used in steelmaking are increasing in cost and the use of scrap will cut costs and reduce energy demands, reducing costs further [25], [37]. Using scrap steel can save approximately £20 per tonne of scrap used.

Alloys have been developed, specifically designed to benefit from the presence of alloying elements that are usually undesirable. M Mujahid et al. discuss a high strength low alloy structural steel with a copper content of 1.6% [7], [38], while Lang Y Ping describes research into a more economical way of producing stainless steels by using nitrogen, usually an undesirable element, to amplify the effects of nickel as a way to reduce resource use and production costs [39]. There is other research into a more effective way of using scrap that makes best use of the alloying elements already present in the scrap which will save money, where the cost saving will depend on current scrap prices at the time of purchase [10].

2.1.5 ALLOY DESIGN

Traditional routes of alloy design and development use much larger scale trials to produce samples. These can be up to 80 kg in size [40] and some alloy development processes involve casting processes such as sand casting and ingot casting [41]. Typically, these will be a good representation of the product that would be produced in a full scale, industrial process.

Larger scale tests have drawbacks and can lead to more material wastage when compared to much smaller alloy tests. The size of sample produced is far more than is required to do several tests to analyse the mechanical properties. These tests often require a lot of planning and can be more time consuming and expensive which is a problem when the development of a new alloy is likely to require numerous tests to develop an alloy which best fits the requirements. As technology progresses and the demand for new materials increases, faster and newer methods to produce prototypes are necessary. In general, these methods produce much smaller samples than traditional routes allowing for less material wastage [42]. RAP allows synthetic alloys to be produced quickly and on a much smaller scale than current alloy development methods [40]. This method is discussed in more detail in section 2.3 Alloy development.

The motivation behind alloy development is varied. Alloys are often designed for a specific application and have set criteria for mechanical properties and other characteristics [43], [44]. Other alloys are more motivated by cost reduction. For example, titanium alloys have been widely researched to replace expensive alloying elements, commonly aluminium, with cheaper alternatives [45].

2.2 PHASES AND ALLOYING SCIENCE

2.2.1 DIFFERENT PHASES IN STEEL
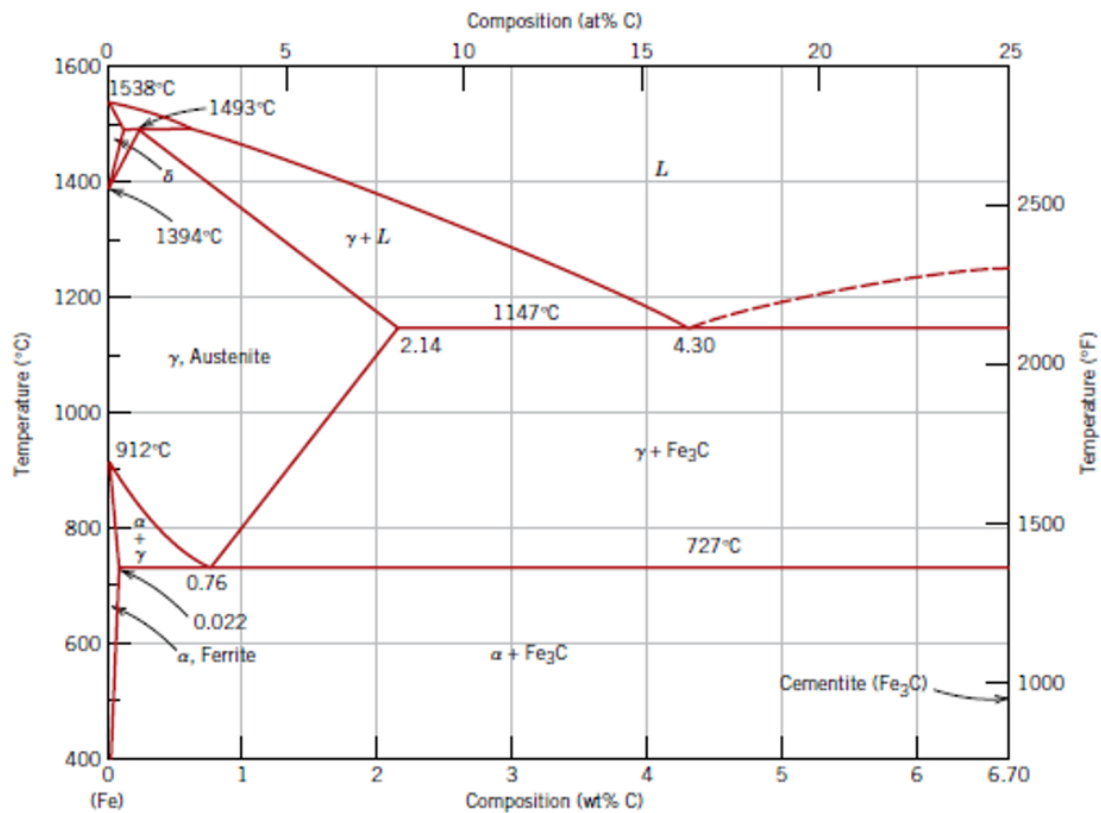
Figure 8 The iron-carbon phase diagram [46]

2.2.1.1 FERRITE

The ferritic phase has a BCC crystal structure. It is a magnetic phase with very low carbon solubility (about 0.02 wt% at room temperature) and it has a low hardness compared to the other phases in steel [47].

When understanding the basics of steel, plain carbon steels are usually discussed first, the phase diagram for which is shown in Figure 8. There are many different types of ferrite including eutectoid, proeutectoid, Widmanstatten, degenerate and bainitic [48]. Eutectoid ferrite forms below the eutectoid temperature of 727°C in a plain carbon steel and forms lathes as part of a pearlitic microstructure (pearlite is discussed in detail in section 2.2.1.4).

Proeutectoid ferrite will form along the existing austenite grain boundaries above the eutectoid temperature when carbon levels are below 0.76 wt% in a plain carbon steel. This form of ferrite forms along grain boundaries where the lattice does not line up between grains and the energy required for initiation and atom diffusion is lower than in the centre of grains.

When ferrite forms, the speed at which the phase grows is dependent on the speed at which carbon can diffuse in the austenite ahead of the interface between the phases [49]. This is dependent on the temperature of the steel. Higher temperatures provide more energy to allow the reaction to happen, but lower temperatures provide a greater driving force. There will be a temperature with the highest rate of transformation which finds the balance between providing enough energy through heat, and enough of a driving force.

2.2.1.2 AUSTENITE

Austenite has an FCC crystal structure and is a common phase in stainless steels. It is not magnetic and not stable at room temperature in plain carbon steels. It is harder than ferrite, making it desirable and many alloying elements are used to stabilise the austenite phase down to room temperature [50]. In general, this phase is not present in most commonly used steel grades.

2.2.1.3 CEMENTITE (Fe₃C)

Cementite is a carbon rich phase not present in pure iron. It is much more brittle than ferrite in plain carbon steels but like ferrite, it can come in many different forms. Proeutectoid cementite can form above the eutectoid temperature in compositions with more than 0.76 wt% carbon and nucleates along grain boundaries. At the eutectoid temperature, eutectoid cementite will then form alongside ferrite to form a pearlitic microstructure. Except for proeutectoid cementite, the phase is rarely found outside of a pearlitic microstructure.

2.2.1.4 PEARLITE

Pearlite is a microstructure rather than a phase and is made of alternating layers of ferrite and cementite. Under a microstructure the different colours of the phases make the steel look like a mother of pearl pattern.

Under equilibrium, pearlite forms below the austenitic transformation temperature. In a 0.76%wt plain carbon steel pearlite will begin to form as the steel cools from the austenitic phase below the equilibrium temperature of 727°C. Under equilibrium temperatures, ferrite and cementite will begin forming at this temperature. Ferrite has a very low carbon solubility so will nucleate in regions of lower carbon concentration. As the phase grows it will reject carbon atoms causing the surrounding areas to increase in carbon concentration. This leads to carbon rich nucleation sites for cementite either side of the ferrite lathes.
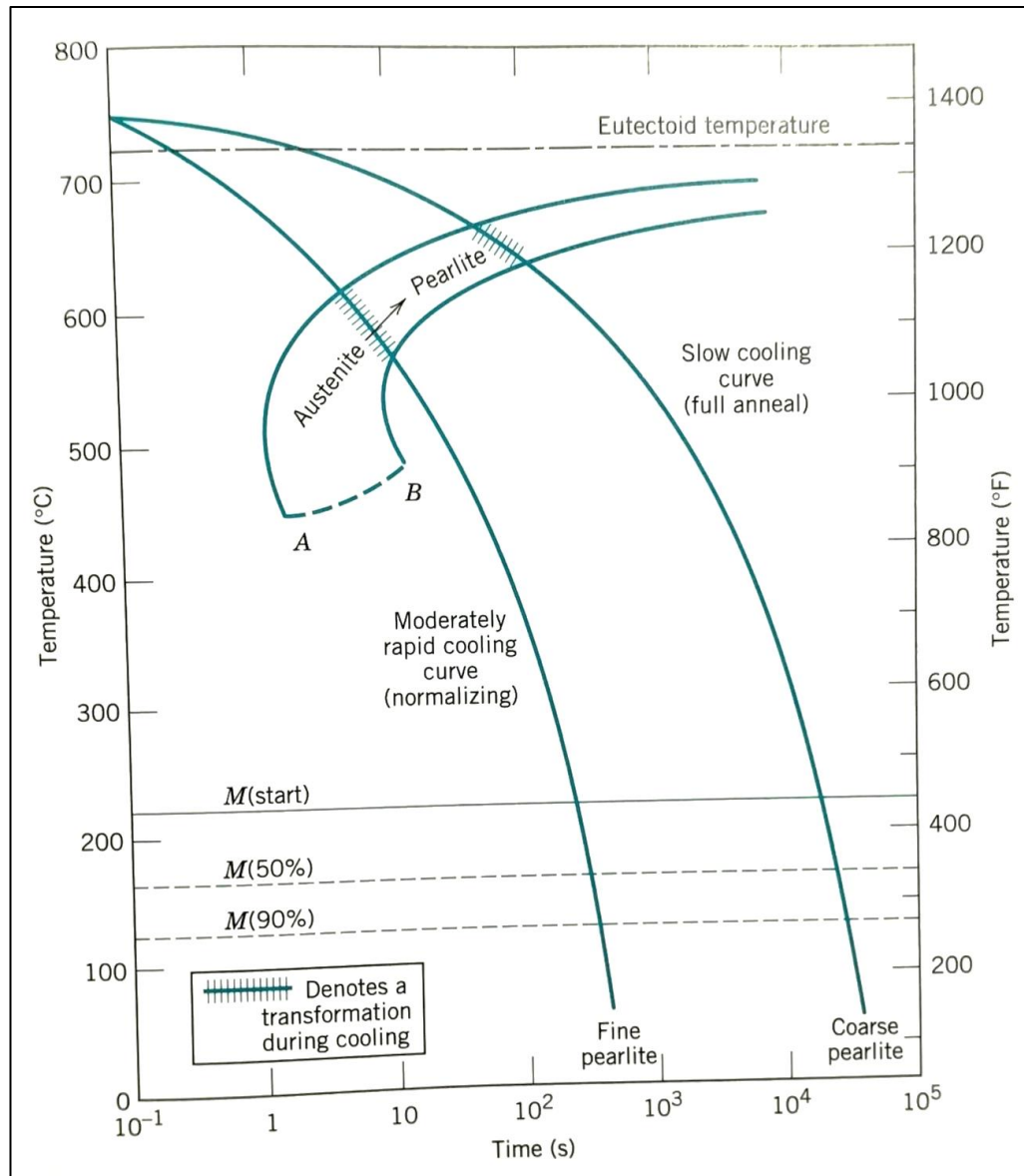
Figure 9 Continuous cooling curve of a eutectoid steel [51]

Lamellar microstructures such as pearlite are present when a structure transforms into two phases which are different but have a combined average composition the same as the parent phase or phases [48]. In the case of pearlite, austenite grains transform into alternating ferrite and cementite layers which have very different compositions but combined they will have the same average composition as the austenite phase present at the eutectoid temperature [48]. The size of the microstructure constituents is dependent of the cooling time. If quenched or cooled quickly the microstructure will not be in equilibrium, resulting in a finer pearlitic microstructure, demonstrated by

Figure 9.

2.2.1.5 MARTENSITE

Martensite is not an equilibrium phase and is a displacive rather than diffusion-based reaction. The chemical composition of martensite is identical to the parent austenite and the transformation can occur at very low temperatures where a diffusion-based transformation would not be feasible. The speed of the reaction front can be much faster than the speed of sound, far quicker than any recorded diffusion transformation, although there are cases of the transformation occurring at high temperatures or at slower speeds.

The phase is a very hard and brittle one [47]. It can be achieved by quenching steel from the austenitic phase to give a very rapid cooling rate which will transform the steel to the BCT martensitic microstructure. Austenite has a high solubility limit for carbon and, if quenched, the carbon can stay in solution but due to the lack of time to diffuse and the solubility of carbon, the phase present is not ferrite, but martensite [52]. Very high levels of carbon lead to an increase in the strength and hardness but the steel will become incredibly brittle [52].

2.2.1.6 BAINITE

Bainite is another phase that is not in equilibrium. It has a medium hardness, above that of ferrite but still less than martensite [47]. It commonly forms when cooling from the austenitic phase and will form in the place of pearlite at high cooling rates.
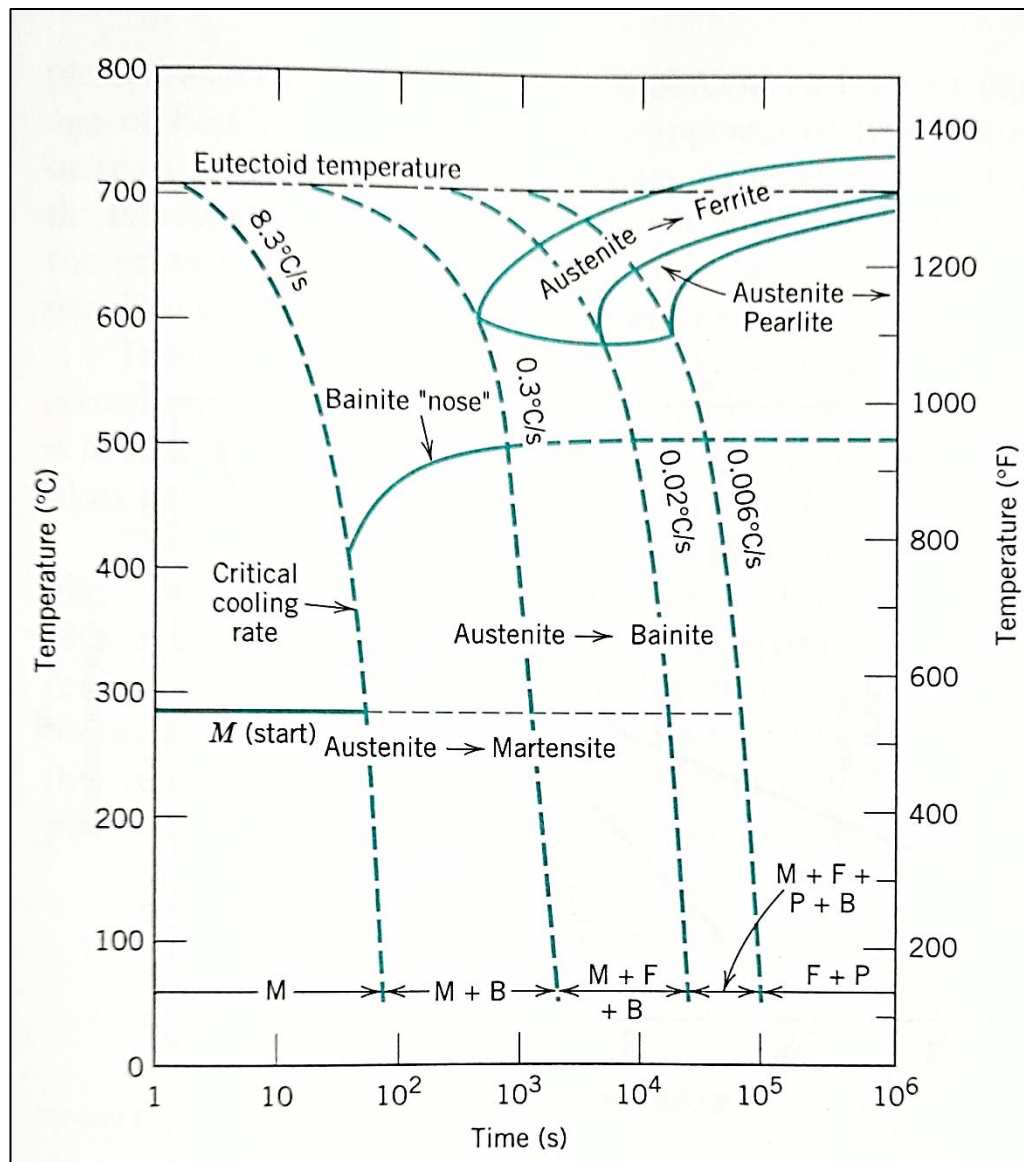
Figure 10 Continuous cooling transformation (CCT) curve indicating the phases present depending on the cooling rate on an alloy steel of unspecified composition [51], [53]

As shown in

Figure 10, the cooling rate will affect the level of transformation possible, and therefore phases present in the cooled steel. Bainite, as a non-equilibrium steel, will only be present in a steel that has cooled slowly enough to prevent the microstructure transforming completely into martensite, but not so slow as to allow all the austenitic region to transform into pearlite.

2.2.1.7 THERMODYNAMICS OF PHASE CHANGE

An equilibrium phase is an arrangement of atoms in its most stable state under the current conditions and will not change with time if held at a constant temperature and pressure in a closed system [54].

Steels take the form of polycrystalline aggregates meaning the strength of the steel is dependent on the strength of the grains and grain boundaries [55]. The grain boundaries are generally the weakest part of the system, so the steel strength is mostly dependant on the strength of the boundaries. This is due to a lower atomic order and a slightly different composition compared to the centre of grains [55]. When a phase is in equilibrium, the system will be thermodynamically stable and the surface tension of each phase on either side of a grain boundary will be exactly the same [55].

Many of the equilibrium phases such as ferrite and austenite are formed by the diffusion of atoms. This atomic diffusion requires time and energy which is not always present in industrial processes, leading to the formation of non-equilibrium phases. Martensite is an example of this and the lattice will be chemically identical to the parent austinite but will be distorted to allow for the dimension change that occurs.

During the formation of an equilibrium, the driving force to lower the Gibbs free energy is present and the temperature will supply enough energy to allow the structure to reach the point of equilibrium. When a non-equilibrium phase forms, the driving force that pushes the steel towards is present, but there is not enough energy to allow the steel to reach equilibrium. This results in a microstructure that has been frozen in place and slows the rate of diffusion of alloying elements to a point where they are negligible.

2.2.1.8 DUAL PHASE STEELS

A dual phase steel is one with a microstructure mostly containing a combination of ferrite and martensite and is particularly common among automotive steels [56], [57]. To achieve the distinctive banded microstructure as shown in Figure 11 a series of heat treatments and rolling processes are usually required to achieve a final product that is both formable and has excellent strength. The combination of a very hard martensite

with the much more ductile ferrite leads to an alloy with properties similar to those of a composite material. This makes dual phase steels a very valuable material, allowing the automotive industry to produce lighter cars, and therefore reduce the carbon dioxide emissions.[56], [58]

Figure 11 Example of a banded dual phase microstructure [59]

2.2.1.9 ELEMENT EFFECTS ON PROPERTIES

The solubility limit in ferrite is due to the size of the interstitial spaces in the BCC lattice (26). Ferrite has both tetrahedral and octahedral sites which have a free space with a radius of 0.036 nm and 0.019 nm respectively. Despite the greater available space in the tetrahedral sites, a substitutional atom such as carbon (radius 0.08 nm) or nitrogen (radius 0.07 nm) will preferentially site at an octahedral site (26). This is due to the nearest neighbours to the solute atoms. The octahedral sites will provide the interstitial atom with two nearest neighbours, rather than the four nearest neighbours present in a tetrahedral site (26). When an interstitial atom is present, the lattice must adjust to account for an atom that is present and larger than the available space, so the nearest neighbours will shift along the <100> direction (26).

Substitutional atoms in ferrite almost always have a linear relationship between the element concentration and the influence on mechanical properties, exceptions include nickel, silicon and cobalt (27).

Austenite has a much higher solubility of atoms such as carbon compared to ferrite. This is due to the larger voids in the austenitic lattice compared to in ferrite which have a radius of 0.052 nm at octahedral sites, nearly twice that of the biggest ferritic void [60]. Despite the larger voids, the austenitic lattice still needs to expand to accommodate the solute atoms.

2.2.2 COMMON TRAMP ELEMENTS AND EFFECTS

All element additions to steel will have an impact of the steel produced, often on the mechanical properties of the final product. A selection of these effects are listed in Table 2.

Table 2 Effects on steel properties from some elements that can be added to steels

Element	Hardness/ hardenabili	Yield stress	Impact strength	Tensile strength	Weldability	Ferrite-Austenite	Ductility
Aluminium			↓			↑	
Antimony	↑			↑	↓		↓
Arsenic	↑			↑	↓		↓
Beryllium						↑	
Bismuth					↓		↓
Boron				↑	↓	↑	
Carbon						↓	
Chromium	↑		↓	↑	↓	↑	↓
Cobalt			↓	↑		↓	
Copper	↑	↑	↑	↑	↓	↓	↓
Gold						↓	
Iridium				↑		↓	
Lead	↑				↓		↓
Manganese	↑	↑		↑	↓	↓	↓
Molybdenum	↑		↑	↑	↑	↑	↓
Nickel	↑		↑	↑	↓	↓	↓
Niobium	↑			↑	↓	↑	↑
Nitrogen	↑			↑	↓	↓	
Osmium						↓	
Palladium						↓	
Phosphorous			↓	↑	↓	↑	↓
Platinum						↓	
Rhodium						↓	
Rutherfordium						↓	
Silicon	↑	↑	↓	↑		↑	↓
Sulphur	↑		↓	↑	↓		
Tantalum						↑	
Tin	↑			↑	↓		↓
Titanium				↑	↓	↑	
Tungsten	↑			↑	↓	↑	↓
Vanadium	↑		↑	↑	↓	↑	
Zinc						↓	
Zirconium						↑	

Element	Hot ductility	Corrosion resistance	Toughness	Machinability	References
Aluminium		↑			[9], [61], [62]
Antimony	↓		↓		[7], [63]
Arsenic	↓		↓		[7], [13]
Beryllium					[62]
Bismuth	↓		↓		[7], [13]
Boron	↓		↓		[7], [62]
Carbon					[62]
Chromium		↑			[7], [9], [13], [63], [64]
Cobalt					[9]
Copper	↓	↑	↓	↓	[7], [25], [37], [63]–[65]
Gold					[62]
Iridium					[62]
Lead	↓	↑	↓	↑	[7], [13], [65]
Manganese				↓	[7], [9], [47], [62], [66]
Molybdenum				↓	[7], [9], [13], [47], [62], [63], [66]–[68]
Nickel		↑		↓	[7], [9], [13], [47], [62]–[64], [66]
Niobium					[7], [13], [47], [62]
Nitrogen				↑	[7], [13], [62]
Osmium					[62]
Palladium					[62]
Phosphorous	↓	↑	↓	↑	[7], [9], [13], [62]
Platinum					[62]
Rhodium					[62]
Rutherfordium					[62]
Silicon	↑			↓	[9], [25], [40], [47], [62], [65], [66], [69], [70]
Sulphur		↓		↑	[7], [9], [13]
Tantalum					[62]
Tin	↓	↑	↓		[7], [37], [63]–[65], [71]
Titanium					[7], [13], [62], [66]
Tungsten				↓	[7], [9], [66]
Vanadium					[7], [9], [13], [62]
Zinc					[62]
Zirconium				↑	[13], [62], [67]
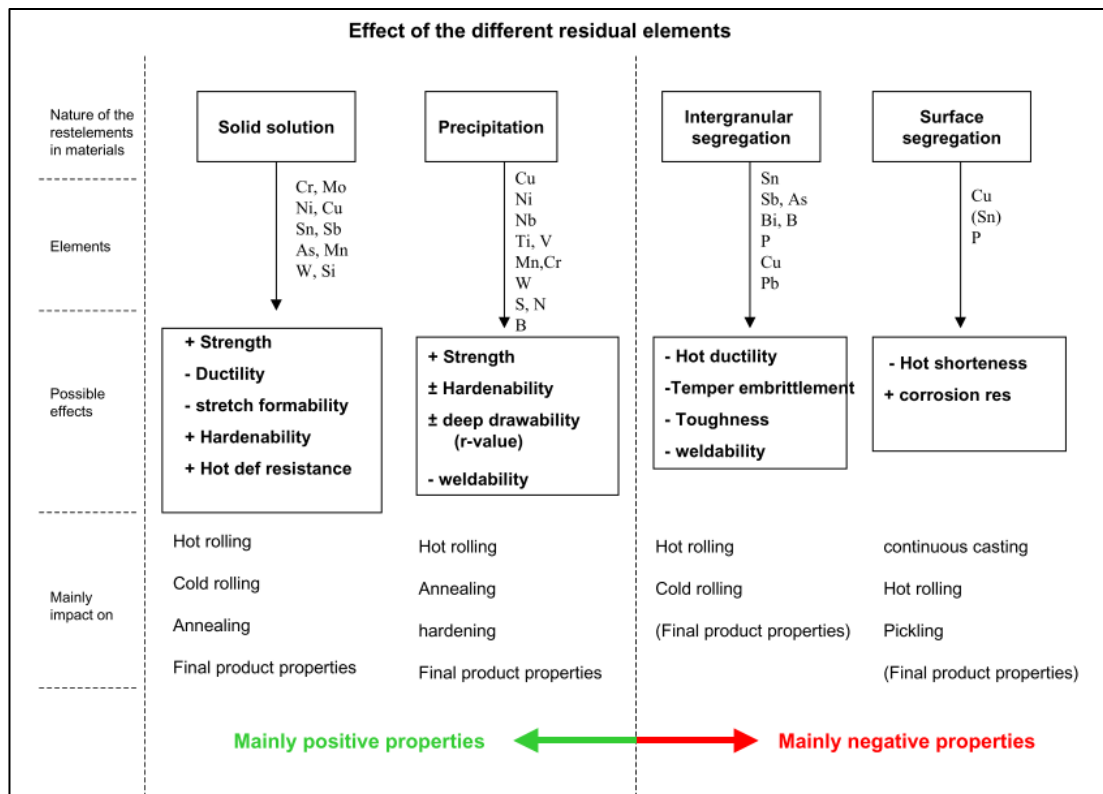
Figure 12 Summary of the typical manner in which common residual elements are present in steel, and the impacts this has on the processing and final products [7]

2.2.2.1 ALUMINIUM (AL)

The addition of aluminium into a steel alloy will decrease the impact strength as nitrides form at grain boundaries [62]. It does improve the corrosion resistance and raises the ferrite – austenite transition temperature [9], [61] in austenitic steels, the addition of aluminium is often countered by the addition of austenite stabilising elements such as manganese and carbon, as is the case in some TWIP steels. With higher levels of aluminium, the austenitic phase will disappear completely [62]. This affects the heat treatments that can occur as any heat treatments that involve heating through the austenitic region are no longer possible [62]. Aluminium additions remove oxygen from the steel and will improve the grain refinement in the final product [13].

2.2.2.2 BORON (B)

Boron is commonly added to steel to affect the hardenability [60]. The effect it has is largely dependent on the type of steel it is added to. Boron added to a hypoeutectoid

steel will improve the hardenability whereas it will decrease the hardenability in hypereutectoid steel and have no effect on eutectoid steel [60].

In finer austenite grains, the hardening effect of boron is increased although if austenizing at high temperatures, the effect is decreased. The optimum concentration of boron lies between 0.0005 – 0.003 wt% and the concentration will have no influence on the martensite transformation temperature [60].

In austenite, the boron becomes part of a solid solution with very low solubility. When the solubility limit has been reached, the boron will migrate to the grain boundaries, suppressing the formation of ferrite as the boron solubility in ferrite is approximately zero although this can be changed by the presence of impurities [41], [60]. Boron can delay the formation of pearlite and bainite as well as ferrite. In steels containing boron, an increase in carbon content in a steel will reduce the hardenability effect that boron has due to borocarbide precipitates that form in the austenite region, reducing the boron concentration throughout the rest of the steel [60]. As boron migrates to the grain boundaries, it is thought that it affects the energy of the surface boundary, this reduces the effects of elements such as copper that lead to steel prone to hot-shortness [7], [41]. While small amounts of boron will strengthen steel alloys, too much boron in the steel will reduce the hardenability and toughness [41], [60]. The reduction in toughness is due to precipitates of Fe_2B at austenite grain boundaries. The hardenability effect in the austenite phase compensates for the loss of hardness due to the low carbon concentration and the fine microstructure without affecting the M_s temperature. The advantage of this is that it reduces the likelihood of quench cracking which is more likely in cooler M_s temperatures [60].

Steels with boron additions must always be alloyed alongside strong nitride formers such as aluminium, titanium and zirconium due to how easily boron will react with nitrogen [60].

2.2.2.3 CARBON (C)

Carbon is probably the most widely used alloying element in steelmaking. When added to pure iron it expands the austenitic region until the point that it is restricted by the eutectoid temperature, below which a pearlitic microstructure forms [62]. It often

reacts with alloying elements to form carbides which in some cases form equilibrium carbide phases in the place of cementite [62]. The presence of carbon has a major effect on the growth rate of ferrite and slows down the formation of ferrite in steels alloyed with other elements as well as carbon. This is due to the effects of other alloying elements such as silicon, aluminium and chromium as a substitutional elements that influence the thermodynamic stability between ferrite and austenite [62].

2.2.2.4 CHROMIUM (Cr)

Chromium is a vital element in steel manufacturing and makes up a significant percentage of the bulk mass in stainless steels, usually at least 13%. It will increase the tensile strength and hardness but has a detrimental effect on the impact strength [9], [13]. Figure 12 shows the way chromium is beneficial in providing solid solution strengthening effects. Chromium atoms sit in solid solution in the steel, strengthening the material and increasing the elastic and shear modulus [7], [47], [67], [72].

The addition of chromium provides excellent corrosion resistance due to the high reactivity, it creates a non-porous protective oxide layer on the surface of the steel. It will slightly increase the eutectoid temperature in the steel by stabilising the ferritic phase [9], [66]. At higher temperatures the chromium in the steel will diffuse to, and precipitate at, grain boundaries forming carbides [62]. These further decrease the steel toughness and can cause a chromium depletion in the areas surrounding the grain boundaries where a lot of the chromium has diffused away. This can leave the steel more susceptible to corrosion. It has a high solubility of 20% of atoms in cementite without affecting the interlamellar spacing in pearlite [62].

2.2.2.5 COPPER (Cu)

Copper is a particularly troublesome tramp element in steel due to the impact on surface finish and difficulties in removing it and is therefore widely researched [7], [12], [17], [63], [65], [73], [74]. Once it has been introduced into the steel, often through copper wires attached to steel components and coatings, it is almost impossible to remove again meaning it will continuously build up and increase the concentration in steel over recycling iterations [73]. This is partly due to copper being

less reactive and more noble than iron [71]. Copper is commonly used to introduce precipitation hardening into a steel such as in structural steels, which can be a main contributor to copper content in scrap [68].

Copper has a maximum solubility of 0.35 wt% in ferrite and 9-10% in austenite and beyond this, will begin to form precipitates [25], [68] although if the concentration exceeds 0.1% copper, a molten layer can form and lead to cracking [22]. Copper atoms will diffuse to the grain boundaries and often form carbides or react with sulphur atoms to form CuS or CuS_2 form elliptical precipitates that weaken the grain boundaries and many of the mechanical properties [25], [37], [65]. This is heavily influenced by the sulphur content in the atmosphere, for example a high sulphur content in the gas present in a coke oven will lead to increased sulphur levels in the steel [68].

Hot shortness results from alloying elements that are less reactive than iron and so do not oxidise when heated, leading to a disproportionally high amount of iron oxidising on the surface, significantly increasing the residual concentration in the layer below the oxidised region [68]. Hot shortness from copper is particularly significant because although it has a solubility limit of 9-10 wt% in austenite, if conditions allow extreme oxidation, copper concentration can increase beyond this [25], [68].

During hot rolling, cracks may occur on the steel surface, caused by the presence of copper. Copper will melt above 1080°C so during processing of 1100-1200°C the copper rich regions will become molten and spread throughout the steel via grain boundaries, leading to grain decohesion and cracking [68].

Below 0.39% the effect on toughness is not significant but copper levels above this can decrease toughness, elongation and bending strength and reduce the hot ductility of the steel leading to hot shortness during rolling processing making the machining of steels with high copper content very challenging [25], [37], [65]. This is due to the increased stress concentration around the copper precipitates which lead to microvoids [65]. On the other hand, copper can increase the UTS, yield and tensile strength and raise the ductile to brittle transition temperature [25], [65]. It has the added benefit of improving the corrosion resistance of the steel [37] and can also harden the bainite phase, decrease the ferrite to austenite transition temperature, expand the austenitic region and refine the microstructure [9], [62], [71].

A proposed way to manage the surface cracking of steel caused by high copper concentrations is by increasing the temperature and oxygen level during heat treatments. This encourages the formation of scale which will be copper rich, which can then be removed be descaling [17].

2.2.2.6 MANGANESE (Mn)

Manganese is a substitutional alloying element that decreases the ferrite to austenite transition temperature by increasing the FCC lattice parameter and stabilising the austenitic phase [62], [66]. It increases stacking fault energy and can either improve or worsen mechanical properties depending on the quantity. When alloyed alongside sulphur, it forms MnS precipitates long the ferrite grain boundaries which introduces stress concentration and encourages void formation. This also increases the yield strength and tensile strength but leads to grain embrittlement. Manganese will react to form carbides and any precipitates present will decrease the steel machinability [9]. The addition of manganese to steel has a solute hardening effect and is a vital component in dual phase steels [47].

2.2.2.7 MOLYBDENUM (Mo)

Molybdenum is a common alloying element because of the beneficial effects it can have on steel. It increases the hardness [13] and both the impact and tensile strength and is a ferrite stabiliser, raising the ferrite – austenite transition temperature and with high enough concentrations, removing the austenitic phase completely [9], [62], [66]. Molybdenum has strengthening effects on steel. It does this through solid solution strengthening [47], [67]. It increases the hardenability, aids the formation of martensite whilst also suppressing the formation of pearlite [47]. It will react readily with carbon in the steel to form carbides which will reduce the machinability of the steel [9], [62].

2.2.2.8 NICKEL (Ni)

Nickel has similar effects to manganese and will increase both the impact and tensile strength and decrease the ferrite – austenite transition temperature, stabilising the austenite phase [9], [66]. Nickel is commonly incorporated into stainless steel and

contributes to the austenitic phase that is normally present at ambient temperatures [62]. In high enough quantities it can eliminate ferrite above room temperature or make it easier to have a metastable austenitic microstructure when quenched [62]. It does have a detrimental effect on the machinability but will not form carbides or nitrides at grain boundaries. Nickel has a hardening effect on steel, helping martensite formation and suppressing pearlite formation [13], [47].

2.2.2.9 SILICON (Si)

Silicon will increase the hardness, yield stress and tensile strength of steel and improves many mechanical properties via solid solution [9], [40], [47], [69]. It has a 10% solubility in ferrite at room temperature and will raise the ferrite to austenite transformation temperature [65], [66], [70]. At higher silicon levels, the austenitic phase will not form, affecting the ability to be heat treated [62]. This can be very useful and 4 wt% silicon can be added to stainless steel to stabilise the ferritic phase [62]. It increases segregation in the steel and encourages copper precipitation, although unlike copper, it does not react to form carbides but is can be oxidised to form slag components so can be removed from a steel melt with relative ease [25]. Silicon reduces the stacking free energy and has negative free energy in the steel and helps with corrosion resistance [65], [69], [70]. Between 700-110°C it reduces the hot ductility, but above 1100°C reports have found that it forms fayalite which helps to improve the hot ductility [65]. Silicon helps to prevent the formation of pearlite and of carbides [47].

2.2.2.10 TIN (Sn)

Tin is another element that will affect a steel in a similar way to copper, but the much bigger atomic radius means the effects are more significant [71]. It is very difficult to remove from steel using metallurgical processes as it is more noble than iron and it will form intermetallic compounds at grain boundaries [37], [65]. These reduce the impact toughness and ductility, in the steel and the increase in tin concentration will decrease the copper solubility and increase the tensile strength of the steel [65], [71]. One of the most common issues associated with tin as a residual element is the hot-

shortness which can occur during a hot working process in steel manufacturing [12], [25], [37], [68], [75], [76]. Tin will also cause issues in cold working and has a strict limit of 0.02 wt% if used for deep drawing [68], [77]. Surface segregation is an issue with high tin contents, this can reduce the creep performance [68]. This is due to the accelerating effects of cavity nucleation from oxides and sulphides [68].

2.2.3 ELEMENT INTERACTIONS

Each alloying element will affect the properties of steel in a unique way, but it is important to recognise that the interaction between multiple elements can enhance or reduce some of the effects. The introduction of some elements will alter the solubility limits of some other elements.

The solubility of tramp elements in steel generally decreases as the steel temperature decreases leading to intermetallic precipitates at grain boundaries [37]. This often leads to surface cracking and an increase in hardness but also in brittle behaviour [37]. Residual elements by definition have unwanted effects on the steel and the levels must be carefully monitored and the effects understood to ensure the steel produced is still of a high enough quality.

The addition of nickel can reduce the effects of copper or tin by stabilising copper rich austenite, raising the melting temperature and preventing the penetration of a molten copper rich phase throughout the steel. It has been proposed as a solution to hot shortness effects [7]. On the other hand, tin amplifies the copper effects due to the reduction of copper solubility in austenite by two thirds, making them particularly important to monitor in combination [17], [68].

When combining copper with nickel, a ratio of 2:1 of Ni:Cu prevents the copper causing surface cracking by the austenitic phase to dissolve a higher concentration of copper, and with some heating conditions a 1:1 ratio was found to be sufficient [17].

A copper equivalent calculation has been proposed as a way to predict the effects of multiple residual elements in a steel [17].

$$Cu_{eq} = Cu + 10Sb + 5Sn + 2As - Ni$$

Equation 2 Copper equivalent in steels [17]

High levels of silicon in a steel can promote a more ductile failure due to the way it repels phosphorous atoms. This limits phosphorous segregation at the grain boundaries and reduces intergranular fracture and the ductile to brittle transformation temperature up to a silicon value of 1 wt% in a Fe-0.2 wt% P steel [78]. In a steel with 0.05 wt% P, additions of 0.5 wt% Si also had a similar effects of reducing intergranular fracture caused by the segregation of phosphorous [79]. Higher silicon levels promoted transgranular fracture and increased the ductile to brittle transformation temperature [78], [79].

A number of issues during the steel processing is as a result of embrittlement, caused by increasing concentrations of elements at grain boundaries. This is related to the solubility of the additional elements in iron, although the solubility of iron typically decreases in higher alloy steels [17].

2.2.4 HEAT TREATMENTS AND ROLLING PROCEDURES

Rolling

This can take the form of cold or warm rolling depending on the steel ductility. The purpose of rolling is to manipulate the microstructure of the steel with the aim of achieving the mechanical properties best suited to the product application.

Hot rolling of steel takes place in the austenite phase which is typically more ductile than a microstructure containing cementite. This allows a greater deformation without subjecting the rolls to excess force. Alloying additions can raise or lower the austenite transition temperature so the composition will affect where this transformation temperature is.

Coiling

The coiling stages involves maintaining the steel at a warm temperature after hot rolling, and below the austenite-ferrite transformation temperature.

Coiling takes place below 727°C, therefore no austenite would be expected. In the target equilibrium state, the microstructure of the steel grades investigated in this thesis would have both ferrite and pearlite present. As Figure 9 shows, using the example of a eutectoid steel, a slower cooling period will lead to a fully annealed coarse pearlitic microstructure which prevents a microstructure containing brittle martensite. [51]

Intercritical annealing

The phases present in the microstructure at this point will depend on the rolling and heat treatment processes of the steel. The intercritical annealing process aims to transform some of the microstructure from one phase to another, in the case of a dual phase steel this may involve transforming austenite into martensite. To achieve martensite, the steel must cool very quickly in order to reach the martensite start temperature before the transformation to pearlite or bainite can begin.

Overaging

An overaging stage holds the steel at a warm temperature for a long time and occurs directly after the intercritical cooling annealing process. In industry the steel would not be quenched immediately to room temperature, instead a warm temperature is maintained for a defined period before fully cooling the steel. [80]
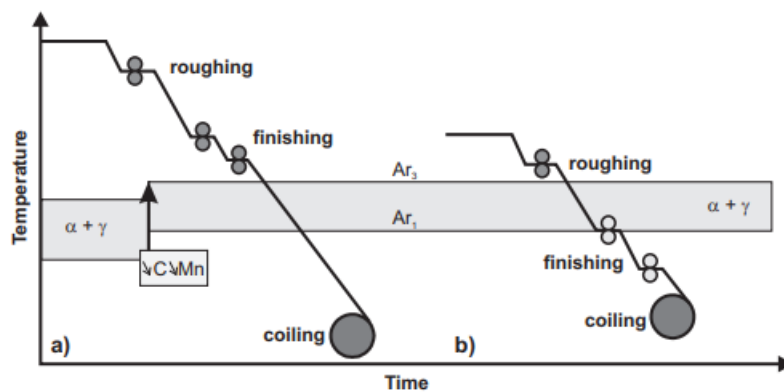
Figure 13 Overview of different rolling approaches showing the rolling schedule of conventional rolling compared to ferritic hot rolling [81]
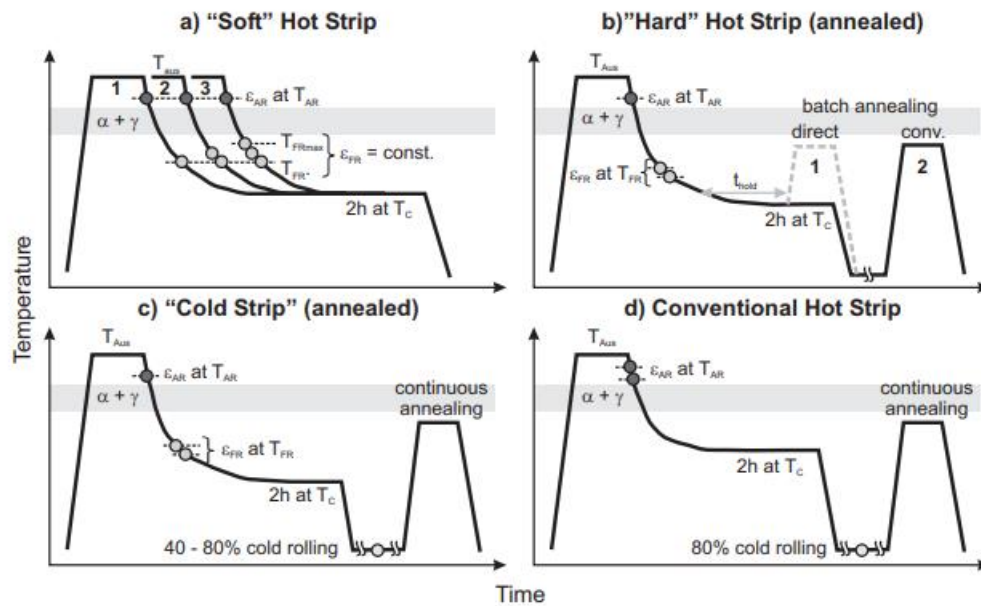
Figure 14 Overview of different rolling approaches [81]

Figure 13 and Figure 14 show an indication of what a rolling schedule can look like. The specific temperatures and timings will vary for each steel grade, but each diagram shows the coils being heated above the ferrite-austenite transformation temperature before hot rolling and coiling.

2.3 ALLOY DEVELOPMENT

Currently new alloys are tested using 80kg trials [40]. This allows for very accurate representation of what the final microstructure is likely to look like and how the mechanical properties will be. The size of the trials can be challenging because they require large volumes of material which slow down development and increase the waste associated with the development stages. The rate of alloy development has increased over recent years with most steel grades having been developed over the past couple of decades [9].

The RAP process has been found to show a lot of promise. In some cases, the manufacturing of a new alloy specimen can be done in a couple of hours, speeding up the alloy development process considerably. RAP covers a variety of manufacturing methods all with different benefits and providing different information.

The properties are not quite the same as the target alloys produced in the volumes that would be made on an industrial scale, often showing less ductility [82] although the chemical compositions are accurate with little macro segregation [83]. Despite the slight inaccuracies in the property values, trends are still able to be seen which has the potential to accelerate the development of new alloys [40], [82].

2.3.1 CURRENT METHODS USED

Technology has made the development of new alloys much faster. Software such as Thermocalc or Calphad allows the user to calculate the phases that would be expected to be present in an alloy of specified composition [83]–[92]. Calphad has been used in the past to develop alloys for disk turbines and made the process far more efficient [86]. This method of alloy development has drawbacks. It is difficult to visualise and produce phase diagrams showing more than simply binary or ternary equilibrium systems [84]. It also avoids considering metastable phases that are often present as a result of processing [84]. As this method will only produce the phases present at equilibrium, this method can only ever be used alongside real-world tests that include the processing conditions used in industry which often mean that the steel contains a phase or phases that are not in equilibrium.

There is not yet a software that can predict the outcome of different compositions as coupled with varying heat treatments and rolling or other working conditions. This means that experimentation still plays a vital role in the development of new alloys. It is important to compare predicted results to experimental data and a combinatorial approach to deepening our understanding of the phase composition and properties of alloys is a common method used [84], [88], [90], [93]–[95].

2.3.2 RAP METHODOLOGY HISTORY AND CURRENT RESEARCH

Combinatorial scientific methods have been in development since the 1960s but became more common in the 1990s where it was initially used to develop pharmaceuticals before the same thought processes were applied to material development [94]. This method has been used to discover and develop

superconducting, catalytic and photoluminescent materials and other new materials for other engineering industries [94], [96]–[99].

Small, rapid alloy development processes are currently being developed and have been shown to cut costs and improve efficiency in alloy development [40], [61], [82]–[84], [86], [100]. A selection of some combinatorial and RAP methods over time are discussed below.

1965: A combinatorial approach to phase diagram development is not new and has been a subject of interest for more than half a century. Kennedy et al. [101] developed a method to deposit three different elements onto a triangular substrate in a way that represents the compositions present on a ternary phase diagram. They focussed their research on the Fe-Cr-Ni alloy system and used electron beam bombardment to evaporate metal from blocks of the pure element. By varying the power of the electron beam used on each element, all elements can be deposited despite the different melting points. By heating the substrate on which the alloy is deposited, equilibrium phases can be found. There were difficulties when choosing the substrate material because it must not alloy with the deposited metal at any temperature present during the deposition or any annealing processes, but the deposited layer must be properly attached. Both molybdenum and stainless steel were found to be appropriate substrate materials. A common issue with vapour deposition is the contamination from gas that can occur. To reduce the effect of gases a high evaporation rate is used, the substrate is protected by a shutter for as long as possible and the process takes place in a high vacuum of approximately 5×10^{-6} Torr [101].

X-ray analysis was used to determine the phases present and alloy composition at each point within the sample. The x-ray technique used has a level of inaccuracy meaning that the results have limited reliability. When compared to information from literature at the time, it was seen that the phases present at each location approximately correspond to what would be expected from an equilibrium diagram, but the phase boundaries are not always in the correct place. It is also important to note that this experiment produced an isothermal diagram at 760°C whilst the information from literature only provided an isothermal ternary diagram at 650°C so some differences

between the two diagrams is to be expected. It was concluded that this method can be used to produce ternary phase diagrams to an acceptable level of accuracy in far less time than previous methods. The authors state that although the sample production is accelerated, the composition and phase analysis is still time consuming so ways to speed up this section of the process would be beneficial [101].

1999: Belov, Naumova and Eskin investigated the Al-Ce-Ni alloy system by producing small casts and using the resulting alloy to characterise and perform mechanical tests. Each alloy was produced using 99.99% pure aluminium and master alloys of Al-20% Ce and Al-20% Ni to introduce nickel and cerium and cast into a 10x20x180 mm graphite mould [102]. To heat treat the ingots, they were held at a constant raised temperature in an electric muffle furnace. To produce slow cooled alloys of the same composition, 10-15 g sections of the original cast were removed and reheated in alumina crucibles in an electric muffle furnace then cooling in either the furnace or in air. A cooling rate similar to industrial casts was able to be achieved giving a good microstructure and therefore reliable values for the mechanical properties. Values for the mechanical properties were found by conducting a three point bend test to which was able to give a reliable value for ultimate strength and an indentation to determine the hardness of the samples. High temperature properties were found by heating the sample to a raised temperature for one hour before conducting a hardness or bend test. The method used was able to advise commercial processing conditions and new aluminium based alloys. [102]

20 alloy variations within the Al-Ce-Ni alloy system were produced which allowed a phase diagram to be formed with the present phases plotted. Optical and SEM methods were used to image and understand the resulting microstructure to find correlations between the phases present, the microstructure and the composition. It was noted that there was some microstructural variation within ingots, especially in those with a composition near to the ternary eutectic point. [102]

The alloys were further heat treated for 5 hours at 400, 450 or 600 °C and viewed to analyse the thermal stability of the microstructure and any changes that may occur. Mechanical properties of the alloys were recorded before and after heat treatments to

gain a better understanding of a ternary alloy system and understand how processing conditions affect it. The resulting alloys were able to compete with industrially produced specimens, helping to validate the methodology. The improves understanding of how processing will affect the microstructure allows for better alloy design. [102]

2006: Pharr, George and Santella used a combinatorial approach to alloy development, focussed on a ternary system of iron, chromium and nickel [94]. Kinetic difficulties prevented a phase diagram for these elements from being studied in the past so Pharr was able to compare the sample data against a calculated phase diagram [94], [103]. Their samples were formed by the thin layer deposition of the alloying elements on 50mm diameter sapphire substrates at a deposition rate of approximately 1nm/s before annealing at 850°C in a vacuum [94]. This temperature was chosen to avoid the evaporation of unacceptably high levels of chromium. The resulting triangular samples contained pure elements at each corner with a concentration gradient throughout the sample which could be measured and matched to a ternary composition grid. From this, corresponding ternary phase diagrams displaying the phases and lattice structures present at each composition were able to be produced. The sample also allowed for the measurement of the alloy hardness and modulus at each composition using a nanoindentation method [94]. The main advantage of this method is that it includes every possible alloy composition but the process did not produce a sample with an even distribution of elements across the specimen meaning the phase locations were not as expected. The shift in location of some compositions and phases could be fixed with longer experimental time, giving the need for a compromise between result quality and processing time. Another improvement could come from increasing the cooling time to lead to more equilibrium conditions [94].

2012: Springer and Raabe produced an extremely fast, semi-continuous method of sample production that allows samples to be made and analysed within a 35 hour timeframe [82]. They emphasised the importance of investigating the effects of microstructure on properties rather than simply understanding the composition, and

therefore, the importance of investigating the effects of heat treatments. The production method used involved a row of five moulds ready for casting. Each mould was filled with a portion of a 4 kg melt, then the melt was adjusted via precise additions of the element of interest to alter the composition. This allowed each sequential cast to contain increasing concentrations of the element to be investigated, in this case, aluminium with concentrations ranging from 0-8 wt.%. Each cast was segmented into nine pieces to allow testing of various heat treatments of the different compositions, producing a total of 45 unique specimens. These samples could then be tested for yield strength, ultimate tensile strength, hardness and elongation to allow for easy comparison [82]. The mechanical property results were not identical to the properties from conventional production techniques but trends between the different compositions were clear and when scaled up to industrial sized production, the mechanical properties of the different alloys are expected to improve slightly, especially the material ductility [82].

2014: Raabe et al. developed this combinatorial work further whilst researching TWIP and austenitic steels [61]. They used the same methodology when investigating a quaternary system of Fe-Mn-Al-C. These specimens were used to further understand the effects of strain hardening on the specimens and the way they correlate to simulation data. This aids the production of better experimental samples with more useful data in the future. It shows that the experimental approach for the high-throughput alloy synthesis can be useful and appropriate [61].

2018: Cristobal et al. studied the effects of copper additions to stainless steel by using an additive alloy melting (ADAM) method [83]. The process researches the homogeneity of the stainless steels with copper additions on both a micro and macro-scale. It was determined that there was no macro-scale variation in composition but on the micro-scale, elements known to stabilise ferrite and austenite were found to segregate as predicted from a phase diagram. Multiple studies were made and produced by melting a section of the base steel with pure copper pieces in an argon atmosphere in a copper crucible, cooled by water any with a central hole containing a

piston. An electric arc from a non-consumable tungsten electrode melts the steel and copper allowing it to fill the hole and when solidified, the piston will lower slightly to leave space for another specimen cast on top of the first. Each melt does not join to the alloy below it meaning that the different compositions can be cast sequentially without issue. The specimens were then separated and prepared for XRF, XRD, OM and EPMA. Testing showed that the composition wt% of each element at points across the width and depth of the samples is very consistent, meaning there is minimal macro-segregation. The specimens contain some residual stresses on the macro-scale and some martensite regions that solidify first due to the cooling rate that would not be predicted from a Schaeffler's diagram. The segregation on the micro-scale involves phases of different compositions and particles particularly rich in certain elements such as copper or manganese [83].

2018: Ratschbacher, Klotz and Eisenbart recently outlined an adaption of this method, used for Cu-Be alloys that uses a diffusion gradient between the two elements [84]. This produces a specimen that includes all the intermediate compositions of the alloy. There is the option to extend this method to use on a system comprised of three different elements. To produce these specimens, samples of different compositions were stacked and diffusion welded and annealed at 900°C for two weeks. The resulting sample could then be sectioned to allow for multiple heat treatment tests. A major advantage of this method is that every possible concentration is present at some point within the specimen and it can be used to find compositions between different alloys. For example, a sample containing alloys of Cu-Ti, Cu-Sn and Cu-Al can be produced. Drawbacks with this method are the number of assumptions that must be made, including that the diffusion is even and perpendicular to the joint between segments. In regions where a multiple phase microstructure forms, it can be difficult to determine the hardness of the whole composition as opposed to the specific phase. The hope is that the method will allow future alloy developments will require fewer experimental iterations by obtaining more information from each test [84].

2019: A machine learning approach to alloy design was presented by Wang et al. using high throughput methodology to develop new aerospace nickel based superalloys [86]. This was done by producing a large specimen made of three different nickel based alloys diffusion bonded together with a concentration gradient of different elements. The samples contained eight different elements and the resulting block was sectioned to allow the sample to be analysed and the hardness tested.

Machine learning technology was used to characterise the microstructure and help integrate the computational and practical sides of alloy development. The microstructure, composition and microhardness data was combined to allow for better predictions of promising alloy compositions. This paper presents a method to produce samples that provide a large quantity of data which can be used to progress the use of machine learning in material design. [86]

2020: Mundhra, Hariharan and Murty used Calphad (CALculation of PHAse Diagram) along with experimental work to design a new alloy [85]. A new Al-Ti-Zr alloy was designed for the aeronautical sector with the aim of decreasing weight and increasing working temperature capability. To achieve this an Al based alloy composition was selected which was predicted to have a high volume fraction of the intermetallic phase ternary trialumnide which is particularly resistant to creep. The aim was to produce an alloy with 50 mol.% intermetallic and 50 mol.% FCC phase with the modelling predictions done using Thermocalc and Calphad software. When a promising composition had been selected, 25 g samples were made by vacuum arc-melting 99.9% purity powder and flipping and remelting the sample five times to ensure homogeneity. Further homogenisation was done by heating at 475 °C for 24 hours in a vacuum and water quenching. XRD was then used to determine the phase composition of the sample. The method to design new alloys by using a combined approach of modelling and experimental work proved very effective with the potential to design more novel alloys in the future. The method did uncover some disagreement between modelled and experimental results for the phases present meaning that experimental work is still necessary to improve databases. [85]

2020: Li et al. used a laboratory sized casting and rolling mill to investigate hydrogen embrittlement of metal strips and the potential effects of using mechanical vibration to optimise the microstructure [104]. A vibration was applied to the melt during solidification because this was found to optimise the microstructure before the metal is fed into the rollers which had rolls of 500 mm diameter and 350 mm wide and was able to replicate industrial processing conditions. They were able to use rolling temperatures over 1500 °C to roll 200 kg of metal at a time with consistent and controlled parameters. A low alloy steel way produced at 20 m/min with a thickness of 2 mm which, when measured, was uniform across the whole 200 kg strip. The research found that adding vibrations to the solidification process is both beneficial for the issue of hydrogen embrittlement in high strength steels, and feasible on an industrial scale. The work also shows that laboratory sized replicas of industrial processes can provide accurate and repeatable results. [104]

2.3.3   RAP FEASIBILITY

A combinatorial method can be used to either refine and optimise existing alloys or to develop new alloys [82], [94], [95]. It has been proven to be a much faster production route to understand trends in the research of new alloys but there are many different methods and approaches that can be used [40], [61], [82]–[86], [88], [90], [93]–[103]. Each has various advantages and limitations, predominantly from the difference between the mechanical property values obtained from the RAP sample tests and the values for the properties of specimens produced on an industrial scale.

2.3.4   SUMMARY

Rapid alloy prototyping is a research method shown to provide useful results in several fields, and the existing work done on metallurgy suggests that the method could be a useful way to research the impacts composition. A better understanding of the effects of residual element levels will allow for a more informed use of scrap steel, allowing lower production costs and associated carbon dioxide emissions. There is currently insufficient research on this topic and little work done on impacts of scrap in steel

making has been published. This thesis proposes a methodology which could alloy rapid research into the impacts of different alloying elements.

CHAPTER 3 MATERIALS AND METHODS

3.1 ALLOYS FOR THIS INVESTIGATION

In this investigation two significantly different steel alloys were selected to develop and test the rapid alloy prototyping routes. One was the Dual Phase DP800 an automotive steel which has been described in chapter 2. The other is 3190, which is an intermediate grade used in the production of various mild steel grades. The target compositions supplied by Tata Steel are given in Table 3.

Table 3 Current industrial tolerance limits and aim compositions for the two steel grades investigated specified in wt%

		Fe	C	Si	Mn	Al (tot)	Nb	Ti
3190	aim	Bal.	0.04					
	min		0.03		0.13	0.015		
	max		0.06	0.025	0.28	0.055	0.002	0.05
DP800	aim	Bal.	0.135	0.25	1.82		0.025	
	min		0.12	0.2	1.72	0.02	0.02	0.02
	max		0.15	0.3	1.92	0.085	0.03	0.04
		P	S	Cr	Mo	Ni	Cu	Sn
3190	aim							
	min							
	max	0.025	0.03	0.06	0.02	0.08	0.08	0.023
DP800	aim			0.55				
	min			0.5				
	max	0.020	0.005	0.6	0.02	0.1	0.12	0.03

This thesis aims to achieve a consistent composition within the limits specified by Tata Steel. The target will be to match the composition of the lab casts to the target levels of each element, first focusing on just carbon, manganese, silicon and residual additions to the iron, before moving on to additional alloying element additions of aluminium, titanium and niobium. As the focus of the work is on the impact of residual elements, the consistency of other alloying additions between casts is vital in order to highlight the effects of the chemistry variation arising from the residual elements.

3.2 (RAP20GP) 20G POWDER METHOD

3.2.1 SAMPLE PRODUCTION

The initial samples were made using a method used previously by J. C. T. Cullen [105] and had a target mass of 20g produced using a powder as the only feedstock for the samples. The powders used had a purity of at least 99% and were weighed out into a small plastic pot using scales to an accuracy of 0.0001g with a total mass of 20g. Residual element additions were added in increments of the current limits applied to the specific grade in industrially produced material. For example, the copper is limited to 0.12 wt% in DP800. The notation used throughout to describe the total levels of the residual elements is described as multiples of the current limit, meaning that Cu 4X would refer to a sample aiming to achieve a total copper level four times greater than the current limit of 0.12 wt%, so would have a target copper level of 0.48 wt%. The powder mixture was manually shaken in a sealed container for 30 seconds to mix the powder and before being compacted into a green body to produce a compaction with a diameter of approximately 10mm. A compacted powder pellet is easier to handle and melt compared to uncompacted powder, due to increased surface contact between particulates. The powder batches were compacted using a Tinius Olsen tensile machine and held under 25kN for 30 seconds, producing a compacted pellet, as demonstrated in Figure 15.
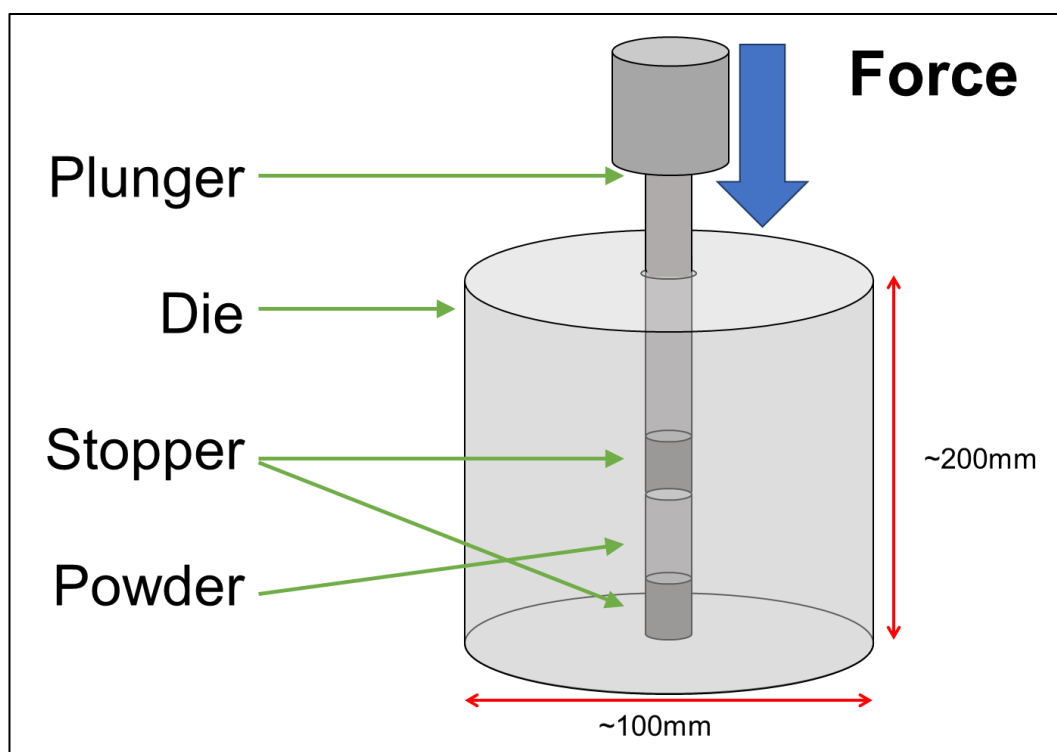
Figure 15 Powder compaction set up – not drawn to scale

To produce the bar cast, the compaction was put into a glove box with an argon atmosphere. The compaction was then placed in a ceramic crucible from Parweld with a 12mm internal diameter and open at both ends in an induction coil where a current was passed through the coil to heat the compacted pellet in a setup shown in Figure 16, and the temperature is monitored by a pyrometer. The current was gradually increased from 60 to 280 A at a rate of approximately 40A per minute until the specimen is molten, after which it is held in a molten state for 5 minutes at 280 A to allow for thorough mixing of all the elements.
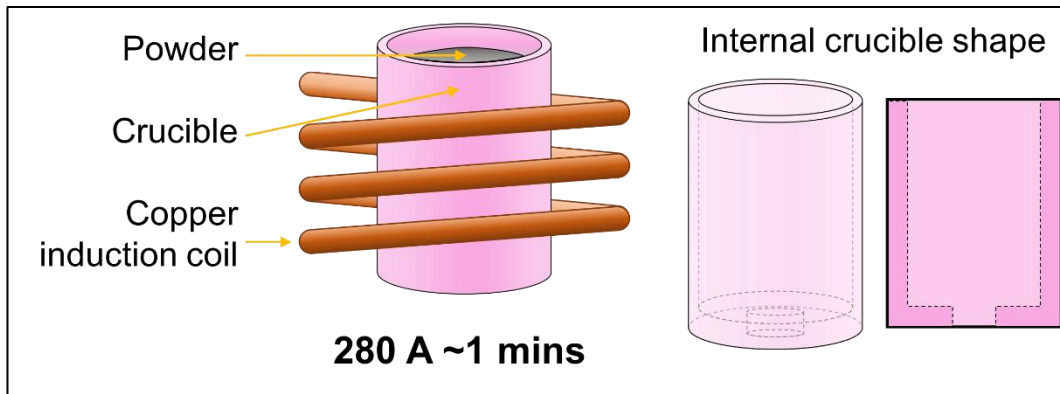
Figure 16 Diagram of melting in induction coil including the internal structure of the crucibles – not drawn to scale

To cast the melt into a bar, the crucible was set to one side as soon as the specimen had solidified throughout and cooled enough to be safe to move, typically when the top surface drops below 1000°C. The samples were cast into a boron nitride mould, propped at an angle beneath the coil, upon which the crucible was placed, ensuring the top of the crucible was within the coil, as demonstrated in Figure 17. When a current was reapplied at 360 A the specimen would remelt and flow into the mould. For the 20g sample, the mould used produced a bar cast of approximately 7x12x30mm.
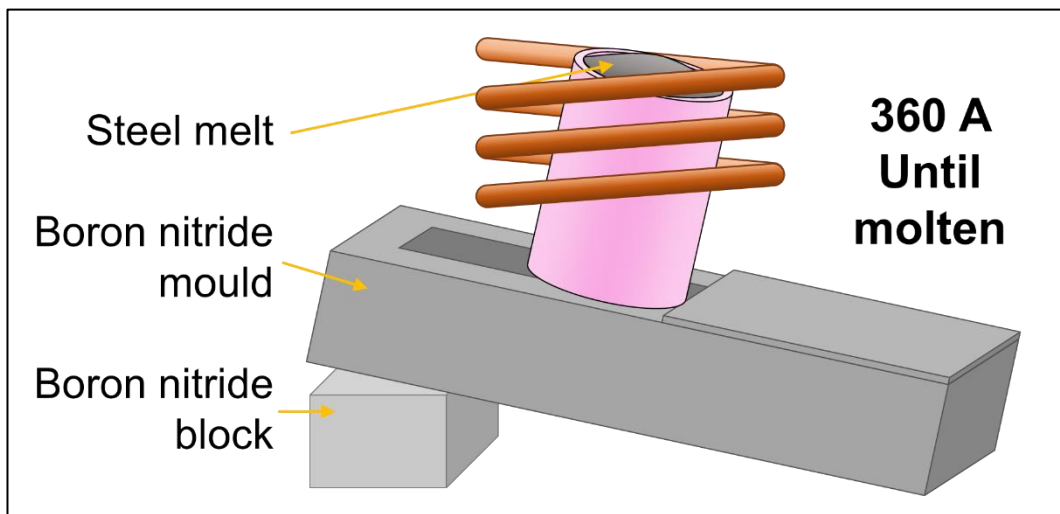
Figure 17 Initial bar casting set up – not drawn to scale

Figure 18 Images of the melting setup and resulting bar casts from the 20g method, showing a powder compaction in a crucible in the induction coil and four bar casts

After casting, the specimens were homogenised in a MTI corporation GSL-1700X vacuum furnace at 850° C for 5 hours. From here, the sample surface was removed and the resulting bar cold rolled by 80% (to an approximate sample thickness of 1.2mm) which was done using a hand powered, table mounted rolling mill. The final heat treatment of the samples was a normalisation process where the sample was held at 900°C for 2 minutes in Nabertherm box furnace with an air atmosphere, and the temperature monitored using a thermocouple attached to the sample. After removing the sample from the furnace, it was left to air cool. The 2 minute normalisation time was decided by testing three different normalisation times, and comparing the microstructure to industrially produced samples, and selecting the time period that gave the closest resemblance.
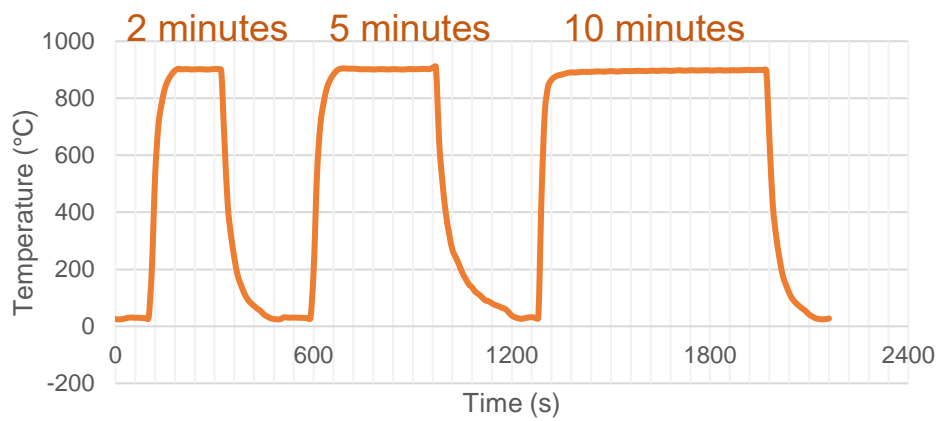
Figure 19 Temperature profile of the three test specimens used to determine the normalising time
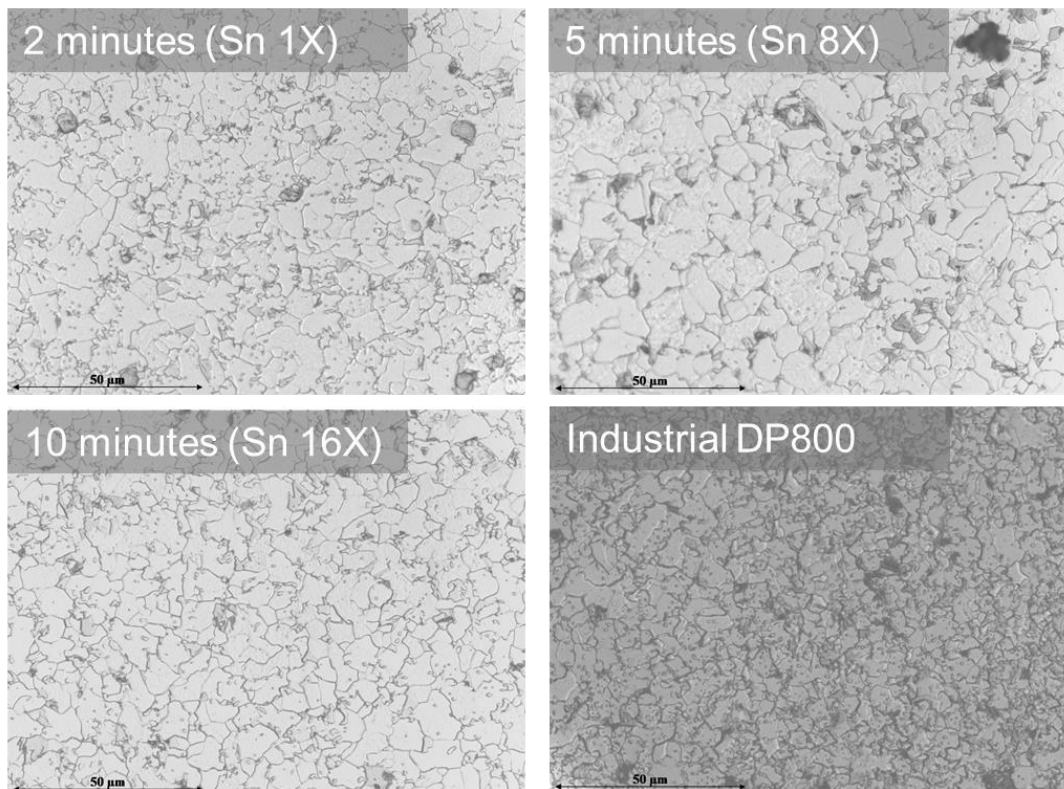
Figure 20 A comparison of microstructures of the test specimens and a section of industrially produced material where Sn 1X is a sample containing a tin level approximately the same as the current industrial limit of 0.03wt%. Sn 8X and Sn16X are eight times and sixteen times this value – 0.24 wt% and 0.48 wt% respectively

Table 4 A comparison of grain sizes between test specimens and the industrially produced sample

Normalising time	Grain size (μm)	
	Horizontal	Longitudinal
2 minutes	5	5
5 minutes	6	7
10 minutes	7	6
DP800 specimen	6	5

A small hand operated rolling mill was used to mimic the rolling processes of the industrial process. Samples were first sanded to remove the surface and thoroughly washed to reduce the potential of rolling any debris in to the material. The rolling mill was only able to roll at ambient temperatures, meaning only cold rolling was possible. The samples were cold rolled with a target reduction of 80%, then were subject to a heat treatment of 900°C for 2 minutes to replicate the coiling process. The sample is then ready to be machined into a tensile bar for the next stage of the process.

3.2.2 TENSILE TESTING

One 20g sample was only large enough to produce one ASTM25 tensile bar with a little excess material at the edges of the material as developed by Zhang et al. [106]. The tensile bars had dimensions shown in Figure 21 were pulled using a Tinius Olsen tensile machine. The samples were mounted in the tensile jaws and pulled at 1mm per minute until failure and extension measured using an epsilon axial clip on mechanical extensometer. The tensile bars are smaller than the A80 bars typically used in industry, so some size effects were expected but research by Zhang et al. [107] shows that these smaller bars can produce comparable results.
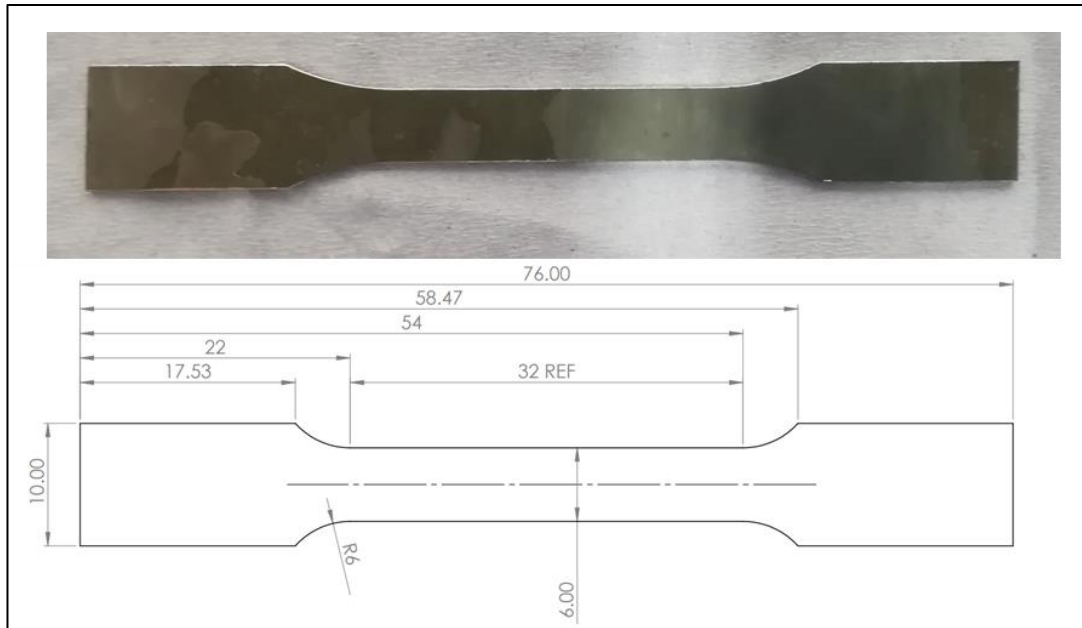
Figure 21 Dimensions of ASTM approved tensile bar for the 20 g rolled samples with units shown in millimetres

3.2.3 HARDNESS TESTING

A section of each specimen was mounted and tested for hardness using a Vicker's hardness test. A Buehler Wilson VH3300 hardness tester was used in conjunction with Diamet software and programmed to make ten indentations across the specimen, with 0.5mm spacing. Each indentation was held for ten seconds with a force of 10N and the indent size automatically measured by the program but checked manually to ensure accuracy.

3.2.4 CORROSION TESTING

Corrosion samples, tested using an open circuit potential setup, were prepared by polishing tensile bar tabs cut off after tensile testing. Using the tabs after the tensile tests made better use of the small specimens which leave little material for repeated tests. The samples had dimensions of approximately 14x10x1mm and the test area was isolated by wrapping insulation tape around the sample 10mm from the bottom. An area was left uncovered above the tape to allow a conductive section of the sample to be clipped to a wire. Before testing the specimen was cleaned again and tested using an open circuit potential. Each sample was immersed in the electrolyte so the

electrolyte just overlapped the bottom edge of the electrical tape. The electrolyte chosen was a 0.1M NaCl poured into a wide glass beaker. The experimental set-up used included a saturated calomel electrode (SCE) constant suspended in the electrolyte next to the test specimen. An experimental set up for open circuit potential is shown in Figure 22, with typical results shown in Figure 23. The tests were left for one hour after which some surface corrosion was visible and the potential difference could be recorded over the time frame by Corrware software.

The open circuit potential test provides a measurement of how reactive the sample surface is, which gives an indication of how susceptible to corrosion the sample is. The final potential difference values after one hour can be compared to identify trends in the reactivity of the samples. [108]
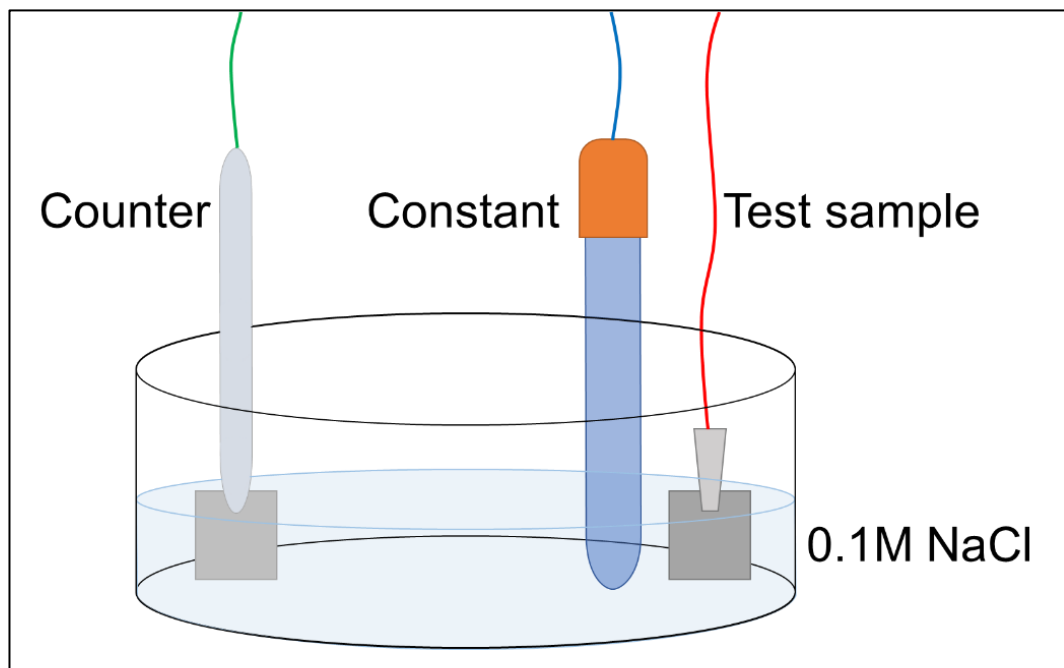
Figure 22 Open circuit potential set up – not drawn to scale
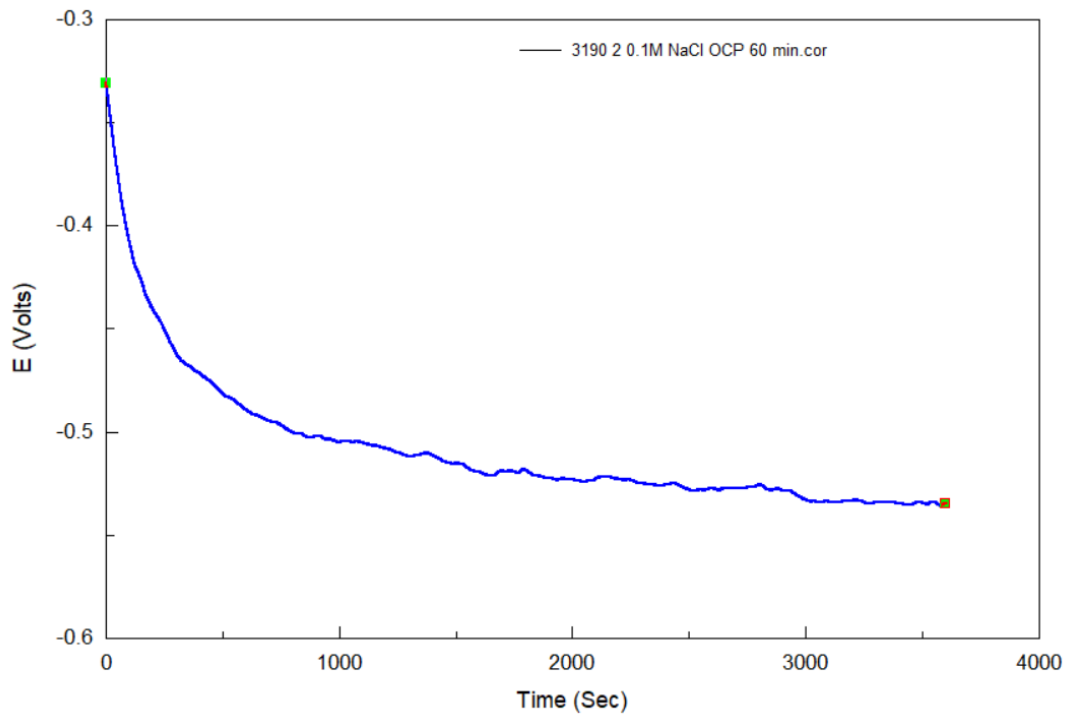
Figure 23 Example of the typical results given by the open circuit potential test

3.2.5   OPTICAL MICROSCOPY

The samples were mounted in a Bakelite compound before being polished according to the Buehler recommended route for stainless and maraging steels as shown in Figure 24 below. After the final polishing stage, the samples were etched using a 2% nital solution to highlight the grain boundaries. The samples were then imaged using a Jeol inverted optical microscope.

Surface	Abrasive / Size	Load - lbs [N] / Specimen	Base Speed [rpm]	Relative Rotation	Time [min:sec]
Sectioning	Abrasive Cutter with a wheel recommended for use on ferrous materials HRC35 -50				
Mounting	Compression, typically with EpoMet				
CarbiMet	120 [P120] to 320 grit [P400] SiC water cooled	6 [27]	300	⊙ ⊛	Until Plane
UltraPad	9 µm MetaDi Supreme Diamond*	6 [27]	150	⊙ ⊛	5:00
TriDent	3 µm MetaDi Supreme Diamond*	6 [27]	150	⊙ ⊛	3:00
ChemoMet	0.05 µm MasterPrep Alumina	6 [27]	150	⊙ ⊛	2:00

Figure 24 Recommended grinding and polishing route for stainless and maraging steels supplied by Buehler [109]

3.2.6 COMPOSITION

To test the elemental composition, optical emission spectrometry (OES) was used on small sections of each specimen. These sections were rolled to make them wide enough to cover the sparking area. The rolled section is big enough to spark the specimen twice on each side producing four sparks for each sample to produce an average composition. An additional method to check the elemental composition is an EDX method which uses an SEM and is most accurate for heavier elements such has manganese but far less reliable for lighter elements, especially carbon. Samples prepared for optical microscopy were also able to be used for EDX analysis, the mounted samples were placed in the sample holder in the SEM and attached with copper wire to ensure good conductivity.

3.2.7 SUMMARY

The results of the 20g method are shown in 4.1 and 4.2, and discussed in 7.1 and 7.2. They show that the methodology can be used to produce a general idea of mechanical properties, but there are variations in the composition, and the sample size means that only one tensile test is possible per cast. Due to this, different methods were considered which produced larger samples and therefore more test specimens allowing test repeats.

3.3 (RAP140GS) 140G SOLIDS METHOD

3.3.1 SAMPLE PRODUCTION

It was possible to produce larger samples using a centrifugal caster, up to approximately 140g. The stock material for the initial tests was an iron bar with solid element additions. The resulting casts were large enough for a series of OES sparks to accurately measure the composition.
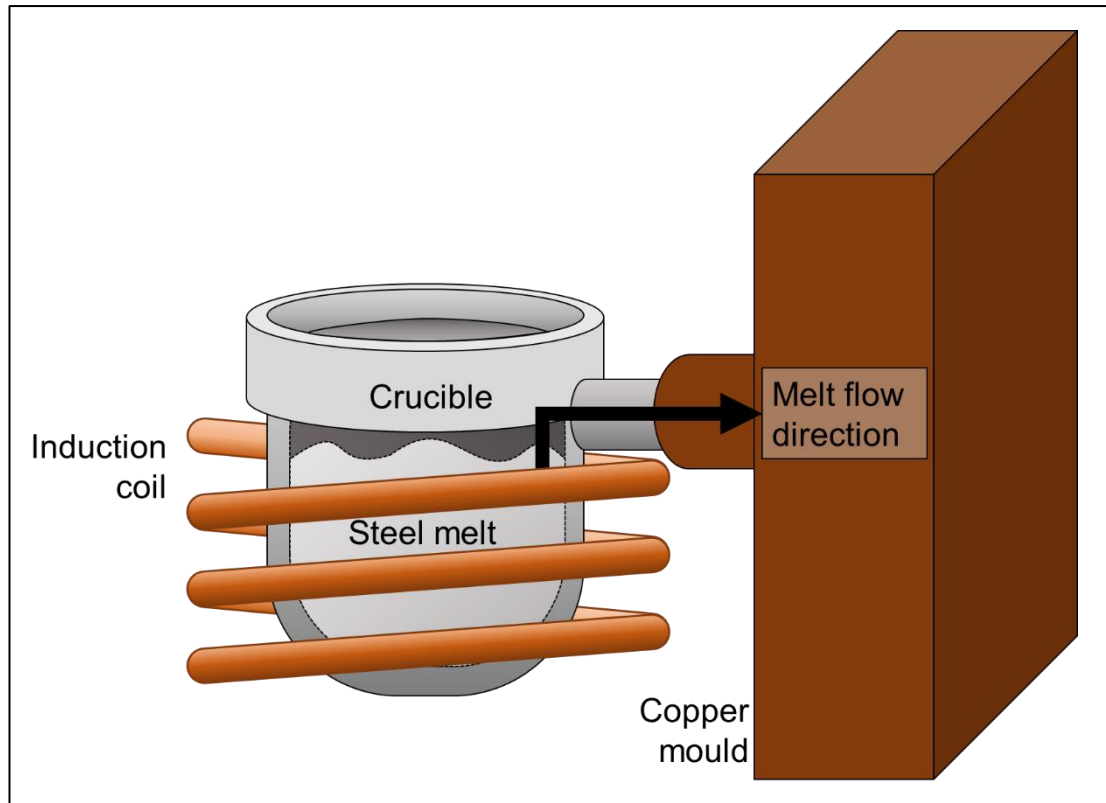
Figure 25 Inner set up of the centrifugal caster – not drawn to scale

The Ultraflex centrifugal caster was loaded with an iron rod to produce the iron content of the alloy, then weighing out additions of manganese, silicon, carbon and residual element additions from solid stock. These additions could then be poured into an alumina crucible with the iron rod and positioned in the centrifugal caster. The heating cycle took approximately 3 minutes until all solids are molten before casting into a copper mould, as shown in Figure 25.

3.3.2 SAMPLE ROLLING

The samples were hot rolled by preheating in the furnace for 5 minutes, at which point the samples were heated through, then pushing through the hot rolling mill where the rolls had been heated to 200°C and were rolling at 50% speed. A reduction to 3mm was achieved in one pass. The samples were then set aside to cool and the surface oxide removed by sandblasting. The samples could then be cold rolled to a further 45% reduction to produce a finished sample.

3.3.3 TENSILE TESTING

The rolled specimens were cut into tensile bars with dimensions shown in Figure 21 and pulled in keeping with the methodology described in 3.2.2, but with the use of an Xsight one video extensometer that uses pixel tracking to measure the changing dimensions of the sample. The centrifugally cast and rolled samples were large enough to produce 3-6 tensile bars, depending on the other desired tests for the material.

3.4 (RAP140GRM) 140G REMELTED METHOD

3.4.1 SAMPLE PRODUCTION

The production method that uses remelted industrial steel is very similar to the centrifugal method using an iron bar detailed in 3.3, with the key difference being the reduced need to add additional alloying elements other than the residual addition. The residual additions are added in solid form to the crucible along with the industrial material. As with other 140g samples, the cast is large enough to hot roll and provides enough material to get more than three ASTM25 tensile bars.

3.4.2 SUMMARY

The results of the two 140g experimentation methods are shown in 5.1 and 5.2 and discussed in 7.4 and 7.5. The remelted and solids routes had the benefit of larger cast sizes, allowing for more samples to be tested from each composition. The feedstocks were decided to be insufficient for the research due to impurities, so the powder route

was investigated again using a larger scale adaption of the 20g powder route investigated initially.

3.5 (RAP40GP) 40G POWDER METHOD

3.5.1 SAMPLE PRODUCTION

The 40g powder route follows largely the same process as the 20g powder route laid out in 3.1 with some key differences. Due to newer equipment availability, the samples could be compacted using a Baleigh Industrial hydraulic press to a force of approximately 90kN. The compaction dies were updated but the basic setup remained the same as is shown in Figure 15.

During the melting process, it was found that holding the melt in a molten state for 1 minute was enough to achieve a homogenous composition. After investigating the as-cast samples prior to homogenisation, the stage was discontinued because it was found that the step had little effect as there was minimal macro segregation of the composition even before the homogenisation step.

Increasing knowledge about the process highlighted the effects of element losses meaning an iterative process was carried out to better understand how to achieve a target composition. The produced samples are listed below.

Table 5 Test samples produced in the pursuit of a consistent composition

Sample Ref	Alloy	Route	Feedstock (Powder or solid)	Elements added
RAP40G_POW_1A	3190	40g	Powder	Fe (Bal), C, Mn, Si
RAP40G_POW_2A	3190	40g	Powder	Fe (Bal), C, Mn, Si
RAP40G_POW_3A	3190	40g	Powder	Fe (Bal), C, Mn, Si
RAP40G_POW_1B	3190	40g	Powder	Fe (Bal), C, Mn, Si
RAP40G_POW_2B	3190	40g	Powder	Fe (Bal), C, Mn, Si
RAP40G_POW_3B	3190	40g	Powder	Fe (Bal), C, Mn, Si
RAP40G_POW_1C	3190	40g	Powder	Fe (Bal), C, Mn, Si
RAP40G_POW_2C	3190	40g	Powder	Fe (Bal), C, Mn, Si
RAP40G_POW_3C	3190	40g	Powder	Fe (Bal), C, Mn, Si
RAP40G_POW_1D	3190	40g	Powder	Fe (Bal), C, Mn, Si, Cr, Al

RAP40G_POW_2D	3190	40g	Powder	Fe (Bal), C, Mn, Si, Cr, Al
RAP40G_POW_3D	3190	40g	Powder	Fe (Bal), C, Mn, Si, Cr, Al
RAP40G_POW_1E	3190	40g	Powder	Fe (Bal), C, Mn, Si, Cr, Al
RAP40G_POW_2E	3190	40g	Powder	Fe (Bal), C, Mn, Si, Cr, Al
RAP40G_POW_3E	3190	40g	Powder	Fe (Bal), C, Mn, Si, Cr, Al
RAP40G_POW_1F	3190	40g	Powder	Fe (Bal), C, Mn, Si, Cr, Al
RAP40G_POW_2F	3190	40g	Powder	Fe (Bal), C, Mn, Si, Cr, Al
RAP40G_POW_3F	3190	40g	Powder	Fe (Bal), C, Mn, Si, Cr, Al
RAP40G_POW_CUR_1	3190	40g	Powder	Fe (Bal), C, Mn, Si, Cr, Al
RAP40G_POW_ CUR_2	3190	40g	Powder	Fe (Bal), C, Mn, Si, Cr, Al
RAP40G_POW_ CUR_3	3190	40g	Powder	Fe (Bal), C, Mn, Si, Cr, Al
RAP40G_POW_NEW_1	3190	40g	Powder	Fe (Bal), C, Mn, Si, Cr, Al
RAP40G_POW_ NEW_2	3190	40g	Powder	Fe (Bal), C, Mn, Si, Cr, Al
RAP40G_POW_ NEW_3	3190	40g	Powder	Fe (Bal), C, Mn, Si, Cr, Al
RAP40G_POW_LIN_1	3190	40g	Powder	Fe (Bal), C, Mn, Si, Cr, Al
RAP40G_POW_ LIN_2	3190	40g	Powder	Fe (Bal), C, Mn, Si, Cr, Al
RAP40G_POW_ LIN_3	3190	40g	Powder	Fe (Bal), C, Mn, Si, Cr, Al

To ensure the composition consistency of the synthetic route, the 40g samples made using powders by measuring masses of powder of at least 99.8% purity in the corresponding wt% without the additions on any residual element additions. The subsequent powder quantities of each element were then adjusted in response to the measured OES composition, intending to converge on the desired composition. For some early tests, a powder mass totalling 45g was used to ensure the mould was completely filled.

The difficulty achieving a consistent composition in the 20g route, was deduced to be, at least in part, due to element losses during the melting processes. These losses were hypothesised to be due to several factors, which are discussed in this chapter, and in more detail in 7.3.3 An iterative method was used to evaluate the material losses in the production of low alloy 3190 steel. The samples were made without any added residual elements, only weighing out carbon, silicon, manganese, and iron powder, aiming focus on fewer elements at first. The compositions of these initial tests, tested on the MACH1 OES, are shown in Table 6 to Table 11 and a visual representation of the progression of element concentrations in Figure 26. It is important to note that the aim element percentage for each iteration does not fit with the industrial chemistry requirements. A piece of industrial material was tested on the OES equipment, and the resulting chemistry reading was used at the target composition to allow for any errors in the machine. The compositions of each iteration are shown below.

Table 6 Composition of 40g synthetic route trial 1

	C	Si	Mn	P	S	Cr	Al	Fe
Aim	0.019	0.017	0.152	0.024	0.013	0.046	0.023	99.63
RAP40G_POW_1A	<0.005	0.031	0.054	0.014	0.014	0.038	0.0041	99.77
RAP40G_POW_2A	<0.005	0.022	0.057	0.013	0.015	0.039	0.0073	99.77
RAP40G_POW_3A	0.007	0.04	0.048	0.014	0.015	0.039	<0.003	99.76
Av.	0.007	0.031	0.053	0.0137	0.0147	0.0387	0.0057	99.767

Table 7 Composition of 40g synthetic route trial 2 (increased C, Mn, lowered Si)

	C	Si	Mn	P	S	Cr	Al	Fe
Aim	0.019	0.017	0.152	0.024	0.013	0.046	0.023	99.63
RAP40G_POW_1B	0.011	0.02	0.063	0.012	0.014	0.039	0.0056	99.76
RAP40G_POW_2B	<0.005	0.017	0.062	0.012	0.015	0.039	0.0036	99.77
RAP40G_POW_3B	0.0053	0.022	0.055	0.011	0.015	0.038	0.0052	99.77
Av.	0.0082	0.0197	0.06	0.0117	0.0147	0.0387	0.0048	99.767

Table 8 Composition of 40g synthetic route trial 3 (increased C, Mn, lowered Si)

	C	Si	Mn	P	S	Cr	Al	Fe
Aim	0.019	0.017	0.152	0.024	0.013	0.046	0.023	99.63
RAP40G_POW_1C	0.012	0.02	0.27	0.0092	0.013	0.039	0.009	99.56
RAP40G_POW_2C	<0.005	0.016	0.22	0.0097	0.014	0.039	0.0044	99.62

RAP40G_POW_3C	0.0058	0.014	0.268	0.011	0.014	0.039	0.0046	99.57
Av.	0.0089	0.0167	0.2557	0.01	0.0137	0.039	0.006	99.583

Table 9 Composition of 40g synthetic route trial 4 (increased C, lowered Mn, unchanged Si, added Cr, Al)

	C	Si	Mn	P	S	Cr	Al	Fe
Aim	0.019	0.017	0.152	0.024	0.013	0.046	0.023	99.63
RAP40G_POW_1D	0.133	0.364	0.341	<0.003	<0.003	0.042	0.033	99.82
RAP40G_POW_2D	0.032	0.054	0.327	<0.003	0.01	0.044	0.019	99.42
RAP40G_POW_3D	0.0051	0.037	0.284	<0.003	0.0058	0.041	0.01	99.53
Batch average	0.0186	0.0455	0.3055	<0.003	0.0079	0.0425	0.0145	99.475

Table 10 Composition of 40g synthetic route trial 5 (increased Al, Cr, lowered Mn, unchanged C, Si)

	C	Si	Mn	P	S	Cr	Al	Fe
Aim	0.019	0.017	0.152	0.024	0.013	0.046	0.023	99.63
RAP40G_POW_1E	0.05	0.022	0.311	<0.003	0.013	0.065	0.048	99.41
RAP40G_POW_2E	0.02	0.031	0.315	0.0033	0.0096	0.043	0.019	99.49
RAP40G_POW_3E	0.038	0.021	0.283	0.0034	0.011	0.042	0.0083	99.52
Batch average	0.029	0.026	0.299	0.00335	0.0103	0.0425	0.01365	99.505

Table 11 Composition of 40g synthetic route trial 5 (increased Al, Cr, lowered Mn, C, Si)

	C	Si	Mn	P	S	Cr	Al	Fe
Aim	0.019	0.017	0.152	0.024	0.013	0.046	0.023	99.63
RAP40G_POW_1F	0.018	0.025	0.137	<0.1	0.013	0.011	0.072	99.47
RAP40G_POW_2F	<0.005	0.014	0.15	0.0098	0.013	0.043	0.021	99.67
RAP40G_POW_3F	<0.005	0.018	0.151	0.0075	0.013	0.042	0.017	99.67
Batch average	0.018	0.016	0.1505	0.0087	0.013	0.0425	0.019	99.67
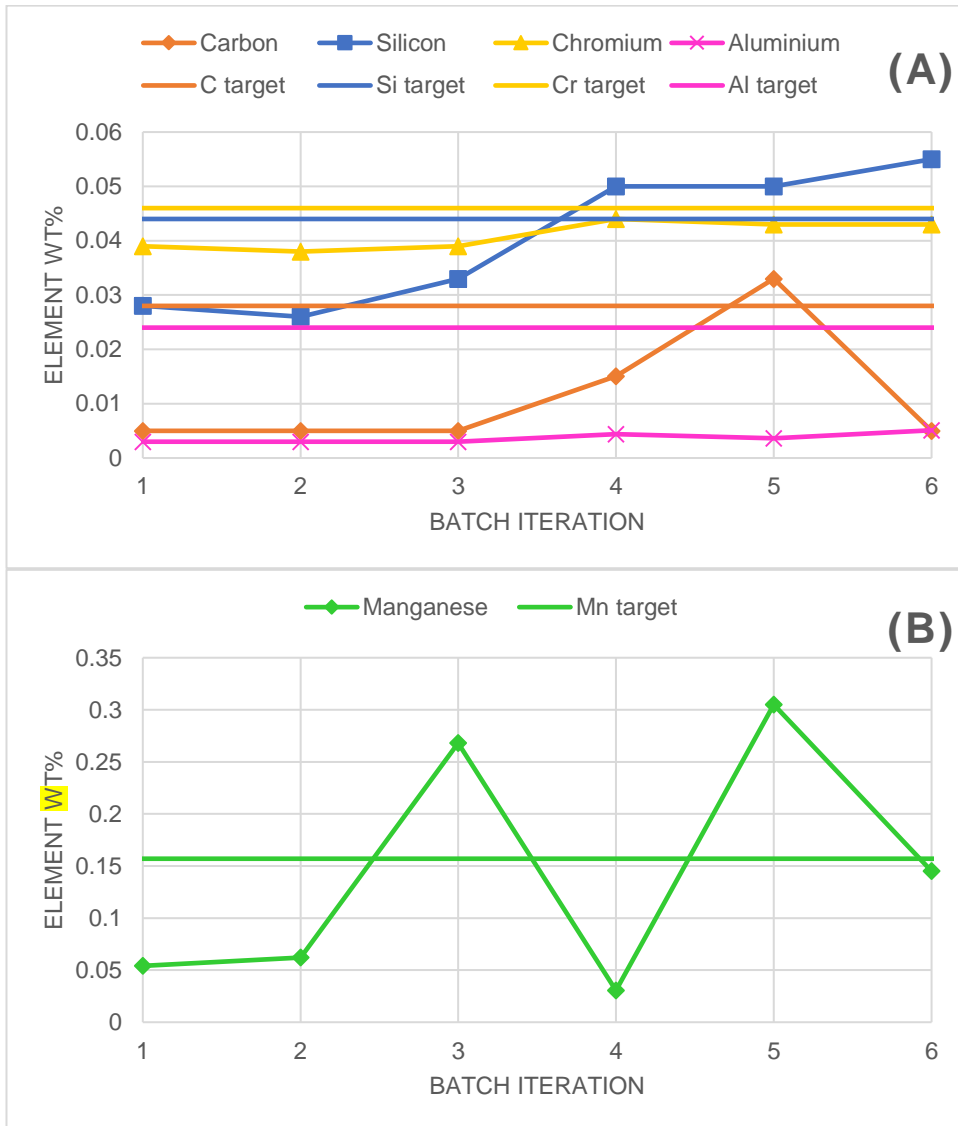
Figure 26(a)&(b) The composition change of subsequent samples made with the aim of getting the correct composition

The element levels in each iteration were based on a calculation using the added element mass and the resulting composition of the samples as shown in Equation 3.

$$\% \; element \; loss = target \; wt\% - average \; wt\%$$

$$New \; target \; mass \; \% = \% \; element \; loss + target \; wt\%$$

Equation 3 Calculation of element losses in iterative composition improvement testing

The resulting values for the element masses in the next batch were then manually adjusted where deemed necessary to avoid some extreme shifts in composition.

After several iterations it became clear that the process was not having the desired results, so attention was turned to other potential sources of element loss.

Due to the continuing difficulty achieving a consistent composition, the element loss was then hypothesised to be attributable to more than just losses during melting. A tested theory was that powder sticking to the plastic mixing pots and therefore not being incorporated into the compacted pellets before melting. Each of the pots would have a powder residue after weighing, but this had been assumed to be a powder mixture representative of the element mix, so a small experiment was devised to evaluate the effects of weighing pots made of different materials on the final outcome. A subsequent test looked at the currently used plastic pots, new pots of a different design, and the current plastic pots, but using old pots that had previously been used to weigh out material instead of new pots. The suspicion was that some of the powder was sticking to the pots, so using old pots with the powder residue rinsed and wiped out may reduce the powder sticking. Three samples were produced using each of the types of pots, with the sample powder masses weighed into each pot. The resulting compositions in the final samples are shown in Table 12.

Table 12 Resulting compositions of trial 3190 made using different pots

Testing pots	OES wt%					
Current pots	Fe	C	Si	Mn	Cr	Al
Aim	99.63	0.019	0.027	0.153	0.046	0.024
RAP40G_POW_CUR_1	99.65	0.026	0.039	0.157	0.043	0.02
RAP40G_POW_ CUR_2	99.62	0.022	0.039	0.163	0.043	0.019
RAP40G_POW_ CUR_3	99.62	0.036	0.032	0.158	0.043	0.019
Average	99.63	0.028	0.0367	0.159	0.043	0.019
New pots						
Aim	99.63	0.019	0.027	0.153	0.046	0.024
RAP40G_POW_NEW_1	99.62	0.005	0.044	0.168	0.044	0.025
RAP40G_POW_ NEW_2	99.62	0.008	0.036	0.167	0.044	0.03
RAP40G_POW_ NEW_3	99.65	0.005	0.033	0.158	0.043	0.02
Average	99.63	0.006	0.0376	0.164	0.0437	0.025
Lined pots						
Aim	99.63	0.019	0.027	0.153	0.046	0.024

RAP40G_POW_LIN_1	99.51	0.018	0.044	0.174	0.045	0.033
RAP40G_POW_ LIN_2	99.6	0.015	0.038	0.169	0.047	0.033
RAP40G_POW_ LIN_3	99.61	0.0083	0.043	0.165	0.045	0.028
Average	99.57	0.0137	0.0416	0.169	0.046	0.031

This test showed that the type of weighing pot did influence the composition of the final material and suggested that the carbon level in particular was influenced by the pot choice.

The pots used were later changed to thick glass containers which minimised the amount of powder sticking to the sides of the pots, therefore reducing that potential source of error.

After this series of tests, a composition and glass weighing pot were selected as being able to give the most consistent results close to the target composition. It was decided to select this choice and try adding some residual elements to the mixture.

Using the 40g approach produces a larger sample of approximately 7x18x60mm. This new geometry was large enough to undertake multiple OES sparks to determine the composition of the material before rolling the sample.

A more recent development employed a different casting method to allow more efficient gravity casting, demonstrated below in Figure 28. A new boron nitride mould was made which allowed for the bar to be vertically cast meaning the positioning of the crucible above the mould is much easier. In initial mould trials, the resulting bar cast has dimensions of approximately 6.5x12.5mm and could be up to 80mm long depending on the amount of material. For a 40g cast, the length would only be approximately 60mm. A later iteration of the mould allowed a wider cast of approximately 6.5x16x45mm. The difference between the two casts is shown in Figure 27.

Figure 27 40g cast from the initial mould trials (left), and the subsequent wider bar cast from a later mould (right)
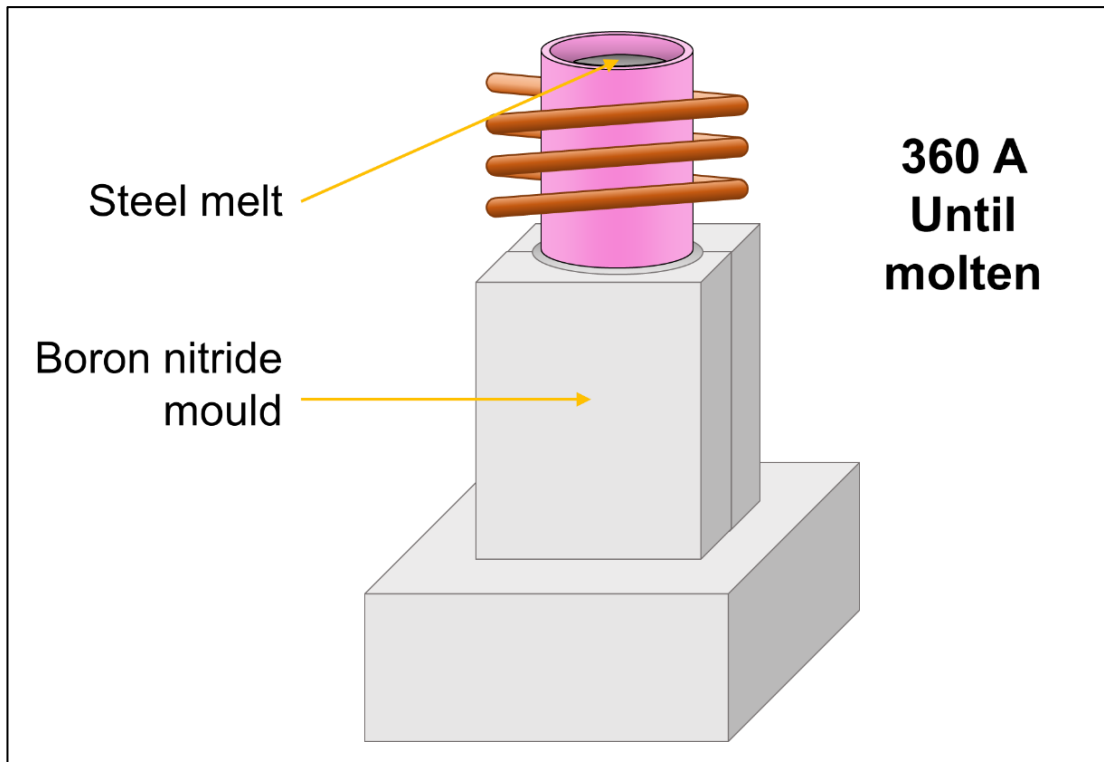
Figure 28 Subsequent bar casting set up

The method varied slightly between steel grades. In the production of the low alloy 3190 material, the samples were normalised in air at 900°C for 5 minutes, rather than

2 minutes as had been used previously as this was found to give the best microstructural results.

At this stage, a mechanical hot rolling mill was available, supplied by International Rolling Mills, allowing for much better control of the rolling process. The samples were able to be hot rolled with the aid of a table top box furnace next to the rolls in which the samples could preheat before being sent through the rolls.

The 40g samples were preheated in a Nabertherm box furnace next to the rolling mill to 1200°C, before being removed and immediately hot rolled, before being moved to a second furnace to coil at 600°C. The method allowed the samples to remain above 900°C throughout the rolling process, then was slow cooled from 600°C by maintaining the furnace temperature until a batch of rolling was complete, then switching off the furnace and leaving to cool, unopened, overnight.

3.5.2 SAMPLE TESTING

The finished rolled 40g samples were sand blasted to remove the oxide scale that formed during the rolling process. The initial longer, narrower 40g samples were able to produce three ASTM25 tensile bars, while the second, slightly shorter, iteration was only able to produce two tensile bars.

Other mechanical tests, such as hardness testing, were undertaken in the same way as described in 3.1, although new equipment availability allowed the use of a video extensometer during the tensile test.

3.5.3 SUMMARY

The results of the 3190 40g experimentation are shown in 6.1 and discussed in 7.6. It shows that the 40g sample size is large enough to produce sample repeats allowing multiple tests per cast, and the compositions achieved were closer to the target values. There were still unexpected element losses during the casting, and a hypothesis discussed in 3.5.1 led to the decision to look again at using solid feedstocks rather than powders.

3.6 (RAP40GS) 40G SOLIDS METHOD

3.6.1 SAMPLE PRODUCTION

The use of solid feedstock in the 40g route was decided to be a potential solution to the problem of element variations that may be coming for powder losses. The process follows most of the same process outlined in 3.5 (RAP40GP) 40g with the exception of a different feedstock and the only compaction necessary was for the high purity electrolytic iron flakes of 99.99% purity.

As before, the method produced gravity cast samples large enough for multiple OES sparks and a hot rolled sample large enough for three ASTM25 tensile bars was possible.

3.7 (RAP40GRM) 40G REMELTED METHOD

3.7.1 SAMPLE PRODUCTION

A variation on the previous 40g route uses remelted industrial material as the feedstock to try and control the element levels in the samples. As with previous 40g methods, the sample is gravity cast and easy to OES test.

3.7.2 SAMPLE TESTING

The cast can be hot rolled and is large enough to provide three ASTM25 tensile bars. The mechanical testing was carried out as described in 3.1 with the addition of a video extensometer.

3.7.3 SUMMARY

Using solid feedstocks was found to have advantages over the powder route as the feedstock was easier to work with and seemed less likely to result in unintentional element losses. The 40g remelted route was used to produce material used to trial and refine the methodology, as described in 3.8.2. Due to the requirement for an industrial feedstock, this method as not investigated further as it would mean the method is only able to research adaptions of grades already produced on an industrial scale and makes the customisation of the composition more challenging.

3.8 (RAP40GMA) 40G MASTER-ALLOYING METHOD

3.8.1 SAMPLE PRODUCTION

After observing the variation between samples produced using the powder route, an alternative 40g method was proposed which involved the addition of master alloys made with binary or tertiary alloys of high purity electrolytic iron and solid alloying additions other master alloys from a supplier. This reduced the potential for material differences through powder losses and makes the weighing out stage far easier to achieve high precision as the masses being weighed out were much larger, by a factor by between 10-100 times. In the initial test of the master alloys, the alloys were made using electrolytic iron and either pure solids or ferro-alloy solid lumps.

Most elements to be added to the synthetic DP800 were required in such small quantities, typically below 0.15wt%, so producing a master alloy with an element addition of approximately 1wt% would allow for more accurate quantities added due to the larger material mass to weigh, and reduced chance of material losses by using solid lumps rather than powders.

The initial master alloys were produced using a range of methods to test and evaluate different approaches.

Fe-Si

Produced using electrolytic iron and solid silicon lump with a target composition of 5wt%. This would lead to an expected mass of 2g of master alloy in a 40g DP800 cast to achieve a silicon composition of 0.25wt%. The initial sample was melted and cooled in the crucible to produce a cylinder cast but after removing from the crucible, it was clear to the eye that the sample was not homogeneous so the sample was remelted and cast into a bar. The resulting cast had a silicon content of 4.664wt% and was warm rolled at 500°C to a strip that was easy to cut with a guillotine.

Fe-Al

Produced using electrolytic iron and William Roland ferro-aluminium master alloy with an existing composition of 36.17wt% aluminium with the target of diluting this to 1wt%. In a 40g DP800 cast, 1.6g of a 1wt% Al master alloy would be needed to achieve an aluminium level of 0.04wt%. During the initial test, aluminium losses were

not accounted for as demonstrated by an aluminium content in the completed master alloy of 0.271wt%. This is due to the reaction between the aluminium and the oxygen already present which form oxides before the remaining, unoxidized aluminium can dissolve into the iron melt. Future master aluminium master alloys used this knowledge to compensate for the losses by adding an amount of aluminium to the initial melt with the aim of removing the existing oxygen from the melt, before adding additional aluminium to the melt to form the final composition. The master alloy was easily cold rolled to a thin strip for easy cutting.

Fe-Cr

Produced using electrolytic iron and solid chromium lump and targeting a chromium level of 10wt%. This estimates that 2.2g of the master alloy would need to be added to produce a synthetic DP800 with 0.55wt% chromium. As with the Fe-Si master alloy, the first attempt at producing this alloy produced a cylinder cast that was visibly not homogeneous and therefore was remelted and cast into a bar. The initial cast was still not homogeneous after remelting so this master alloy was remade from scratch. The new cast was made in the same way as the initial cast but was held in a molten state for 5 minutes before casting to increase the sample homogeneity. The new master alloy achieved a composition of 9.971wt% chromium with six consistent oes sparks across the length of the sample and on the top and bottom surfaces meaning that homogeneity was able to be achieved. The successful sample was able to be cold rolled to a thin strip before being cut into appropriately sized pieces.

Fe-Ti

Produced from electrolytic iron and an existing William Roland ferro-titanium master alloy with 70wt% titanium, which was diluted to a target of 1wt% titanium. Approximately 1.2g of this master alloy would need to be added to a 40g DP800 sample to achieve 0.03wt% titanium. The completed master alloy had a titanium level of 0.857wt%, the slight loss in titanium possibly coming from reaction with the oxygen within the melt. This sample was also easy to cold roll to an appropriate thickness before cutting to size.

Fe-Nb

Produced using electrolytic iron and a ferro-niobium master alloy from William Roland containing 65.85wt% niobium. This was diluted to a target of 1wt% niobium which would mean that 1g of this master alloy would need to be added to a 40g DP800 sample to achieve a niobium level of 0.025wt%. The niobium master alloy achieved a niobium level very close to the target, with a composition of 1.008wt% niobium. This sample was able to be cold rolled before cutting.

Fe-Mn-C

Produced using electrolytic iron and a combination of a ferro-manganese master alloy from William Roland containing 75.73wt% manganese and 6.95wt% carbon, and pure manganese flakes. This master alloy targeted a composition of 1wt% carbon and 13.4wt% manganese, the correct ratio for a DP800 steel. To produce a 40g sample, 5.4g of the master alloy would need to be added to provide a carbon level of 0.135wt% and manganese level of 1.81wt%. This combined element approach could be prone to error if the element ratio within the master alloy is not quite correct, but if successful could make the sample production stage simpler with a far more consistent ratio of element additions. The resulting master alloy had a carbon level of 0.938wt% and a manganese level of 13.981wt%. This is close to the intended values but the ratio between the elements is not quite on target, meaning it made the element composition of future samples made using this master alloy more challenging. An additional challenge became apparent during the warm rolling process at 500°C where, at a thickness on 2mm, the sample was so badly cracked that it could not be rolled any further but was still too thick to cut safely. The brittle nature of the sample made it possible to snap by placing the strip in a vice and bending using pliers, but the resulting chunks were of unpredictable and inconsistent sizing making it challenging to weigh out the subsequent samples using precise quantities of the master alloy.

Initial master alloy batch

An initial batch of three samples were made using the master alloys, all targeting the sample composition to test the accuracy and precision of the new method. These samples were made with the intention of being a first attempt at a new method. The master alloys were able to be added more easily than small solid particles, and with fewer losses than the powder route.

Fe-Mn

After concluding that using the ferro-manganese master alloy was not the optimal way to produce a master alloy, a new approach was made by making a new manganese master alloy from electrolytic iron and high purity manganese flakes with an aim of 10wt% manganese. This master alloy was then warm rolled at 500°C to a thin strip, with far less cracking than the previous Mn-C-Fe master alloy, allowing a thinner thickness to be achieved and the material was therefore easier to cut into pieces for measuring and weighing out.

Fe-C

The lack of success with the Mn-C-Fe master alloy meant another master alloy was also necessary to incorporate the carbon into future samples. The master alloys were again made using electrolytic iron with the addition of carbon solids cut from a pure carbon rod with a target composition of 1wt%. These master alloys were then warm rolled at 500°C to an appropriate thickness to easily cut and add to future samples.

3.8.2 ROLLING SCHEDULE

The rolling and heat treatments are vital to achieving the correct microstructure in a dual phase steel. To test this, several 40g casts were made by remelting industrial DP800 before putting them through the proposed rolling schedule. When the route was developed, a number of residual free, fully synthetic DP800 casts were made using the same process as the samples with added residual elements to determine what the finished sample would look like after the full process. This allowed for determination of any differences between samples from the same production method, to see the difference compared with the remelted industrial DP800 subject to the same heating and rolling processes, and with a final product industrial DP800 that has undergone the industrial process this work is aiming to replicate. The initial rolling route tested is shown in Table 13;

Table 13 Summary of stages in initial rolling route

Stage	Temperature (°C)	Reduction %	Dimension change (mm)	Time

Hot rolling	1000-1200 (entry) to 900+ (exit)	63%	6-2.3	
Coiling	630 (sample entry temp) 610 (furnace temp)			Furnace cool until cold
Cold roll	Room temperature	45%	2.3-1.25	
Intercritical cooling annealing	800			2 minutes
Overaging	325			15 minutes
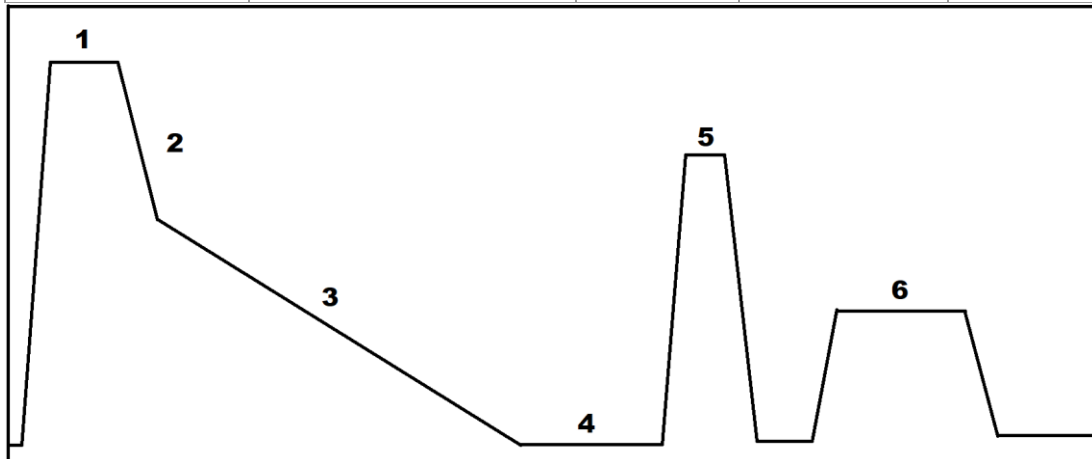
Figure 29 Rolling schedule stages

The heating and rolling schedule shown in Figure 29 indicates the heat and rolling schedule for the samples. The subsequent stages are as follows;

1. Preheat in box furnace at 1250°C in air for 5 minutes
2. Hot roll sample to a 63% reduction with an entry temperature >1150°C and an exit temperature <900°C cooling in air until 650°C
3. At 650°C sample is placed in a second box furnace at 610°C, then furnace cooled over many hours
4. Sand blast to remove scale and cold roll to a further 45% reduction
5. Intercritical annealing at 800°C in box furnace
6. Overaging at 325°C in box furnace

The surface of the sample blocks was removed prior to rolling to minimise that number of impurities imbedded into the sample surface. After cleaning, the samples could be

hot rolled. The hot rolling mill, made by International Rolling Mills, includes an inline furnace, allowing hot rolling of future samples.

Earlier samples were both hot and cold rolled using a rolling mill designed for hot rolling with rolls that could be preheated to 200°C if necessary. Later samples were able to be cold rolled with a new mill, also supplied by International Rolling Mills mill better suited to cold rolling.

The intercritical annealing stage was carried out in a box furnace with an air atmosphere. Each sample was placed in the furnace for 4 minutes 15 seconds. From test samples, it was found that the samples took approximately 2 minutes 15 seconds to reach 790°C. The samples remained in the furnace for a further 2 minutes, where the surface temperature averaged 804°C, after which they were removed and placed in front of a fan, cooling the sample surface by approximately 400°C in the 10 seconds after leaving the furnace. An example of the temperature profile of the test can be seen in Figure 30.
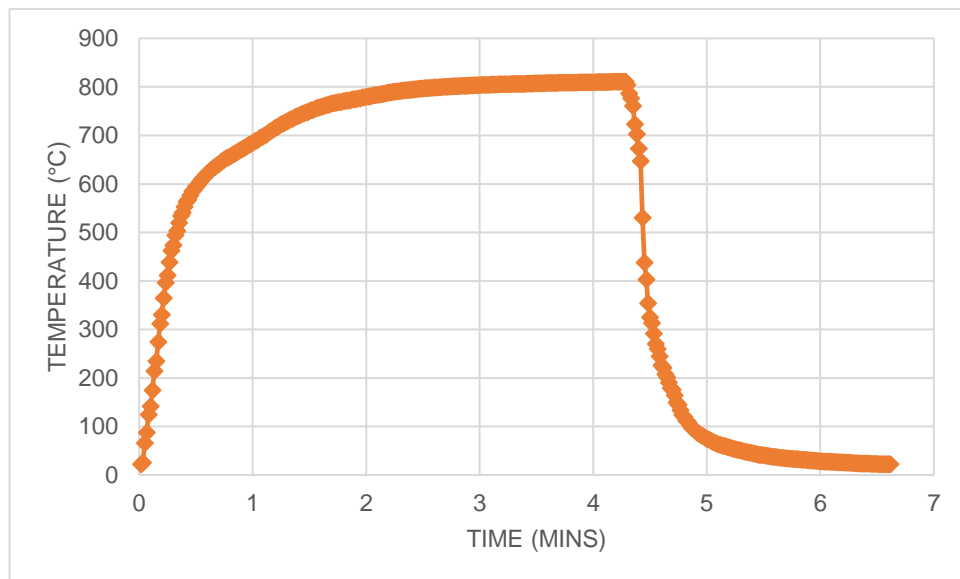
Figure 30 Temperature of synthetic residual free sample during a 2 minute 800°C intercritical annealing heat treatment

For the overaging stage, the samples were heat treated in batches of 3 samples. It was found that the samples took a long time to reach the desired temperature, so the target time of 15 minutes overaging was measured from the moment the sample surface reached 310°C. It took approximately 5 minutes for the test samples to reach this stage,

so samples were placed in the furnace for a total of 20 minutes before removing from the furnace and leaving to cool without the assistance of a fan or any other flow of air. The resulting heat cycle gave a surface temperature of 322.6°C over the 15 minutes overaging section of the cycle. The sample then cooled by 90°C over the first 10 seconds after leaving the furnace. An example of the sample surface temperature throughout the test is shown in Figure 31. As the furnace door was not able to be closed easily when the samples had a thermocouple attached, it was decided that the samples would all be left in the furnace for 20 minutes without a thermocouple attached.
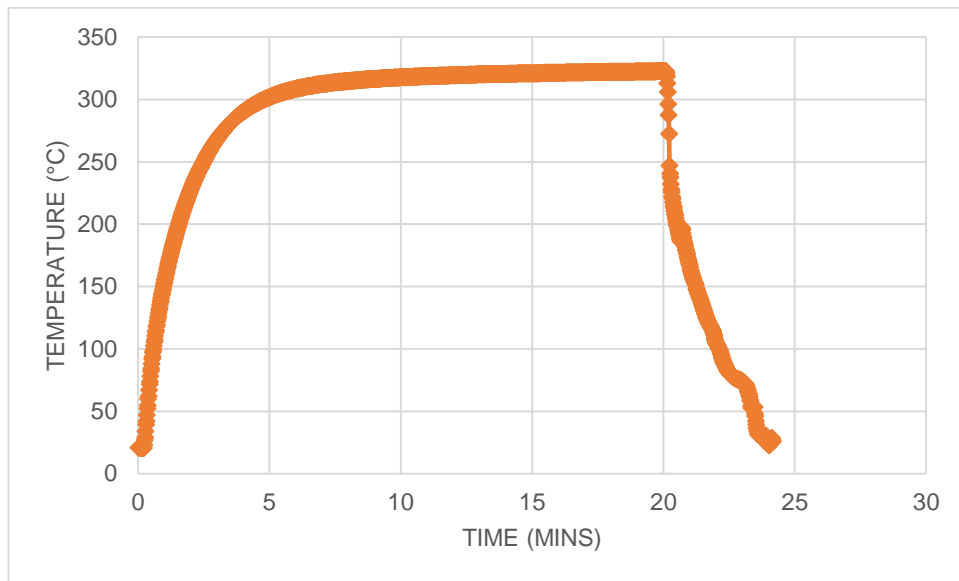
Figure 31 Temperature of industrial DP800 test sample during a 20 minute overaging heat treatment trial

3.8.3   SAMPLE TESTING

These samples were large enough to check the composition using an OES, and the OES used was one in The Steel and Metals Institute (SaMI), a research site for Tata Steel Europe, which gives more reliable results than the one available in the MACH1 labs. The other testing steps were the same as described in 3.1 with the inclusion of a video extensometer.

3.8.4   SUMMARY

The master alloy method was concluded to be to most promising method investigated in this thesis. The composition of the samples was quite consistent, the mechanical

properties showed increasing strength and hardness with the increasing residual levels, and the microstructure looked similar to the industrial equivalents, shown in 7.7. Further work on the heat treatments and rolling schedules has been done as a result of the success of the initial method development to achieve a product very similar to the industrial counterpart, as discussed in 8.2.

3.9 METHOD SUMMARIES

Throughout the research carried out, not only was the effect of residual elements investigated, but the RAP process was varied and improved throughout the work. These methods are summarised for easy comparison in Table 14 below.

Table 14 Methods summary of different sample production routes

Method #	RAP20G	RAP40G _POW	RAP40G _EI	RAP40G _MA	RAP40G _SOL	RAP140G _FE_BAR	RAP140G _CF_RM
Mass (g)	20	40	40	40	40	140	140
Iron feedstock	Powder	Powder	Electrolytic iron	Electrolytic iron	Remelt	Iron bar	Remelt
Additions feedstock	Powder	Powder	Solids	Master alloys	Solids	Solids	Solids
Melting method	Glove box	Glove box	Glove box	Glove box	Glove box	Centrifugal caster	Centrifugal caster
Hot rolling?	No	Yes	Yes	Yes	Yes	Yes	Yes
No. tensile bars	1	3	3	2-3	3	3-6	3-6

3.9.1 SUMMARY

The different methodologies investigated in this thesis have been explained, developing the previously used RAP20G process which used a powder feedstock to produce enough material for one tensile test, into larger casts with improved compositional accuracy and enough material for repeated tests. The powder route was replaced with a master alloy route which instead used high purity ferro-alloys as the feedstock, and other equipment had gradually become available which allowed the

sample processing to better match the heat treatments and rolling schedule of the industrial process.

CHAPTER 4   TESTING AND EVALUATION OF EXISTING RAP ROUTE

In this chapter some of the preliminary attempts at producing synthetic versions of DP800 and 3190 are presented, completed using an existing method previously developed by J. C. T Cullen [105].

4.1   PRELIMINARY RESULTS 20G DP800 STEEL

DP800 is an automotive steel with relatively high levels of alloying additions, shown in Table 3. It would be expected that the other elements already present in the composition would minimise the impacts of the residual elements because there is so much else influencing the properties. For example, the high levels of manganese and carbon with strengthen the material and increase the hardness, meaning the existing variation in composition make it challenging to determine precisely how much of the changing properties are due to the residual elements. The tight constraints on the product meant that not only must the composition be carefully controlled, there must also be an elaborate sequence of rolling and heat treatments on the samples to mimic the industrially produced version being attempted to recreate.

4.1.1   INTRODUCTION AND SAMPLE OVERVIEW

The existing RAP20G route used the method of an existing route [105] to make synthetic DP800 with additions of copper, tin, and nickel, as described in (RAP20GP) 20g powder method and summarised below and in Figure 32. This initial exploratory work aimed to understand the benefits and limitations of the RAP method developed to date and see if it was able to give an insight into the effects of residual elements on DP800, a dual phase automotive steel.

4.1.1.1   METHOD SUMMARY (DP800 20G POWDER ROUTE)

- 20g sample size
- Gravity cast

- Powder feedstock
- One tensile bar per sample
- Cold rolled to an 80% reduction (approximately 6mm to 1.2mm)
- Normalised at 900°C for 2 minutes
- OES testing challenging due to small sample size
- Testing included tensile, corrosion, hardness and microscopy

This method provided a good basis for the initial tests and understanding of the process and being able to begin looking at and improving the way samples are made. The small sample size made it challenging to do an OES test to check the composition. Where OES tests were possible, only four sparks could be made due to the small sample size, and due to the lack of measurement of tin in the available OES, the samples with additions of tin were assumed to have a composition equivalent to that of the proportions of each element weighed out to input into the samples.

The positioning of the crucible and the mould meant that when the sample was cast, the flow of the metal had a directionality along the sample, replicating part of the industrial process. The glove box used to melt the samples contained an argon atmosphere with an oxygen level typically below 100ppm, meaning minimal oxygen made its way into the sample.

Figure 32 Overview of RAP20G route

The samples considered in this section are listed in Table 15, where the notation used describe the total levels of the residual elements is described as multiples of the current limit.

Table 15 Initial 20g DP800 samples which did not include a control specimen

Sample Ref	Alloy	Route	Feedstock (Powder or solid)	Elements added
RAP20G_DP_POW_CuX1	DP800	20G	Powder	Fe (Bal), C, Mn and Si + residual Cu
RAP20G_DP_POW_CuX4	DP800	20G	Powder	Fe (Bal), C, Mn and Si + residual Cu
RAP20G_DP_POW_CuX8	DP800	20G	Powder	Fe (Bal), C, Mn and Si + residual Cu
RAP20G_DP_POW_CuX12	DP800	20G	Powder	Fe (Bal), C, Mn and Si + residual Cu

RAP20G_DP_POW_CuX16	DP800	20G	Powder	Fe (Bal), C, Mn and Si + residual Cu
RAP20G_ DP_POW_SnX1	DP800	20G	Powder	Fe (Bal), C, Mn and Si + residual Sn
RAP20G_ DP_POW_SnX4	DP800	20G	Powder	Fe (Bal), C, Mn and Si + residual Sn
RAP20G_ DP_POW_SnX8	DP800	20G	Powder	Fe (Bal), C, Mn and Si + residual Sn
RAP20G_DP_POW_SnX12	DP800	20G	Powder	Fe (Bal), C, Mn and Si + residual Sn
RAP20G_DP_POW_SnX16	DP800	20G	Powder	Fe (Bal), C, Mn and Si + residual Sn
RAP20G_ DP_POW_NiX1	DP800	20G	Powder	Fe (Bal), C, Mn and Si + residual Ni
RAP20G_ DP_POW_NiX4	DP800	20G	Powder	Fe (Bal), C, Mn and Si + residual Ni
RAP20G_ DP_POW_NiX8	DP800	20G	Powder	Fe (Bal), C, Mn and Si + residual Ni
RAP20G_DP_POW_NiX12	DP800	20G	Powder	Fe (Bal), C, Mn and Si + residual Ni
RAP20G_DP_POW_NiX16	DP800	20G	Powder	Fe (Bal), C, Mn and Si + residual Ni

4.1.2 COMPOSITION

The addition of three different elements (Cu, Sn, Ni) to a synthetic DP800 was investigated at five different residual levels based on the current industrial residual limit. The levels added were 1X, 4X, 8X, 12X, and 16X the current limit of each residual element as shown in Table 3. The synthetic steel samples were a simplified version of the industrial grade, with only Fe, C, Mn and Si added in addition to the residual element. A table of the target and achieved compositions is shown in Table 16, and summarised in Figure 33.

Table 16 Composition of the RAP20G_ DP_POW samples, those with Cu and Ni additions were measured with an OES, those with Sn additions were calculated by weighed element levels. All measurements are presented at wt%

	FE	C	MN	SI	RESIDUAL
RAP20G_DP_POW_CUX1	**97.5900**	0.1660	1.7910	0.2650	0.0730
RAP20G_DP_POW_CUX4	**97.3400**	0.1350	1.9980	0.2560	0.1560
RAP20G_DP_POW_CUX8	**97.3800**	0.1390	1.8470	0.2520	0.2680
RAP20G_DP_POW_CUX12	**96.9700**	0.1300	1.9770	0.2640	0.4010
RAP20G_DP_POW_CUX16	**96.9800**	0.1130	1.9180	0.2420	0.5340
RAP20G_ DP_POW_SNX1	**97.7860**	0.1310	1.8205	0.2490	0.0135
RAP20G_ DP_POW_SNX4	**97.7648**	0.1315	1.8198	0.2475	0.0365
RAP20G_ DP_POW_SNX8	**97.7180**	0.1320	1.8190	0.2525	0.0785
RAP20G_DP_POW_SNX12	**97.6816**	0.1285	1.8184	0.2510	0.1205
RAP20G_DP_POW_SNX16	**97.6060**	0.1324	1.8178	0.2488	0.1949
RAP20G_ DP_POW_NIX1	**97.4400**	0.0930	1.9320	0.2540	0.0490
RAP20G_ DP_POW_NIX4	**97.4400**	0.0960	1.8300	0.2870	0.1110
RAP20G_ DP_POW_NIX8	**97.3400**	0.0910	1.8800	0.2920	0.1840
RAP20G_DP_POW_NIX12	**97.2400**	0.0980	1.9290	0.2710	0.2460
RAP20G_DP_POW_NIX16	**97.0400**	0.0910	1.9930	0.2920	0.3370
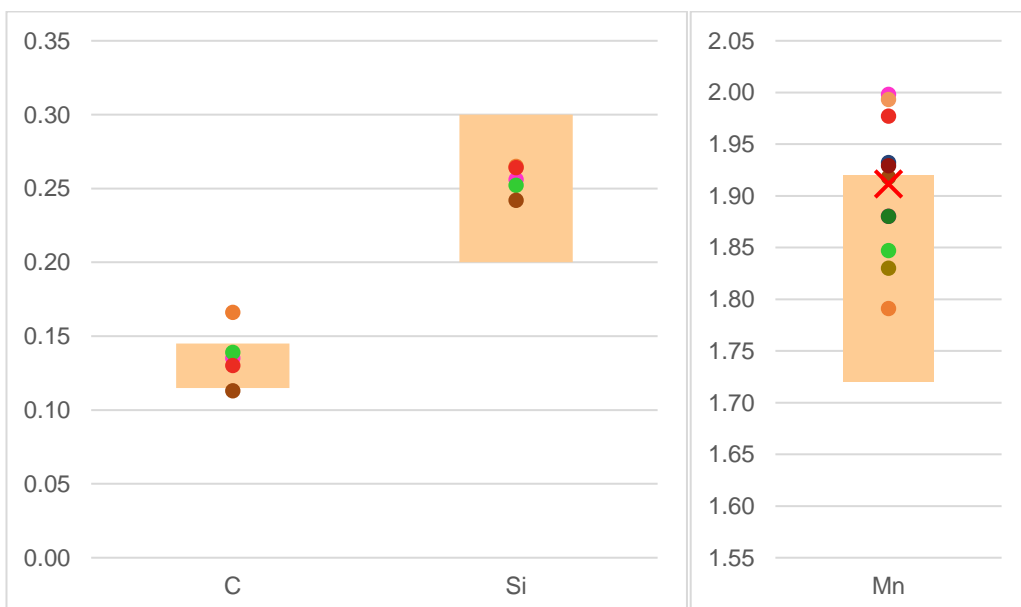
Figure 33 Compositional overview of RAP20G_DP_POW samples

4.1.3 NORMALISATION

As shown by Figure 34 below, the surface temperature of the synthetic DP800 samples was recorded over the first minute after leaving the furnace, giving an estimate of the sample cooling rate.

Cooling rate (°C/s)	
Average	11.11
Range	4.44
Standard deviation	1.12
R²	
Average	0.891
Standard deviation	0.0279
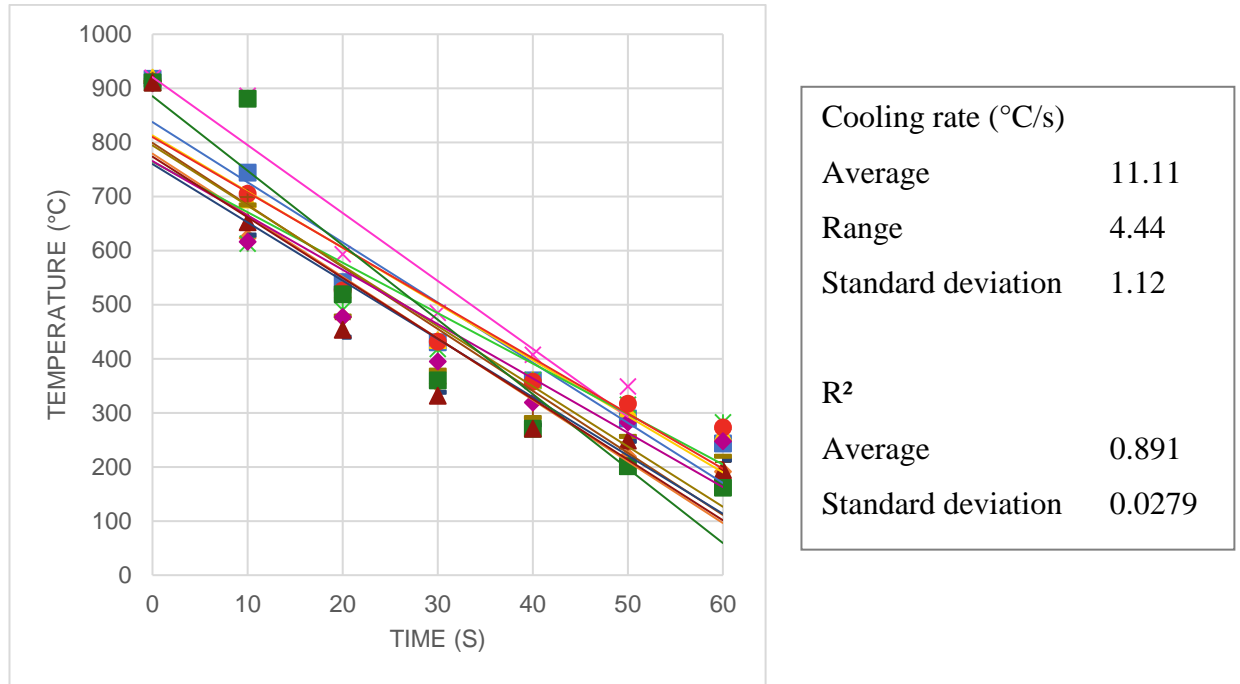
Figure 34 Temperature of RAP20G_ DP_POW samples over the first minute after removal from the furnace

Figure 34 shows a drop in temperature of the 15 samples from about 900°C to 200°C over the first minute of cooling after leaving the furnace, with an error of approximately ±100°C.

4.1.4 CORROSION

The corrosion effects of the different elements in the synthetic DP800 have seen summarised in Figure 35. It would be expected that copper, tin and nickel would all improve the corrosion resistance, as summarised in Table 2, but the results show that only the copper had a noticeable change in reactivity with the increasing residual content. The measured potential difference compared to the saturated calomel electrode constant of the samples after one hour remained very similar, mostly between

-0.5 and -0.6V for all nickel and tin samples, while the higher copper levels lead to a potential difference of -0.33 after one hour.
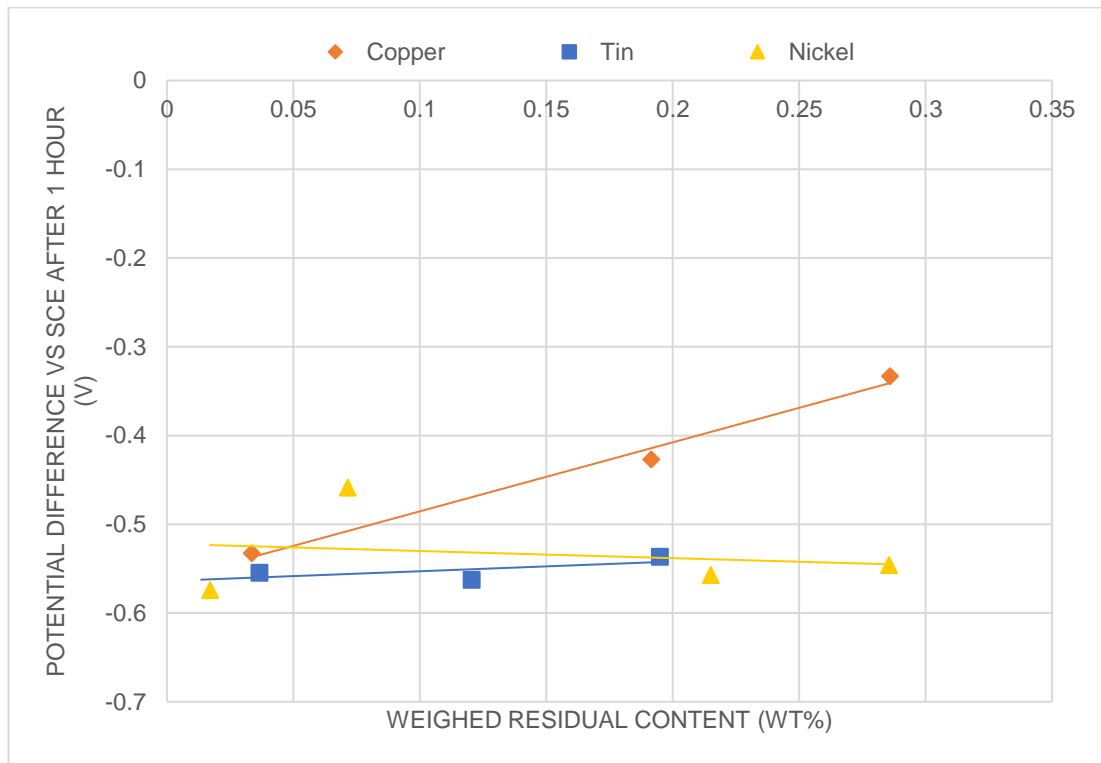
Figure 35 Corrosion results RAP20G_DP_POW samples Optical Microscopy

The microstructure of the RAP20G_ DP_POW samples is seen in the optical microscopy images in Figure 36 to Figure 41. The selected microstructures show the clearest image from the two samples with the highest and lowest residual levels for each residual element addition. The resulting microstructures appear to be mostly ferritic with a small amount of a second phase.
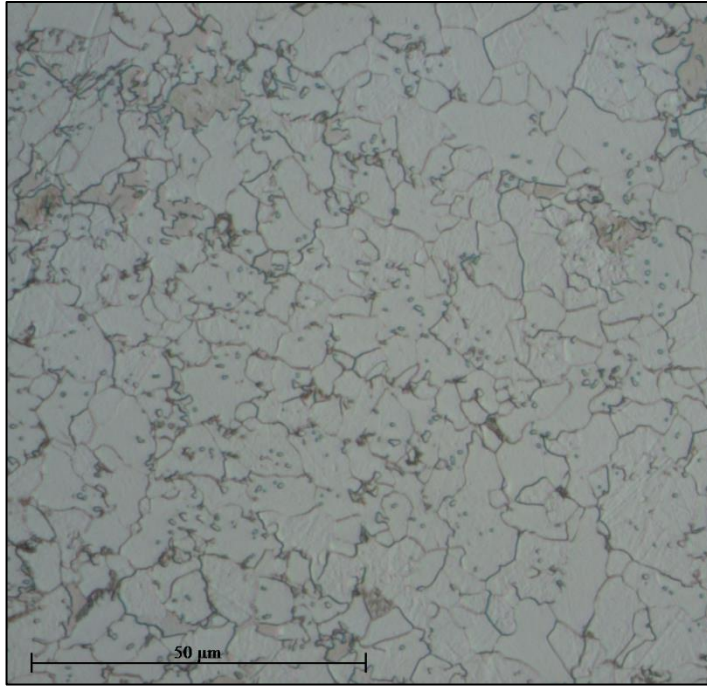
Figure 36 Optical image of RAP20G_DP_POW_CuX4
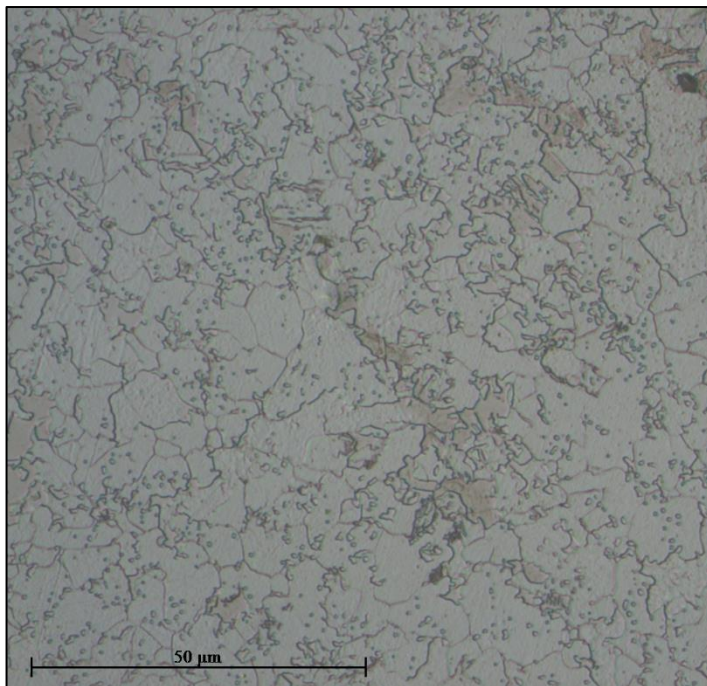
Figure 37 Optical image of RAP20G_DP_POW_CuX16
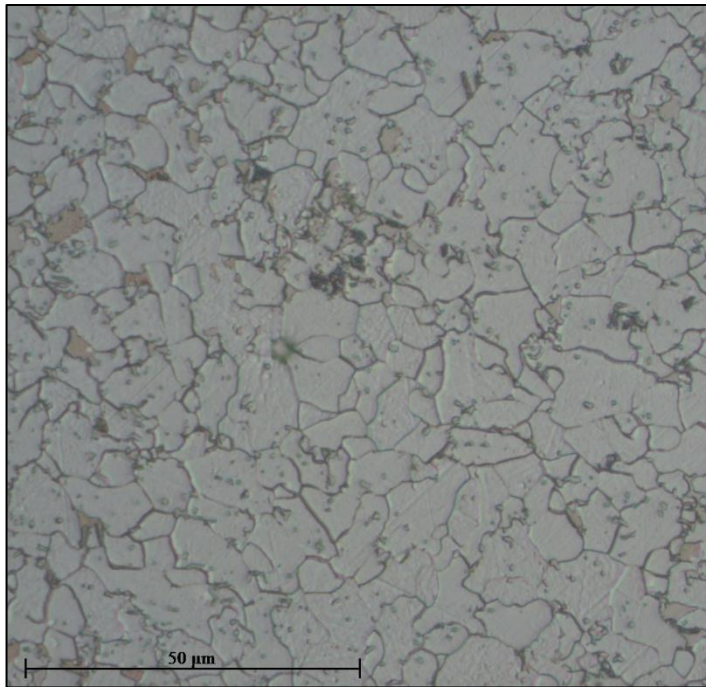
Figure 38 Optical image of RAP20G_ DP_POW_SnX4
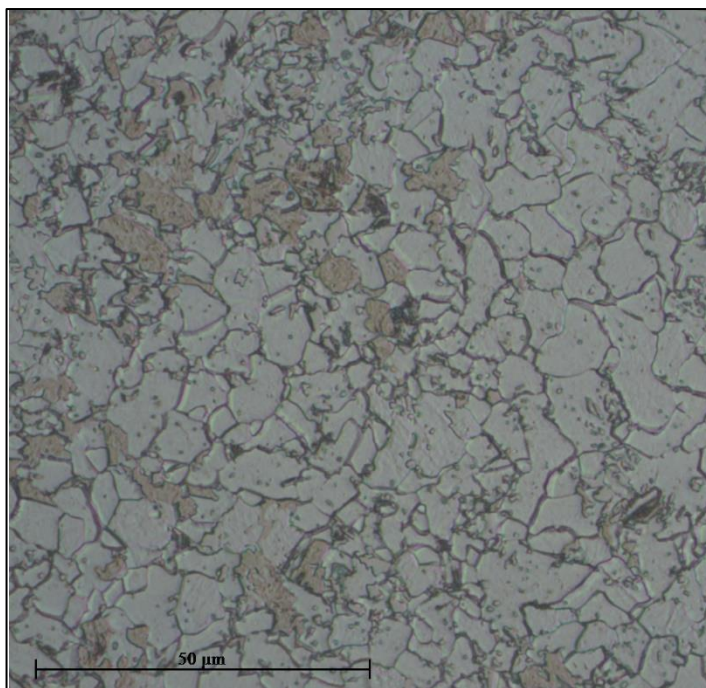
Figure 39 Optical image of RAP20G_DP_POW_SnX12
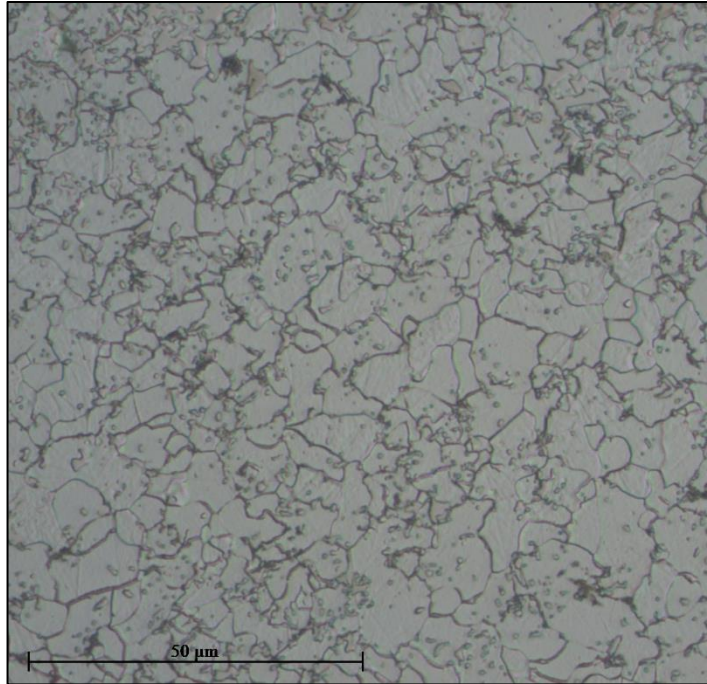
Figure 40 Optical image of RAP20G_ DP_POW_NiX1
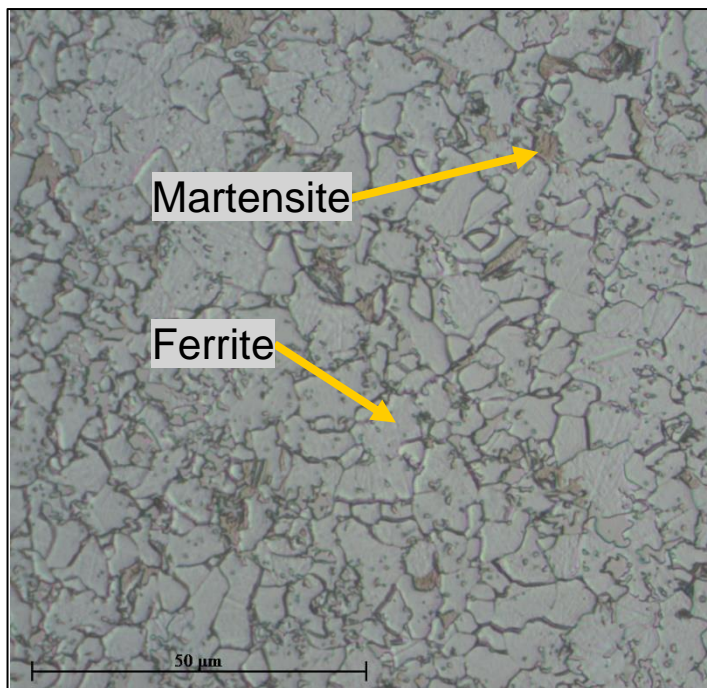
Figure 41 Optical image of RAP20G_DP_POW_NiX12 with labelled phases

Figure 36 to Figure 41 show optical microscopy images from a selection of the samples, showing what appears as a mostly ferritic microstructure with some martensitic regions, as labelled in Figure 41.
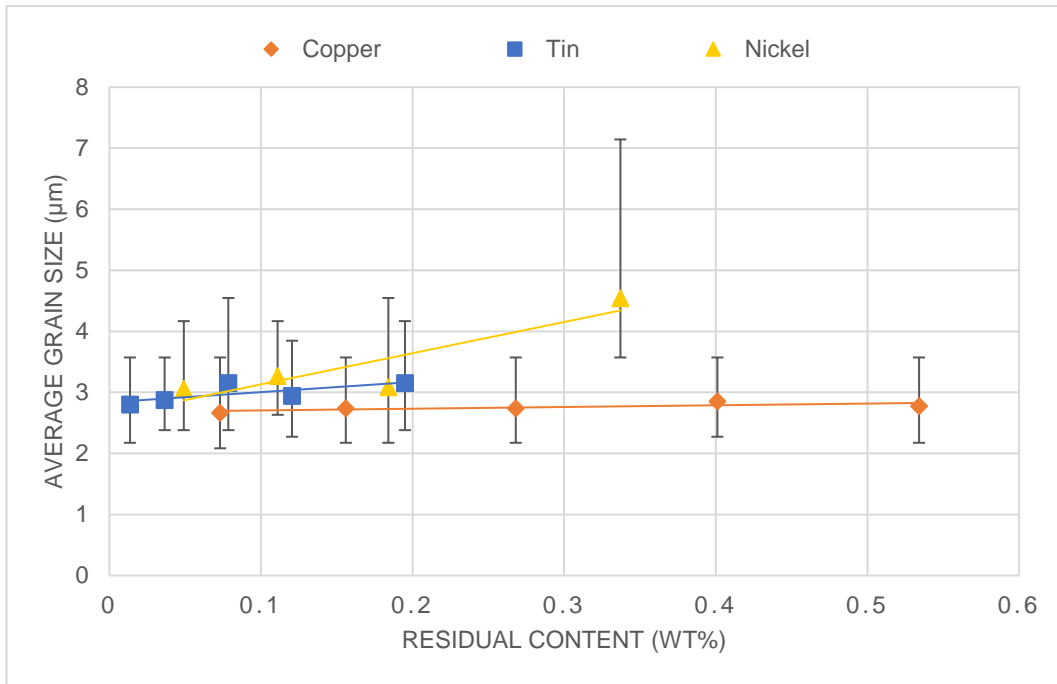
Figure 42 Average grain size for the RAP20G_DP_POW samples with residual additions with error bars showing the highest and lowest average grain size of the regions sampled

Figure 42 shows the average grain size of the different samples, where the average grain size of the samples with copper and tin additions display very little variation, remaining approximately 3µm. The sample containing 0.34wt% nickel had a measured average grain size of 4.5µm, larger than in any other sample.

4.1.5   HARDNESS
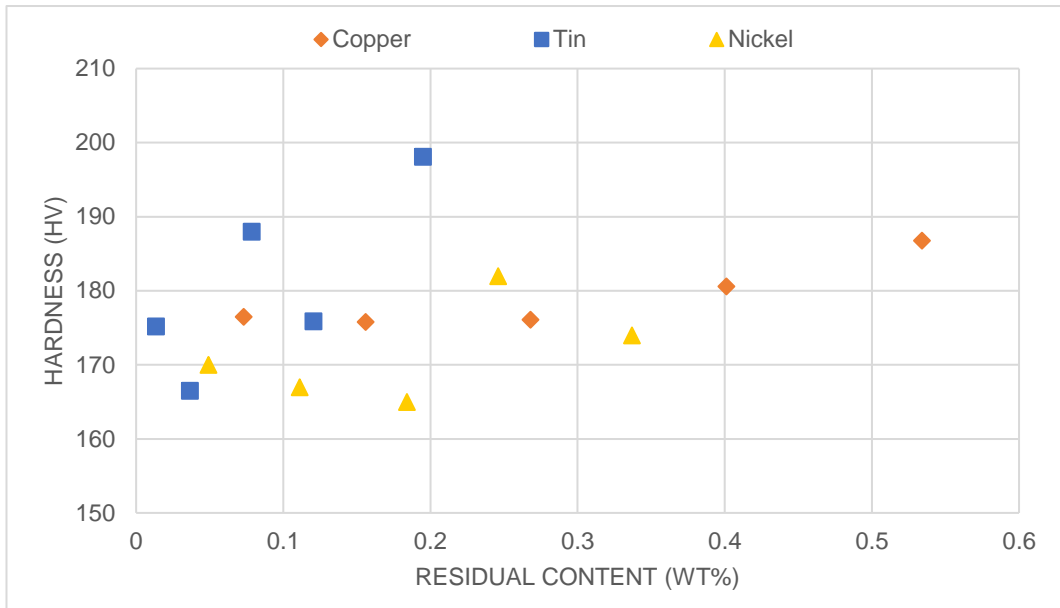
Figure 43 Harness results for the RAP20G_DP_POW samples

Figure 43 shows that all the residual elements tested increased the hardness of the steel samples, especially the samples containing increased levels of tin, but the results contained some scatter.

4.1.6 TENSILE RESULTS
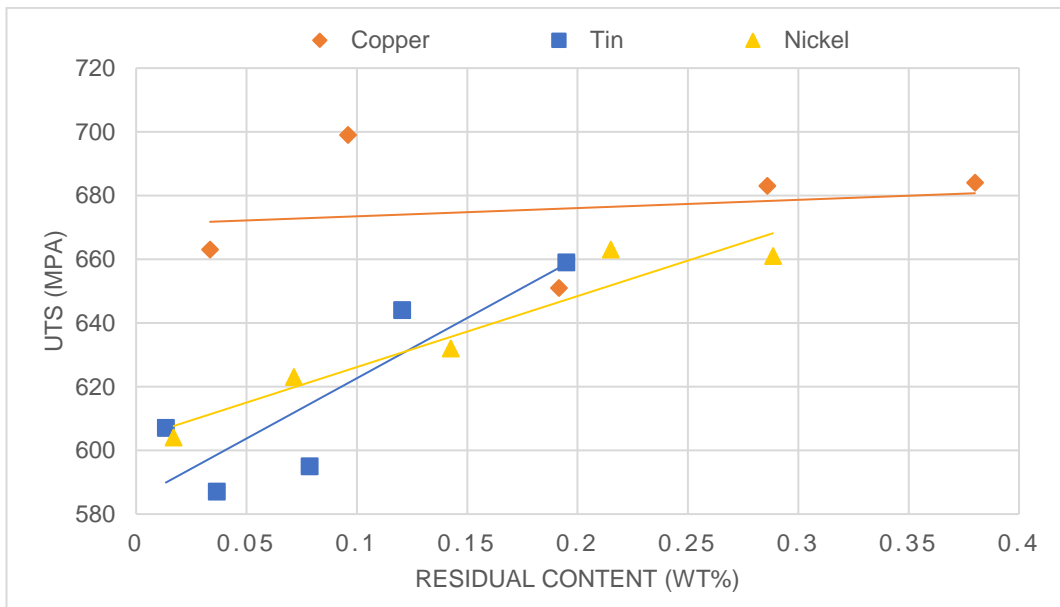
Figure 44 UTS values for the RAP20G_DP_POW samples where the trendlines have been included to show the trends that could be suggested from this data, but due to the

scatter in the results it would be advisable not to use the trendlines as proof of a
correlation
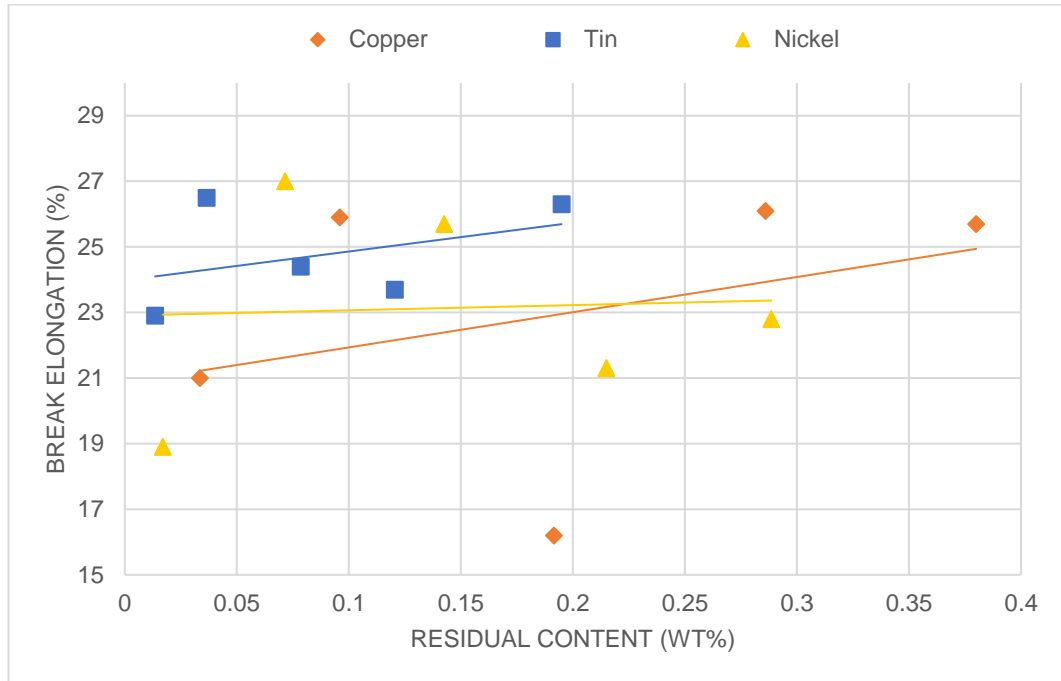
Figure 45 Break elongation values for the RAP20G_DP_POW samples where the trendlines have been included to show the trends that could be suggested from this data, but due to the scatter in the results it would be advisable not to use the trendlines as proof of a correlation

Figure 44 and Figure 45 show some of the results from the tensile tests of the samples. The scatter presented is more significant than the expected scatter between industrially produced material, which has an average UTS of 834MPa in products with a gauge between 0.8-1.4mm, and typically falls between 810 and 860MPa.

4.2 PRELIMINARY RESULTS 20G 3190

4.2.1 INTRODUCTION AND SAMPLE OVERVIEW

3190 is an intermediate steel grade that, depending on subsequent rolling and heat treatments, may be appropriate for many different customer specifications. The steel grade has a much lower level of alloying elements compared to many other grades and there are fewer heat treatments necessary to replicate the industrial equivalent. This means the effects of the residual elements may be much clearer and easier to see due to the lack of other potential variables between the samples, be those variations in

composition, or differences in the rolling stage of the samples, especially as hot rolling is not necessary; cold rolling followed by a heat treatment is enough.

4.2.1.1 METHOD SUMMARY (DP800 20G POWDER ROUTE)

The existing RAP20G route was used to make synthetic DP800 with additions of copper, tin, and nickel, as described in 3.2 and summarised below and in Figure 46.

- 20g sample size
- Gravity cast
- Powder feedstock
- One tensile bar per sample
- Cold rolled to an 80% reduction (approximately 6mm to 1.2mm)
- Normalised at 900°C for 2 minutes
- OES testing challenging due to small sample size
- Testing included tensile, corrosion, hardness and microscopy

This method provided a good basis for the initial tests and understanding of the process and being able to begin looking at and improving the way samples are made. The small sample size made it challenging to do an OES test to check the composition. Where OES tests were possible, only four sparks could be made due to the small sample size, and due to the lack of measurement of tin in the available OES, the samples with additions of tin were assumed to have a composition equivalent to that of the proportions of each element weighed out to input into the samples.

The positioning of the crucible and the mould meant that when the sample was cast, the flow of the metal had a directionality along the sample, replicating part of the industrial process. The glove box used to melt the samples contained an argon atmosphere with an oxygen level typically below 100ppm, meaning minimal oxygen made its way into the sample.

Figure 46 Overview of RAP20G route

The 3190 samples produced using this method are summarised below in Table 17, where the notation used describe the total levels of the residual elements is described as multiples of the current limit.

Table 17 Initial 20g 3190 samples which did not include a control

Sample Ref	Alloy	Route	Feedstock (Powder or solid)	Elements added
RAP20G_3190_POW_CuX1	3190	20G	Powder	Fe (Bal), C, Mn and Si + residual Cu
RAP20G_3190_POW_CuX4	3190	20G	Powder	Fe (Bal), C, Mn and Si + residual Cu
RAP20G_3190_POW_CuX8	3190	20G	Powder	Fe (Bal), C, Mn and Si + residual Cu
RAP20G_3190_POW_CuX12	3190	20G	Powder	Fe (Bal), C, Mn and Si + residual Cu
RAP20G_3190_POW_CuX16	3190	20G	Powder	Fe (Bal), C, Mn and Si + residual Cu
RAP20G_ 3190_POW_SnX1	3190	20G	Powder	Fe (Bal), C, Mn and Si + residual Sn
RAP20G_ 3190_POW_SnX4	3190	20G	Powder	Fe (Bal), C, Mn and Si + residual Sn
RAP20G_ 3190_POW_SnX8	3190	20G	Powder	Fe (Bal), C, Mn and Si + residual Sn
RAP20G_3190_POW_SnX12	3190	20G	Powder	Fe (Bal), C, Mn and Si + residual Sn

RAP20G_3190_POW_SnX16	3190	20G	Powder	Fe (Bal), C, Mn and Si + residual Sn
RAP20G_ 3190_POW_NiX1	3190	20G	Powder	Fe (Bal), C, Mn and Si + residual Ni
RAP20G_ 3190_POW_NiX4	3190	20G	Powder	Fe (Bal), C, Mn and Si + residual Ni
RAP20G_ 3190_POW_NiX8	3190	20G	Powder	Fe (Bal), C, Mn and Si + residual Ni
RAP20G_3190_POW_NiX12	3190	20G	Powder	Fe (Bal), C, Mn and Si + residual Ni
RAP20G_3190_POW_NiX16	3190	20G	Powder	Fe (Bal), C, Mn and Si + residual Ni
RAP20G_ 3190_POW_CrX1	3190	20G	Powder	Fe (Bal), C, Mn and Si + residual Cr
RAP20G_ 3190_POW_CrX4	3190	20G	Powder	Fe (Bal), C, Mn and Si + residual Cr
RAP20G_ 3190_POW_CrX8	3190	20G	Powder	Fe (Bal), C, Mn and Si + residual Cr
RAP20G_3190_POW_CrX12	3190	20G	Powder	Fe (Bal), C, Mn and Si + residual Cr
RAP20G_3190_POW_CrX16	3190	20G	Powder	Fe (Bal), C, Mn and Si + residual Cr
RAP20G_ 3190_POW_MoX1	3190	20G	Powder	Fe (Bal), C, Mn and Si + residual Mo
RAP20G_ 3190_POW_MoX4	3190	20G	Powder	Fe (Bal), C, Mn and Si + residual Mo
RAP20G_ 3190_POW_MoX8	3190	20G	Powder	Fe (Bal), C, Mn and Si + residual Mo
RAP20G_3190_POW_MoX12	3190	20G	Powder	Fe (Bal), C, Mn and Si + residual Mo
RAP20G_3190_POW_MoX16	3190	20G	Powder	Fe (Bal), C, Mn and Si + residual Mo

4.2.2 COMPOSITION

The 20g powder approach to the low alloy 3190 steel investigated five different levels (1X, 4X, 8X, 12X, 16X) which are multiplications of the current residual limit set by Tata of five different common residual elements (Cu, Ni, Sn, Cr, Mo).   The compositions of these samples is shown in Table 18.

Table 18 Composition of the RAP20G_3190_POW samples measured using different methods, all samples were measured with an OES, except those with Sn additions were calculated by weighed element levels

	FE	C	MN	SI	RESIDUAL
RAP20G_3190_POW_CUX1	99.52	0.005	0.204	0.01	0.08
RAP20G_3190_POW_CUX4	99.36	0.008	0.218	0.013	0.203

RAP20G_3190_POW_CUX8	99.21	0.0088	0.214	0.011	0.361
RAP20G_3190_POW_CUX12	99.19	0.005	0.078	0.01	0.522
RAP20G_3190_POW_CUX16	99.01	0.005	0.132	0.011	0.655
RAP20G_ 3190_POW_SNX1	99.7790	0.0420	0.1650	0.0040	0.0100
RAP20G_ 3190_POW_SNX4	99.7475	0.0420	0.1650	0.0040	0.0415
RAP20G_ 3190_POW_SNX8	99.7080	0.0422	0.1658	0.0040	0.0800
RAP20G_3190_POW_SNX12	99.6670	0.0421	0.1654	0.0040	0.1215
RAP20G_3190_POW_SNX16	99.6280	0.0422	0.1658	0.0040	0.1600
RAP20G_ 3190_POW_NIX1	99.57	0.005	0.156	0.01	0.048
RAP20G_ 3190_POW_NIX4	99.5	0.005	0.159	0.01	0.116
RAP20G_ 3190_POW_NIX8	99.41	0.005	0.144	0.01	0.219
RAP20G_3190_POW_NIX12	99.33	0.005	0.134	0.01	0.322
RAP20G_3190_POW_NIX16	99.28	0.005	0.121	0.01	0.399
RAP20G_ 3190_POW_CRX1	99.58	0.005	0.127	0.01	0.058
RAP20G_ 3190_POW_CRX4	99.55	0.005	0.122	0.01	0.098
RAP20G_ 3190_POW_CRX8	99.41	0.005	0.147	0.01	0.21
RAP20G_3190_POW_CRX12	99.32	0.005	0.148	0.01	0.305
RAP20G_3190_POW_CRX16	99.24	0.005	0.149	0.01	0.382
RAP20G_ 3190_POW_MOX1	99.61	0.005	0.152	0.01	0.0165
RAP20G_ 3190_POW_MOX4	99.57	0.005	0.178	0.01	0.027
RAP20G_ 3190_POW_MOX8	99.6	0.005	0.168	0.01	0.019
RAP20G_3190_POW_MOX12	99.59	0.005	0.153	0.01	0.039
RAP20G_3190_POW_MOX16	99.57	0.005	0.161	0.01	0.048
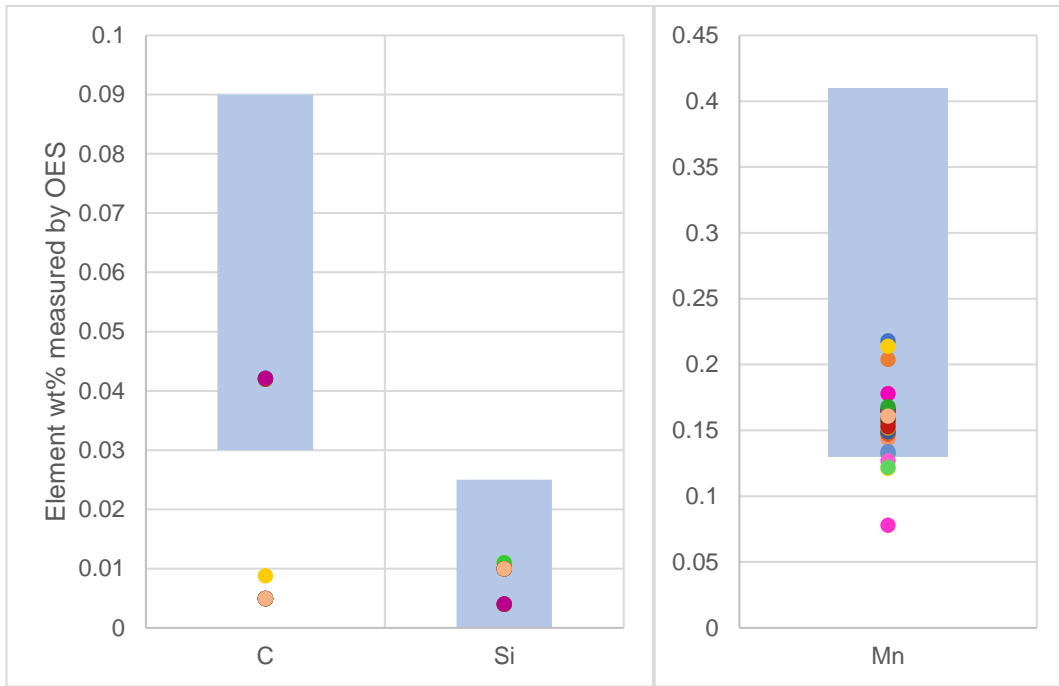
Figure 47 Compositional overview of RAP20G_3190_POW samples

4.2.3 NORMALISATION

The sample temperature was monitored throughout the whole normalisation process and it was found that each sample had similar cooling rates as shown by Figure 48. The average cooling rate over the first minute after removing the sample from the furnace for the 3190 batches was 8.5 °C/s.
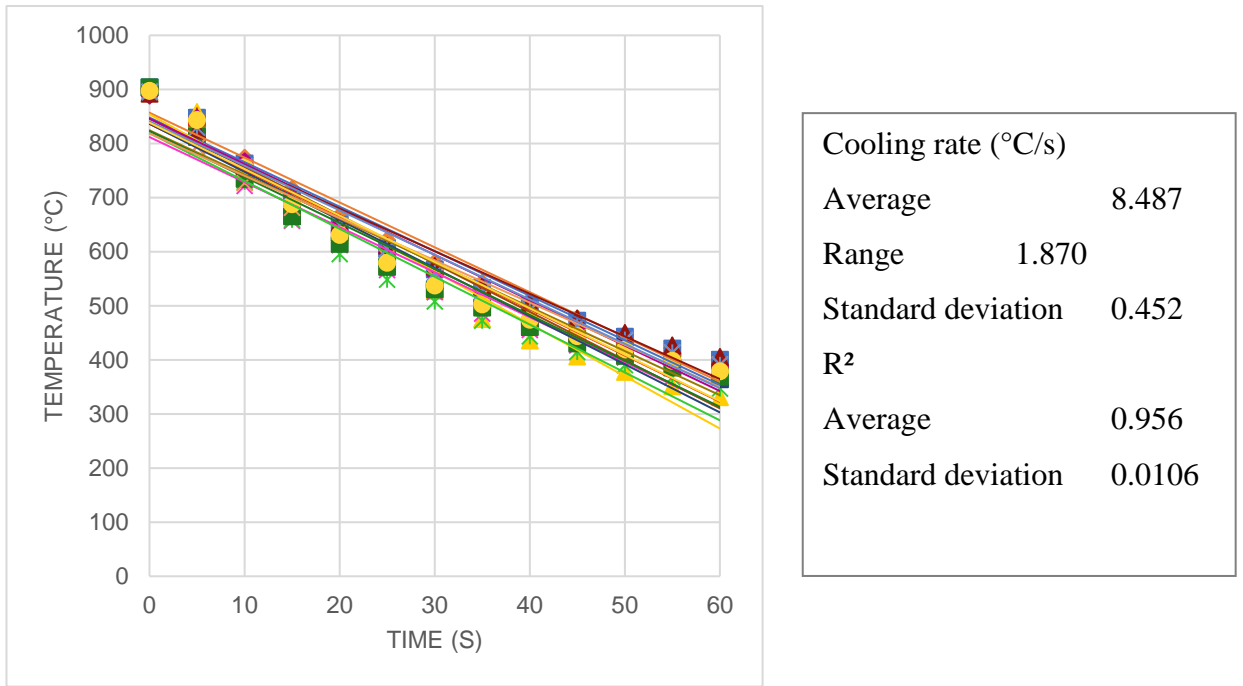
Figure 48 Temperature of RAP20G_3190_POW samples over the first minute after removal from the furnace

Figure 48 shows a drop in temperature of the 25 samples from about 850°C to 350°C over the first minute of cooling after leaving the furnace, with an error of approximately ±50°C.

4.2.4   CORROSION

Figure 49 shows the corrosion measurements for the RAP20G_3190_POW samples as measured using an open circuit potential setup.
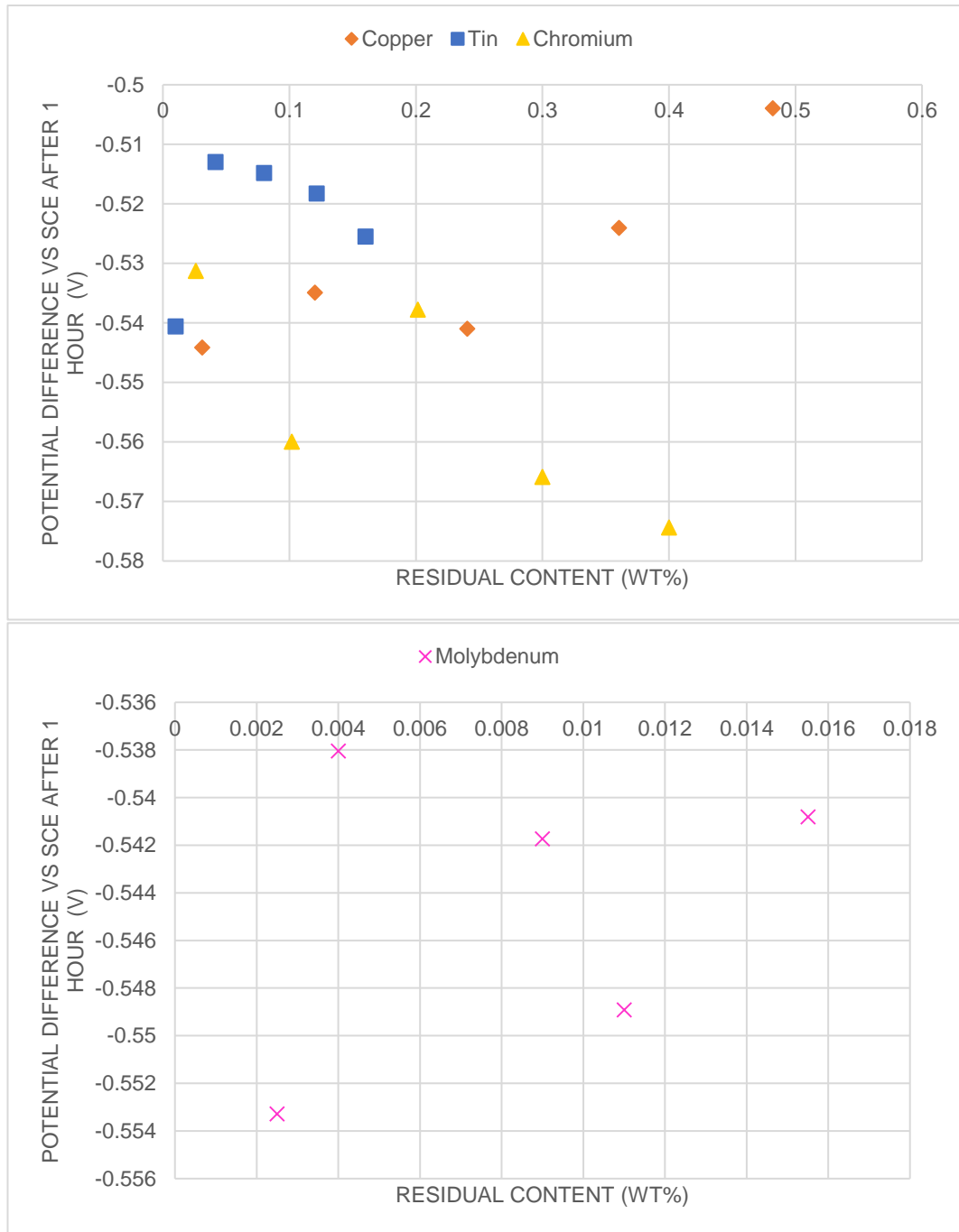
Figure 49 Corrosion results for the RAP20G_3190_POW samples (Mo results presented on a separate graph for clarity due to low residual content)

Figure 49 shows the potential difference when compared to a saturated calomel electrode, showing the results contain a lot of scatter with all residual additions. The amount of scatter in the results means a change in potential difference cannot be quantified for the molybdenum and tin. It can be seen that the lowest to highest copper

additions show a potential difference change from approximately -0.544 to -0.504, whereas the lowest to highest chromium levels show a potential difference change from approximately -0.531 to -0.574.

4.2.5 HARDNESS
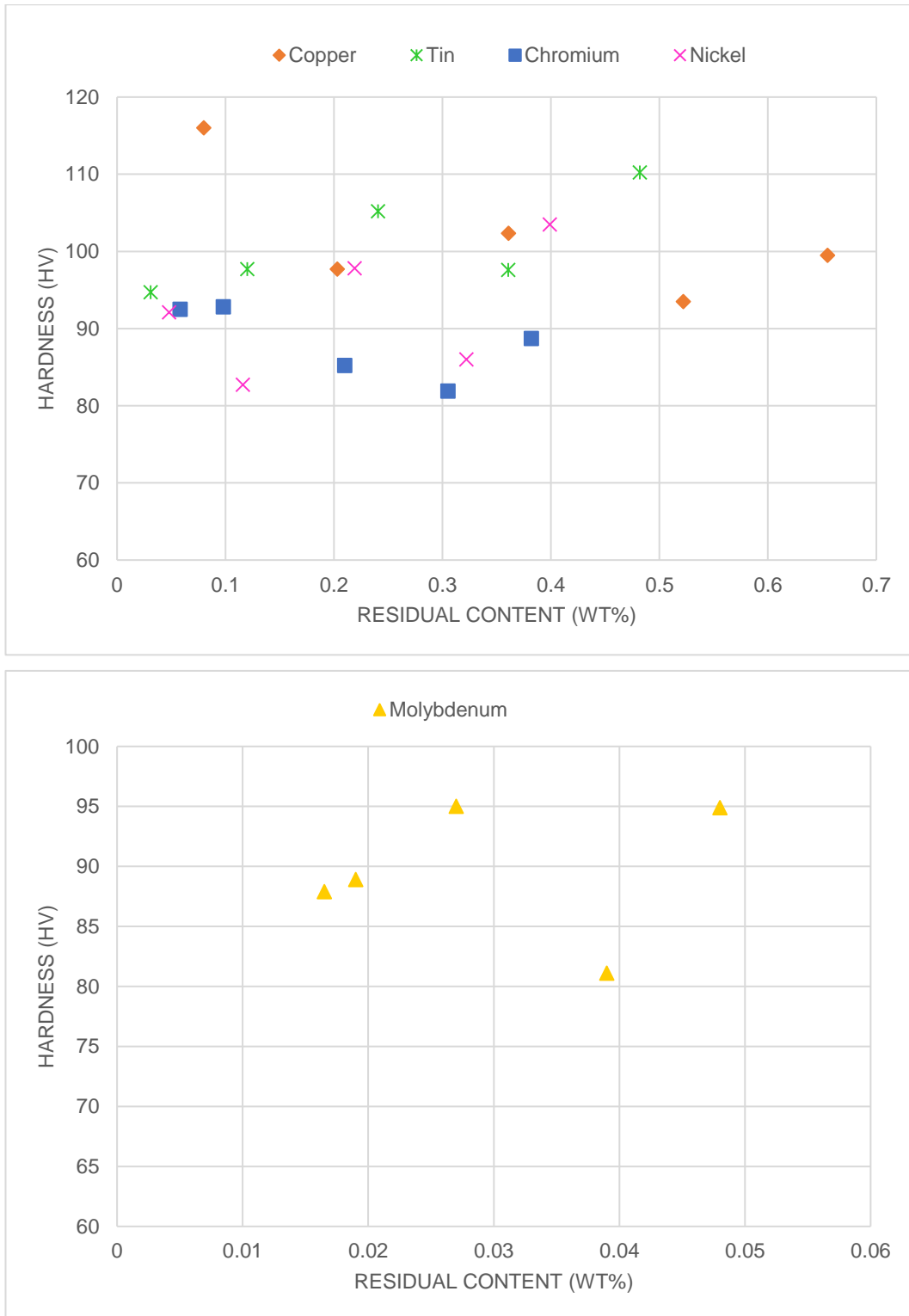
Figure 50 Harness results for the RAP20G_3190_POW samples compared against the residual content as measured by an OES, with the exception of tin which was calculated

based on the wt% of powder added to the mix (Mo results presented on a separate graph for clarity due to low residual content)

The hardness values for the RAP20G_3190_POW samples are shown in Figure 50. The data contains a lot of scatter, making it hard to identify a correlation.

4.2.6 OPTICAL MICROSCOPY

The microstructures of some of the samples is shown in Figure 51 to Figure 60.
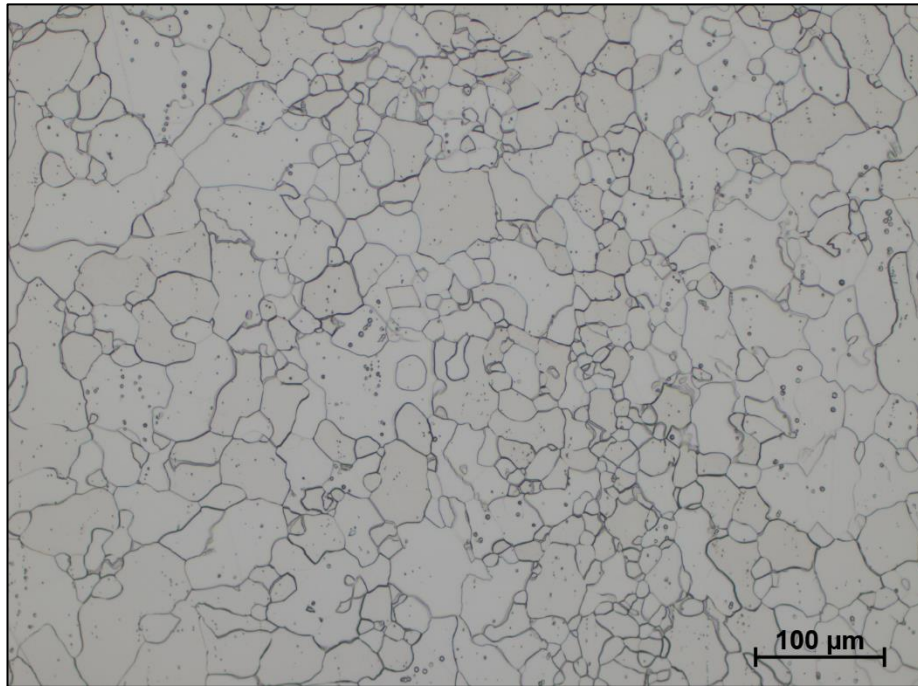
Figure 51 Optical image of RAP20G_3190_POW_CuX1
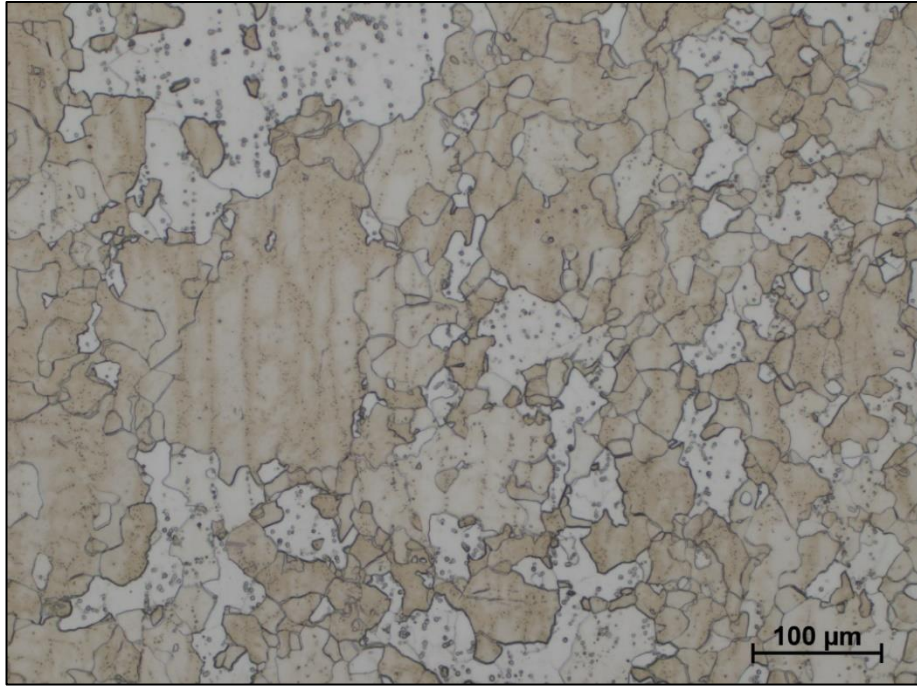
Figure 52 Optical image of RAP20G_3190_POW_CuX16
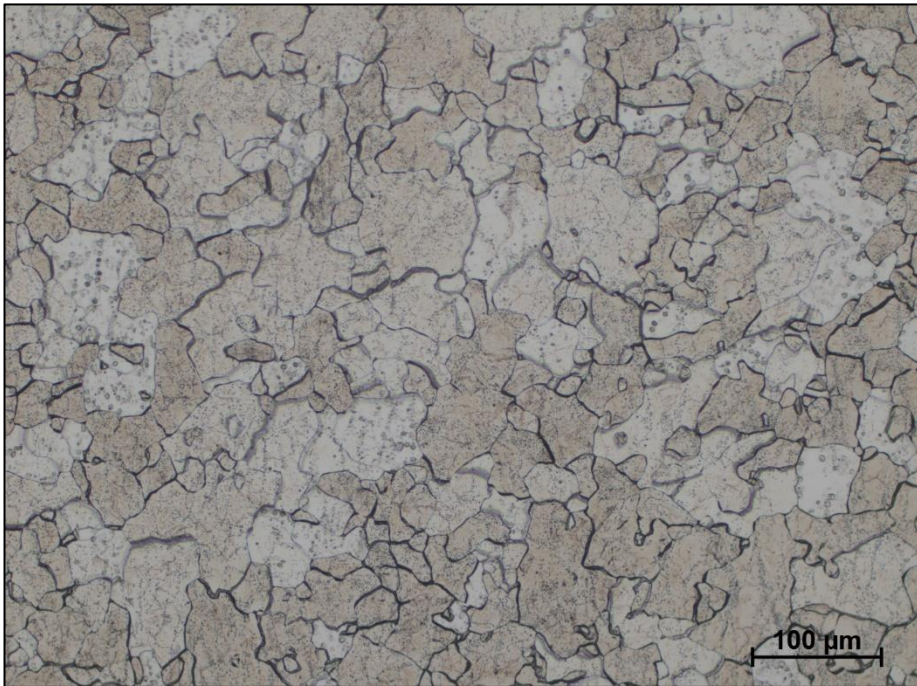
Figure 53 Optical image of RAP20G_ 3190_POW_SnX1
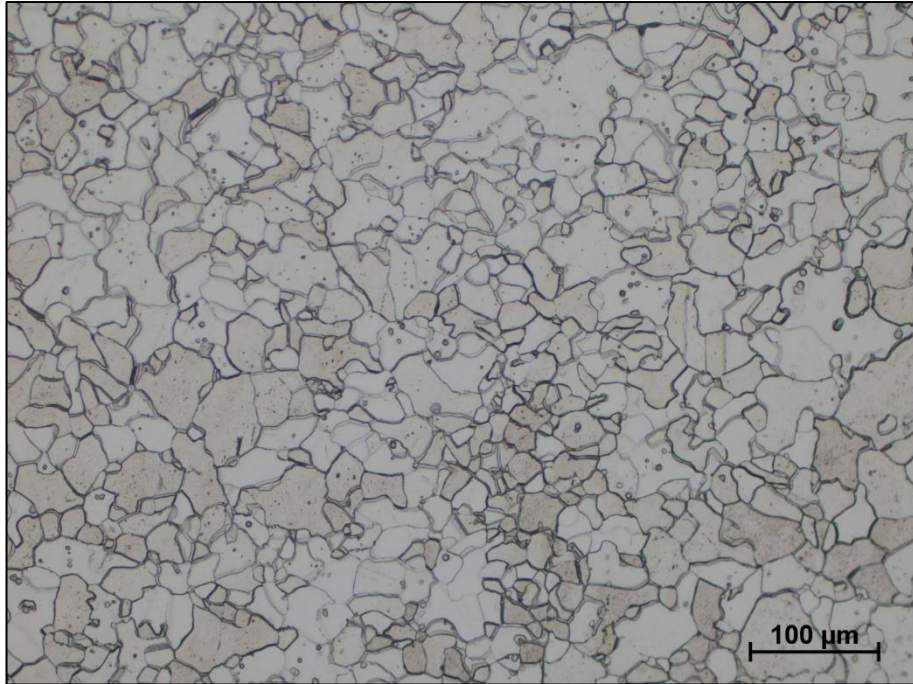
Figure 54 Optical image of RAP20G_3190_POW_SnX16
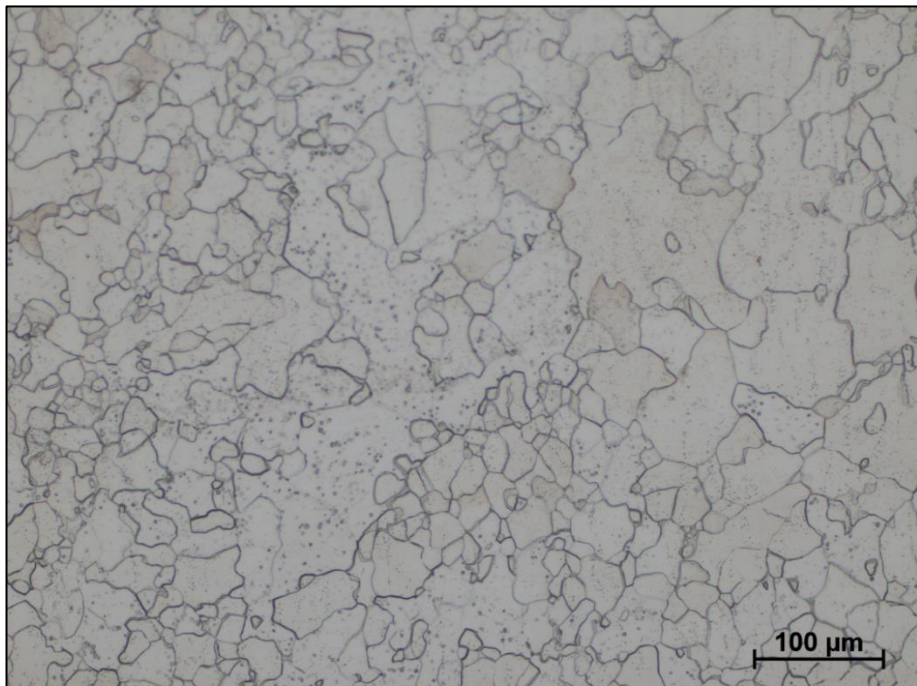
Figure 55 Optical image of RAP20G_ 3190_POW_CrX1
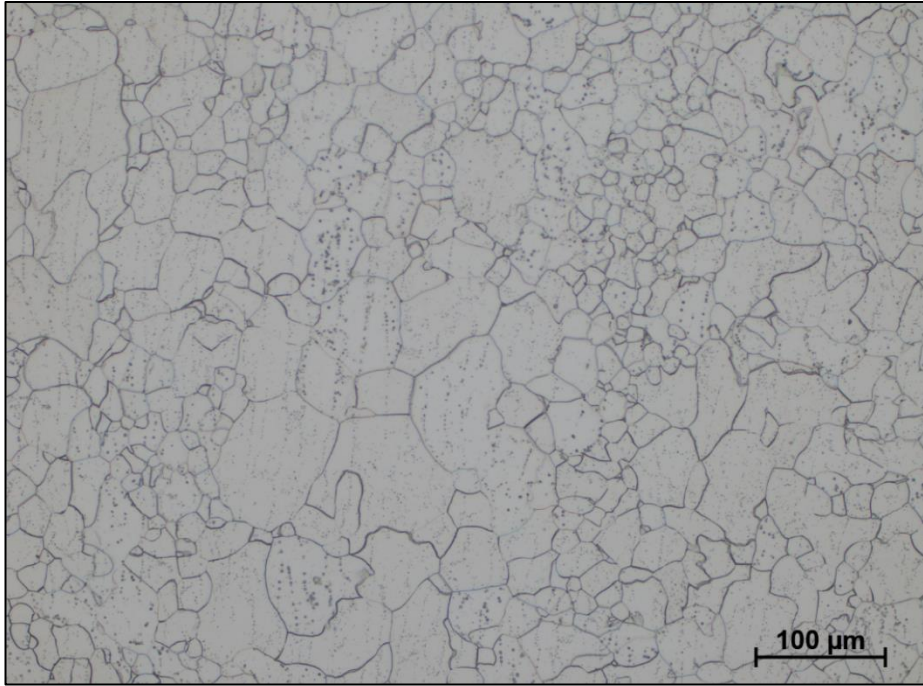
Figure 56 Optical image of RAP20G_3190_POW_CrX16
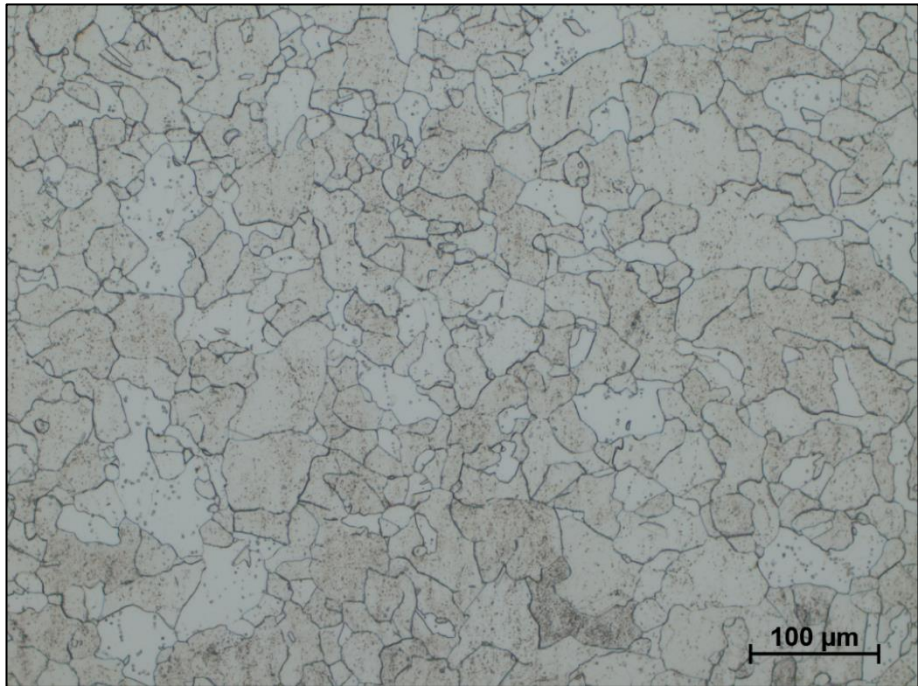
Figure 57 Optical image of RAP20G_ 3190_POW_MoX1
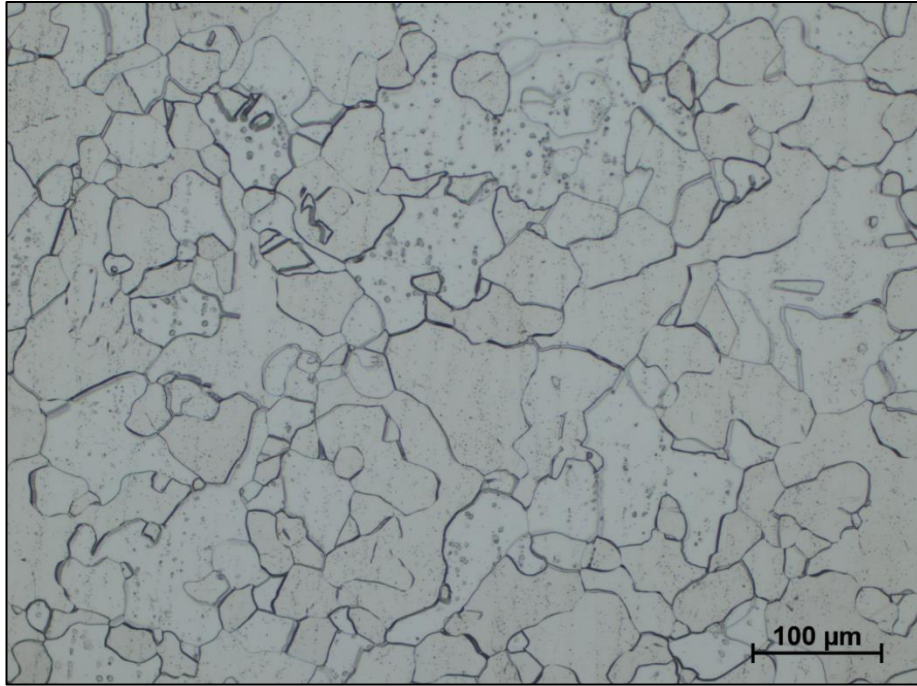
Figure 58 Optical image of RAP20G_ 3190_POW_MoX16
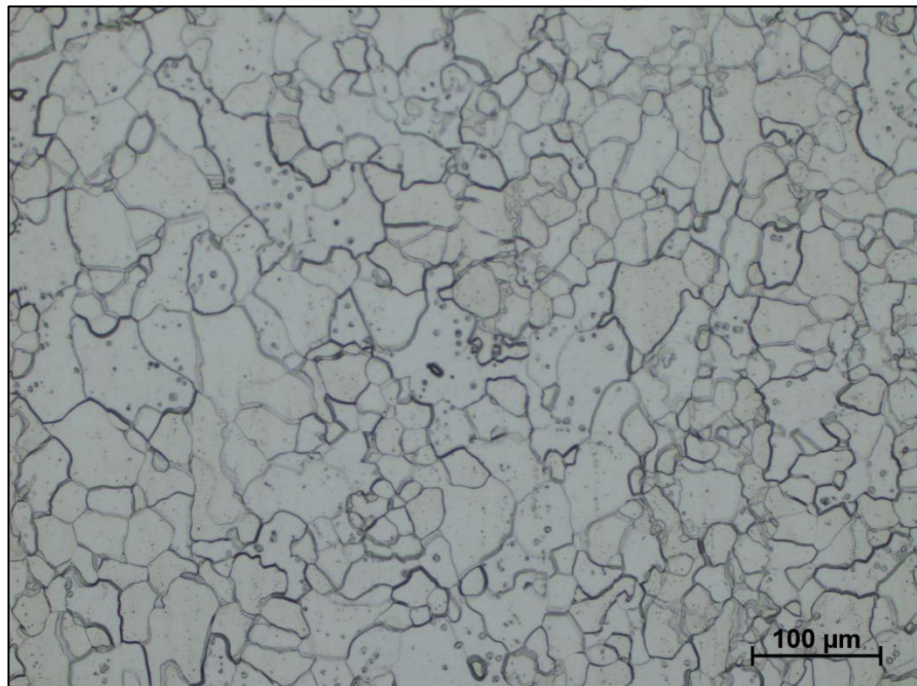
Figure 59 Optical image of RAP20G_ 3190_POW_NiX1
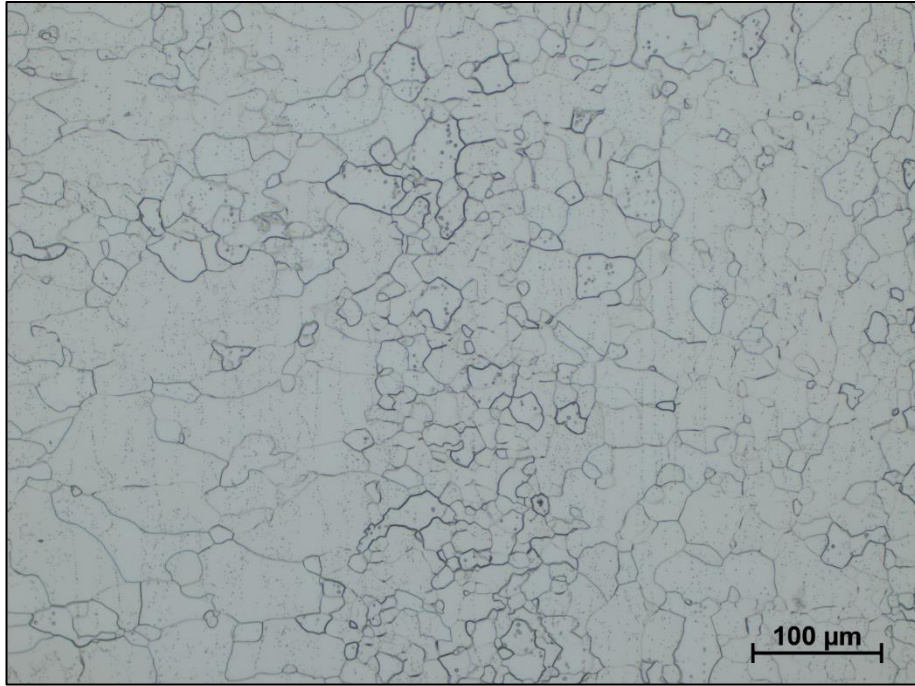
Figure 60 Optical image of RAP20G_ 3190_POW_NiX16

Figure 51 to Figure 60 show the microstructures of some of the samples, showing that the samples have fully ferritic microstructures at all residual levels.
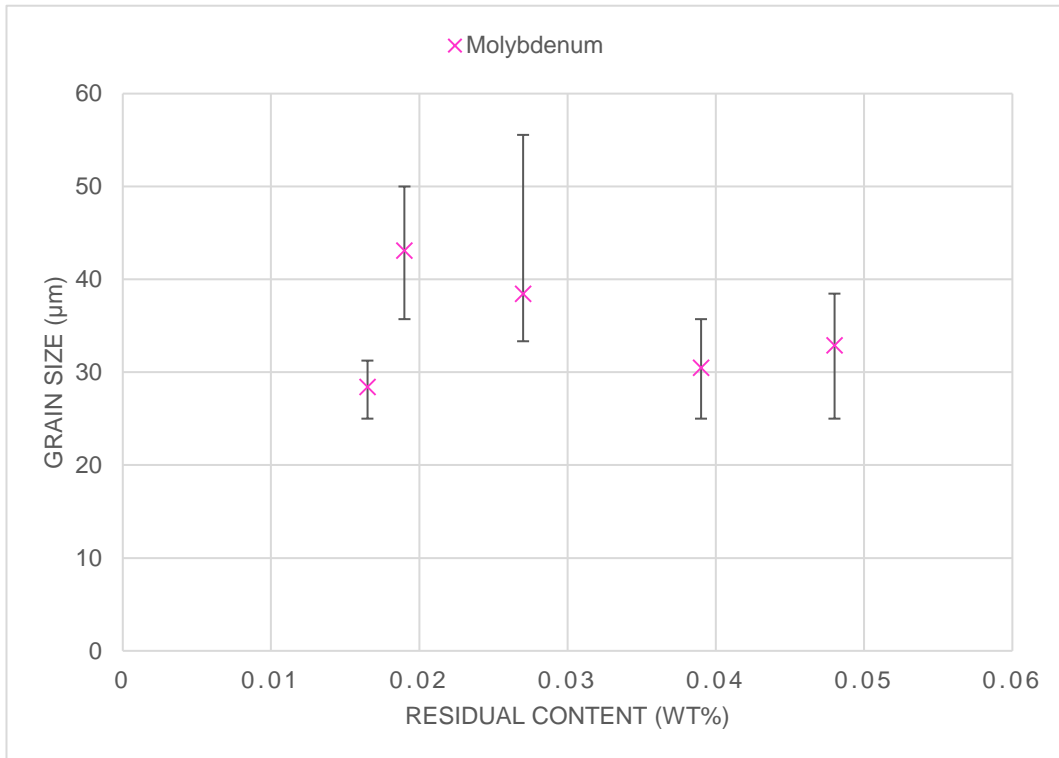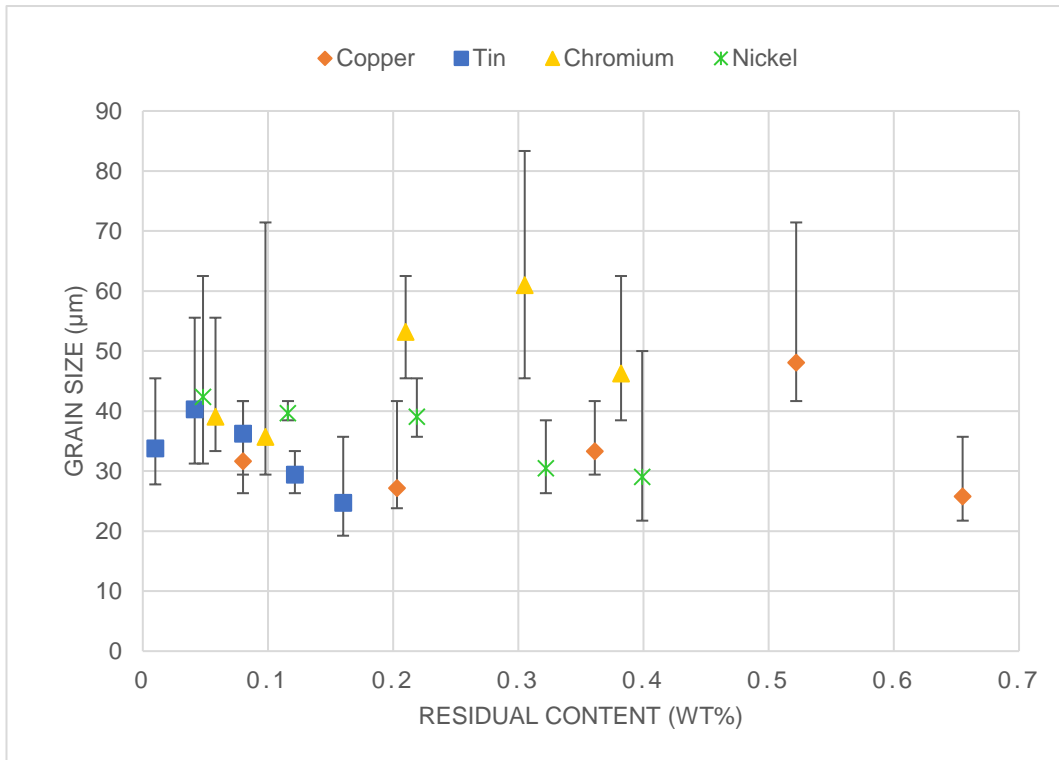
Figure 61 Grain sizes of RAP20G_ 3190_POW samples

Figure 61 shows the average grain sizes of the samples, showing the grain size generally has a range over 15µm within each sample. There is little change in the average grain size between the extremes of the element additions.

4.2.7 TENSILE
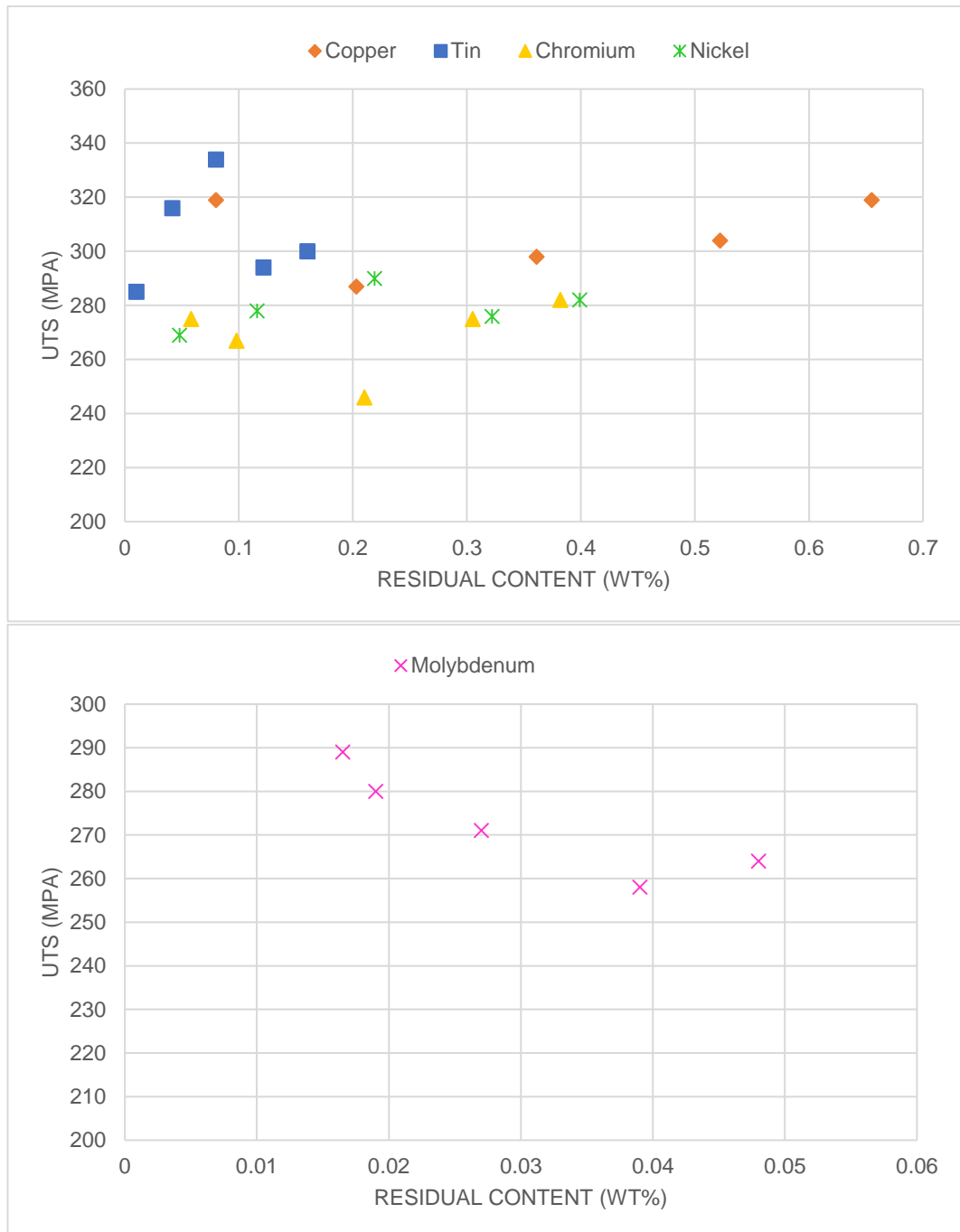
Figure 62 UTS values for the RAP20G_ 3190_POW samples (Mo results presented on a separate graph for clarity due to low residual content)

Figure 62 shows the UTS results from the RAP20G_ 3190_POW samples. The samples with increasing levels of molybdenum suggests a softening effect, with a UTS decreasing from 290MPa to 265MPa. The other residual element additions do not show a noticeable impact to the UTS values.
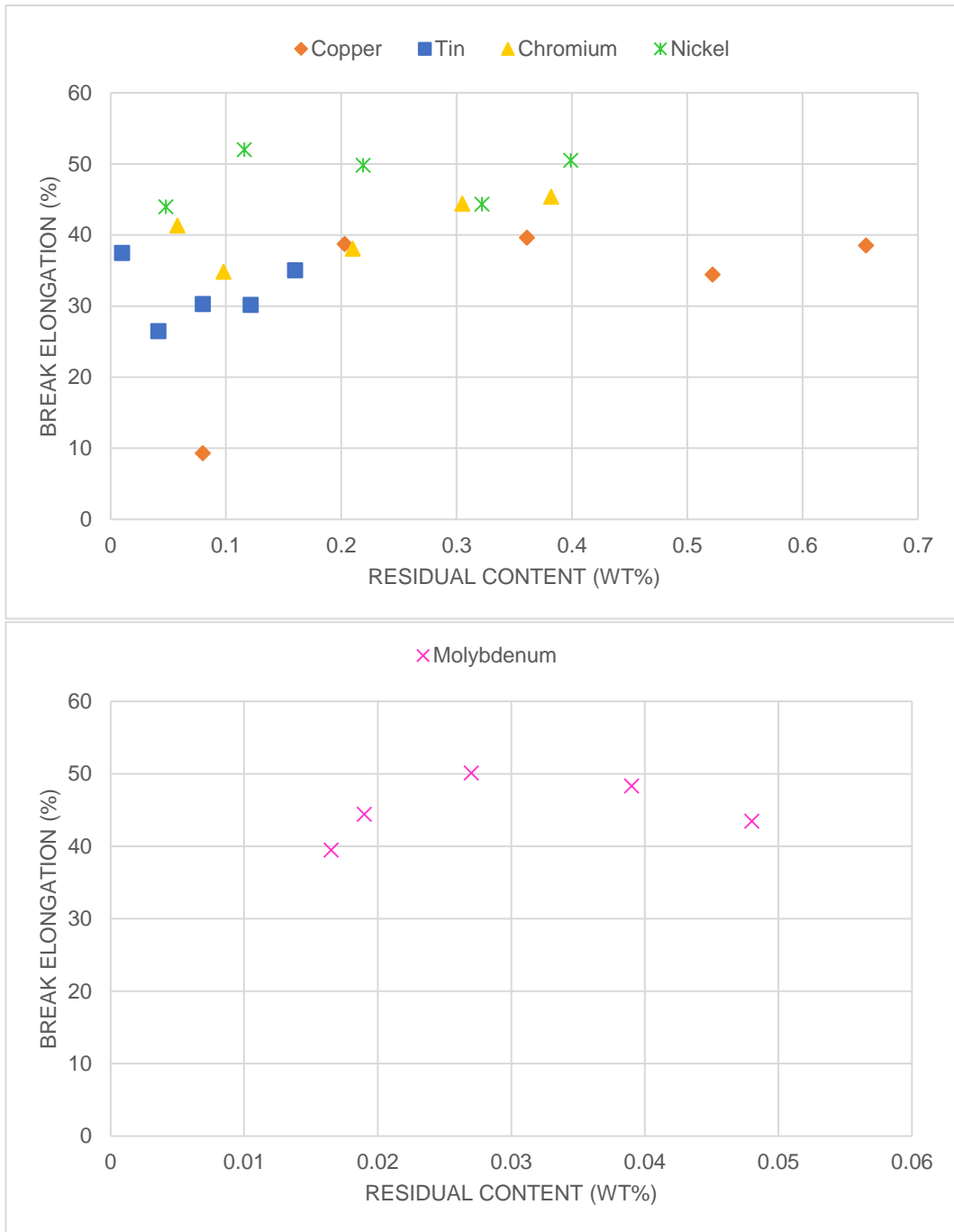
Figure 63 Break elongation values for the RAP20G_ 3190_POW samples (Mo results presented on a separate graph for clarity due to low residual content)

Figure 63 shows the break elongation results from the RAP20G_ 3190_POW samples. The increasing residual element additions do not show a noticeable impact to the break elongation values.

4.2.8   XRD
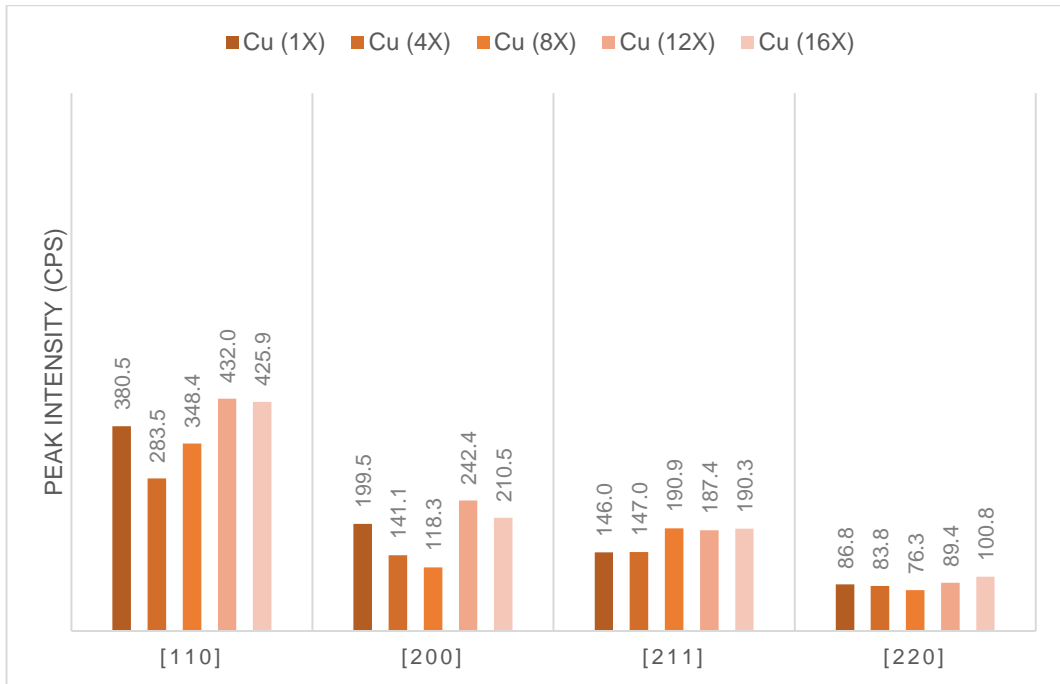
Figure 64 The intensity of XRD peaks representing different crystal structures in RAP20G_3190_POW_Cu samples
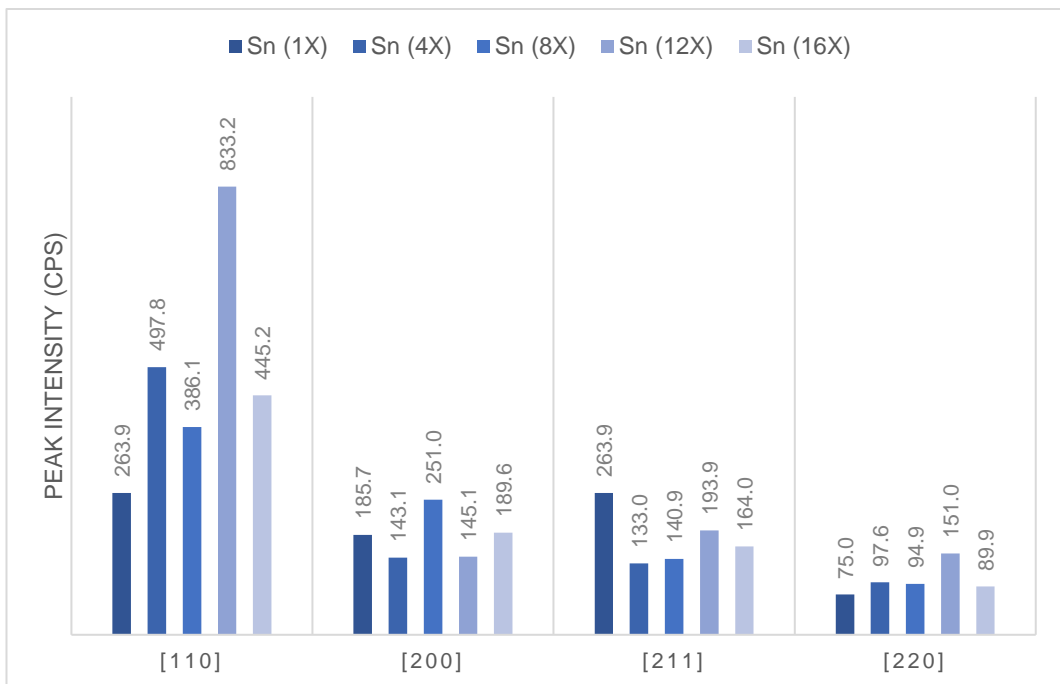
Figure 65 The intensity of XRD peaks representing different crystal structures in RAP20G_3190_POW_Sn samples
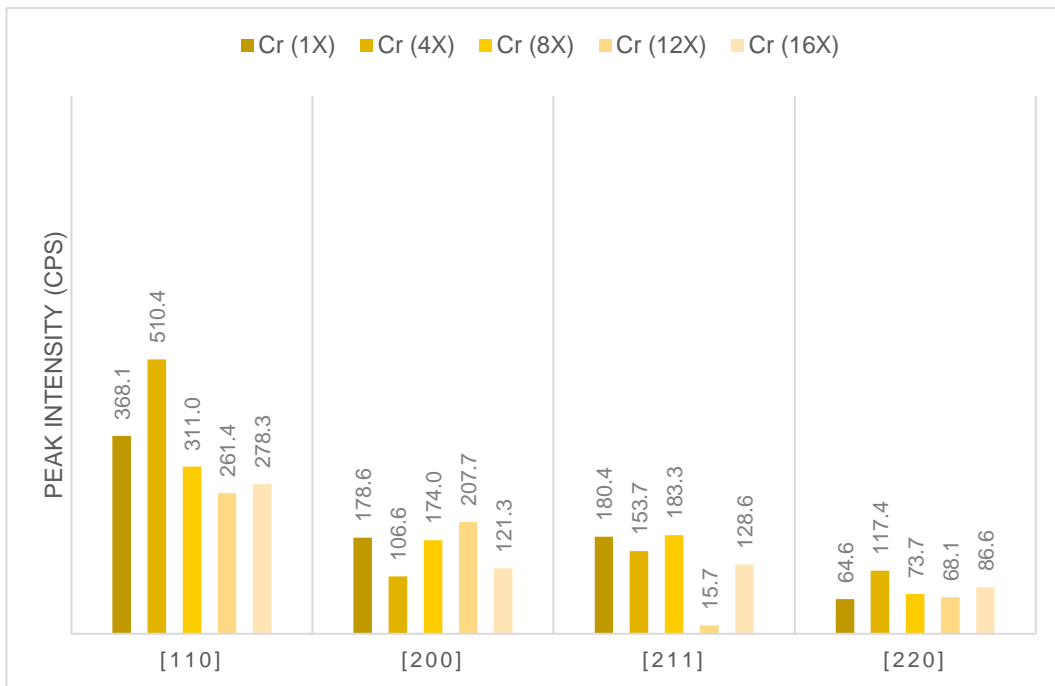
Figure 66 The intensity of XRD peaks representing different crystal structures in RAP20G_3190_POW_Cr samples
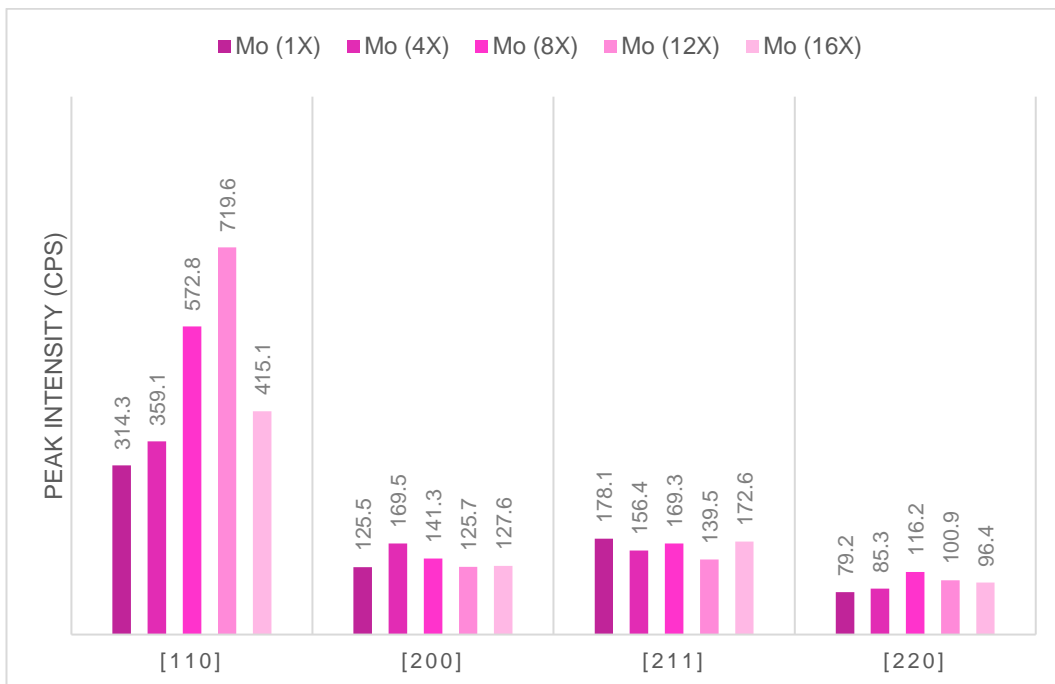
Figure 67 The intensity of XRD peaks representing different crystal structures in RAP20G_3190_POW_Mo samples
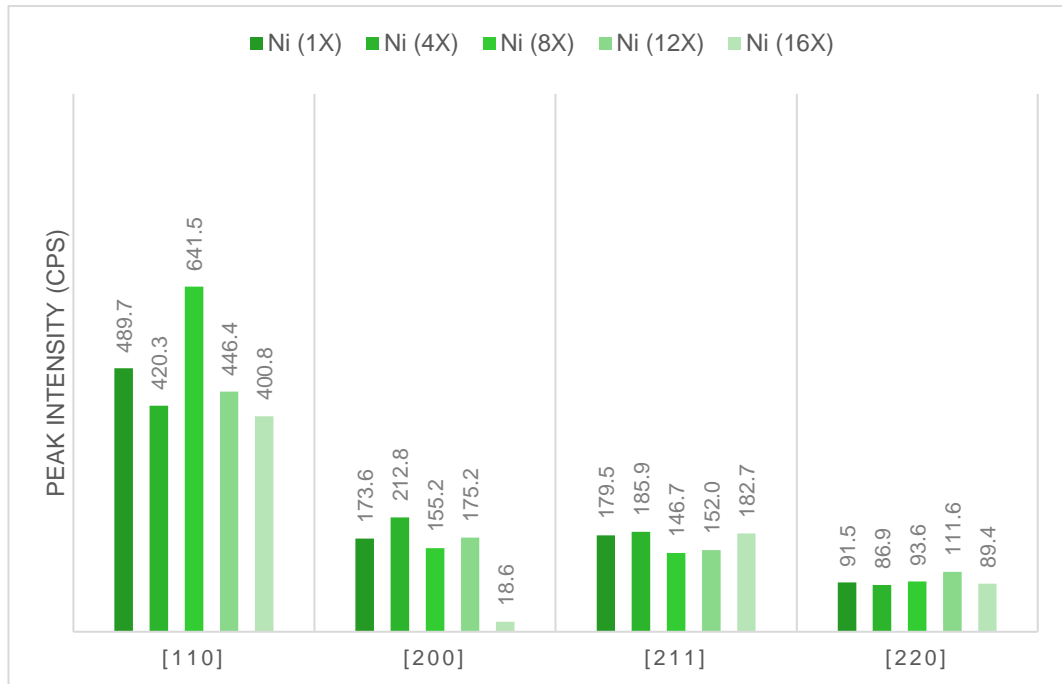
Figure 68 The intensity of XRD peaks representing different crystal structures in RAP20G_3190_POW_Ni samples

The XRD graphs shown in Figure 64 to Figure 68 demonstrate the phase distribution of the samples with different residual elements and levels. Only the tin and molybdenum samples showed a correlation of the orientation of the internal structure, with the intensity of the [110] direction increasing with higher levels of these elements. The other elements did not show a correlation.

4.3   SUMMARY OF EVALUATION OF EXISTING ROUTES

The initial results followed a previously established 20g powder route to produce an array of samples of both DP800 grade and 3190 grade with residual additions that included copper, tin, nickel, molybdenum, and chromium. The samples were cold rolled and heat treated to produce one strip of steel per composition, from which a singular tensile bar was able to be produced and some tensile and hardness testing, and some microscopy work could be completed. This resulted in a series of results with no sample repeats and a lot of scatter in the results to the extent that it was decided that a different approach that allowed multiple test specimens to be produced from each cast was a priority.

CHAPTER 5   IMPROVED RAP ROUTES

5.1   RESULTS (140G) 3190

5.1.1   INTRODUCTION AND SAMPLE OVERVIEW 3190 140G REMELT ROUTE

In response to the 20g samples being too small to produce more than one tensile bar per cast, and due to a centrifugal caster becoming available, a potential route was investigated with a sample size of 140g, initially of 3190 material, producing more material and allowing test repeats from each cast. Remelted industrial material was used with the aim of improving the compositional consistency, summarised below and in Figure 69.

5.1.1.1   METHOD SUMMARY (3190 140G REMELT ROUTE)

- 140g sample size
- Centrifugally cast
- Solid feedstock (remelted industrial material)
- 3 tensile bars per sample
- Hot rolling possible
- Samples large enough for easy OES testing

Remelted industrial steel was melted with solid lumps of residual elements added to the crucible. The 140g route used the centrifugal caster to produce a larger sample from which, more material was produced for various tests. The use of industrially produced steel as the base feedstock made the sample production quicker due to there being far less weighing out to do, and the combination of all elements already in the industrial feedstock removes the probability of human error when weighing out alloying element additions. This feedstock also includes all micro-alloying elements necessary, removing the need to simplify the composition to minimise variations between samples.
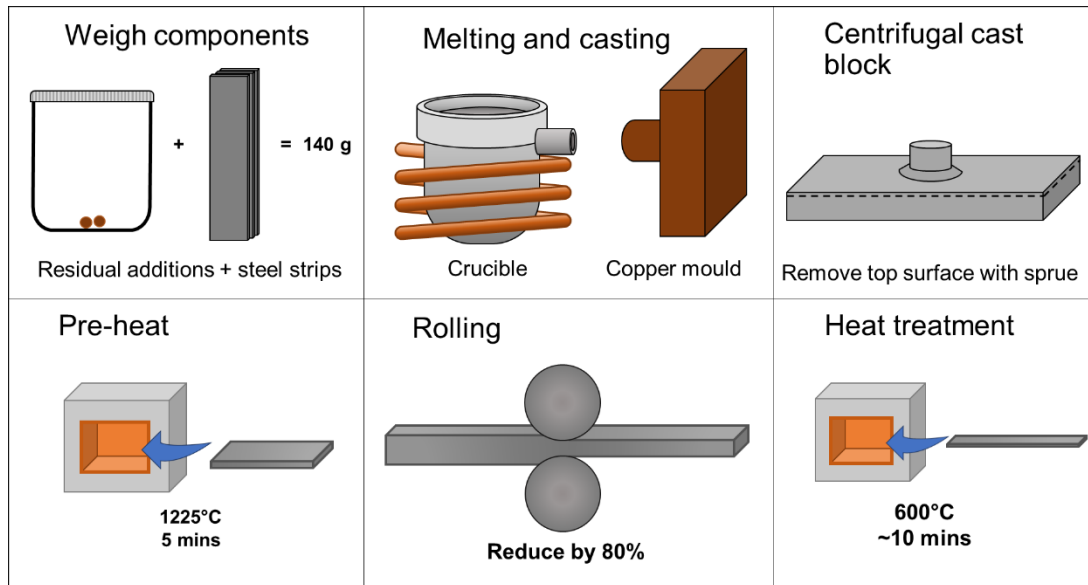
Figure 69 Overview of RAP140G _CF_RM method

The samples made using remelted industrial material are listed below in Table 19. The total levels of the residual elements is described as multiples of the current industrial limit.

Table 19 Centrifugally cast 3190 from remleted material, where
RAP140G_3190_CF__RM RF is a control sample

Sample Ref	Alloy	Route	Feedstock (Powder or solid)	Elements added
RAP140G_ 3190_CF__RM RF	3190	140G	Solid	Remelted industrial strip
RAP140G_ 3190_CF__RM CuX1	3190	140G	Solid	Remelted industrial strip + residual Cu
RAP140G_ 3190_CF__RM CuX4	3190	140G	Solid	Remelted industrial strip + residual Cu
RAP140G_ 3190_CF__RM CuX8	3190	140G	Solid	Remelted industrial strip + residual Cu
RAP140G_ 3190_CF__RM CuX12	3190	140G	Solid	Remelted industrial strip + residual Cu
RAP140G_ 3190_CF__RM CuX16	3190	140G	Solid	Remelted industrial strip + residual Cu
RAP140G_ 3190_CF_RM_CrX1	3190	140G	Solid	Remelted industrial strip + residual Cr
RAP140G_ 3190_CF_ RM_CrX4	3190	140G	Solid	Remelted industrial strip + residual Cr
RAP140G_ 3190_CF_ RM_CrX8	3190	140G	Solid	Remelted industrial strip + residual Cr
RAP140G_ 3190_CF_ RM_CrX12	3190	140G	Solid	Remelted industrial strip + residual Cr

RAP140G_ 3190_CF_ RM_CrX16	3190	140G	Solid	Remelted industrial strip + residual Cr

5.1.2 COMPOSITION

Table 20 shows the composition of several casts made from remelting industrial steel with additions of copper and chromium. The other elements in the samples stay mostly within the acceptable range of the element in an industrial version of the steel and the residual element increase in a linear manner as more of each element was added as is shown by Figure 70 and Figure 71.

Table 20 Composition of centrifugally cast 3190 made from remelted industrial steel

	Fe (wt%)	C (wt%)	Mn (wt%)	Si (wt%)	Cu/Cr (wt%)
Pre-melt composition	99.63	0.019	0.152	0.017	0.0081
RAP140G_3190_CF__ RM RF	99.55	0.02	0.194	0.0048	0.017
RAP140G_3190_CF__ RM CuX1	99.65	0.016	0.113	0.022	0.042
RAP140G_3190_CF__ RM CuX4	99.54	0.03	0.111	0.018	0.148
RAP140G_3190_CF__ RM CuX8	99.35	0.036	0.123	0.022	0.312
RAP140G_3190_CF__ RM CuX12	99.22	0.023	0.128	0.021	0.457
RAP140G_3190_CF__ RM CuX16	99.09	0.012	0.101	0.018	0.62
RAP140G_3190_CF_ RM_CrX1	99.68	0.0093	0.117	0.021	0.054
RAP140G_ 3190_CF_ RM_CrX4	99.66	0.011	0.118	0.018	0.082
RAP140G_3190_CF_ RM_CrX8	99.62	0.0088	0.116	0.017	0.13
RAP140G_3190_CF_ RM_CrX12	99.52	0.016	0.126	0.022	0.203
RAP140G_3190_CF_ RM_CrX16	99.47	0.01	0.12	0.019	0.266
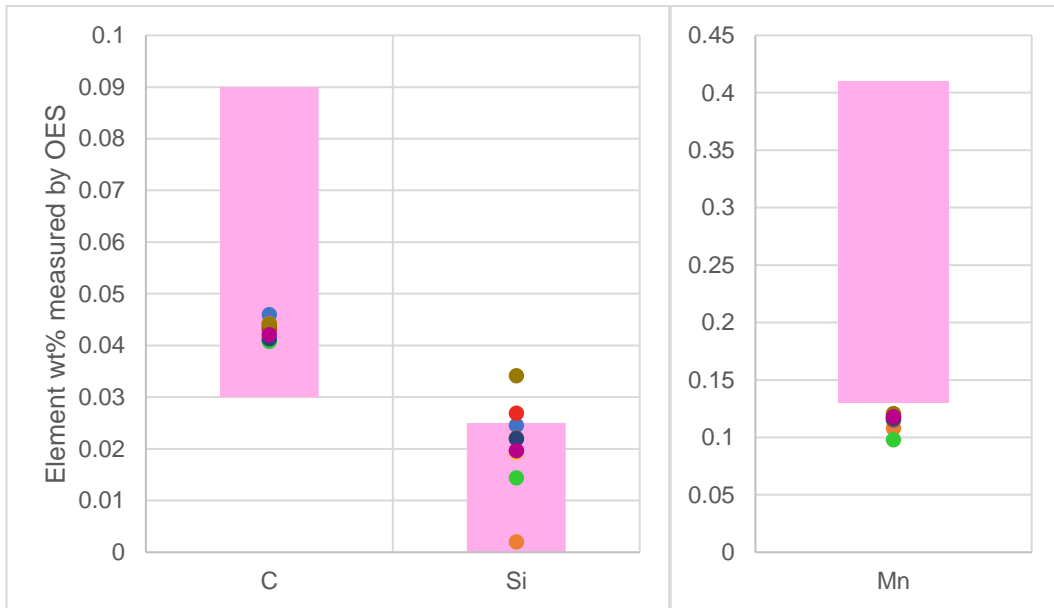
Figure 70 Compositional overview RAP140G_3190_CF samples
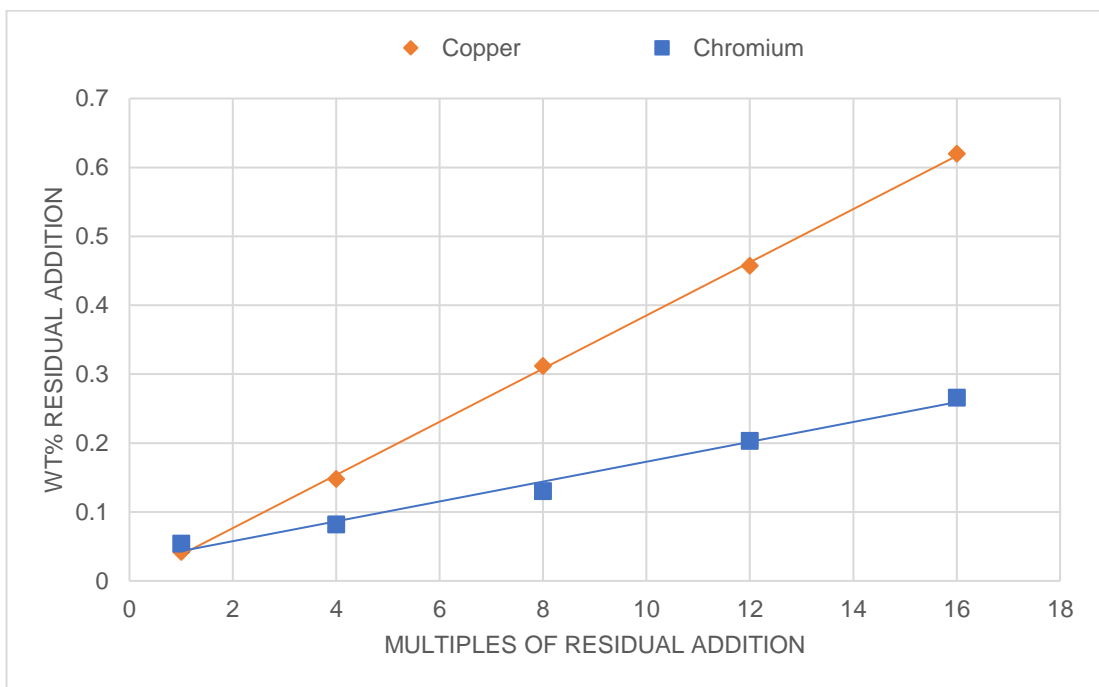
Figure 71 Residual variations within RAP140G_3190_CF__RM samples

5.1.3 HARDNESS
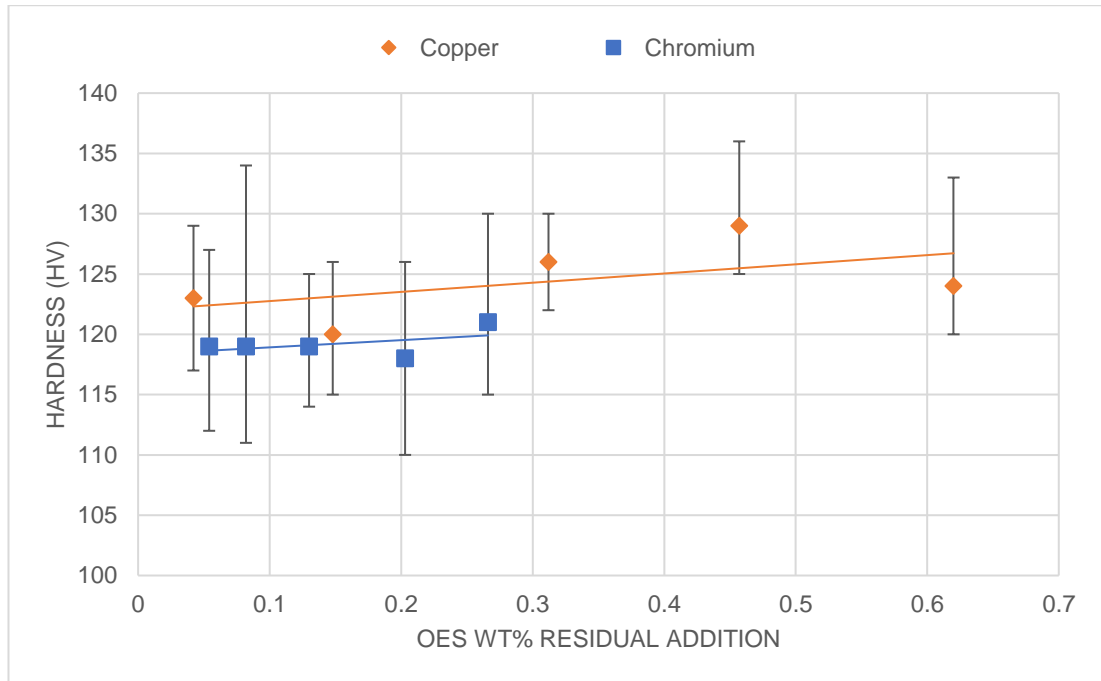
Figure 72 The hardness of as cast RAP140G_3190_CF__RM with copper and chromium additions showing the average hardness and the maximum and minimum hardness of each cast

The 140g 3190 casts were hardness tested in their as cast state. The hardness values can be seen in Figure 72, showing a slight hardening effect of both copper and chromium.

5.2   RESULTS 140G DP800 CENTRIFUGALLY CAST

5.2.1   INTRODUCTION AND SAMPLE OVERVIEW DP800 140G SOLIDS

As with the investigation into the production of 3190 in the centrifugal caster, it was decided to also investigate DP800 with the same method, allowing multiple test repeats from each cast as summarised below and in Figure 73. In this batch, pure materials solids were used to replicate the industrial material.

5.2.1.1   METHOD SUMMARY (3190 140G SOLIDS ROUTE)

- 140g sample size
- Centrifugally cast
- Solid feedstock
- Multiple tensile bars per sample (3-6)
- Hot rolling possible
- Samples large enough for easy OES testing

Scaling up to a 140g melt allows for more usable material per melt, and therefore more samples per composition which eliminates the need for repeated melts to obtain enough material to repeat tests because each cast, when rolled, was large enough to make six ASTM tensile bars. This also means that the composition and rolling profile is consistent for each residual level. The caster is under an argon atmosphere and when casting, the molten metal flows from the crucible into the mould, entering the mould at the centre and spreading outwards which does not reflect the industrial casting process and required close attention to the microstructure of the samples. The use of iron bar and other element solids made the melting process easy, and the resulting sample was easy to hot roll, helped by having a sample size that loses heat less quickly than smaller samples. As discussed in later sections, it was found that the iron bar used in the initial centrifugal tests only had a purity of 99% and left the final material with inclusions that significantly altered the mechanical properties. The use of high purity iron flakes was trialled in the place of iron bar in an attempt to reduce the number of inclusions. This was done by placing iron flakes in the crucible with the other solid element additions but the lack of contact area between the flakes prevented the material

from melting and the sample was not made. It was found that in order to successfully melt the iron flakes in the centrifugal caster, the flakes had to be first compacted. This added a significant amount of work time to the weighing out process and it was decided that the three tensile bars produced by the 40g route was sufficient, in addition to the fact that the glove box used for the smaller casts was able to achieve a cleaner atmosphere with a lower oxygen level.
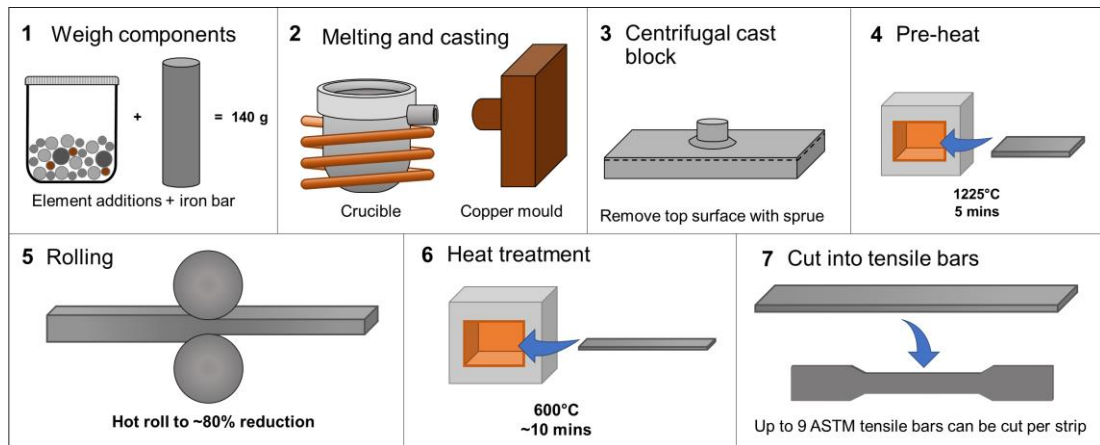
Figure 73 Summary of RAP140G _FE_BAR method

The samples produced using the iron bar feedstock are listed below in Table 21. The total levels of the residual elements is described as multiples of the current industrial limit.

Table 21 Centrifugally cast DP800 samples made using an iron bar feedstock

Sample Ref	Alloy	Route	Feedstock (Powder or solid)	Elements added
RAP140G_DP800_FE_BAR_RES-FREE	DP800	140G	Solid	Fe (Bal), C, Mn and Si
RAP140G_DP800_FE_BAR_CuX1	DP800	140G	Solid	Fe (Bal), C, Mn and Si + residual Cu
RAP140G_DP800_FE_BAR_CuX4	DP800	140G	Solid	Fe (Bal), C, Mn and Si + residual Cu
RAP140G_DP800_FE_BAR_CuX8	DP800	140G	Solid	Fe (Bal), C, Mn and Si + residual Cu
RAP140G_DP800_FE_BAR_CuX10	DP800	140G	Solid	Fe (Bal), C, Mn and Si + residual Cu

| RAP140G_DP800_FE_BAR_CuX15 | DP800 | 140G | Solid | Fe (Bal), C, Mn and Si + residual Cu |
| RAP140G_DP800_FE_BAR_CuX20 | DP800 | 140G | Solid | Fe (Bal), C, Mn and Si + residual Cu |

5.2.2 COMPOSITION

The composition of the initial samples made using iron bar can be seen in Table 22 and summarised in Figure 74.

Table 22 Composition of centrifugally cast DP800 made with iron bar with all element levels shown in wt%

	C	Si	Mn	P	S	Cr	Cu	Fe	Other (max)
RAP140G_3190_FE_BAR_RES-FREE	0.106	0.243	1.809	0.016	0.011	0.043	0.0081	97.68	0.084
SD	0.0067	0.014	0.058	0.0015	0.00088	0.00082	0.00093	0.082	/
Weighed wt%	0.1136	0.1429	2.2181	0	0	0	0	95.9705	0
RAP140G_3190_FE_BAR_CuX1	0.114	0.233	1.184	0.0071	0.0089	0.042	0.025	97.52	0.077
SD	0.012	0.022	0.07	0.0015	0.0015	0.0005	0.0026	0.111	/
Weighed wt%	0.1167	0.1450	2.2542	0	0	0	0	97.4659	0
RAP140G_3190_FE_BAR_CuX4	0.119	0.283	1.855	0.01	0.0061	0.043	0.115	97.48	0.0935
SD	0.013	0.0079	0.032	0.00086	0.00061	0.00094	0.0032	0.058	/
Weighed wt%	0.1623	0.1707	2.2576	0	0	0	0	97.3174	0
RAP140G_3190_FE_BAR_CuX8	0.129	0.278	1.897	0.0077	0.011	0.043	0.224	97.21	0.0953
SD	0.022	0.034	0.069	0.0015	0.0011	0.0011	0.0082	0.106	/
Weighed wt%	0.1155	0.1445	2.2543	0	0	0	0	97.3057	0
RAP140G_3190_FE_BAR_CuX10	0.165	0.261	1.687	0.013	0.01	0.042	0.303	97.44	0.078
SD	0.013	0.013	0.041	0.0005	0.00092	0.00094	0.0073	0.072	/
Weighed wt%	0.1635	0.1666	2.2018	0	0	0	0	97.2380	0
RAP140G_3190_FE_BAR_CuX15	0.119	0.281	1.931	0.008	0.011	0.045	0.459	97.02	0.1263
SD	0.015	0.0076	0.033	0.00085	0.0014	0.00071	0.0032	0.028	/
Weighed wt%	0.1178	0.1445	2.2546	0	0	0	0	97.1087	0
RAP140G_3190_FE_BAR_CuX20	0.152	0.252	1.813	0.015	0.011	0.042	0.594	97.04	0.085
SD	0.008	0.0071	0.016	0.00085	0.00065	0.00093	0.0071	0.027	/
Weighed wt%	0.1580	0.1704	2.2490	0	0	0	0	96.9638	0
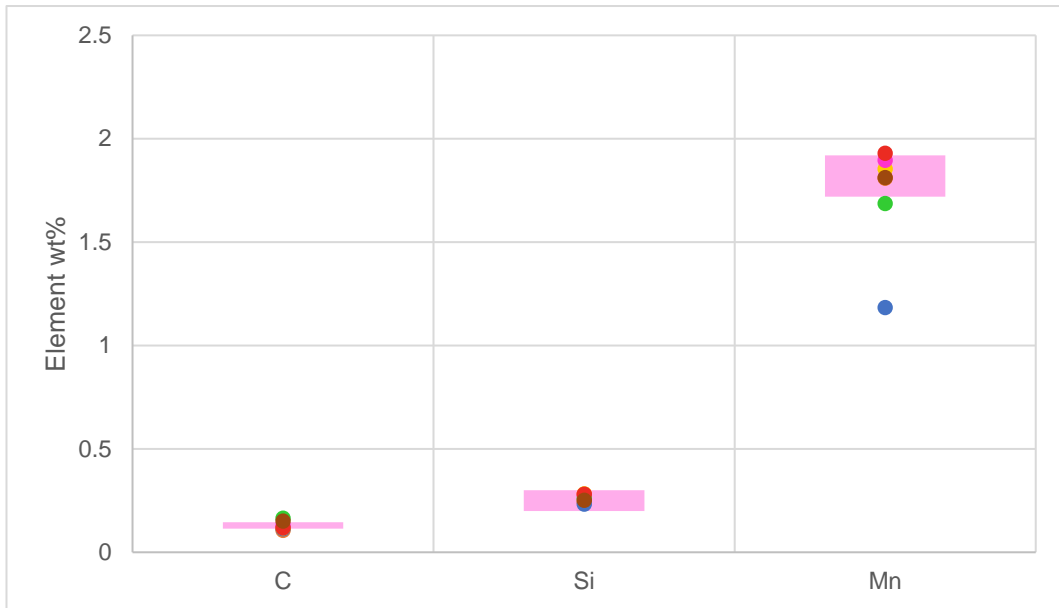
Figure 74 Compositional overview of RAP140G_DP800_FE_BAR samples

5.2.3 MICROSTRUCTURE
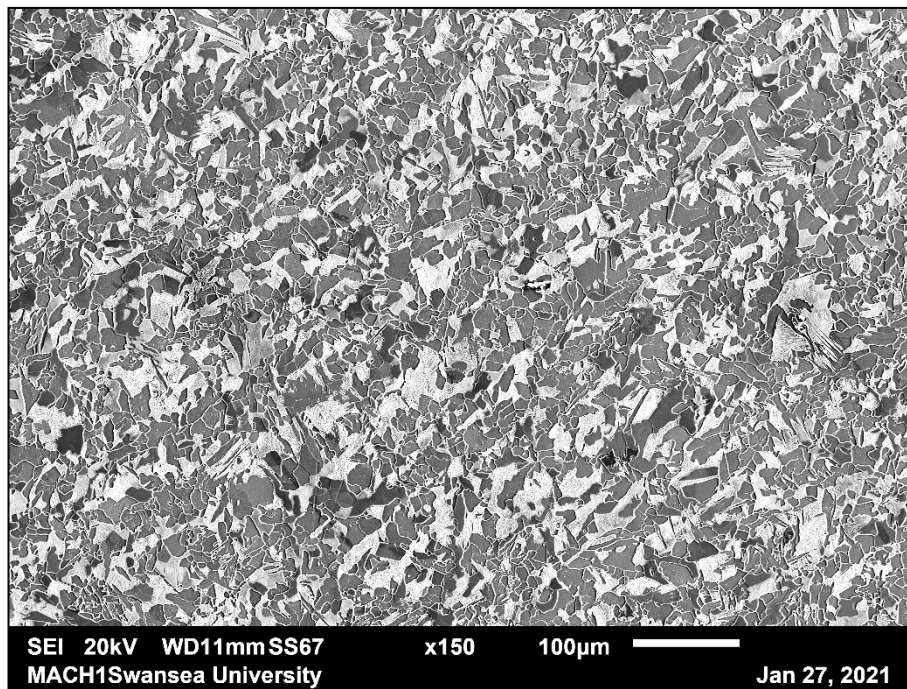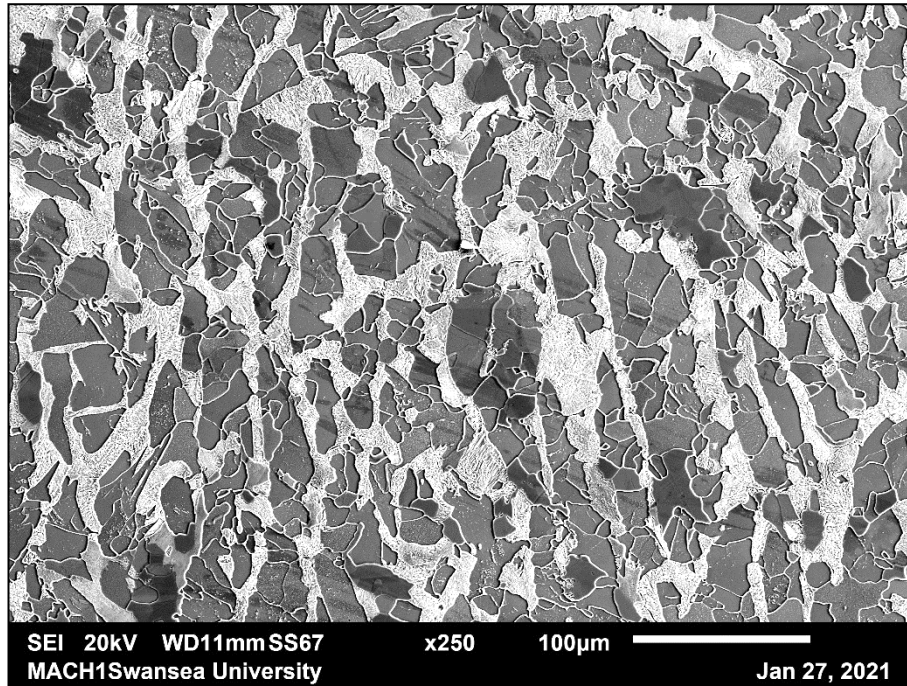
Figure 75 SEM images of RAP140G_ DP800_FE_BAR_CuX15 (rolling direction diagonal)
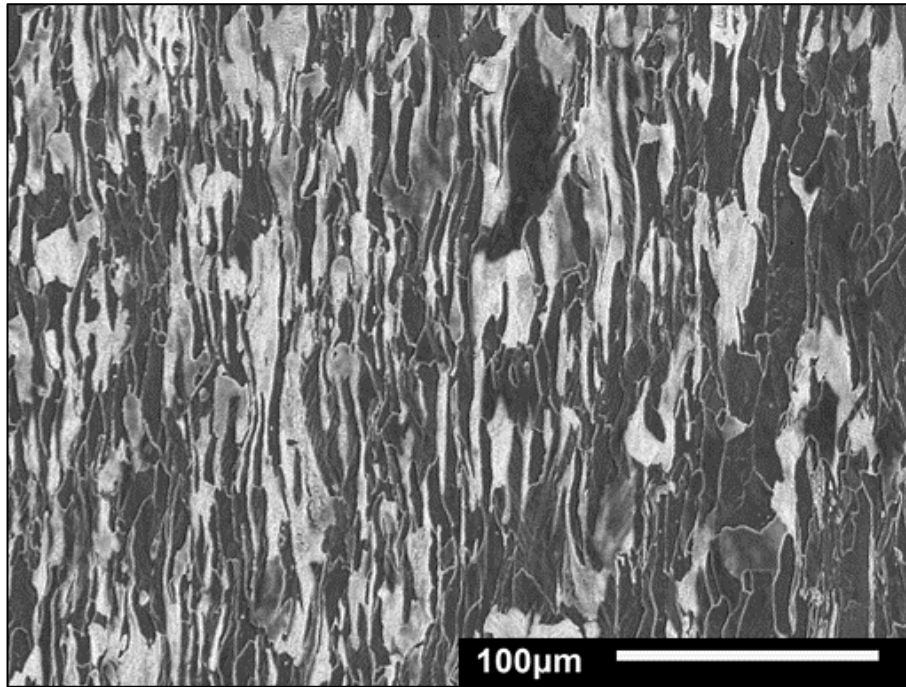
Figure 76 RAP140G_ DP800_FE_BAR_CuX4 microstructure after hot rolling (rolling direction vertical)
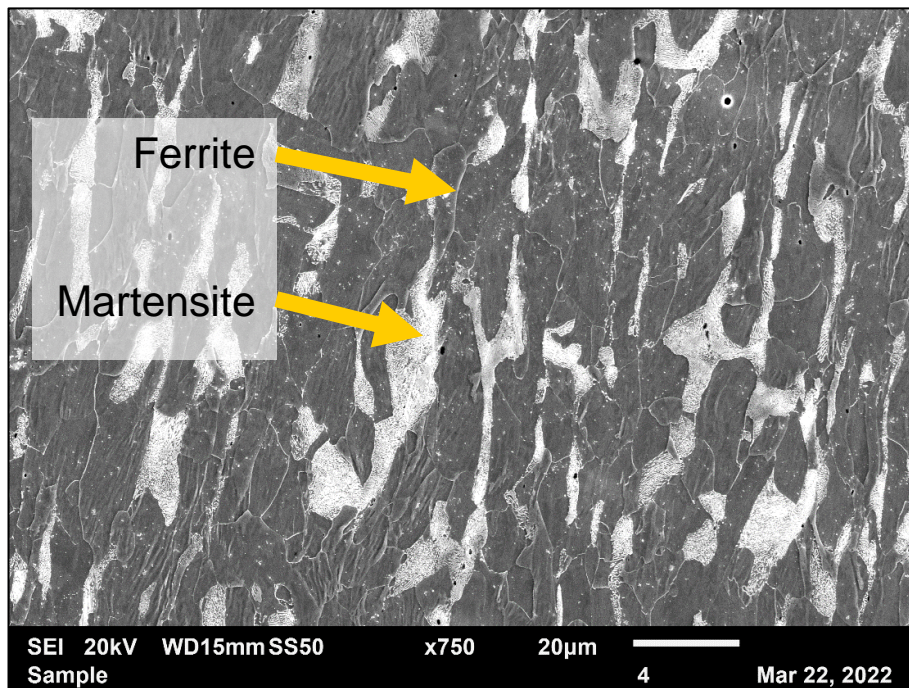
Figure 77 RAP140G_ DP800_FE_BAR_RES-FREE microstructure after hot rolling (rolling direction vertical) with labelled phases

The microstructure of the samples after the rolling processes can be seen in Figure 75 to Figure 79 where the traditional banded microstructure of martensitic islands in a ferritic sea can be clearly seen, and the phases are labelled in Figure 77. This can be compared to an example dual phase microstructure in Figure 11.
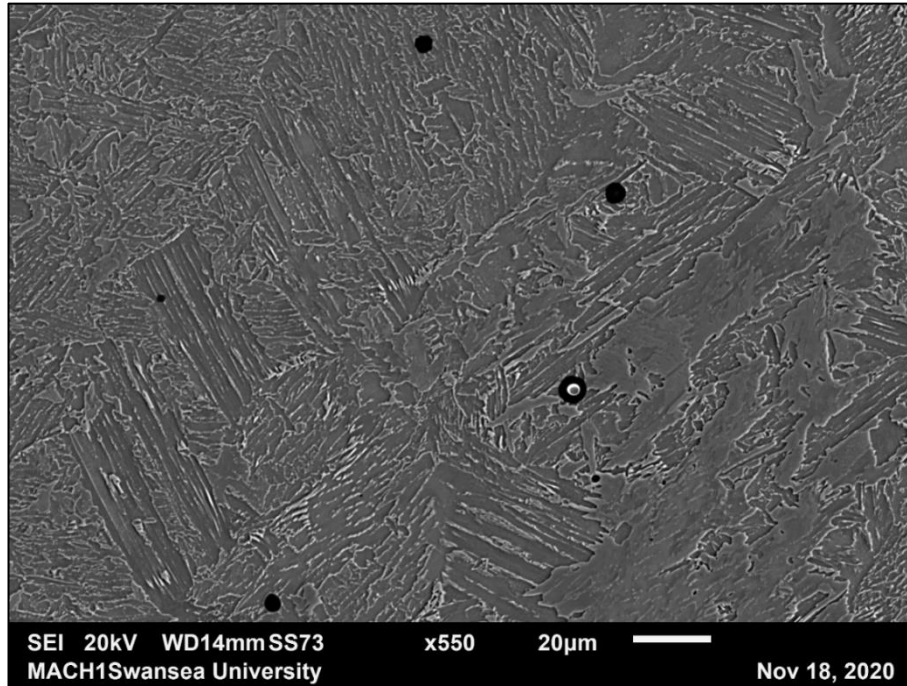
Figure 78 SEM image of oxides present in RAP140G_ DP800_FE_BAR_CuX4
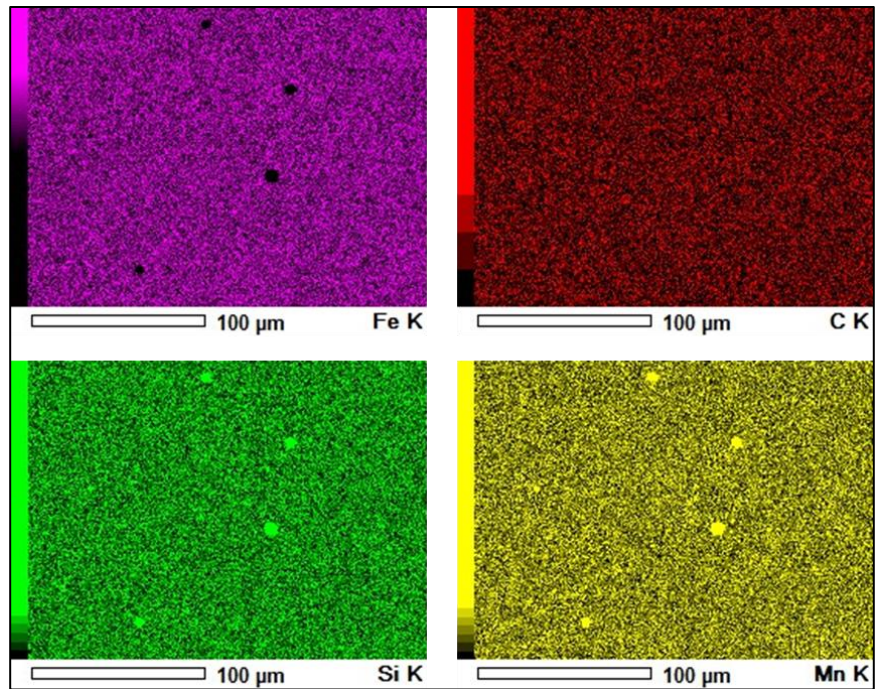
Figure 79 EDX results for oxides present in RAP140G_ DP800_FE_BAR_CuX4
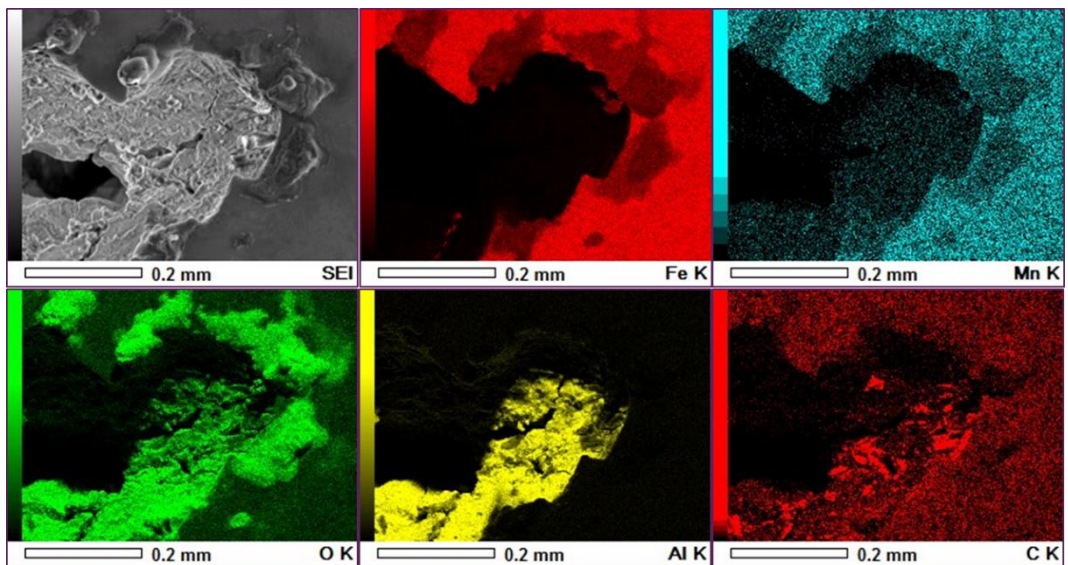
Figure 80 EDX results for a large pore present in RAP140G_ DP800_FE_BAR_CuX4

Figure 78 to Figure 80 show some of the pores found in sample RAP140G_ DP800_FE_BAR_CuX4, and an EDX analysis of some features.

146

5.2.4 TENSILE
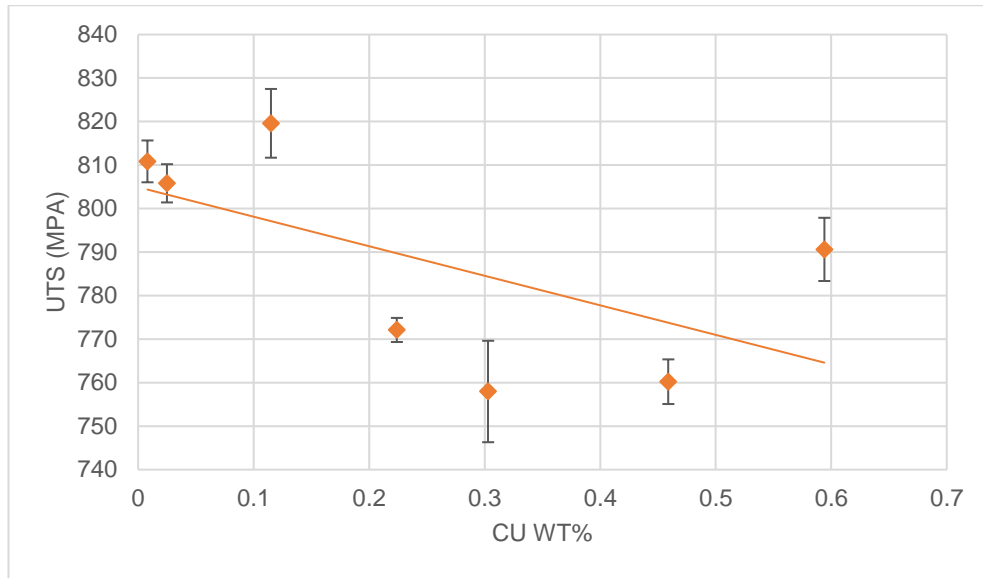
Figure 81 The UTS of RAP140G_ DP800_FE_BAR_Cu samples
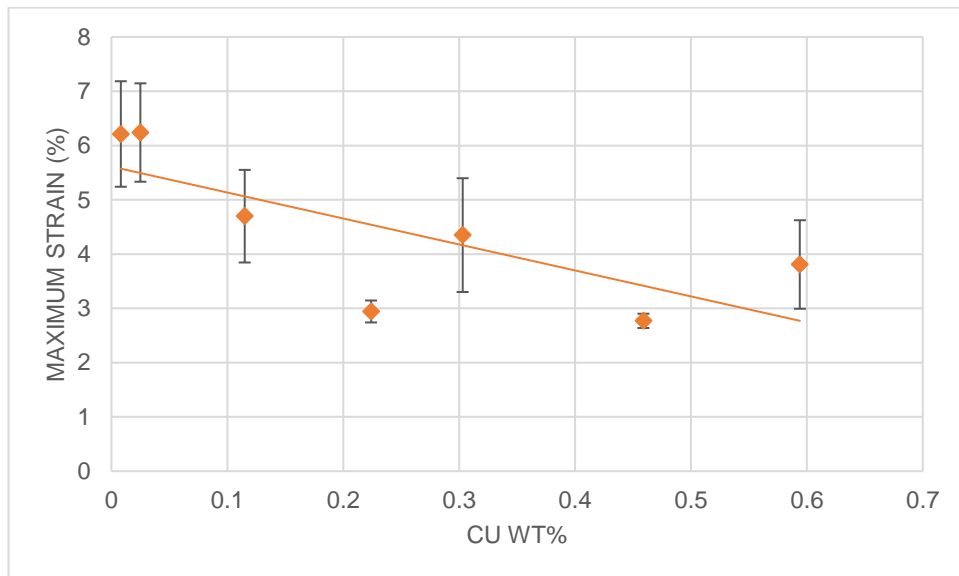
Figure 82 The maximum strain of RAP140G_ DP800_FE_BAR_Cu samples
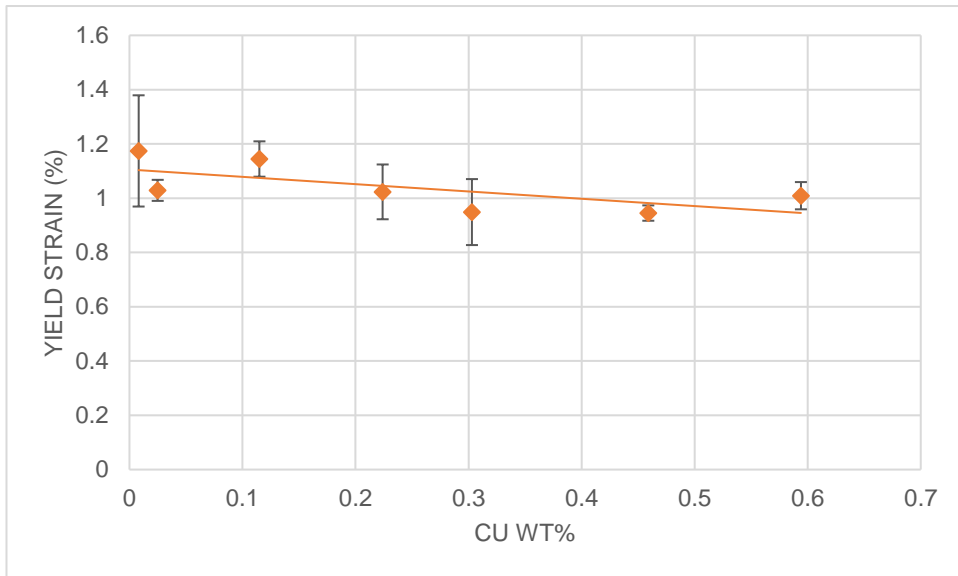
Figure 83 The yield strain of RAP140G_ DP800_FE_BAR_Cu samples
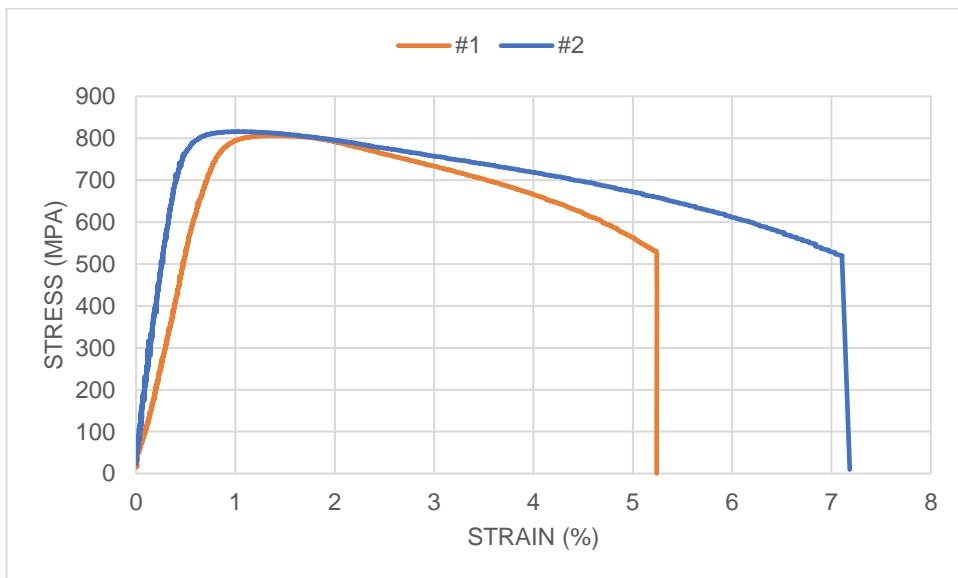
Figure 84 The stress-strain curves for the two RAP140G_ DP800_FE_BAR_CuX1 samples
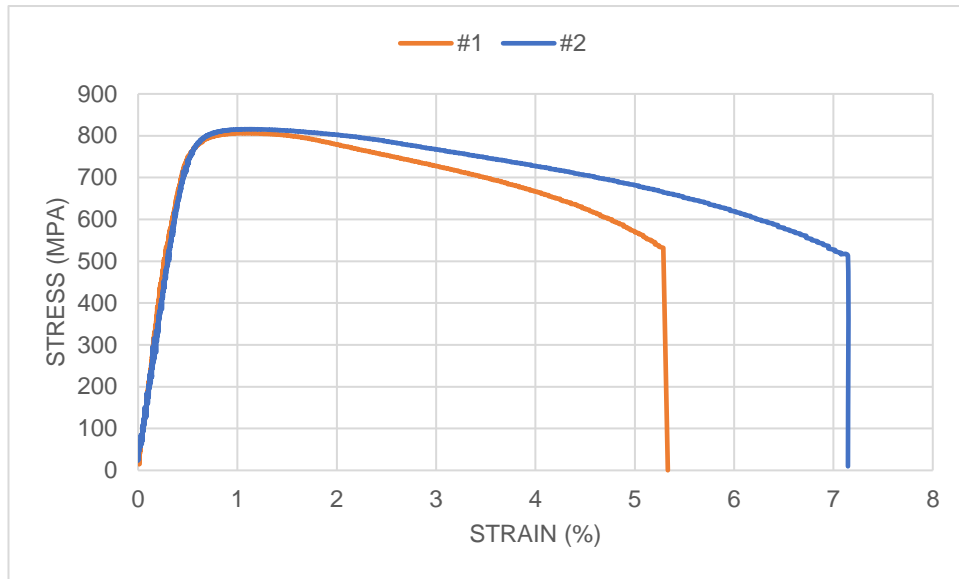
Figure 85 The stress-strain curves for the two RAP140G_ DP800_FE_BAR_CuX16 samples

Figure 81 to Figure 83 plot the mechanical property results of samples with increasing copper levels, and Figure 84 and Figure 85 show example stress strain curves. The graphs suggest that increasing copper levels decrease the UTS, and maximum strain of the material, although the yield strain remains similar for all samples. The example stress strain curves show that the samples had continuous yielding and a brittle fracture.

5.2.5 HARDNESS
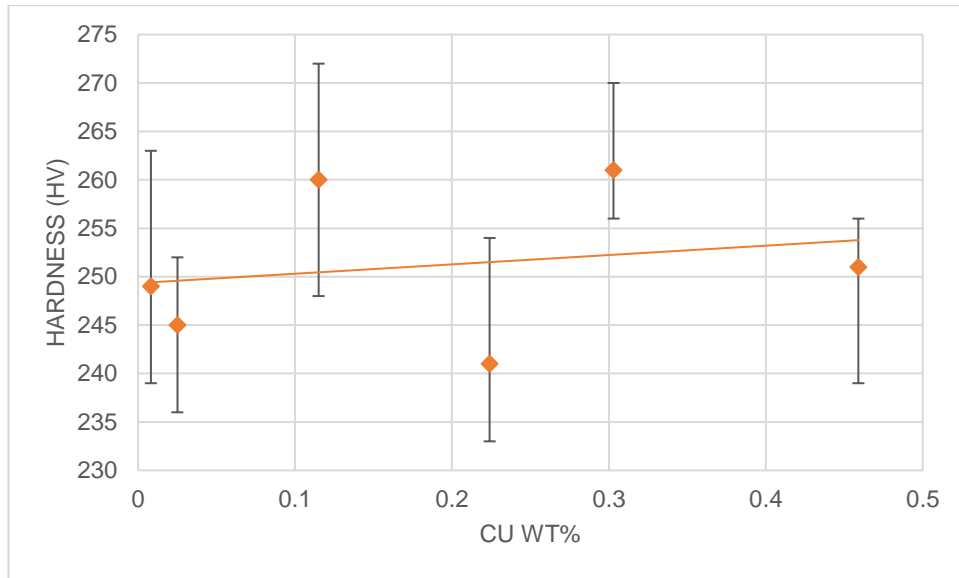
Figure 86 The hardness of RAP140G_ DP800_FE_BAR_Cu samples

Figure 86 shows the hardness results of the samples, showing little impact of the increasing copper levels.

5.3 SUMMARY OF 140G ROUTE

The 140g casts produced using the centrifugal caster allowed for more test specimens to be produced per composition which meant that repeated tests could be performed. There were unfortunately some difficulties with the feedstock, especially the iron bar which was found to contain inclusions which led to very brittle tensile samples that did not achieve the expected elongation values. The composition still lacked consistency, it was decided to look again at the powder route but scaled up to allow multiple samples.

CHAPTER 6   FINAL TESTING OF OPTIMISED ROUTE

6.1   3190 RESULTS 40G POWDER ROUTE

6.1.1   INTRODUCTION AND SAMPLE OVERVIEW 3190 40G POWDER ROUTE

The powder route was revisited, this time with a 40g cast now available with the aim of using the method of the 20g route but scaled up to allow for sample repeats. Extensive research, shown in 3.5.1, was undertaken prior to the inclusion of residual elements with the aim of achieving a composition that is both consistent and within target.

6.1.1.1   METHOD SUMMARY (3190 40G REMELT ROUTE)

- 40g sample size
- Gravity cast
- Powder feedstock
- 3 tensile bars per sample
- Hot rolling possible
- Samples large enough for easy OES testing

An initial improvement was the scale up from 20g to 40g which produced a sample which was larger and, when rolled, was able to provide enough material for three ASTM tensile bars. The casts has the same flow direction as the 20g method and were wide enough to easily test the composition several OES sparks, and this information meant the composition was easier to monitor and adjust. It was found that some elements are more readily lost through the weighing, melting and casting process in often unpredictable ways, whilst other elements had a tendency to be picked up during the process. This allowed for an adjustment of these elements to achieve a composition which is closer to the target values. This method development also coincided with the new availability of a hot rolling mill. Whilst the samples were small enough that they

quickly lost heat, they were still able to be hot rolled, giving a production method which could more closely replicate the processing conditions of steel grades on an industrial scale.
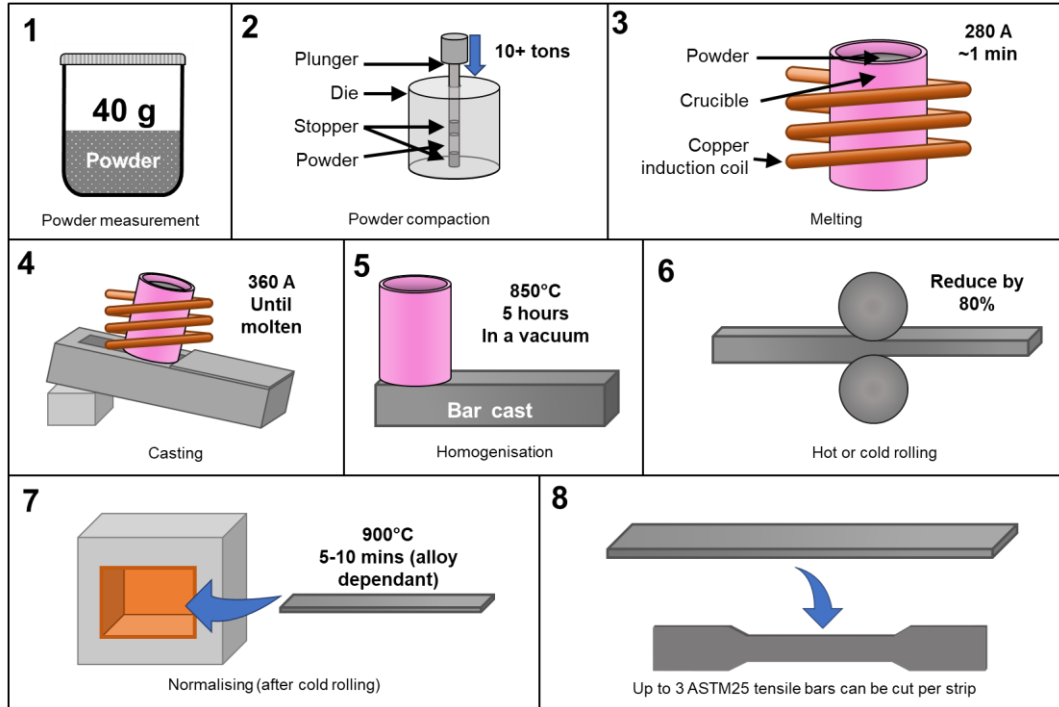
Figure 87 Overview of RAP40G _POW route

The samples considered in this section were as follows, where the notation used describe the total levels of the residual elements is described as multiples of the current limit.

Table 23 Samples produced to make 40g 3190 replicas

Sample Ref	Alloy	Route	Feedstock (Powder or solid)	Elements added
RAP40G_POW_CuX1	3190	40g	Powder	Fe (Bal), C, Mn, Si, Al and Cr + residual Cu
RAP40G_POW_CuX4	3190	40g	Powder	Fe (Bal), C, Mn, Si, Al and Cr + residual Cu
RAP40G_POW_CuX8	3190	40g	Powder	Fe (Bal), C, Mn, Si, Al and Cr + residual Cu
RAP40G_POW_CuX12	3190	40g	Powder	Fe (Bal), C, Mn, Si, Al and Cr + residual Cu
RAP40G_POW_CuX16	3190	40g	Powder	Fe (Bal), C, Mn, Si, Al and Cr + residual Cu
RAP40G_POW_CuX24	3190	40g	Powder	Fe (Bal), C, Mn, Si, Al and Cr + residual Cu

RAP40G_POW_CuX36	3190	40g	Powder	Fe (Bal), C, Mn, Si, Al and Cr + residual Cu
RAP40G_POW_CrX1	3190	40g	Powder	Fe (Bal), C, Mn, Si and Al + residual Cr
RAP40G_POW_CrX4	3190	40g	Powder	Fe (Bal), C, Mn, Si and Al + residual Cr
RAP40G_POW_CrX8	3190	40g	Powder	Fe (Bal), C, Mn, Si and Al + residual Cr
RAP40G_POW_CrX12	3190	40g	Powder	Fe (Bal), C, Mn, Si and Al + residual Cr
RAP40G_POW_CrX16	3190	40g	Powder	Fe (Bal), C, Mn, Si and Al + residual Cr
RAP40G_POW_CrX24	3190	40g	Powder	Fe (Bal), C, Mn, Si and Al + residual Cr
RAP40G_POW_CrX36	3190	40g	Powder	Fe (Bal), C, Mn, Si and Al + residual Cr
RAP40G_POW_SnX1	3190	40g	Powder	Fe (Bal), C, Mn, Si, Al and Cr + residual Sn
RAP40G_POW_SnX4	3190	40g	Powder	Fe (Bal), C, Mn, Si, Al and Cr + residual Sn
RAP40G_POW_SnX8	3190	40g	Powder	Fe (Bal), C, Mn, Si, Al and Cr + residual Sn
RAP40G_POW_SnX12	3190	40g	Powder	Fe (Bal), C, Mn, Si, Al and Cr + residual Sn
RAP40G_POW_SnX16	3190	40g	Powder	Fe (Bal), C, Mn, Si, Al and Cr + residual Sn
RAP40G_POW_SnX24	3190	40g	Powder	Fe (Bal), C, Mn, Si, Al and Cr + residual Sn
RAP40G_POW_SnX36	3190	40g	Powder	Fe (Bal), C, Mn, Si, Al and Cr + residual Sn
RAP40G_POW_NiX1	3190	40g	Powder	Fe (Bal), C, Mn, Si, Al and Cr + residual Ni
RAP40G_POW_NiX4	3190	40g	Powder	Fe (Bal), C, Mn, Si, Al and Cr + residual Ni
RAP40G_POW_NiX8	3190	40g	Powder	Fe (Bal), C, Mn, Si, Al and Cr + residual Ni
RAP40G_POW_NiX12	3190	40g	Powder	Fe (Bal), C, Mn, Si, Al and Cr + residual Ni
RAP40G_POW_NiX16	3190	40g	Powder	Fe (Bal), C, Mn, Si, Al and Cr + residual Ni
RAP40G_POW_NiX24	3190	40g	Powder	Fe (Bal), C, Mn, Si, Al and Cr + residual Ni
RAP40G_POW_NiX36	3190	40g	Powder	Fe (Bal), C, Mn, Si, Al and Cr + residual Ni
RAP40G_POW_MoX1	3190	40g	Powder	Fe (Bal), C, Mn, Si, Al and Cr + residual Mo
RAP40G_POW_MoX4	3190	40g	Powder	Fe (Bal), C, Mn, Si, Al and Cr + residual Mo
RAP40G_POW_MoX8	3190	40g	Powder	Fe (Bal), C, Mn, Si, Al and Cr + residual Mo
RAP40G_POW_MoX12	3190	40g	Powder	Fe (Bal), C, Mn, Si, Al and Cr + residual Mo
RAP40G_POW_MoX16	3190	40g	Powder	Fe (Bal), C, Mn, Si, Al and Cr + residual Mo

RAP40G_POW_MoX24	3190	40g	Powder	Fe (Bal), C, Mn, Si, Al and Cr + residual Mo
RAP40G_POW_MoX36	3190	40g	Powder	Fe (Bal), C, Mn, Si, Al and Cr + residual Mo

6.1.2 COMPOSITION

The composition of the 40g route is shown in Table 25 and Table 26 and summarised in Figure 88. Table 26 Chemical compositions of 3190 40g samples made using the powder route with Ni, Sn and Mo residual additions.

and shows that most of the elements fall short of the target values detailed in Table 3. This is despite the efforts catalogued in 3.5.1 to achieve a composition within the range set out in Table 3.

Table 24 Target residual addition wt% for 3190 with Cu or Cr additions

	x1	x4	x8	x12	x16	x24	x36
Cr wt.%	0.025	0.1	0.2	0.3	0.4	0.6	0.9
Cu wt.%	0.03	0.12	0.24	0.36	0.48	0.72	1.08

Table 25 Chemical compositions, hardness and grain sizes of 3190 40g samples made using the powder route with Cu and Cr residual additions. Crx1 sample did not have enough remaining material to test with an OES so target Cr wt% is used [1]

Ref. ID	Cu	Cr	C	Mn	Si	S	P	Grain size (µm)	Hardness (HV$_1$)
Baseline	0.001	0.017	0.014	0.137	0.067	0.01	0.0037	16.1 ± 1.5	108.6 ± 10
Cu x1	0.0295	0.018	0.022	0.134	0.035	0.015	0.0038	18.2 ± 0.7	106.2 ± 8
Cu x4	0.111	0.017	0.020	0.139	0.020	0.015	0.0038	17.1 ± 0.6	103.9 ± 8
Cu x8	0.224	0.019	0.019	0.144	0.024	0.011	0.0023	15.9 ± 1.4	105.0 ± 4
Cu x12	0.33	0.016	0.016	0.136	0.023	0.015	0.0033	19.2 ± 2.1	116.4 ± 6
Cu x16	0.441	0.017	0.017	0.141	0.073	0.0165	0.003	15.6 ± 0.9	116.1 ± 7
Cu x24	0.676	0.016	0.023	0.138	0.019	0.01	0.0032	19.4 ± 1.2	113.3 ± 7
Cu x36	1.03	0.017	0.022	0.139	0.020	0.016	0.0034	17.2 ± 0.9	120.7 ± 9
Average	N/A	0.017	0.02	0.14	0.024	0.014	0.0033	N/A	N/A
St. Dev.		0.001	0.003	0.003	0.006	0.003	0.0005		
Cr x1	--	0.025	0.030			0.0133		17.5 ± 0.9	96 ± 3
Cr x4	--	0.101	0.013	0.139	0.019	0.016	0.0032	21.9 ± 0.7	108.9 ± 10

Cr x8	--	0.201	0.021	0.143	0.038	0.015	0.003	15.6 ± 0.8	97 ± 4
Cr x12	--	0.294	0.016	0.131	0.014	0.016	0.0033	23.4 ± 1.7	108.8 ± 12
Cr x16	--	0.395	0.036	0.134	0.016	0.012	0.0023	14.9 ± 1.6	100 ± 6
Cr x24	--	0.578	0.015	0.129	0.012	0.016	0.0033	21.9 ± 1.1	95.8 ± 6
Cr x36	--	0.867	0.022	0.126	0.012	0.011	0.0033	16.3 ± 0.5	100.9 ± 7
Average	N/A	N/A	0.022	0.134	0.0185	0.014	0.003	N/A	N/A
St. Dev.			0.008	0.006	0.01	0.002	0.0004		

Table 26 Chemical compositions of 3190 40g samples made using the powder route with Ni, Sn and Mo residual additions.

	C	Si	Mn	P	S	Cr	Mo	Ni	Cu	Sn
Ni1	0.006	0.014	0.135	0.0042	0.0095	0.019	0	0.034	0.001	0
Ni4	0.016	0.021	0.138	0.0043	0.0103	0.018	0	0.107	0.002	0
Ni8										
Ni12	0.006	0.013	0.137	0.0039	0.0097	0.019	0	0.308	0.001	0
Ni16	0.007	0.014	0.135	0.0036	0.0099	0.019	0	0.403	0.001	0
Ni24	0.021	0.017	0.135	0.004	0.0095	0.019	0	0.594	0.002	0
Ni36	0.009	0.015	0.136	0.0038	0.0103	0.017	0	0.842	0.001	0
Average	0.011	0.016	0.136	0.0040	0.0099	0.019			0.001	0
Sn1										
Sn4	0.009	0.012	0.133	0.0042	0.0093	0.018	0	0.004	0.001	0.036
Sn8	0.019	0.017	0.132	0.0039	0.0091	0.016	0	0.003	0.001	0.071
Sn12	0.03	0.026	0.124	0.0038	0.0091	0.015	0	0.001	0.001	0.114
Sn16	0.023	0.024	0.12	0.0042	0.0083	0.016	0	0.002	0.001	0.145
Sn24	0.025	0.028	0.125	0.0044	0.0084	0.016	0	0.002	0.001	0.222
Sn36	0.026	0.024	0.122	0.0044	0.0085	0.016	0	0.002	0.001	>0.330
Average	0.022	0.022	0.126	0.0042	0.0088	0.016		0.002	0.001	
Mo1	0.02	0.014	0.132	0.0041	0.0096	0.017	0.001	0.004	0.001	0
Mo4	0.021	0.013	0.132	0.0038	0.0092	0.016	0.006	0.003	0.001	0
Mo8	0.014	0.011	0.127	0.0037	0.0095	0.017	0.01	0.004	0.001	0
Mo12	0.007	0.021	0.136	0.0037	0.0092	0.019	0.017	0.004	0.001	0
Mo16	0.015	0.014	0.134	0.0035	0.0099	0.017	0.016	0.003	0.001	0
Mo24	0.017	0.015	0.134	0.0038	0.0089	0.016	0.028	0.004	0.002	0

Mo36	0.009	0.015	0.133	0.004	0.009	0.017	0.038	0.004	0.001	0
Average	0.015	0.015	0.133	0.0038	0.0093	0.017		0.004	0.001	0
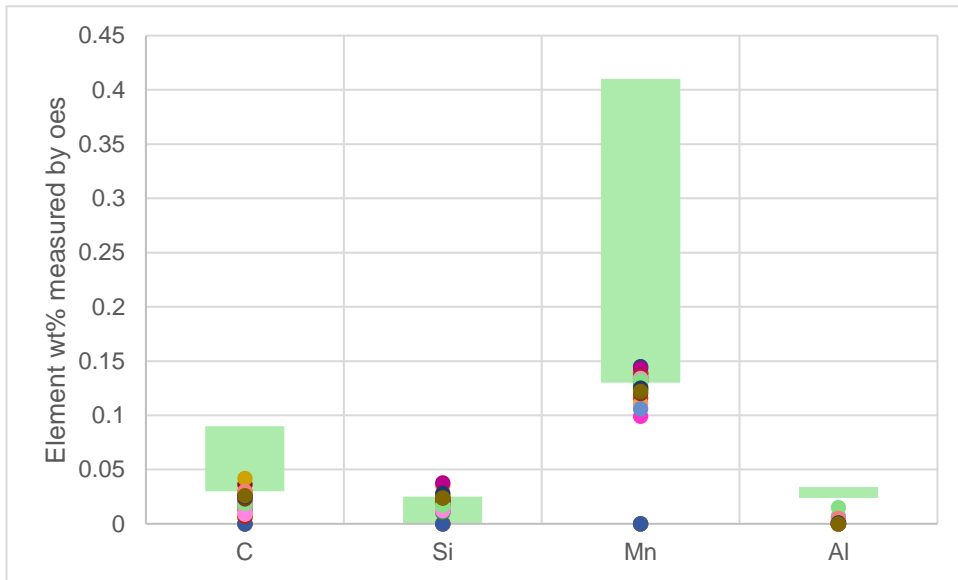
Figure 88 Compositional overview of RAP40G_POW samples

6.1.3   TENSILE

Figure 89 to Figure 98 show the tensile properties of the RAP40G_POW samples with copper and chromium additions. These results were presented also in [1].
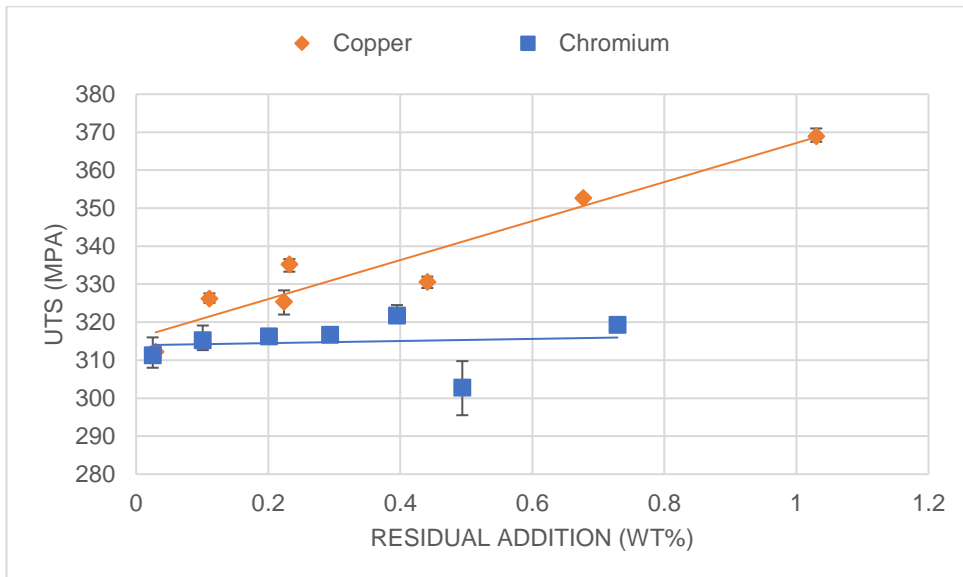
Figure 89 The ultimate tensile strength of RAP40G_POW with copper and chromium additions
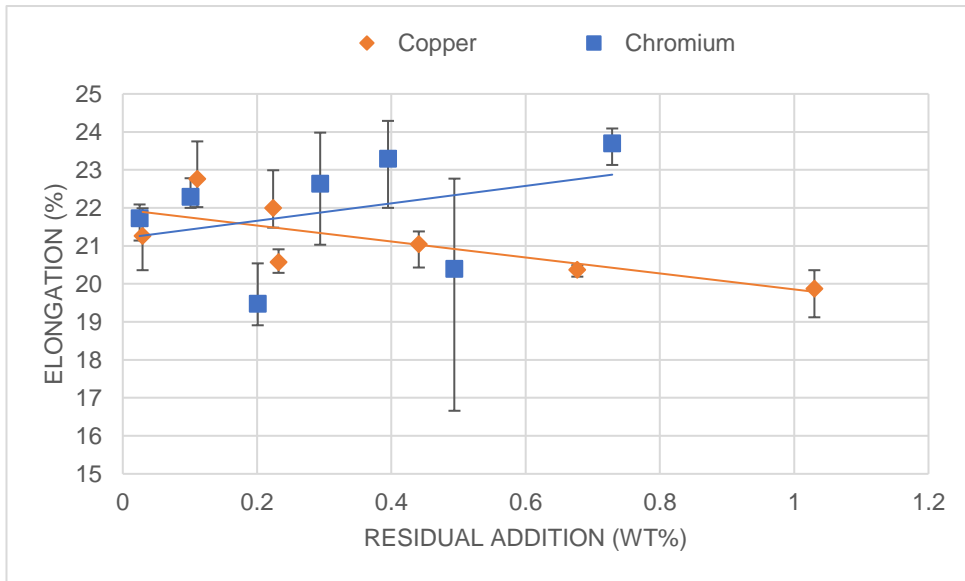
Figure 90 The uniform elongation of RAP40G_POW with copper and chromium additions
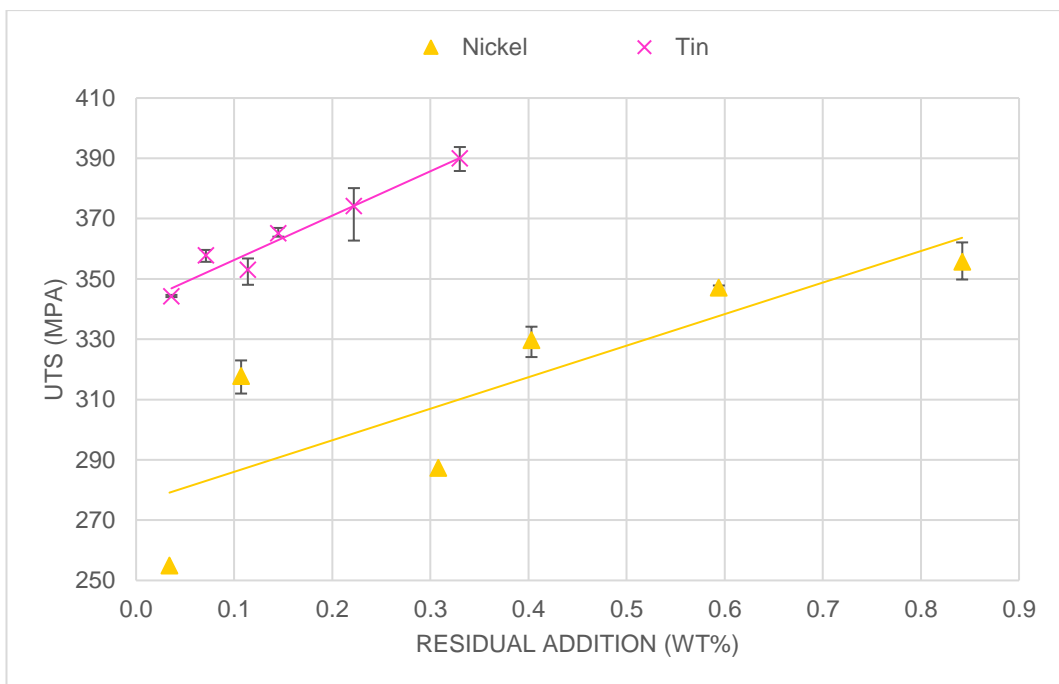
Figure 91 The ultimate tensile strength of RAP40G_POW with tin and nickel additions
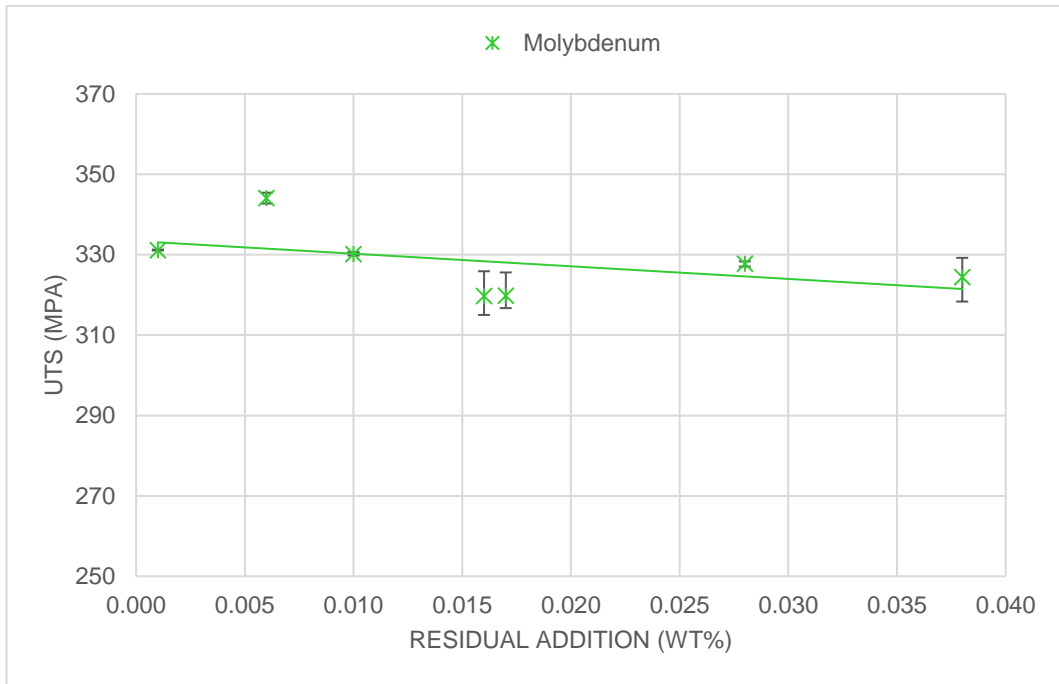
Figure 92 The ultimate tensile strength of RAP40G_POW_Mo
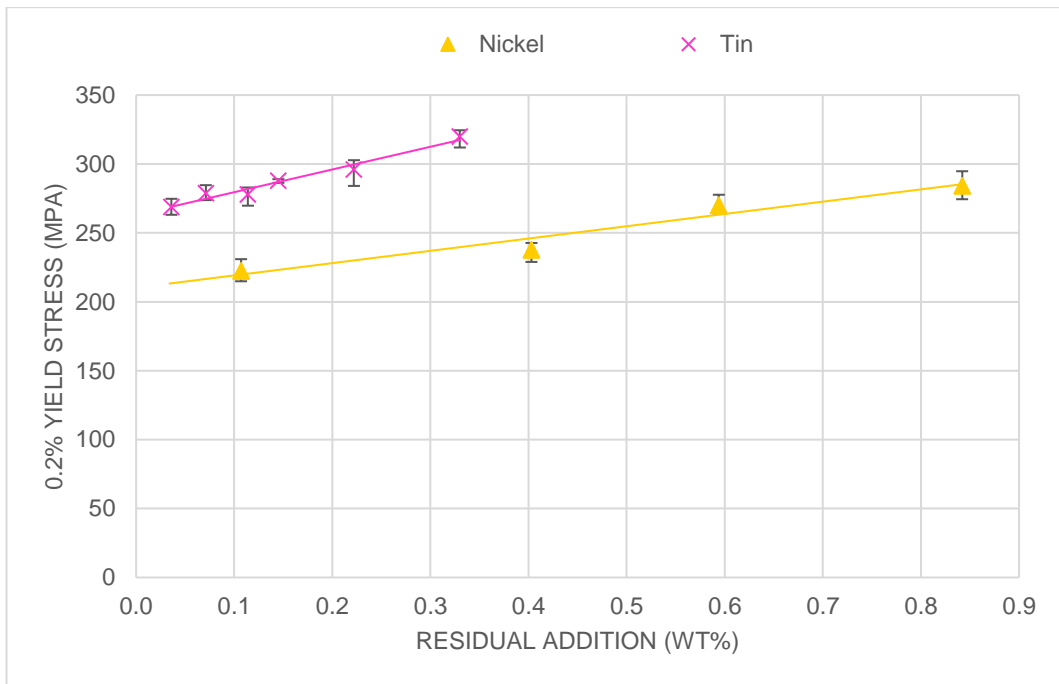
Figure 93 The 0.2% proof strength of RAP40G_POW with tin and nickel additions
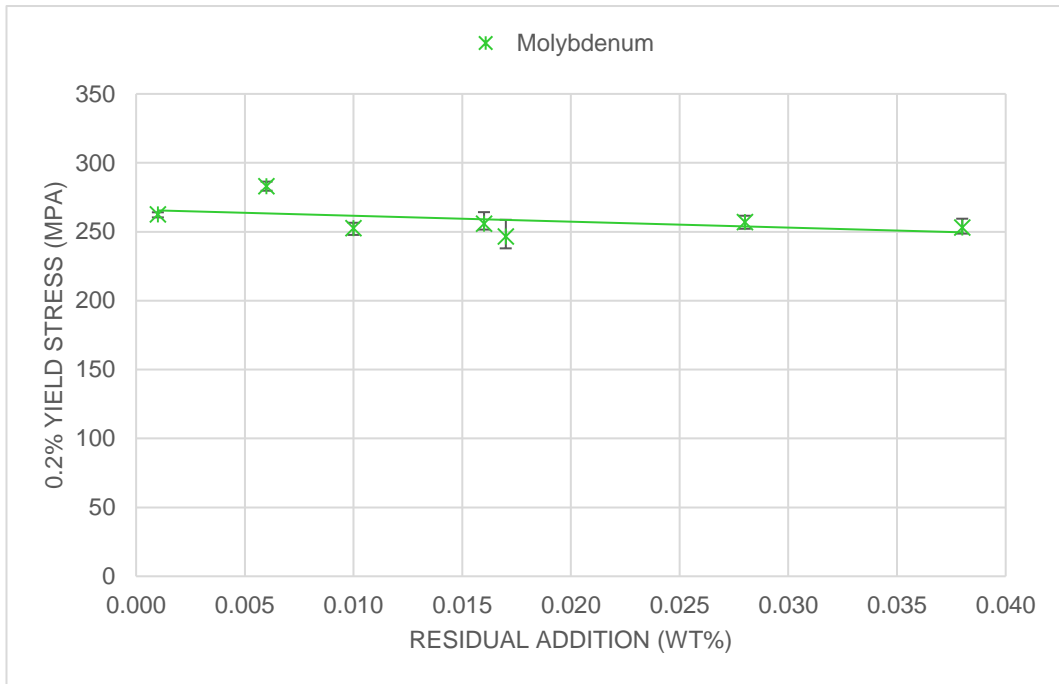
Figure 94 The 0.2% proof strength of RAP40G_POW_Mo
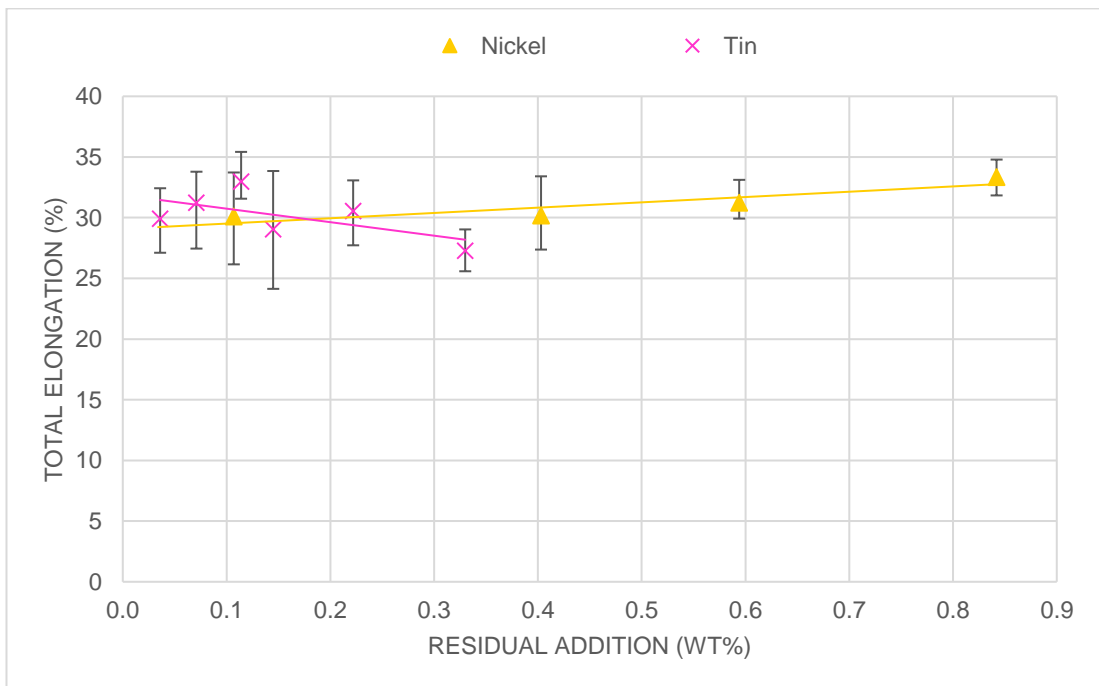
Figure 95 The maximum elongation of RAP40G_POW with tin and nickel additions
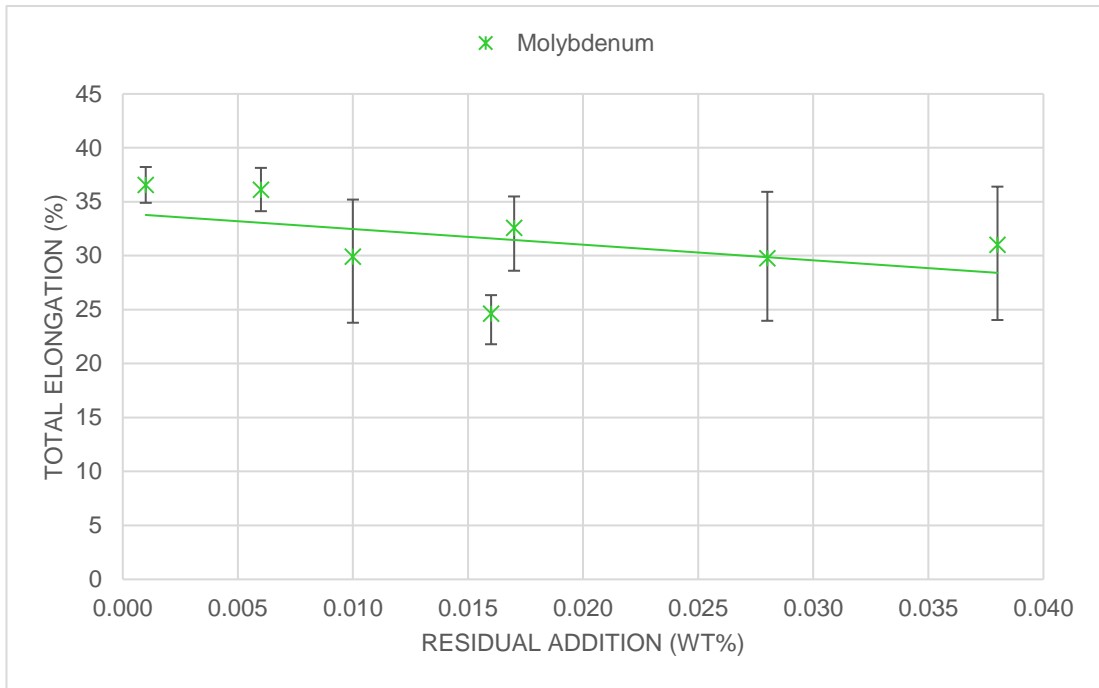
Figure 96 The maximum elongation of RAP40G_POW_Mo
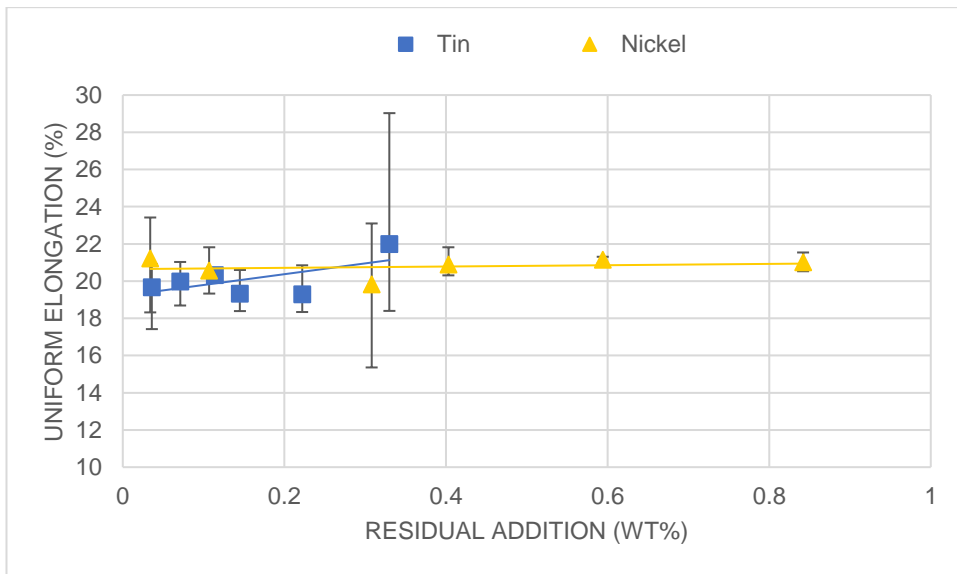
Figure 97 The uniform elongation of RAP40G_POW with tin and nickel additions
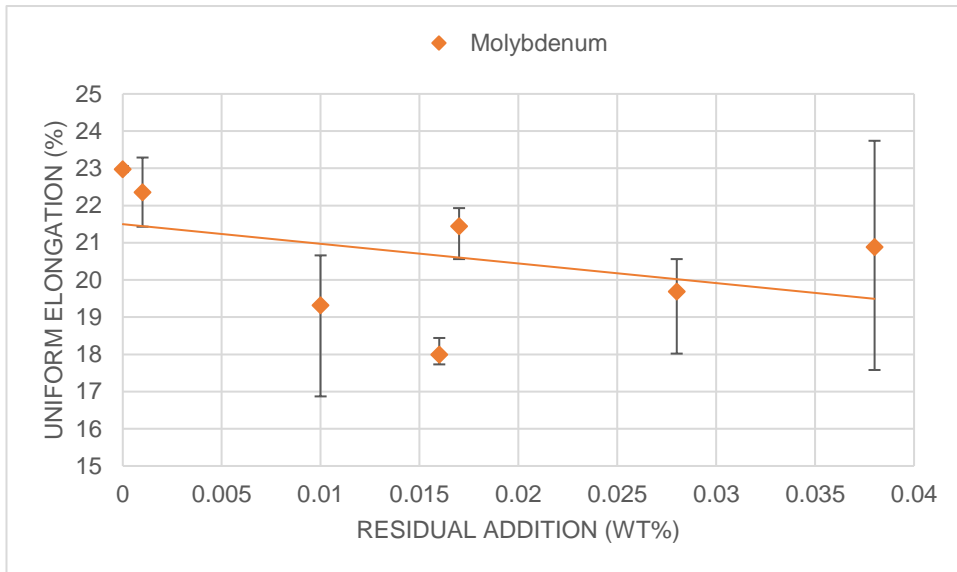
Figure 98 The uniform elongation of RAP40G_POW_Mo

Figure 89 to Figure 98 show the tensile results for the RAP40G_POW samples which suggest that higher levels of copper, nickel and tin increased the UTS of the material, but only copper had a significantly detrimental effect on the elongation. Molybdenum and chromium were shown to have much less effect on the material at the levels investigated.

A carbon equivalent equation was considered with the aim of comparing the samples in a way that considered the varying levels of several levels rather than just the intentionally added residual element. The carbon equivalent equation below is an adaption of one used by Tata Steel, with tin added (shown in red) due to the exclusion of tin from the original equation. Tin was placed where it is based on some research suggesting that tin has similar effects as copper but is more potent [7]. The positioning of tin in the equation below reflects this.

$$C_{eq} = C + \frac{Mn}{6} + \frac{Cr + Mo + V + Sn}{5} + \frac{Cu + Ni}{15}$$

Equation 4 Adjusted carbon equivalent calculation with consideration of tin levels
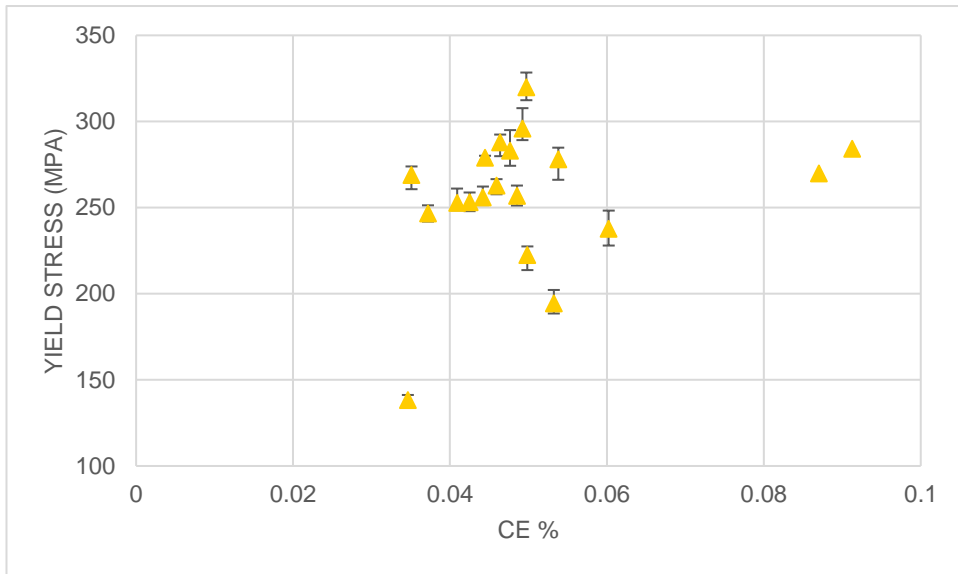
Figure 99 Yield stress of RAP40G_POW samples plotted against the carbon equivalent of each sample
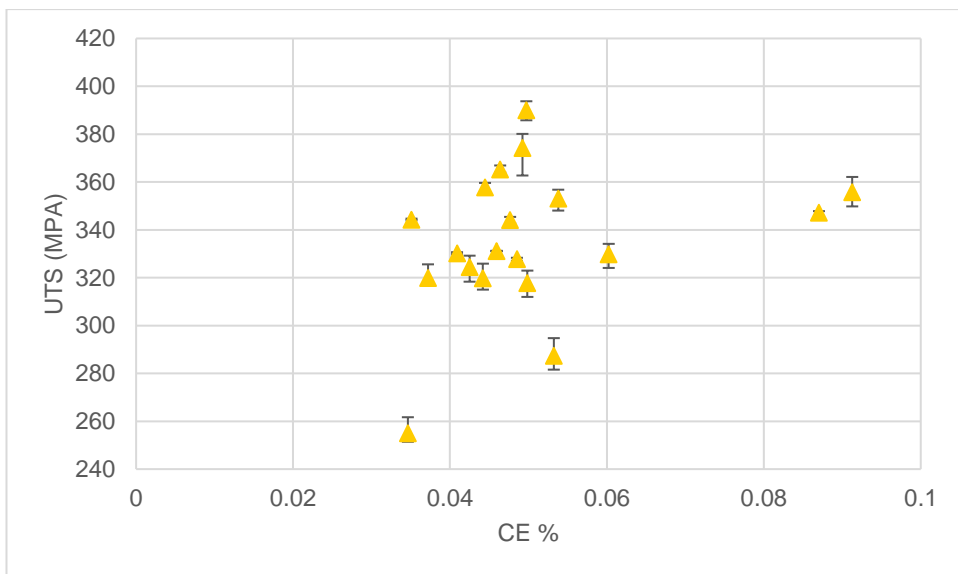
Figure 100 UTS of synthetic RAP40G_POW samples plotted against the carbon equivalent of each sample
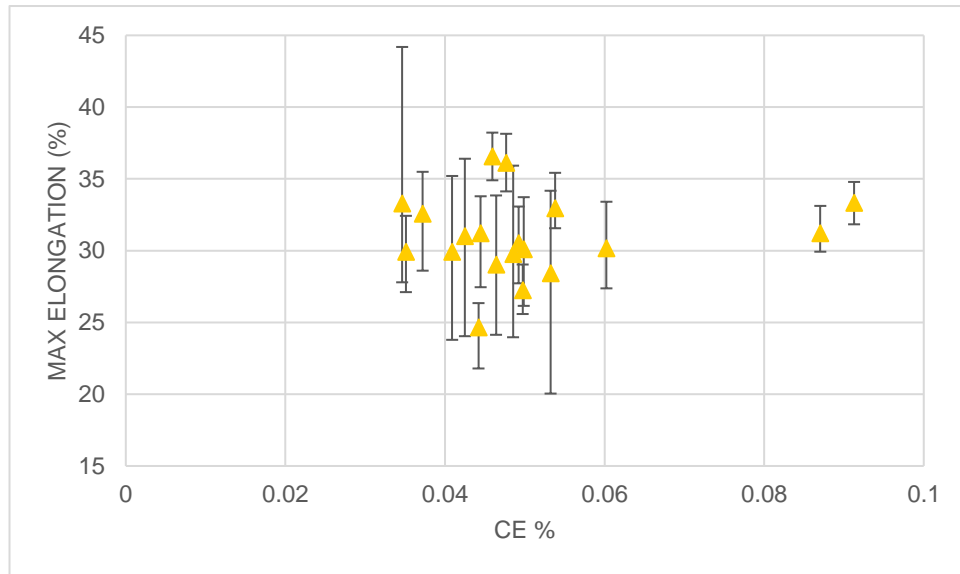
Figure 101 Manimum elongation of RAP40G_POW samples plotted against the carbon equivalent of each sample
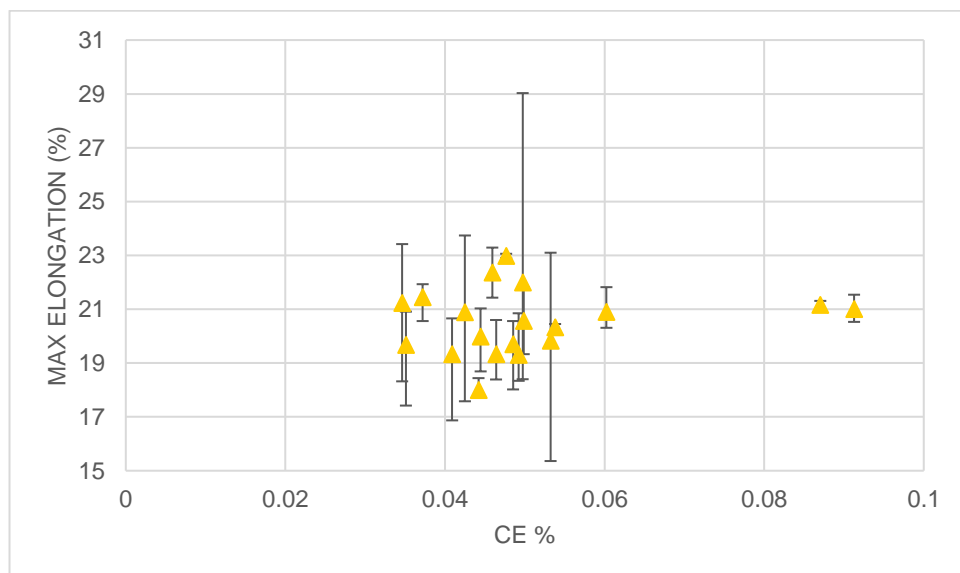
Figure 102 Uniform elongation of RAP40G_POW samples plotted against the carbon equivalent of each sample

Figure 99 to Figure 102 show the mechanical properties of the samples, plotted using a carbon equivalent value rather than plotting simply against the residual content. The results contain a lot of scatter, making it difficult to establish a trend in the data.
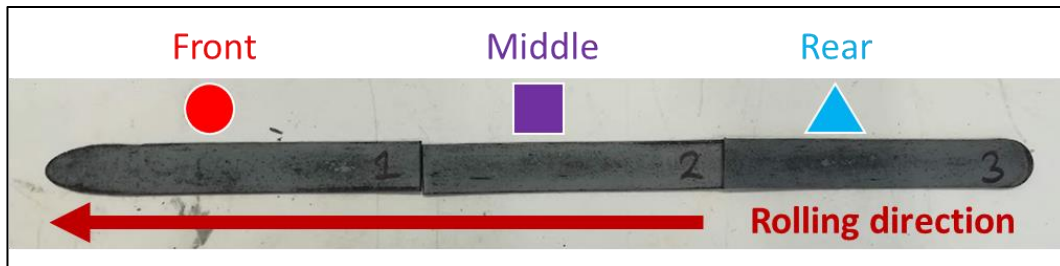
Figure 103 Labelled image of a rolled strip indicating the rolling direction and the regions from which each tensile bar was taken
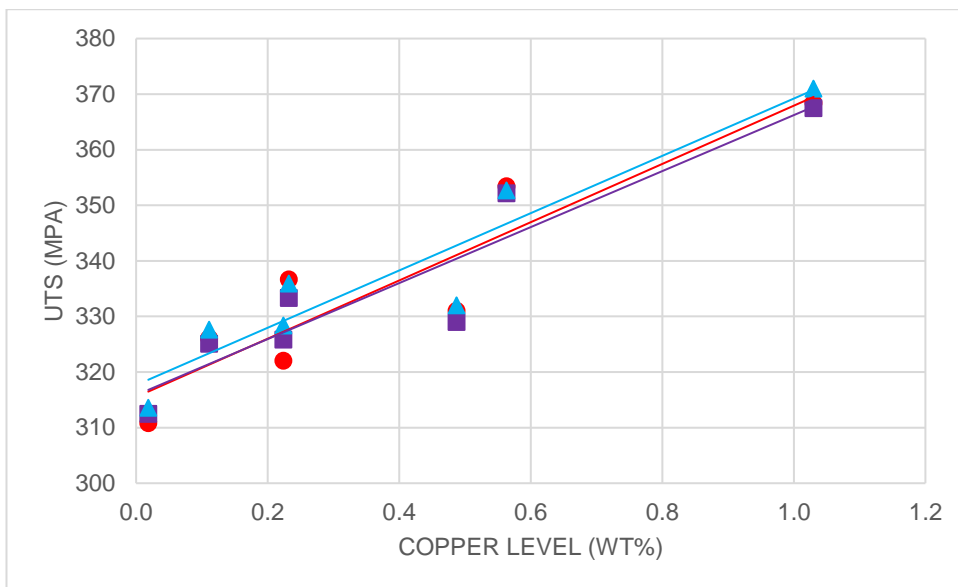
Figure 104 A comparison of the ultimate tensile strength of different regions of synthetic 3190 samples made using the 40g powder route with copper additions
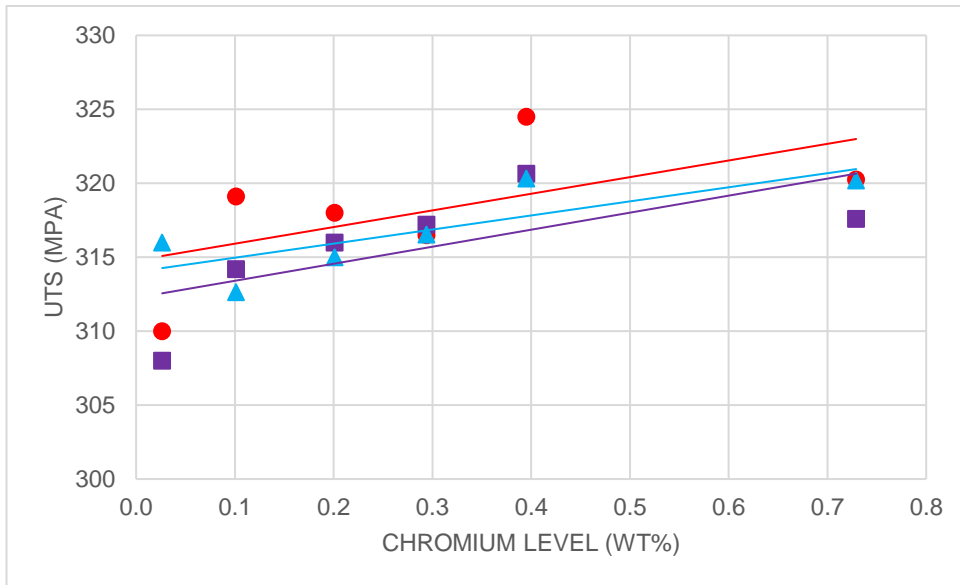
Figure 105 A comparison of the ultimate tensile strength of different regions of synthetic 3190 samples made using the 40g powder route with chromium additions
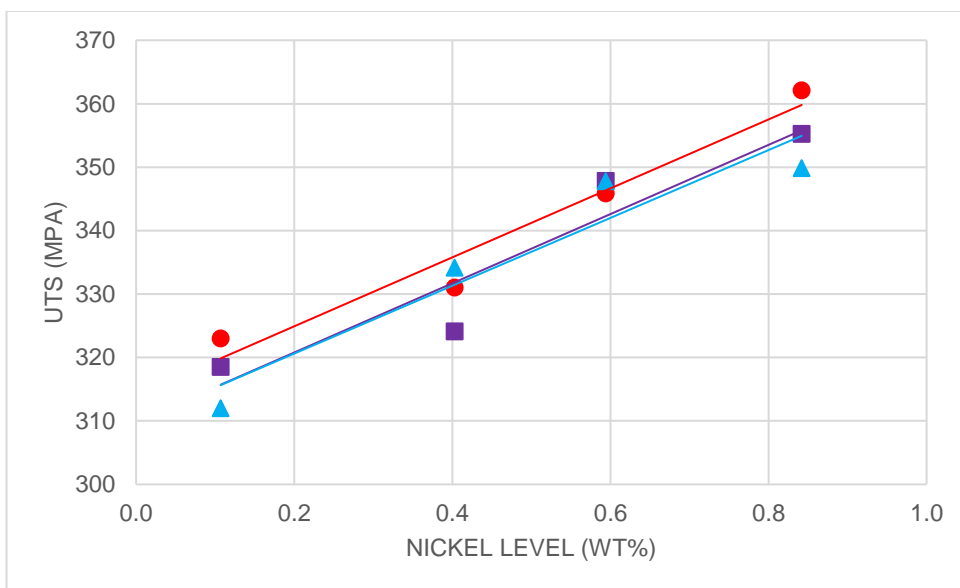
Figure 106 A comparison of the ultimate tensile strength of different regions of synthetic 3190 samples made using the 40g powder route with nickel additions
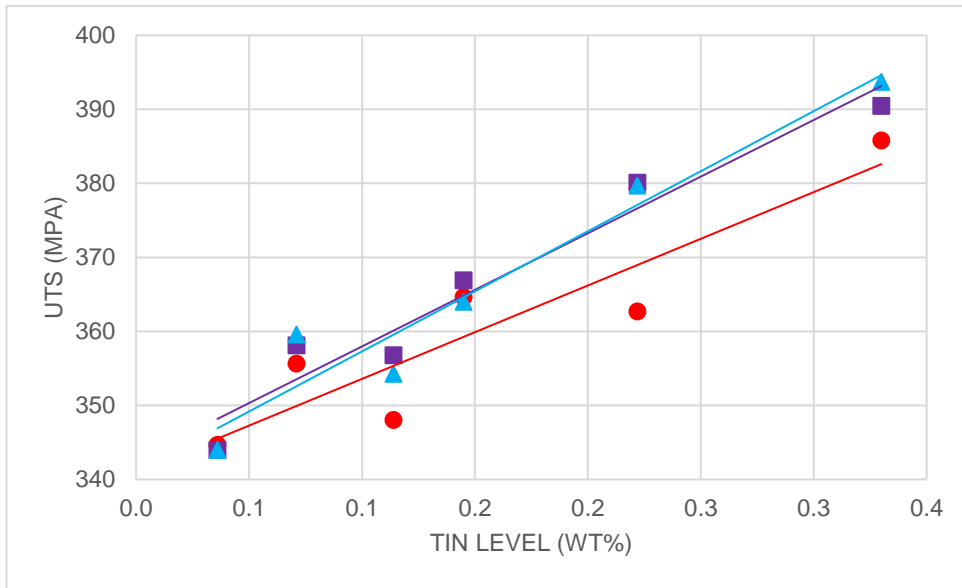
Figure 107 A comparison of the ultimate tensile strength of different regions of synthetic 3190 samples made using the 40g powder route with tin additions
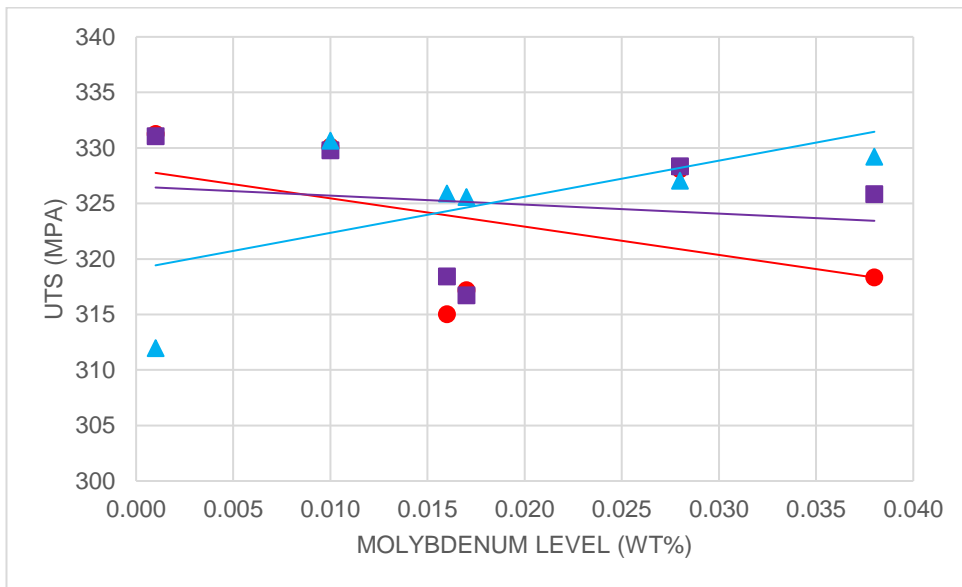
Figure 108 A comparison of the ultimate tensile strength of different regions of synthetic 3190 samples made using the 40g powder route with molybdenum additions
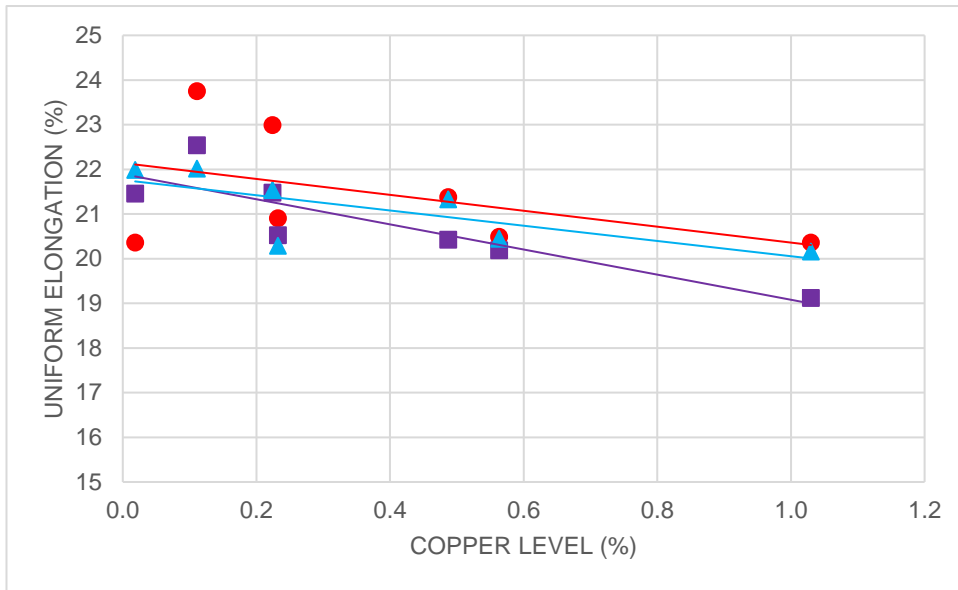
Figure 109 A comparison of the uniform elongation of different regions of synthetic 3190 samples made using the 40g powder route with copper additions
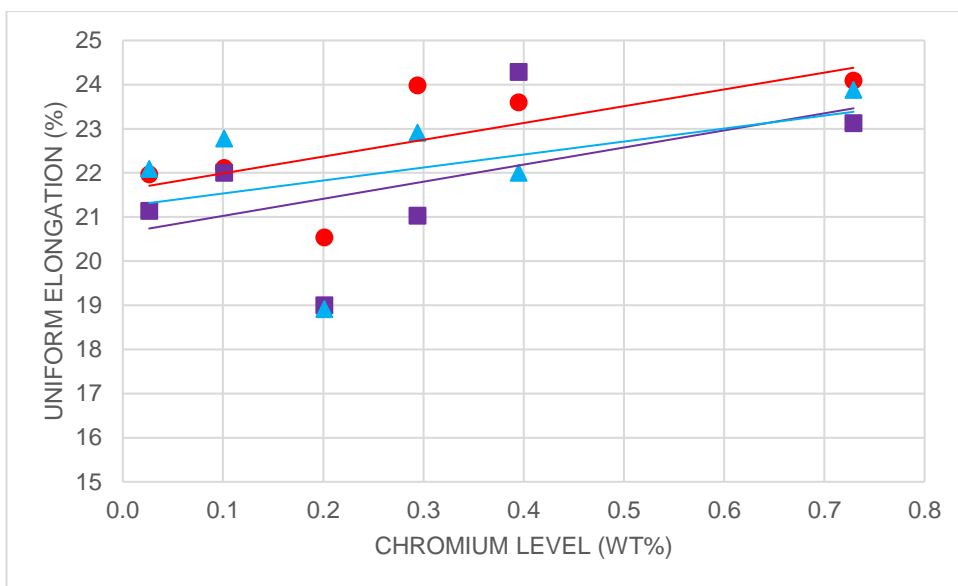
Figure 110 A comparison of the uniform elongation of different regions of synthetic 3190 samples made using the 40g powder route with chromium additions
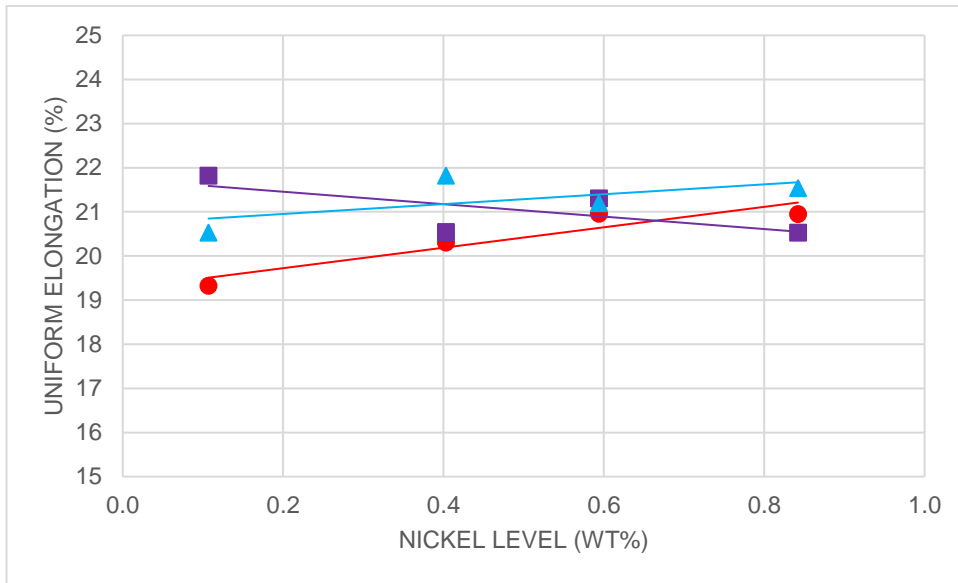
Figure 111 A comparison of the uniform elongation of different regions of synthetic 3190 samples made using the 40g powder route with nickel additions
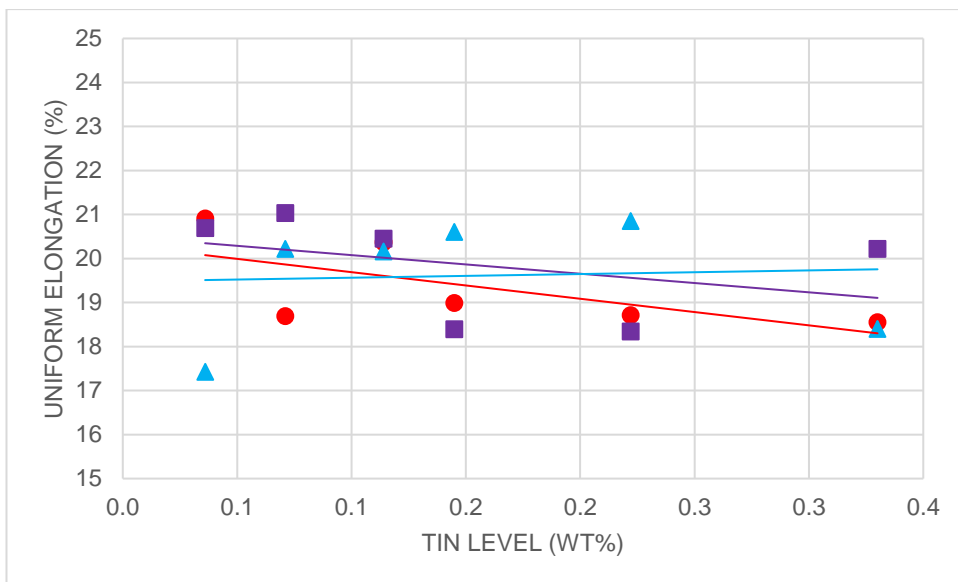
Figure 112 A comparison of the uniform elongation of different regions of synthetic 3190 samples made using the 40g powder route with tin additions
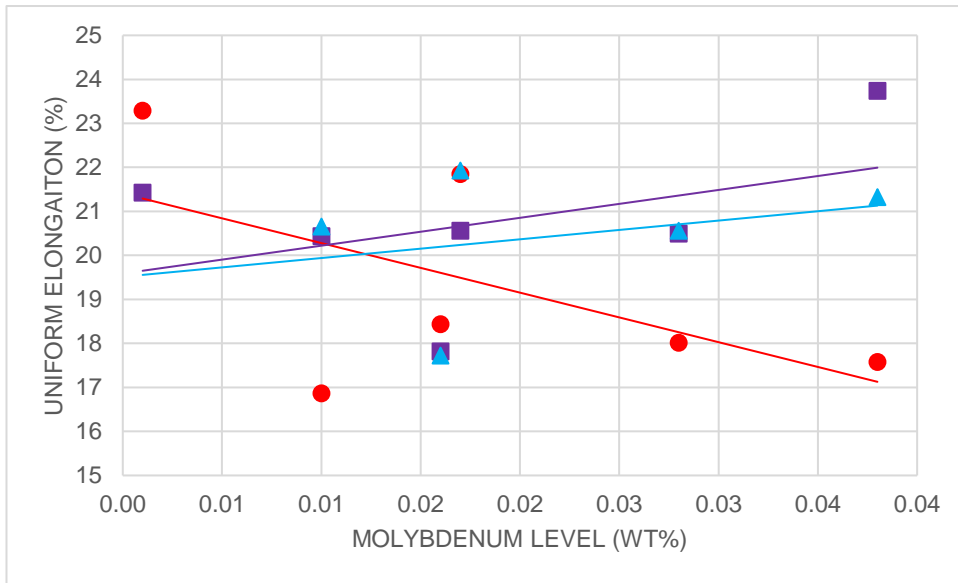
Figure 113 A comparison of the uniform elongation of different regions of synthetic 3190 samples made using the 40g powder route with molybdenum additions

Figure 104 to Figure 113 show a comparison between the properties of the tests completed from each point in the sample. The figures show that each point of the final rolled sample will have similar properties.

Regression analysis is a way to consider several measurable variables when looking at a set of data. The analyses here considered all the intentionally added elements and are discussed in more detail in 7.6.3.
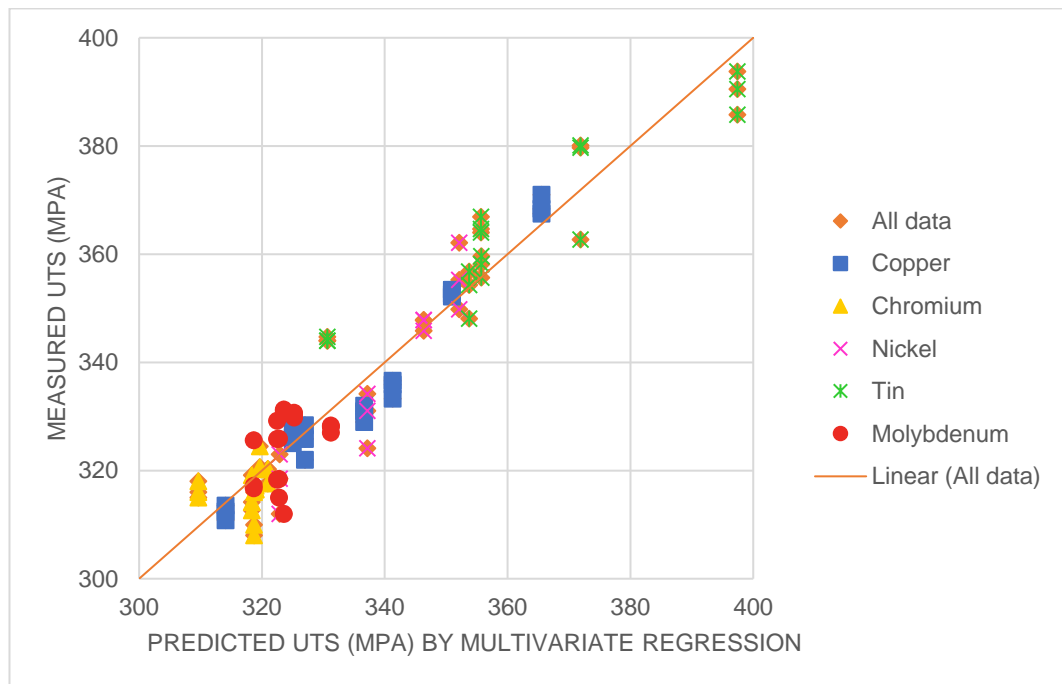
Figure 114 Regression analysis of the ultimate tensile strength of synthetic 3190 samples made using the 40g powder route with various residual additions – R²=0.917

The UTS regression analysis shown in Figure 114 produced the following equation;

UTS (MPa)=356+139C-373Si-226Mn-14Cr+27Mo+37Ni+1159Al+226Sn+43Cu
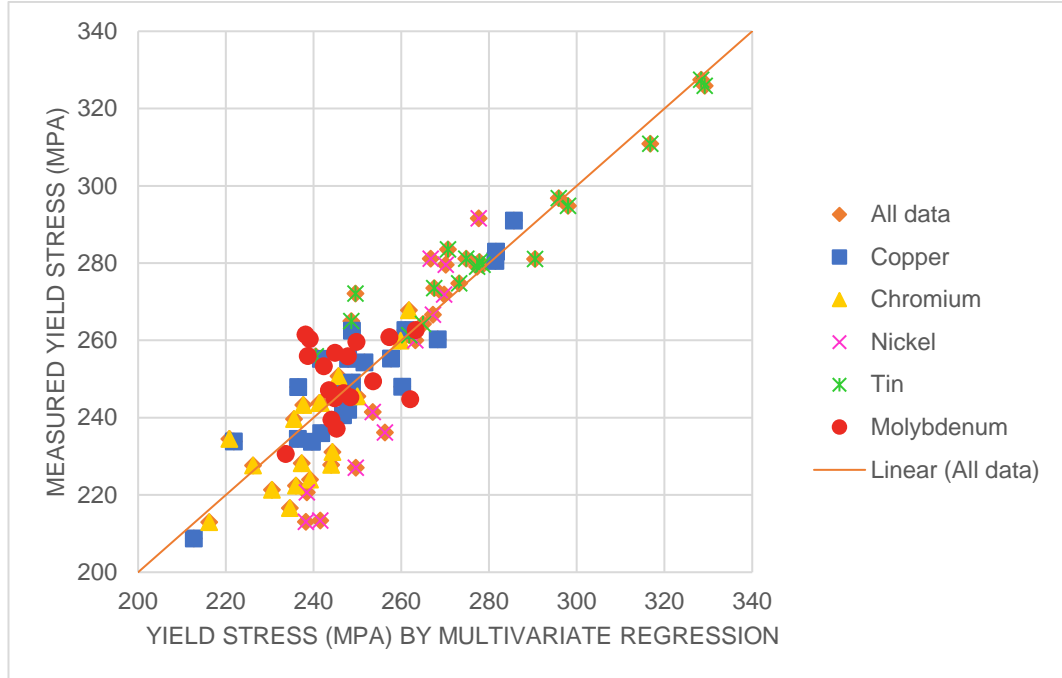
Figure 115 Regression analysis of the yield stress of synthetic 3190 samples made using the 40g powder route with various residual additions – R²=0.838

The yield stress regression analysis shown in Figure 115 produced the following equation;

YS(MPa)=243+734C-867Si+480Mn-3639P-

5268S+27Cr+469Mo+42Ni+263Al+270Sn+43Cu
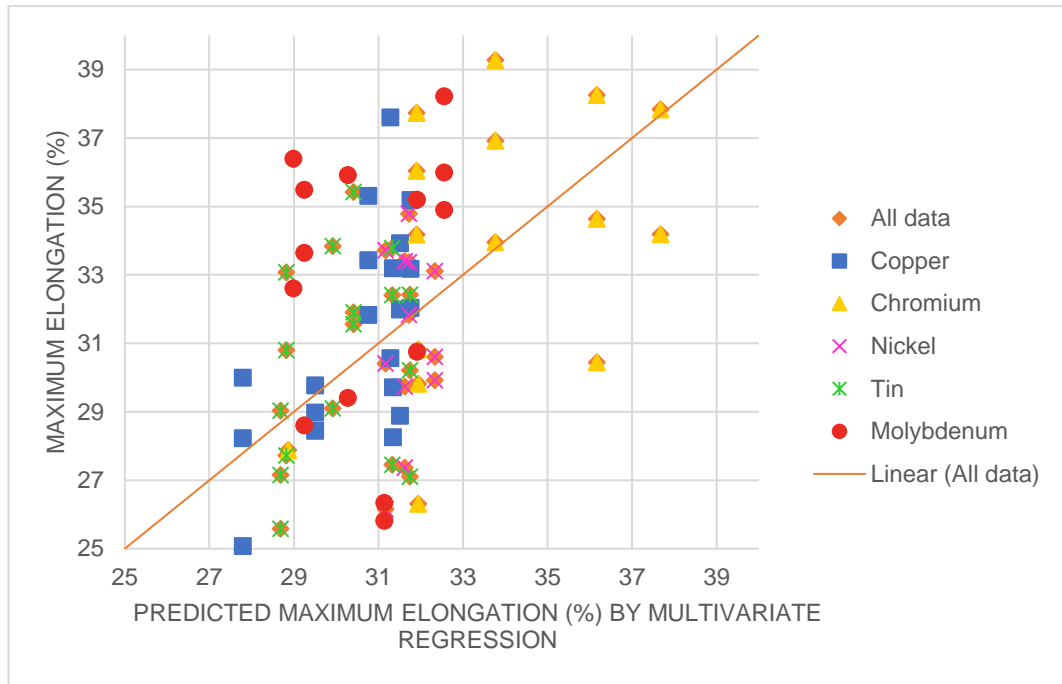
Figure 116 Regression analysis of the maximum elongation of synthetic 3190 samples made using the 40g powder route with various residual additions – R^2=0.243

The maximum elongation regression analysis shown in Figure 116 produced the following equation;

Elong_max(%)=32+85C-168Si+7Mn+7Cr-67Mo+0.2Ni-8Al-8Sn-Cu
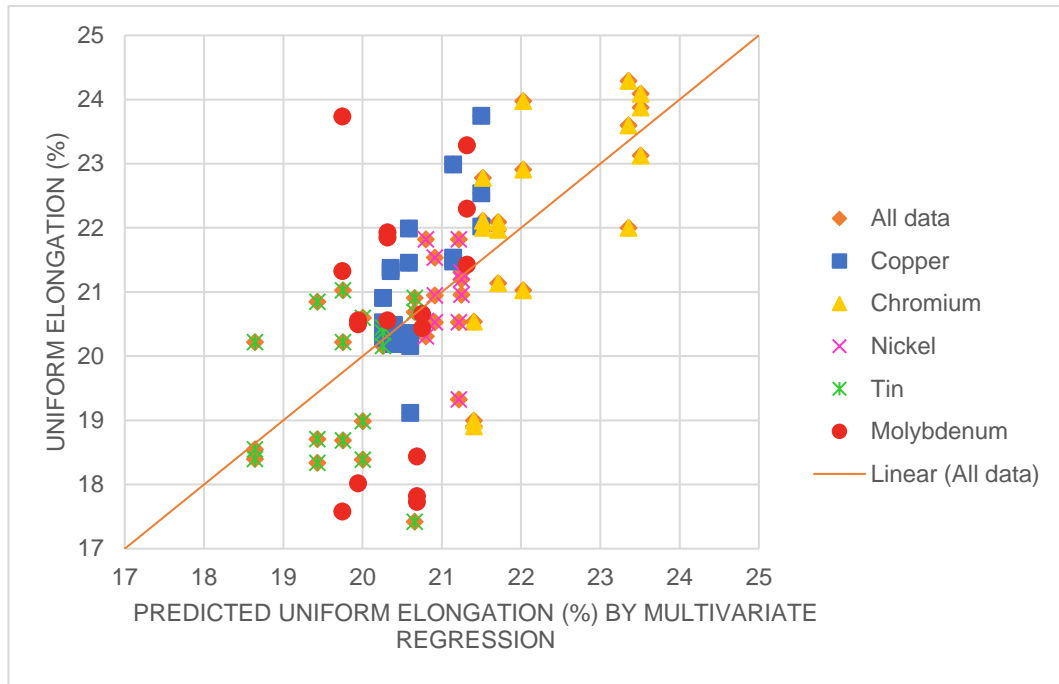
Figure 117 Regression analysis of the uniform elongation of synthetic 3190 samples made using the 40g powder route with various residual additions – $R^2=0.377$

The uniform elongation regression analysis shown in Figure 117 produced the following equation;

Elong_uniform=19+39C-9Si+16Mn+4Cr-31Mo-0.07Ni-63Al-8Sn-Cu

Figure 114 to Figure 117 shows the results of using a regression analysis method to determine a link between the composition and the final properties. The UTS and yield stress results show a strong correlation with the composition with R-values of 0.917 and 0.838 respectively. The maximum elongation and uniform elongation on the other hand showed little correlation, with R-values of 0.243 and 0.377 respectively.

6.1.4   MICROSCOPY
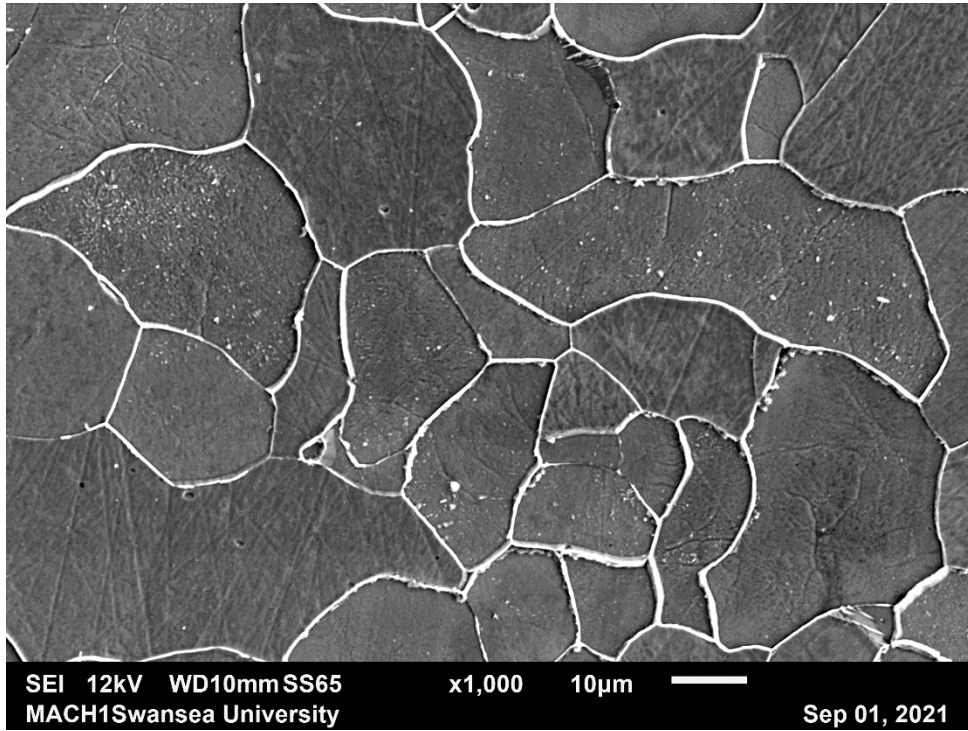
Figure 118 RAP40G_POW_CuX4 from [1]
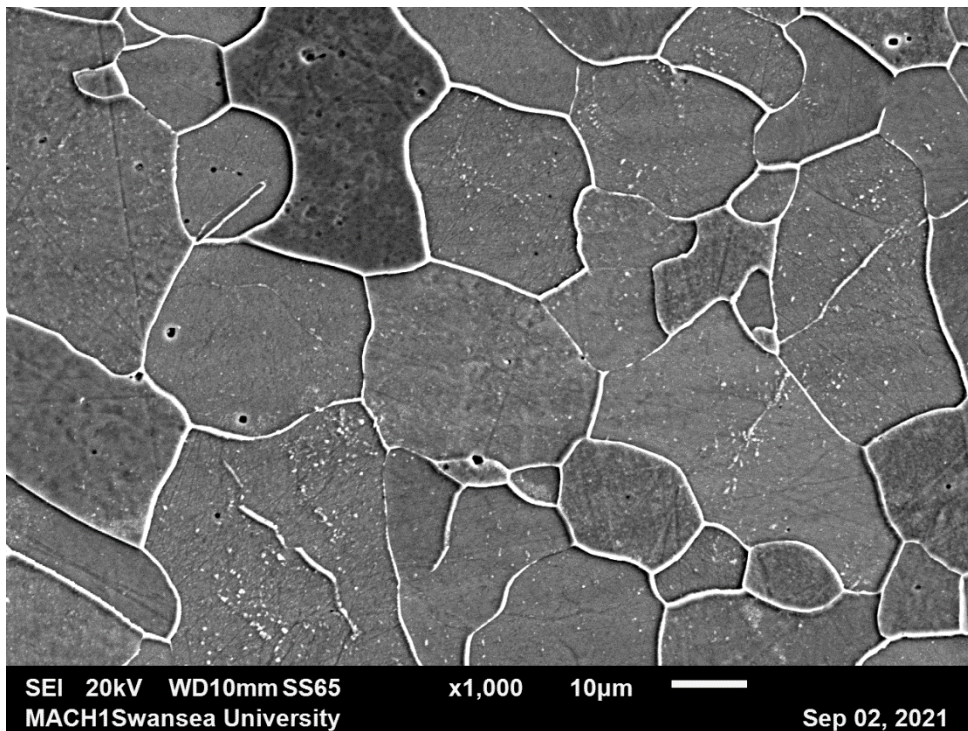
Figure 119 RAP40G_POW_CuX36 from [1]
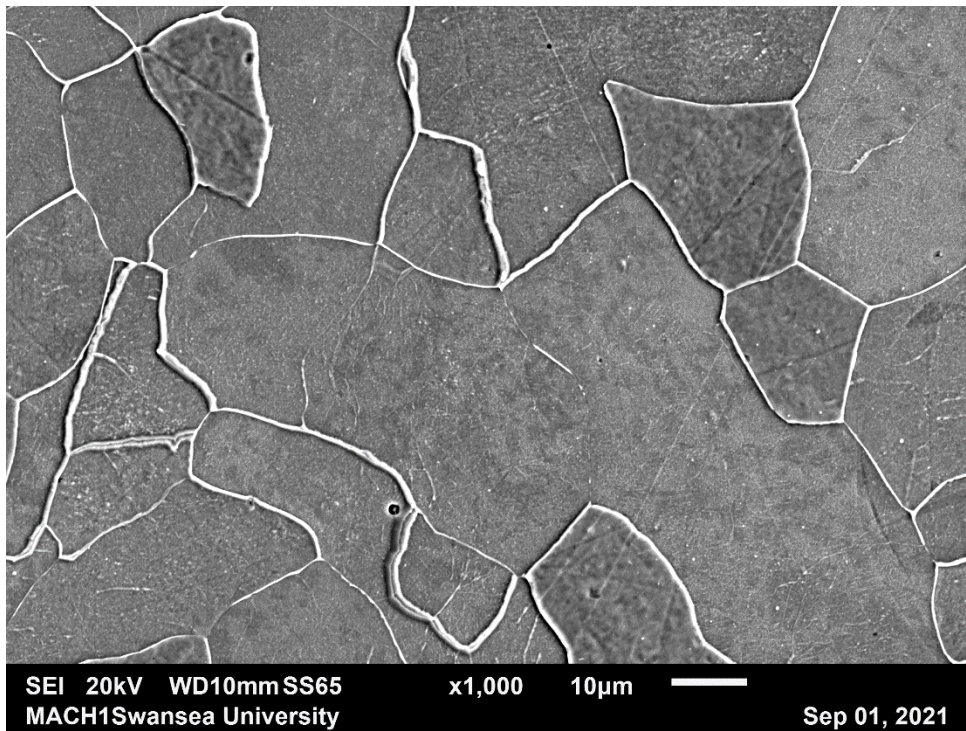
Figure 120 RAP40G_POW_CrX4 from [1]
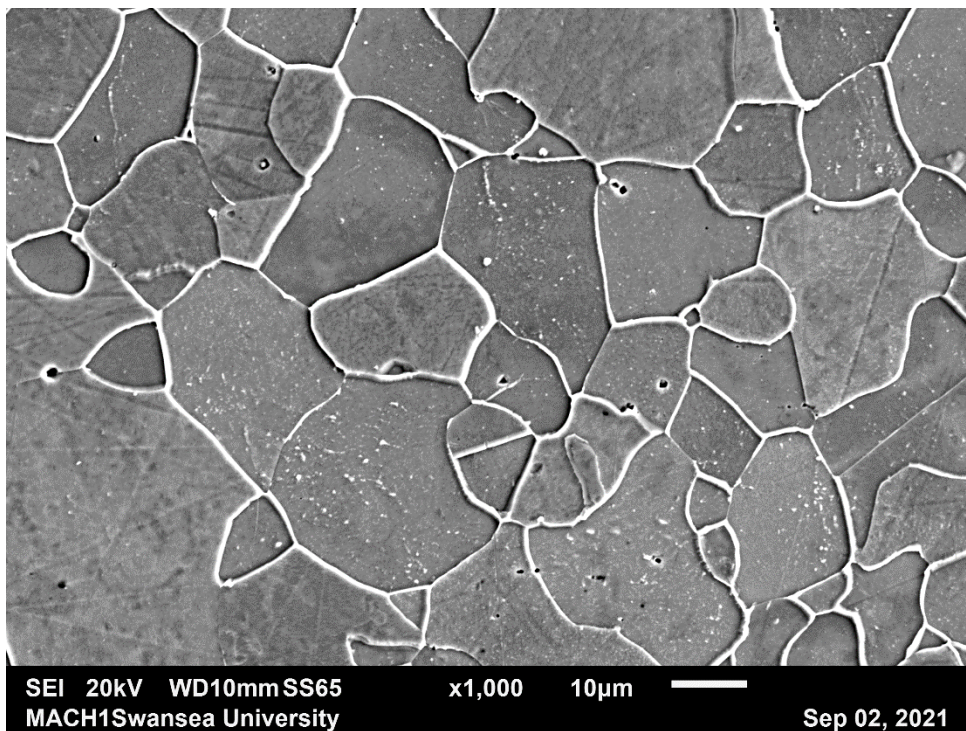
Figure 121 RAP40G_POW_CrX36 from [1]
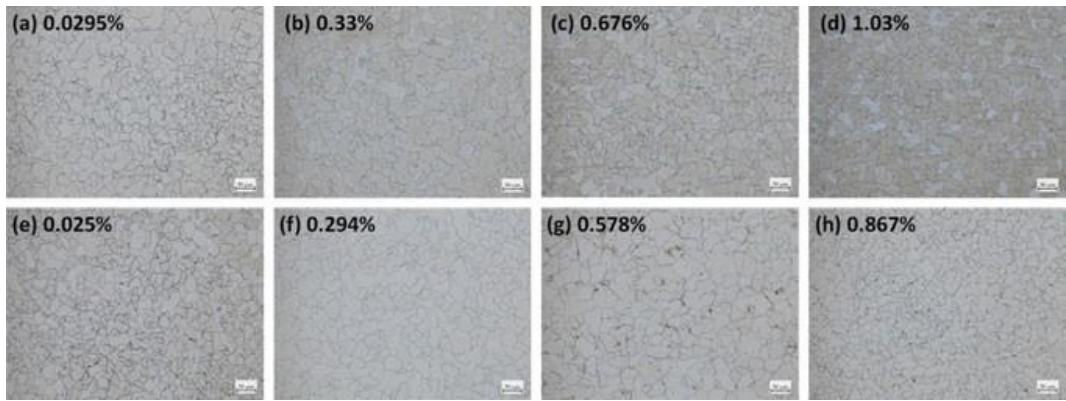
Figure 122 RAP40G_POW with copper and chromium additions optical images taken from [1], where images (a-d) show samples with increasing levels of copper, and (e-h) show samples with increasing levels of chromium
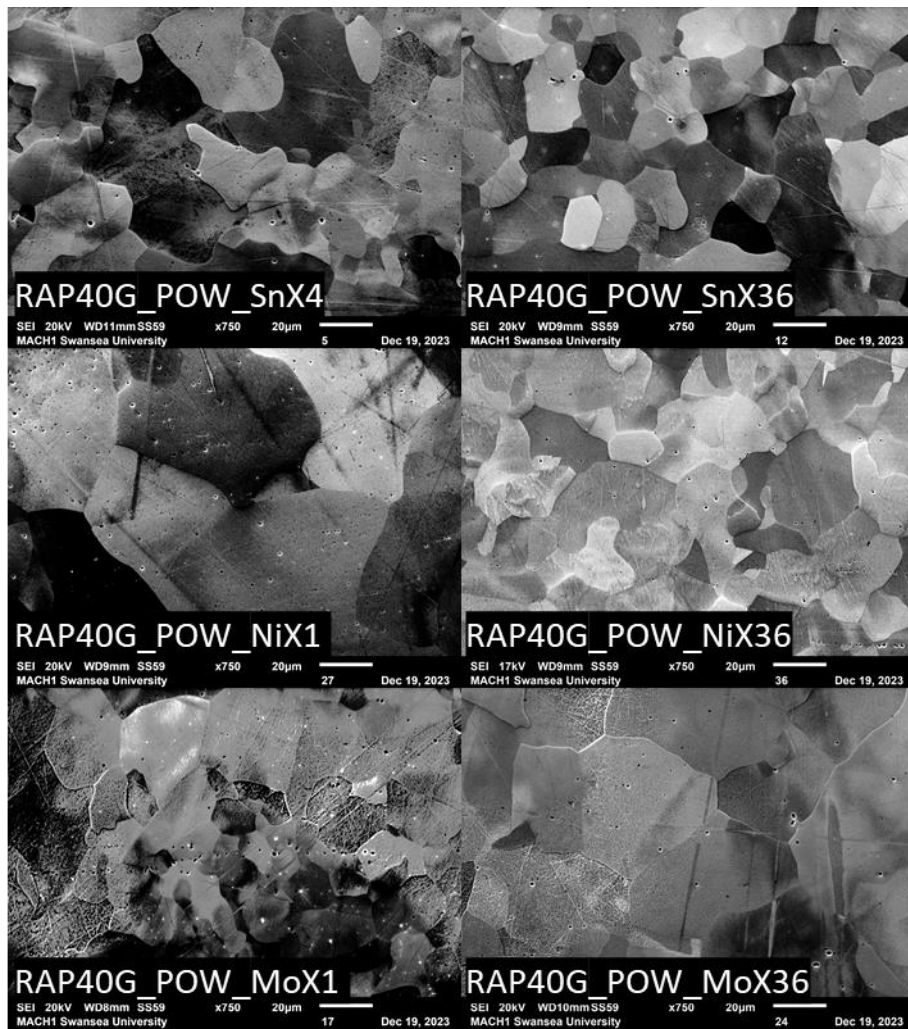
Figure 123 SEM image of RAP40G_POW with Ni, Mo and Sn

Figure 118 to Figure 123 shows optical and SEM microscopy of a selection of samples, showing the changes to the composition has no noticeable effect on the microstructures of the samples which all appear to be fully ferritic.

6.1.5 HARDNESS
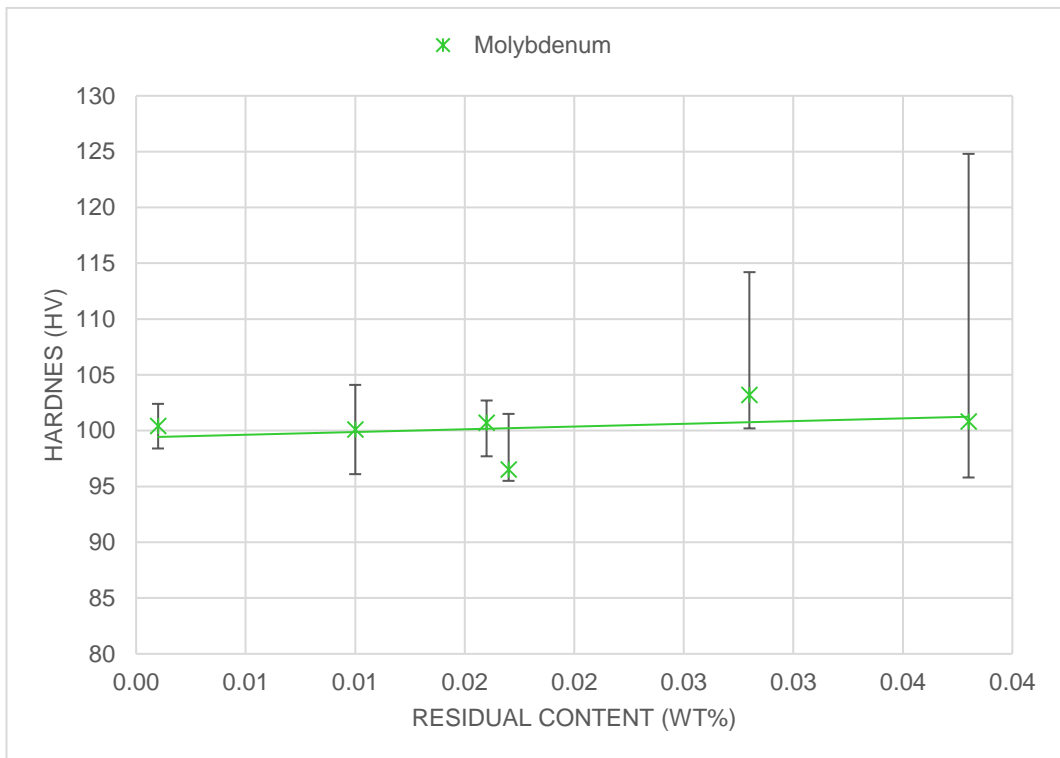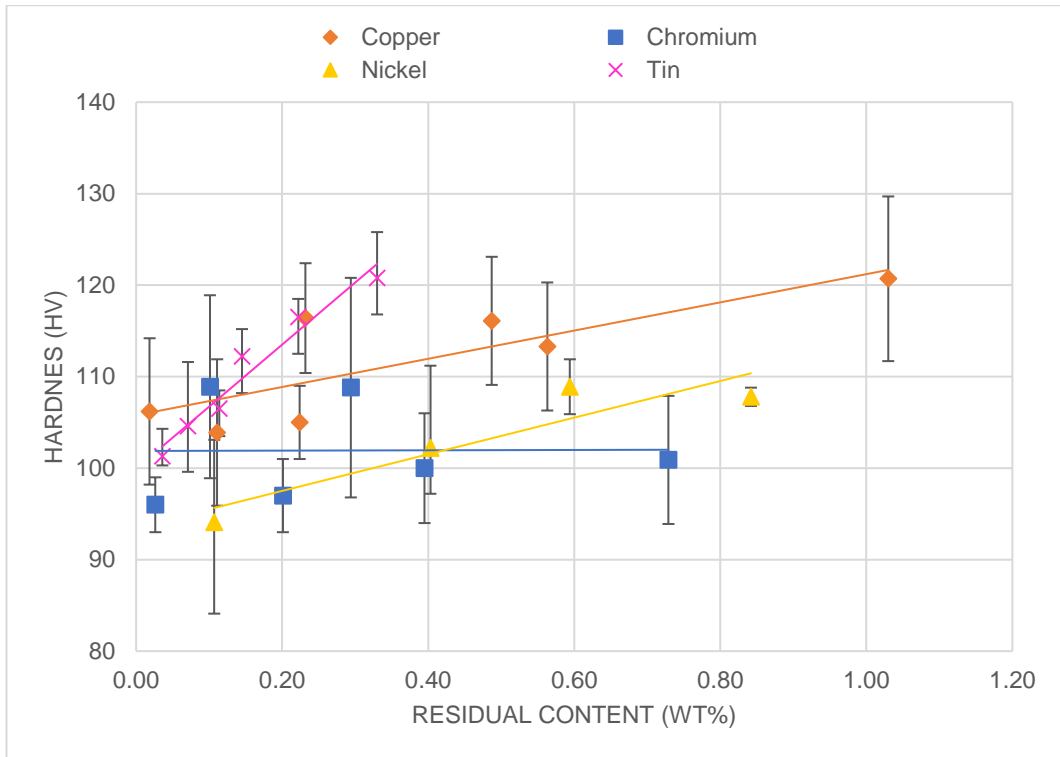
Figure 124 Hardness of RAP40G_POW

The hardness of the samples are shown in Figure 124 where increasing copper, nickel and tin are shown to have a hardening effect on the steel samples.
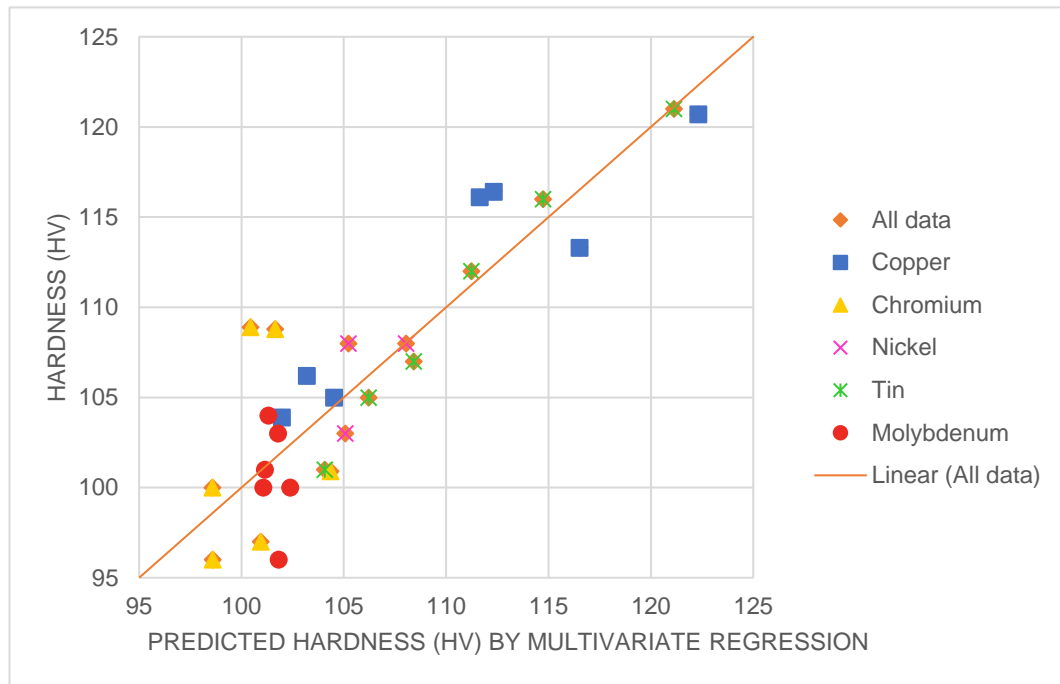
Figure 125 Regression analysis of the average hardness of synthetic 3190 samples made using the 40g powder route with various residual additions, without removing any anomalous data points – R2=0.764

The hardness regression analysis shown in Figure 125 produced the following equation;

Hardness(Hv)=124-105C+24Si-164Mn-Cr-8Mo+8Ni+61Al+57Sn+22Cu

Figure 125 shows that a regression analysis approach presents a correlation between the sample composition and the hardness values measured in the sample.
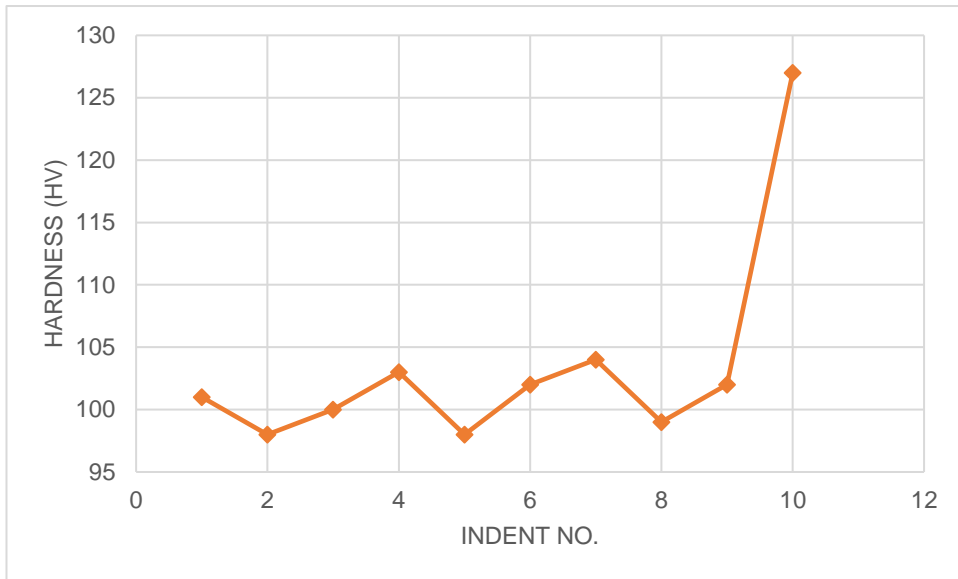
Figure 126 Hardness values measured by each indent of the synthetic 3190 sample made using the 40g powder route with a molybdenum addition of 36x the industrial limit, indicating a situation where an anomalous data point was removed from the data set
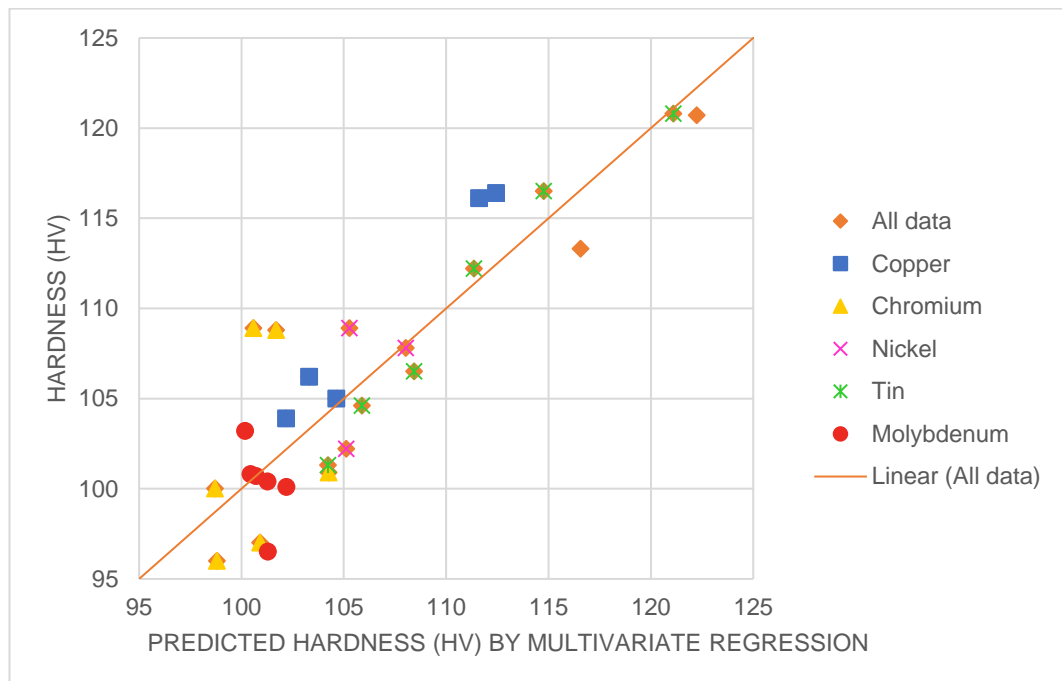
Figure 127 Regression analysis of the average hardness of synthetic 3190 samples made using the 40g powder route with various residual additions, after removing anomalous data points from the average hardness calculation of each sample – R2=0.770

The hardness regression analysis shown in Figure 127 produced the following equation;

Hardness(Hv)=125-100C+23Si-165Mn-2Cr-48Mo+7Ni+28Al+56Sn+22Cu

Figure 127 shows that discounting anomalous results from the regression analysis approach has a slight impact on the strength of the correlation, increasing the R-value to 0.770 compared to 0.764 in Figure 126.

6.1.6   SUMMARY OF FINAL 3190 40G TESTING

Using the 40g method to investigate 3190 material allowed for multiple test specimens to be produced per composition with a compositional consistency that has improved compared to previous methods. The higher levels of residual elements were generally shown to strengthen and harden the material whilst reducing the ductility.

6.2   DP800 RESULTS (40G/SOLIDS)

6.2.1   INTRODUCTION AND SAMPLE OVERVIEW DP800 40G SOLIDS ROUTE)

The difficulties achieving a consistent composition eventually lead to the use of solids in the 40g route. A master alloy method was developed and was able to minimise the material losses, allowing the effects of the residual elements to be highlighted.

6.2.1.1   METHOD SUMMARY (DP800 40G MASTER ALLOY ROUTE)

- 40g sample size
- Gravity cast
- Solid feedstock (lab made master alloys)
- 2-3 tensile bars per sample (dependant on shape of mould)
- Hot rolling possible
- Samples large enough for easy OES testing

Due to the difficulty in achieving an accurate composition, especially with smaller element levels, a number of master alloys of each of these elements was investigated to provide a solution. The elements were diluted using electrolytic iron to a target level

of about 1%, 5%, or 10%, allowing the elements required in the smallest quantities to be much easier to weigh out. These master alloys were made in 40g batches using either existing ferro-alloys, or element solids in addition to the electrolytic iron. The casts were cold rolled where possible, and hot rolled in the case of more brittle alloys, until a point where they were easy to cut into pieces. The subsequent alloys were then weighed out to the required masses and mixed with another mass of electrolytic iron to make up a new 40g sample. The electrolytic iron was compacted before melting to assist with the melting process.
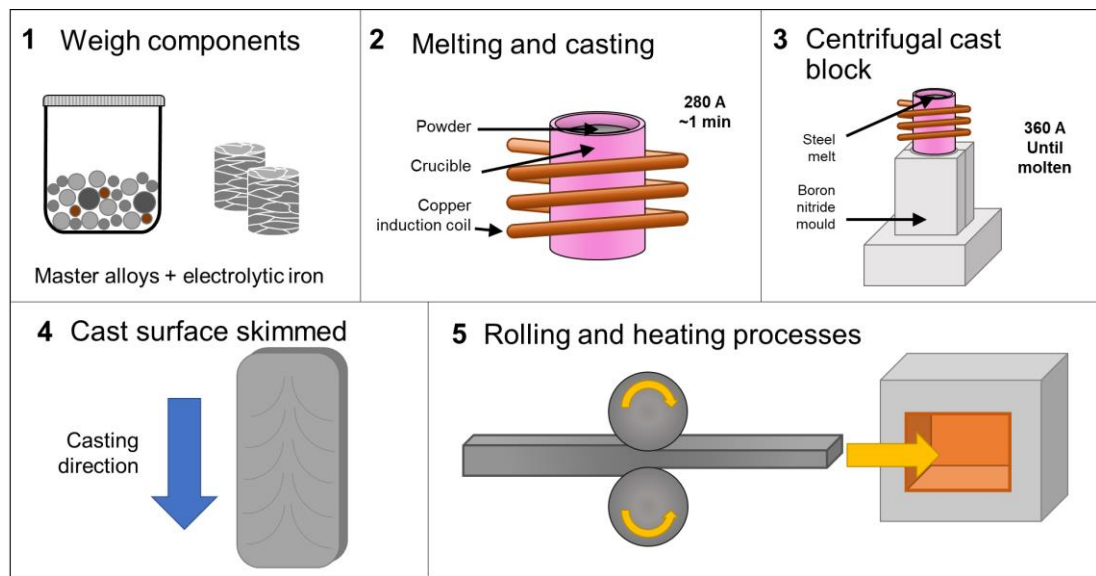
Figure 128 Overview of RAP40G _MA route

The samples considered in this section were as follows, where the notation used describe the total levels of the residual elements is described as multiples of the current limit.

Table 27 Synthetic DP800 samples made using the master alloy method

Sample Ref	Alloy	Route	Feedstock (powder or solid)	Elements added
RAP40G_MA_SOL_RF	DP800	40g	Solid (master alloy)	Fe (Bal), C, Mn, Si, Ti, Nb, Al and Cr
RAP40G_MA_SOL_CuX1	DP800	40g	Solid (master alloy)	Fe (Bal), C, Mn, Si, Ti, Nb, Al and Cr + residual Cu
RAP40G_MA_SOL_CuX4	DP800	40g	Solid (master alloy)	Fe (Bal), C, Mn, Si, Ti, Nb, Al and Cr + residual Cu

RAP40G_MA_SOL_CuX8	DP800	40g	Solid (master alloy)	Fe (Bal), C, Mn, Si, Ti, Nb, Al and Cr + residual Cu
RAP40G_MA_SOL_CuX12	DP800	40g	Solid (master alloy)	Fe (Bal), C, Mn, Si, Ti, Nb, Al and Cr + residual Cu
RAP40G_MA_SOL_CuX16	DP800	40g	Solid (master alloy)	Fe (Bal), C, Mn, Si, Ti, Nb, Al and Cr + residual Cu
RAP40G_MA_SOL_CuX24	DP800	40g	Solid (master alloy)	Fe (Bal), C, Mn, Si, Ti, Nb, Al and Cr + residual Cu
RAP40G_MA_SOL_CuX36	DP800	40g	Solid (master alloy)	Fe (Bal), C, Mn, Si, Ti, Nb, Al and Cr + residual Cu
RAP40G_MA_SOL_SnX1	DP800	40g	Solid (master alloy)	Fe (Bal), C, Mn, Si, Ti, Nb, Al and Cr + residual Sn
RAP40G_MA_SOL_SnX4	DP800	40g	Solid (master alloy)	Fe (Bal), C, Mn, Si, Ti, Nb, Al and Cr + residual Sn
RAP40G_MA_SOL_SnX8	DP800	40g	Solid (master alloy)	Fe (Bal), C, Mn, Si, Ti, Nb, Al and Cr + residual Sn
RAP40G_MA_SOL_SnX12	DP800	40g	Solid (master alloy)	Fe (Bal), C, Mn, Si, Ti, Nb, Al and Cr + residual Sn
RAP40G_MA_SOL_SnX16	DP800	40g	Solid (master alloy)	Fe (Bal), C, Mn, Si, Ti, Nb, Al and Cr + residual Sn
RAP40G_MA_SOL_SnX24	DP800	40g	Solid (master alloy)	Fe (Bal), C, Mn, Si, Ti, Nb, Al and Cr + residual Sn
RAP40G_MA_SOL_SnX36	DP800	40g	Solid (master alloy)	Fe (Bal), C, Mn, Si, Ti, Nb, Al and Cr + residual Sn
RAP40G_MA_SOL_NiX1	DP800	40g	Solid (master alloy)	Fe (Bal), C, Mn, Si, Ti, Nb, Al and Cr + residual Ni
RAP40G_MA_SOL_NiX4	DP800	40g	Solid (master alloy)	Fe (Bal), C, Mn, Si, Ti, Nb, Al and Cr + residual Ni
RAP40G_MA_SOL_NiX8	DP800	40g	Solid (master alloy)	Fe (Bal), C, Mn, Si, Ti, Nb, Al and Cr + residual Ni
RAP40G_MA_SOL_NiX12	DP800	40g	Solid (master alloy)	Fe (Bal), C, Mn, Si, Ti, Nb, Al and Cr + residual Ni
RAP40G_MA_SOL_NiX16	DP800	40g	Solid (master alloy)	Fe (Bal), C, Mn, Si, Ti, Nb, Al and Cr + residual Ni
RAP40G_MA_SOL_NiX24	DP800	40g	Solid (master alloy)	Fe (Bal), C, Mn, Si, Ti, Nb, Al and Cr + residual Ni

RAP40G_MA_SOL_NiX36	DP800	40g	Solid (master alloy)	Fe (Bal), C, Mn, Si, Ti, Nb, Al and Cr + residual Ni

Table Composition of the initial master alloys made in a 40g batch

6.2.2 COMPOSITION

	C	Mn	Al	Si	S	P	Ti	Cr
Fe-Si	0	0.003		4.664	0.0008			0.001
Fe-Al	0.027	0.009	0.271	0.058	0.0019	0.0024	0	0.012
Fe-Cr	0	0	0	0.031	0.0061	0.013	0	9.971
Fe-Ti	0.015	0.002	0.038	0.019	0.0007	0.0016	0.857	0.007
Fe-Nb	0.022	0.01	0	0.042	0.0026	0.003	0.007	0.001
Fe-Mn-C	0.938	13.981	0	0.031	0.0005	0.0099	0	0.029
(cont.)	Nb	Ta	Mo	Ni	Mg	Co	V	W
Fe-Si	0		0.004	0	0.0001			
Fe-Al	0	0.007	0.003	0.004		0.001	0.018	0
Fe-Cr	0		0	0	0.005		0.001	0.003
Fe-Ti	0.004	0.007	0.006	0.005		0.003	0.037	0
Fe-Nb	1.008	0.013	0.003	0		0.001	0.004	0
Fe-Mn-C	0.004		0.002	0		0.005	0.001	0

Table 28 Composition of the first batch of synthetic DP800 made using lab-made master alloys tested using the MACH1 OES

		MACH1 OES							
		C	Si	Mn	Cr	Al	Nb	Ti	Fe
		0.135	0.25	1.81	0.55	0.04	0.025	0.03	Bal.
Cast #1	Mean	0.118	0.246	1.622	0.48	0.0056	0.025	0.023	97.23
	SD	0.0083	0.015	0.066	0.021	0.001	0.0015	0.00063	0.112
Cast #2	Mean	0.107	0.258	1.565	0.505	0.0065	0.027	0.026	97.25
	SD	0.0051	0.0075	0.038	0.0001	0.00059	0.0014	0.00089	0.053
Cast #3	Mean	0.114	0.273	1.593	0.509	0.0067	0.026	0.022	97.2
	SD	0.0083	0.033	0.038	0.018	0.0031	0.0025	0.0011	0.098

Table 29 Composition of the second batch of synthetic DP800 made using lab-made master alloys tested using the SaMI OES

		SaMI OES							
		C	Si	Mn	Cr	Al	Nb	Ti	Fe
		0.135	0.25	1.81	0.55	0.04	0.025	0.03	Bal.

		C	Si	Mn	Cr	Al	Nb	Ti	Fe
Cast #1	Mean	0.12	0.278	1.672	0.551	0.004	0.025	0.02	97.255
	SD	0.004	0.003	0.007	0.002	0	0	0.001	0.011
Cast #2	Mean	0.111	0.286	1.624	0.549	0.005	0.026	0.022	97.303
	SD	0.004	0.003	0.008	0.004	0	0.001	0	0.011

Table 30 Composition of the third batch of residual-free synthetic DP800 sample with adjusted composition

	C	Si	Mn	Cr	Al	Nb	Ti	Fe
Target	0.115-0.145	0.2-0.3	1.72-1.92	0.5-0.6	0.02-0.08	0.02-0.03	0.02-0.04	Bal
Sample 1	0.112	0.255	1.738	0.535	0.051	0.025	0.022	97.191
Sample 2	0.111	0.251	1.723	0.546	0.004	0.025	0.019	97.251
Sample 3	0.122	0.253	1.737	0.542	0.077	0.025	0.028	97.129
Average	0.115	0.253	1.733	0.541	0.044	0.025	0.023	97.190
SD	0.003-0.013	0.002-0.007	0.005-0.025	0.002-0.003	0.001-0.005	0-0.001	0.001	0.01-0.025

Table 31 Composition of synthetic DP800 made using the master alloy method, measured with an OES

		Mn	C	Si	Cr	Al	Nb	Ti	Ni	Cu	Sn	Fe	Target Res
Cu	Cu1	1.794	0.152	0.24	0.555	0.108	0.029	0.028	0.006	0.028	0.003	96.995	0.024
	Cu4	1.807	0.151	0.244	0.557	0.106	0.029	0.028	0.006	0.112	0.003	96.894	0.096
	Cu8	1.789	0.15	0.244	0.554	0.102	0.029	0.028	0.006	0.207	0.003	96.828	0.192
	Cu12	1.808	0.145	0.245	0.557	0.103	0.028	0.028	0.006	0.283	0.003	96.732	0.288
	Cu16	1.799	0.133	0.298	0.554	0.105	0.029	0.028	0.005	0.378	0.003	96.6	0.384
	Cu24	1.746	0.149	0.248	0.555	0.106	0.029	0.028	0.006	0.601	0.003	96.468	0.576
	Cu36	1.777	0.148	0.238	0.558	0.101	0.029	0.028	0.006	0.892	0.003	96.158	0.864
Sn	Sn1	1.769	0.15	0.246	0.554	0.103	0.028	0.029	0.005	0	0.011	97.043	0.01
	Sn4	1.775	0.15	0.244	0.553	0.111	0.029	0.028	0.006	<0.000	0.043	96.997	0.04
	Sn8	1.828	0.154	0.241	0.553	0.106	0.029	0.028	0.006	<0.000	0.083	96.91	0.08
	Sn12	1.842	0.156	0.238	0.561	0.109	0.028	0.024	0.006	0	0.126	96.845	0.12
	Sn16	1.995	0.172	0.244	0.589	0.126	0.029	0.029	0.007	0	0.169	96.577	0.16
	Sn24	1.785	0.154	0.244	0.556	0.114	0.03	0.028	0.005	0	0.256	96.761	0.24
	Sn36	1.792	0.141	0.251	0.561	0.099	0.028	0.028	0.005	<0.001	0.357	96.702	0.36
Ni	Ni1	1.752	0.152	0.292	0.554	0.111	0.029	0.028	0.028	<0.000	0.003	96.986	0.018
	Ni4	1.779	0.151	0.298	0.559	0.099	0.029	0.028	0.072	<0.000	0.003	96.92	0.072
	Ni8	1.764	0.151	0.293	0.554	0.109	0.029	0.029	0.15	<0.000	0.003	96.856	0.144
	Ni12	1.798	0.154	0.285	0.554	0.114	0.029	0.028	0.21	<0.000	0.003	96.764	0.216
	Ni16	1.831	0.162	0.304	0.556	0.101	0.029	0.029	0.278	0	0.003	96.628	0.288
	Ni24	1.818	0.145	0.291	0.559	0.113	0.029	0.028	0.415	<0.000	0.003	96.536	0.432
	Ni36	1.801	0.134	0.295	0.556	0.106	0.028	0.028	0.599	<0.000	0.003	96.387	0.648
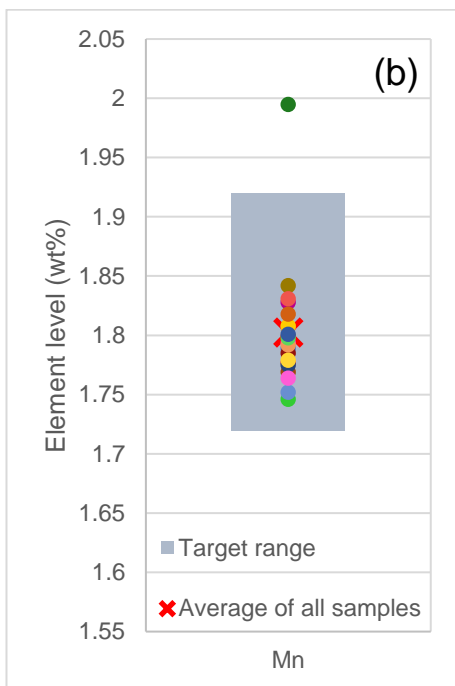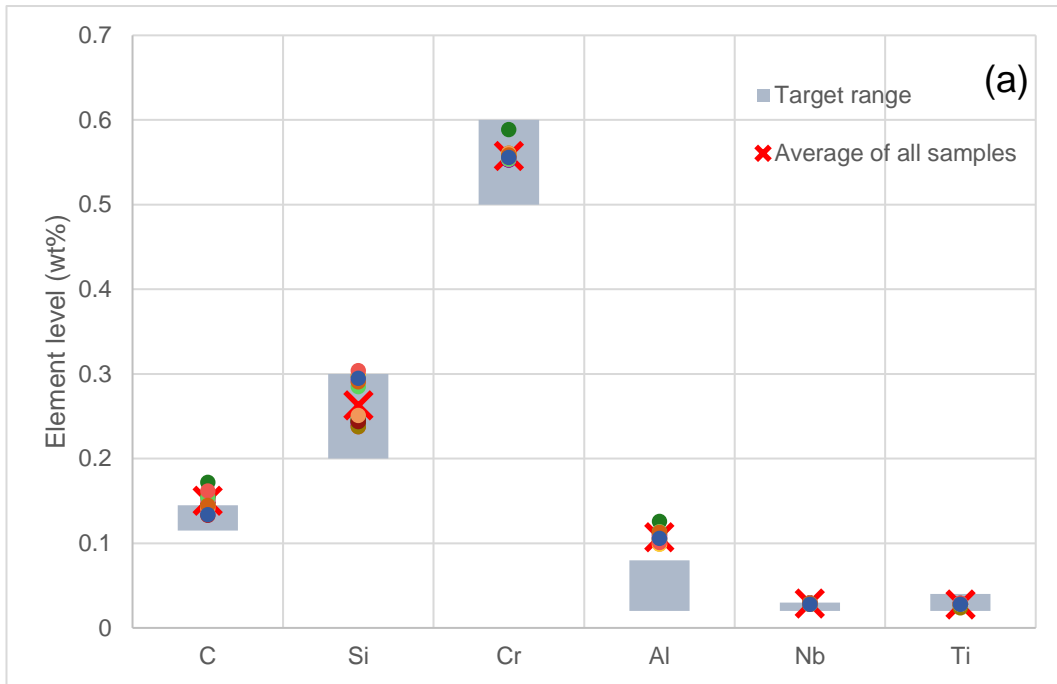
Figure 129 (a) & (b) Composition of RAP40G_MA_SOL, comparing the measured values to the target range. Manganese is shown in Figure (b) due to the difference in scale needed

Figure 129 indicates the spread of compositions measured in each of the samples with residual additions. The full data set for the final samples is available in Table 31.
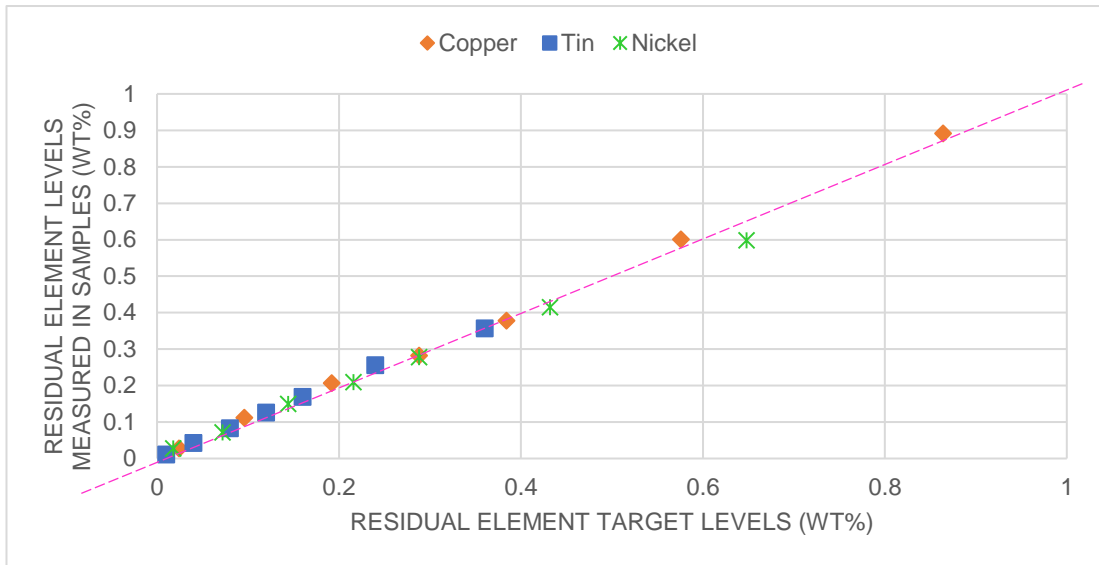
Figure 130 Comparison between the measured residual levels and target values in the RAP40G_MA_SOL samples made using the master alloy method

When looking at the compositions shown in Table 29 one clear issue with samples is the lack of aluminium. This was a reoccurring source of inconsistency in previous samples and it was clear in the aluminium master alloy that even introducing aluminium via a ferro-alloy still leads to significant element losses, assumed to be due to oxidation, but the exact cause was not able to be traced. In the first batch of residual-free DP800 there was no attempt made to compensate for the element losses to determine how much aluminium was being lost in the melt. The resulting composition indicated that the amount of aluminium left in the samples were almost completely undetectable by the OES. It was decided that a more accurate way of determining the aluminium losses was to look to the aluminium loss in the master alloy and use this to calculate an additional amount of aluminium to add to the melt to compensate for the losses. That gave a compensation requirement of 0.29g per 40g, equivalent of an extra 0.12wt% aluminium in addition to the aluminium requirement in the final product. Looking at the aluminium losses from the 40g aluminium master alloy, the aim composition was 1wt% Al, but the final composition, as measured by an OES gave an aluminium level of 0.271wt%. This means there were losses of approximately 0.2916g Al from the added to the master alloy via the ferro aluminium, assuming the given composition of the ferro aluminium matched what was given on the data sheet provided.

A single sample, aiming to test the effectiveness of the compensation method for the different elements, was made after the first batch with an adjusted composition focused on improving the aluminium, carbon and manganese. These elements were chosen because these elements were outside the acceptable composition range for the specific alloy. The silicon level was also adjusted because, despite being within the required range, the achieved composition was still higher than target value and the purpose of the sample was to achieve a composition as close to the target as possible.

The aluminium compensation was added in the form of a solid mass of aluminium to the initial melt with the initial iron flakes and other master alloys. The aluminium master alloy was the last lump added to the melt. This aimed to use the pure aluminium lump to react with and remove the oxygen within the sample, which is likely the cause of the aluminium losses due to the far higher reactivity of aluminium compared to iron. As can be seen from Table 30, the third attempt at achieving a DP800 composition gave an aluminium level considerably higher than the initial batch, but this was a significant over compensation, and the aluminium was several times higher than the target composition, meaning there was a need to make another sample with a further adjusted aluminium level. This initial test sample had a total aluminium addition of 0.29g pure aluminium solids and 5.7g of the 0.271wt% aluminium master alloy. The total aluminium added to the sample from these two sources was 0.31g Al out of a total initial mass of all combined elements before melting of 40.43g.

The aluminium level in the next completed sample was measured to be 0.688wt%, equivalent to approximately 0.235g aluminium spread throughout the whole 40g sample. This means there is a loss of only 0.07g Al during the melting, in contrast to the master alloy production, which lost 0.29g Al. This leads to the suggestion that the aluminium losses during melting are not consistent between samples, or there has been a miscalculation at some point in the process.

Due to this significant overcompensation, the aluminium level of 0.688wt% in the resulting sample was not only off the target of 0.04wt%, but far outside the tolerance of 0.02-0.08wt%, meaning another test sample was needed to determine a better way to achieve the correct aluminium level. This sample was also used to improve the

carbon and manganese levels which, in both the first batch and the subsequent adjusted sample, were below the target level.

In the adjusted sample a greater amount of the Mn-C-Fe master alloy was added but not enough to bring the level of the manganese up in line with the lower limit of the tolerance range. It was hypothesised after this point that the combined manganese and carbon master alloy may not be the best way to add these elements because of the difficulty in getting the carbon-manganese ratio correct in the master alloy, so more master alloys were made.

The Fe-Mn master alloy was made using high purity electrolytic iron and manganese flakes with a target composition of 10wt% manganese. The Fe-C master alloy also used high purity electrolytic iron and used slices of pure carbon rod to introduce the carbon into the alloy with a target of 1wt% carbon. An additional Fe-Al was made by adding an aluminium level that significantly overcompensated for the aluminium losses that would occur during the melting process, this time aiming for a target of 5wt% aluminium by adding pure aluminium solids to electrolytic iron.

The iterative process lead to a batch of samples with a composition, as given in Table 31, that mostly falls within the target range shown in Table 3, although it is clear that the aluminium level within the 0.02-0.08wt% was not able to be achieved, instead giving an average of approximately 0.11wt%.

The residual elements included in these samples closely matched the target levels, as shown by Figure 130, and when coupled with the compositions shown in Figure 129 show that these samples have achieved a very consistent composition, with the most significant difference being the level of residual elements.

6.2.3 MICROSTRUCTURE
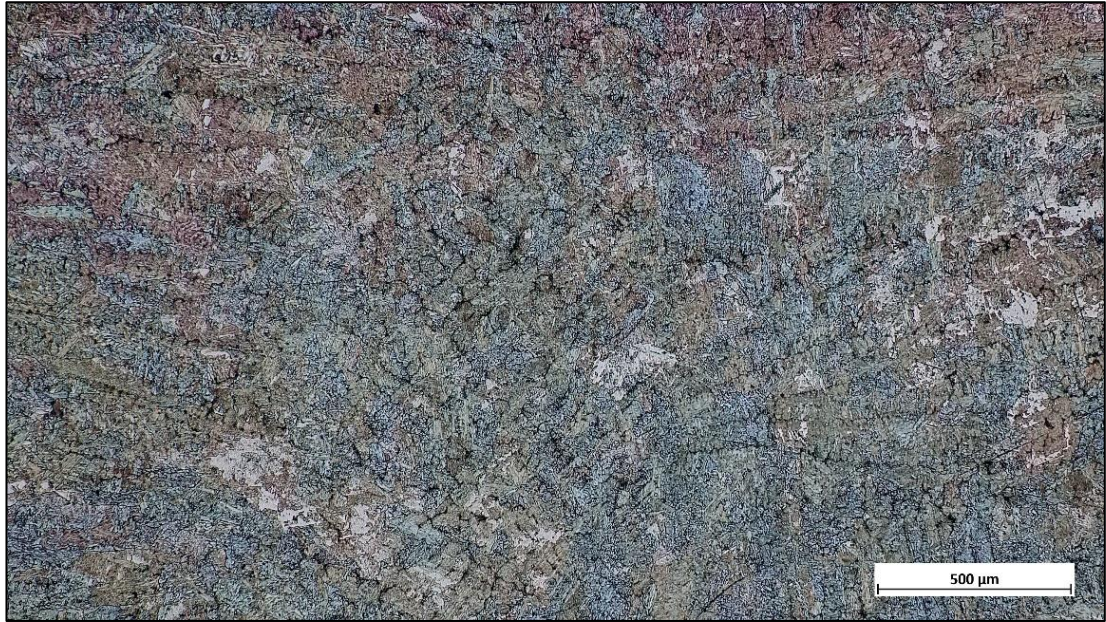
Figure 131 Optical image of the as-cast microstructure in RAP40G_MA_SOL_RF showing the centre of the sample in the narrower plane

Figure 132 Optical image of the as-cast microstructure in RAP40G_MA_SOL_RF showing the edge of the sample in the narrower plane
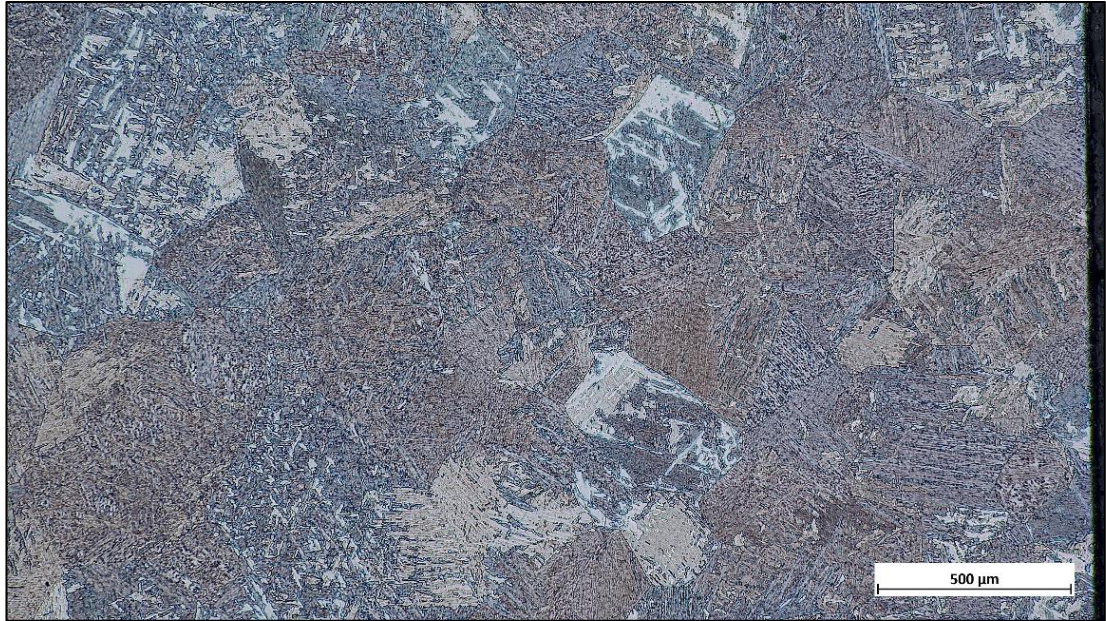
Figure 133 Optical image of the as-cast microstructure in RAP40G_MA_SOL_RF showing the centre of the sample in the wider plane
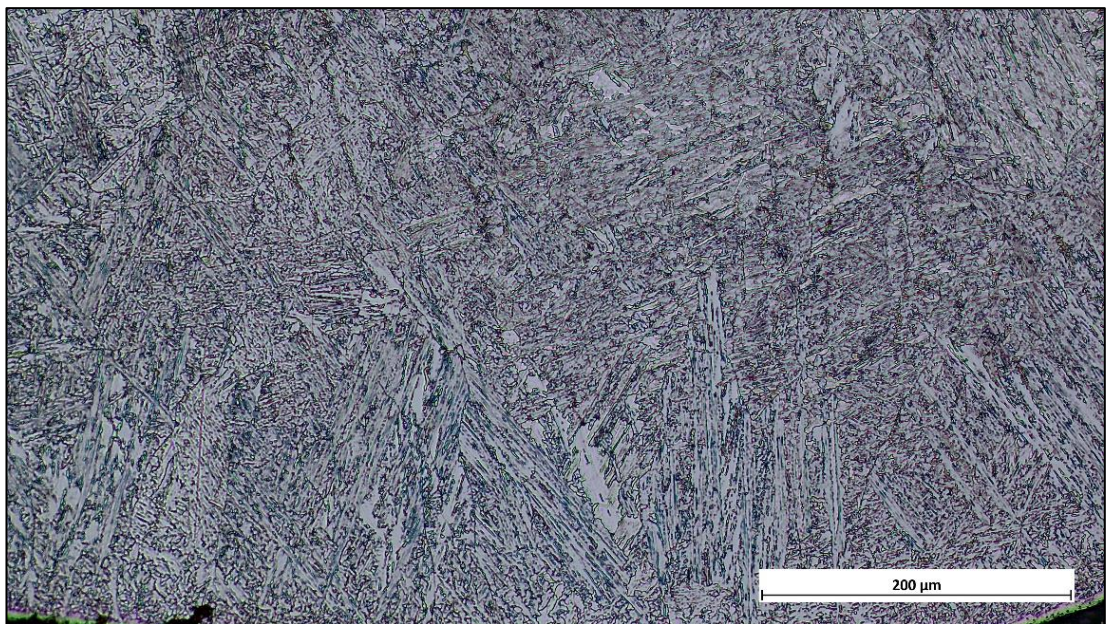
Figure 134 Optical image of the as-cast microstructure in RAP40G_MA_SOL_RF showing the bottom of the sample in the wider plane
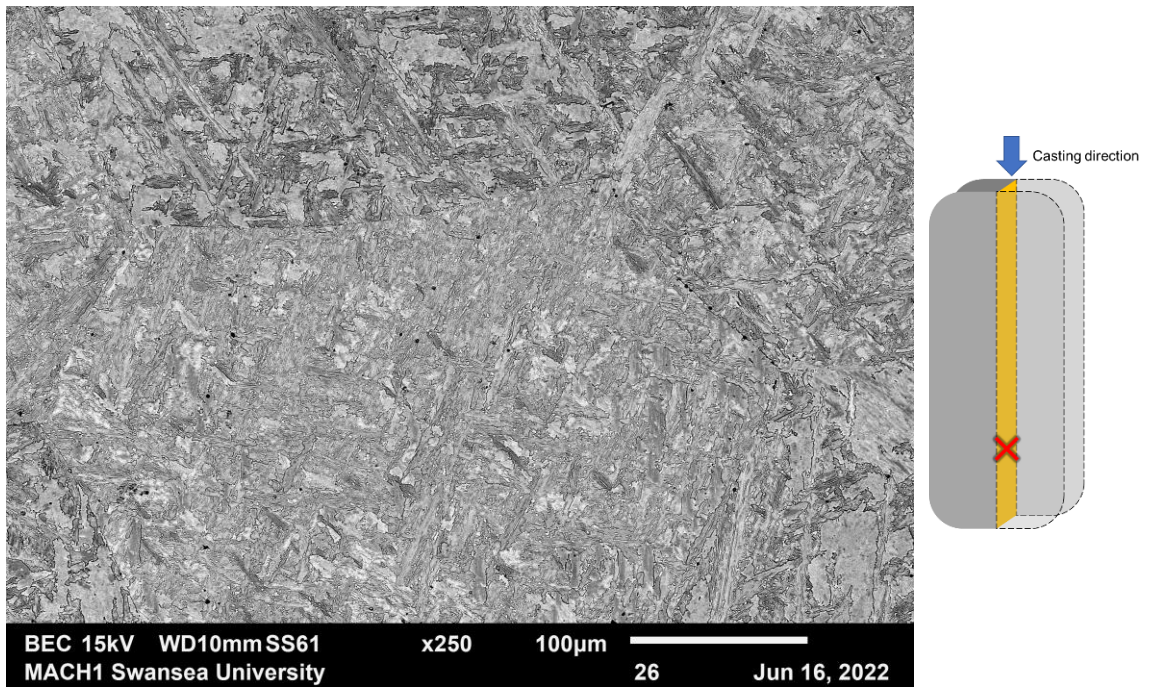
Figure 135 Microstructure of the as-cast DP800 made using master alloys
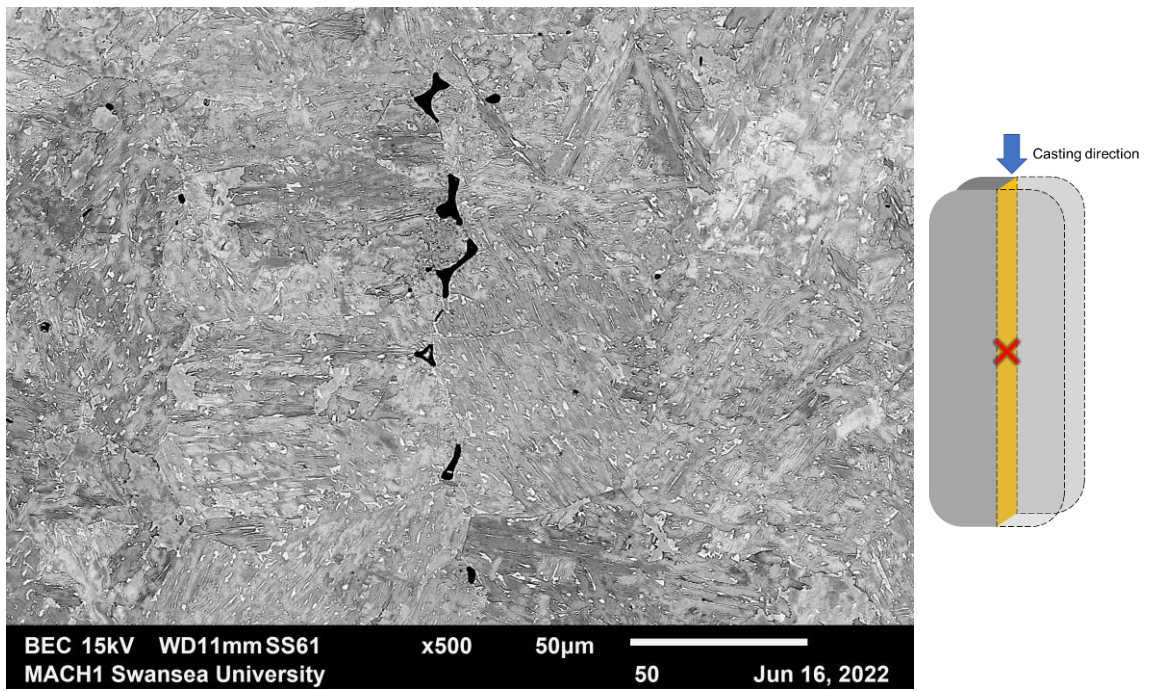
Figure 136 Pore in the microstructure of the as-cast DP800 made using master alloys
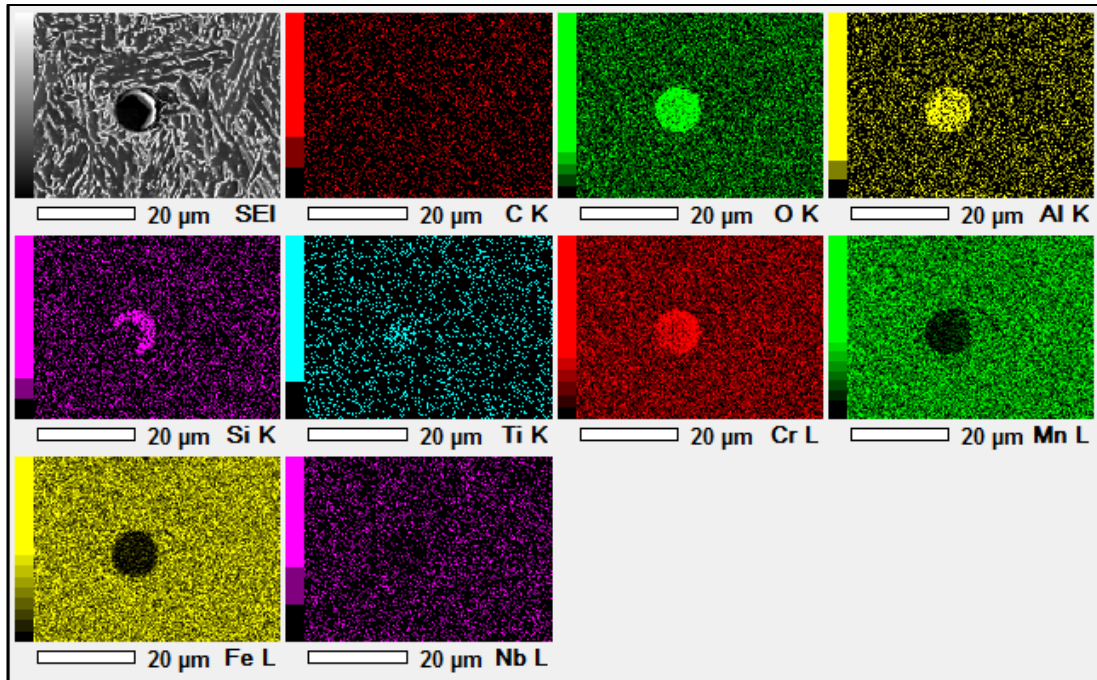
Figure 137 EDX analysis of an oxide inclusion in the as-cast microstructure RAP40G_MA_SOL_RF found towards the edge of the sample in the narrower plane
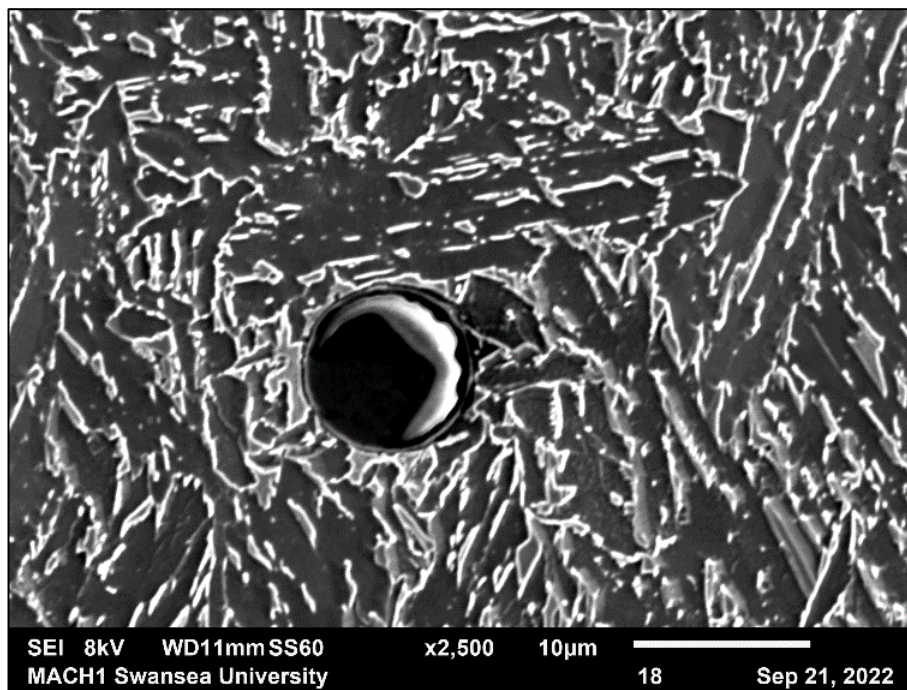
Figure 138 SEM image of an oxide inclusion in the as-cast microstructure in RAP40G_MA_SOL_RF found towards the edge of the sample in the narrower plane
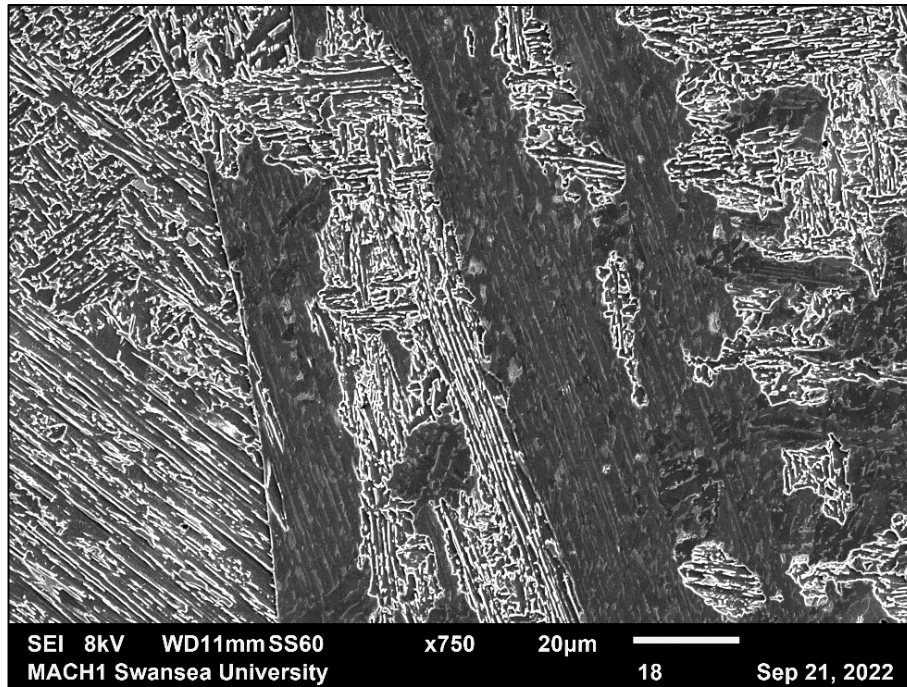
Figure 139 SEM image of the as-cast microstructure RAP40G_MA_SOL_RF showing multiple phases towards the centre of the sample in the narrower plane
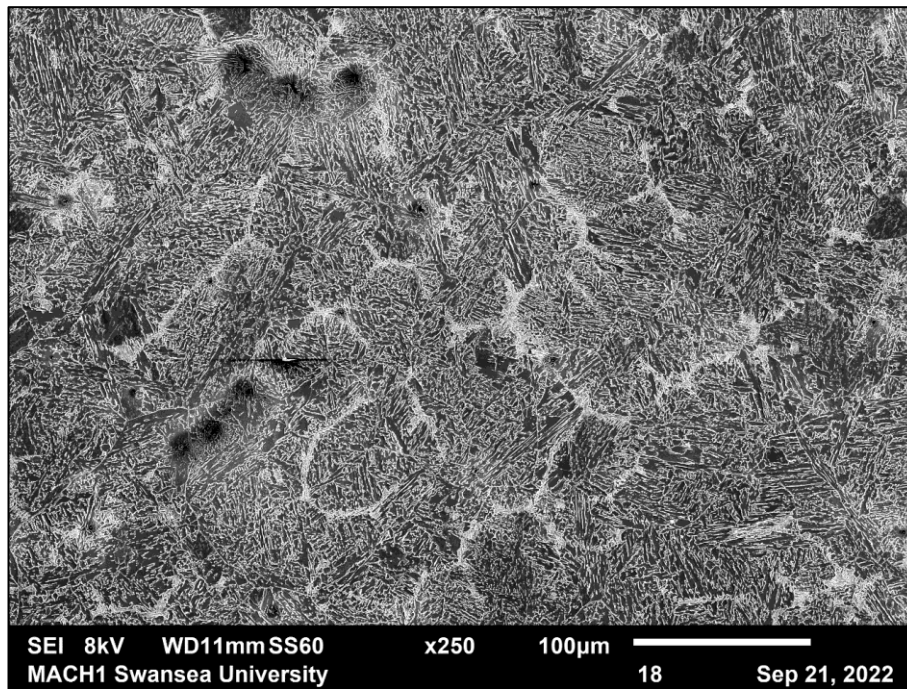
Figure 140 SEM image of the as-cast microstructure in RAP40G_MA_SOL_RF showing the centre of the sample in the narrower plane

As can be seen in Figure 131 to Figure 140, the as-cast microstructure shows the presence of at least two different phases. The as-cast microstructure is equiaxed and contains some pores and oxide inclusions.
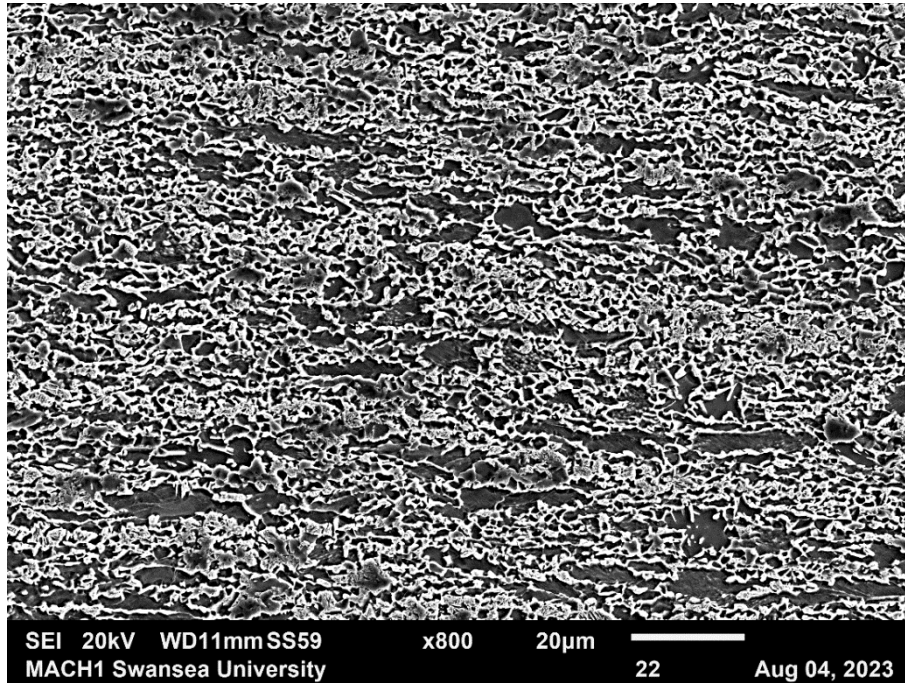
Figure 141 Remelted material, having undergone the same processing as the synthetic samples
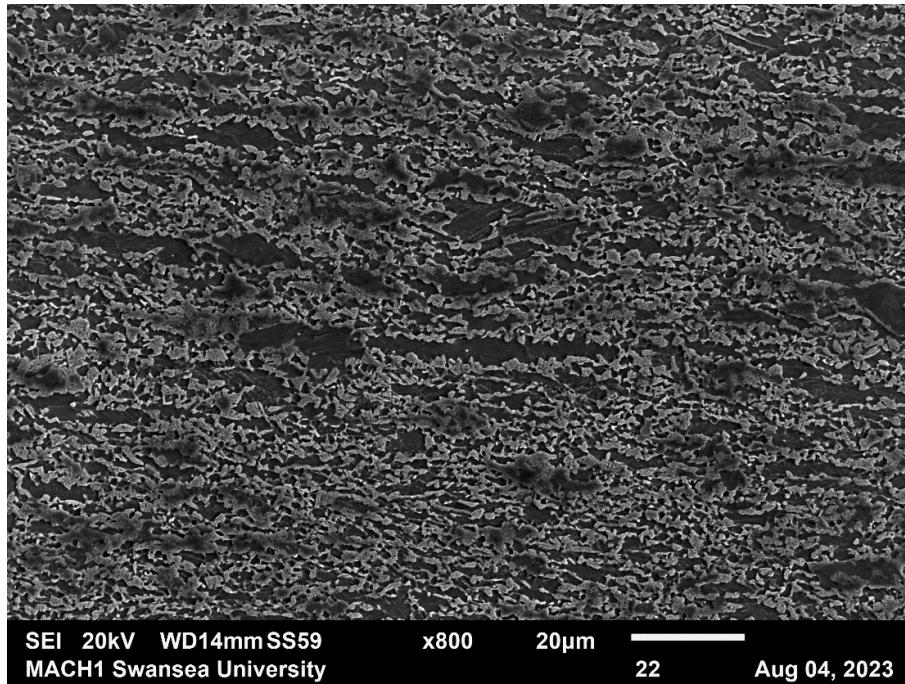
Figure 142 RAP40G_MA_SOL_CuX1 SEM image
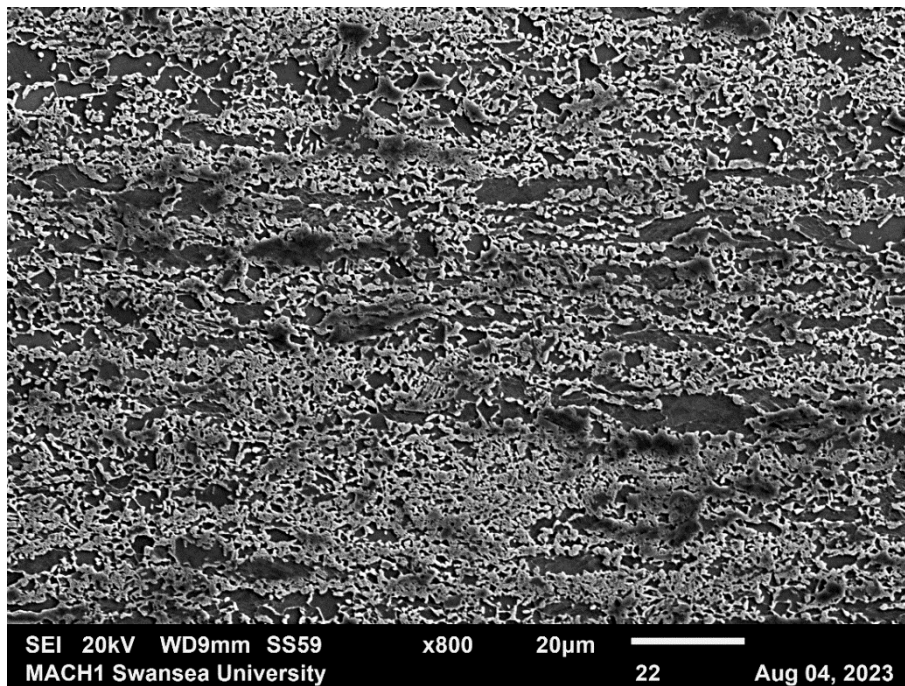
Figure 143 RAP40G_MA_SOL_CuX16 SEM image
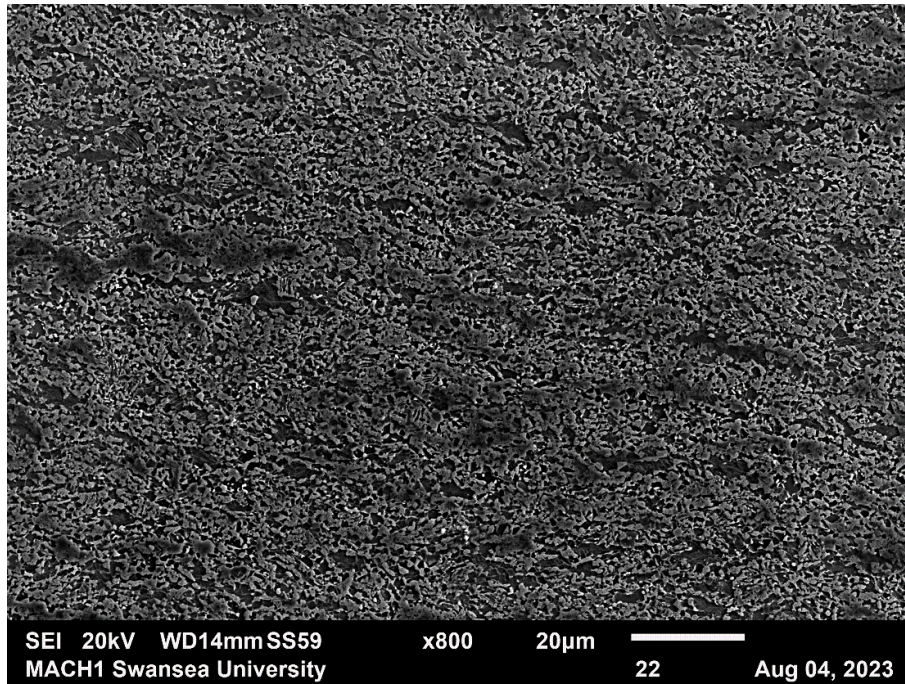
Figure 144 RAP40G_MA_SOL_CuX36 SEM image
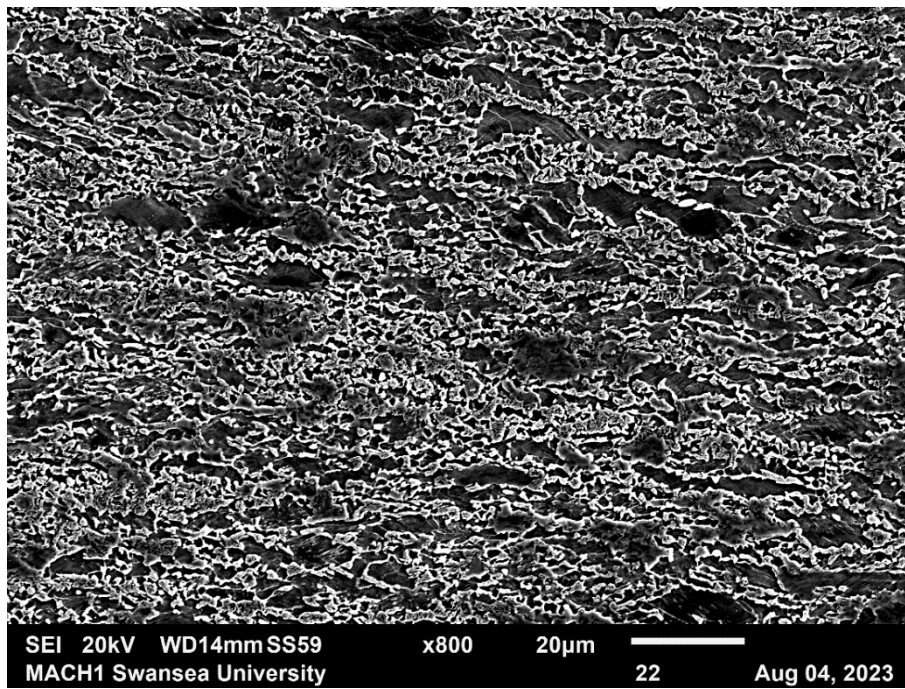
Figure 145 RAP40G_MA_SOL_SnX1 SEM image
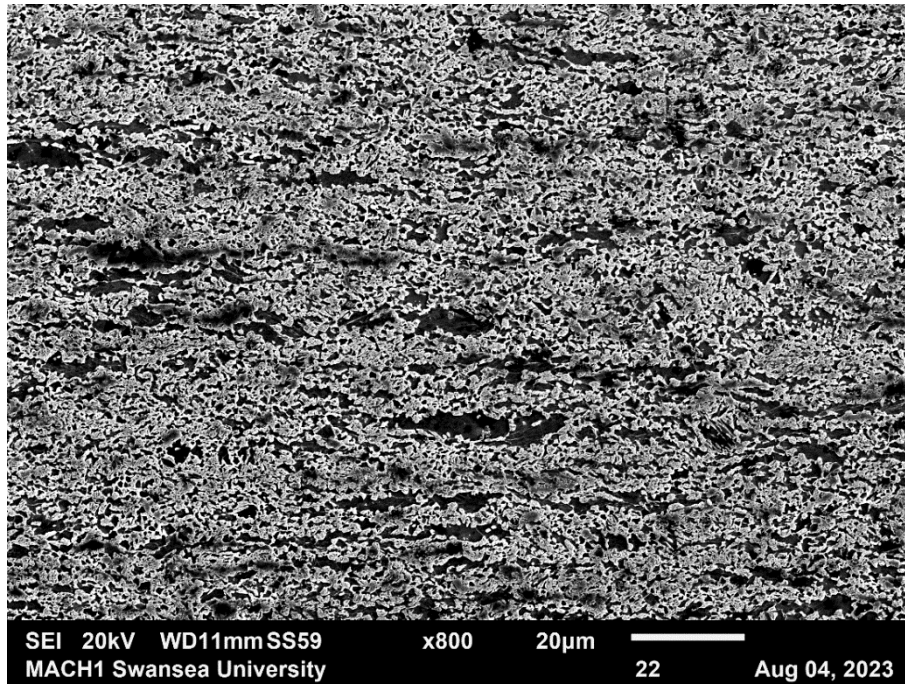
Figure 146 RAP40G_MA_SOL_SnX16 SEM image
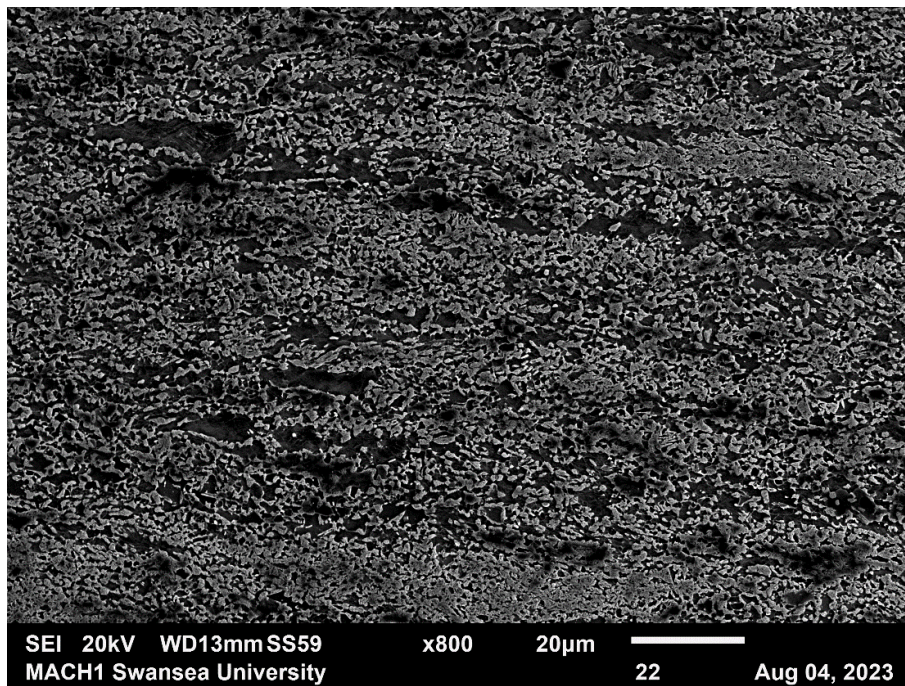
Figure 147 RAP40G_MA_SOL_SnX36 SEM image
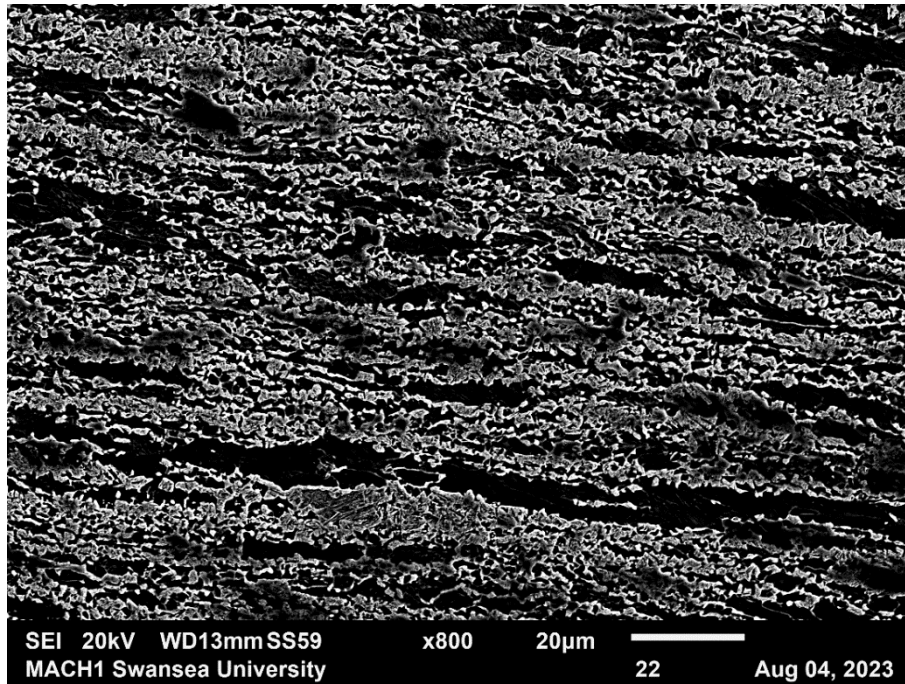
Figure 148 RAP40G_MA_SOL_NiX1 SEM image
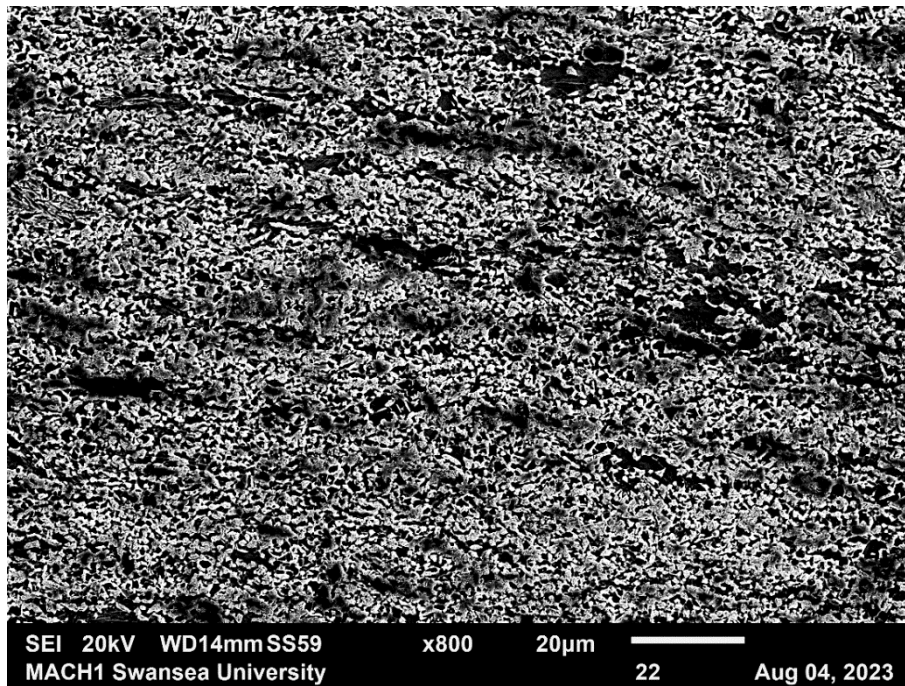
Figure 149 RAP40G_MA_SOL_NiX16 SEM image
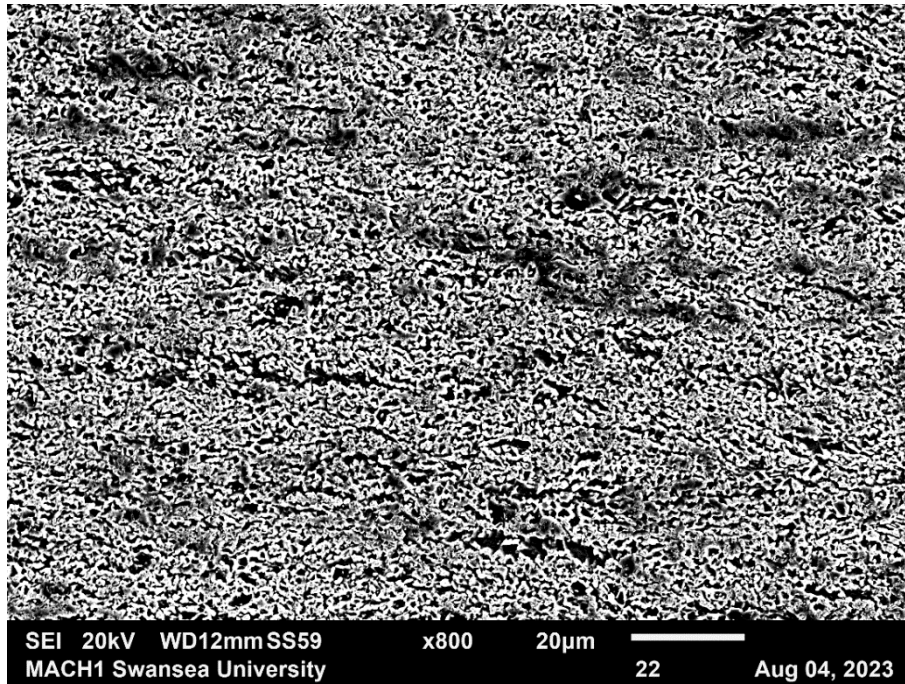
Figure 150 RAP40G_MA_SOL_NiX36 SEM image
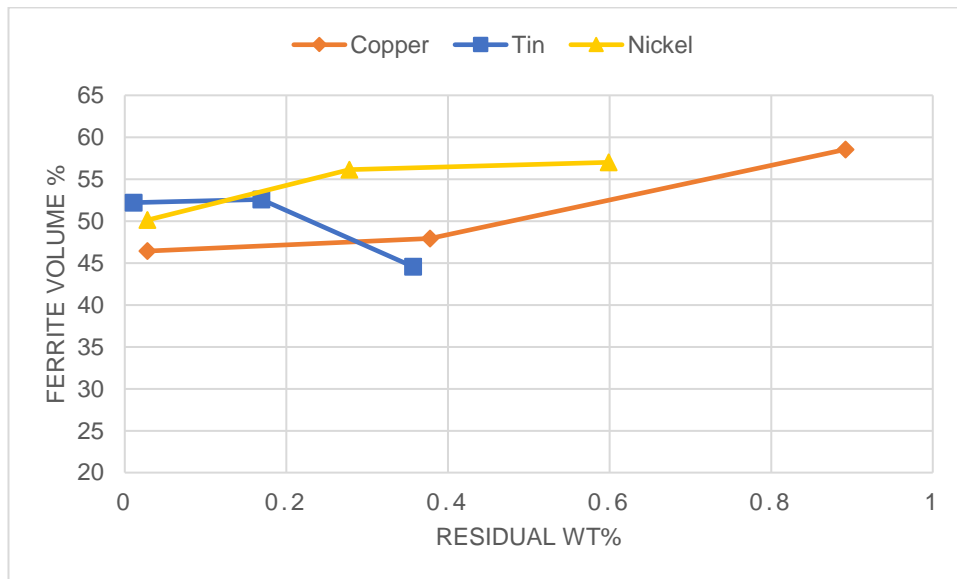
Figure 151 Percentage of ferrite present in the microstructure in a selection of the RAP40G_MA_SOL samples

The final microstructures of the synthetic DP800 with residual additions are shown in Figure 141 to Figure 150, with a summary of the ferrite content of the samples presented in Figure 151. The ferrite volume increased slightly at the higher copper and nickel levels, and decreased at the lower tin levels. The phase fraction was calculated

using ImageJ software to determine the percentage of an image occupied by each phase.

6.2.4 TENSILE
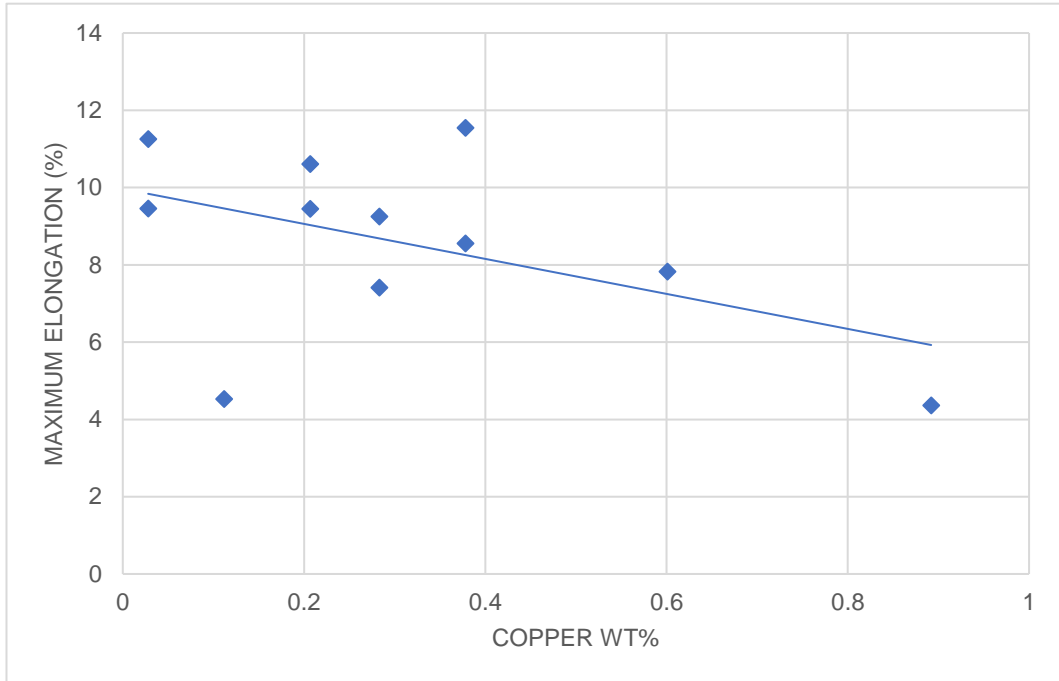
Figure 152 Break elongation of RAP40G_MA_SOL_Cu samples
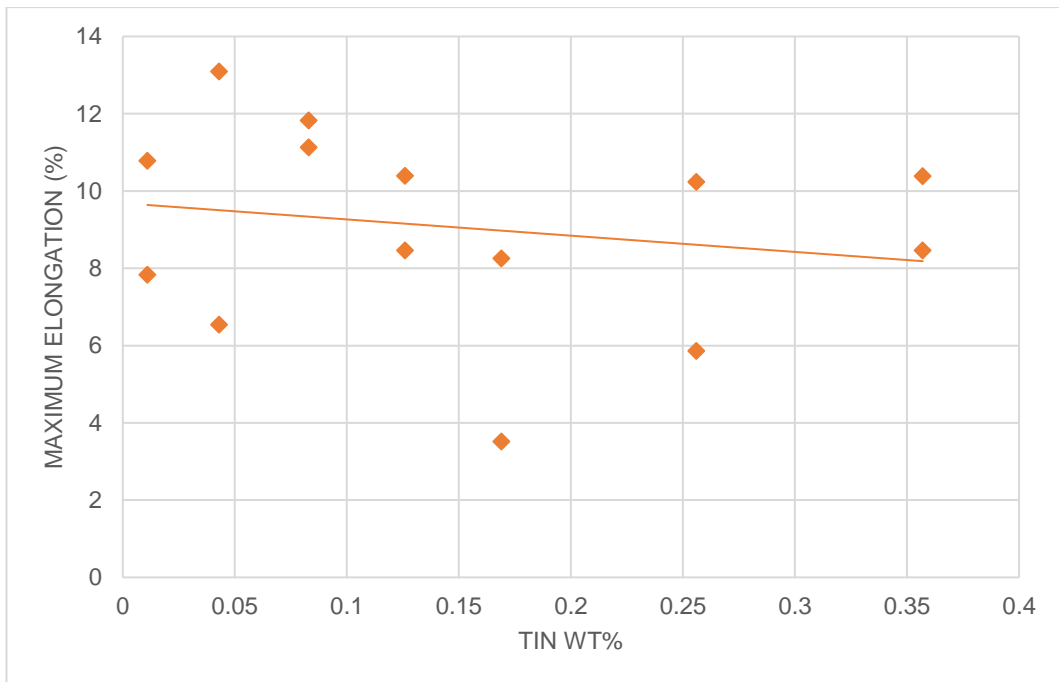
Figure 153 Break elongation of RAP40G_MA_SOL_Sn samples
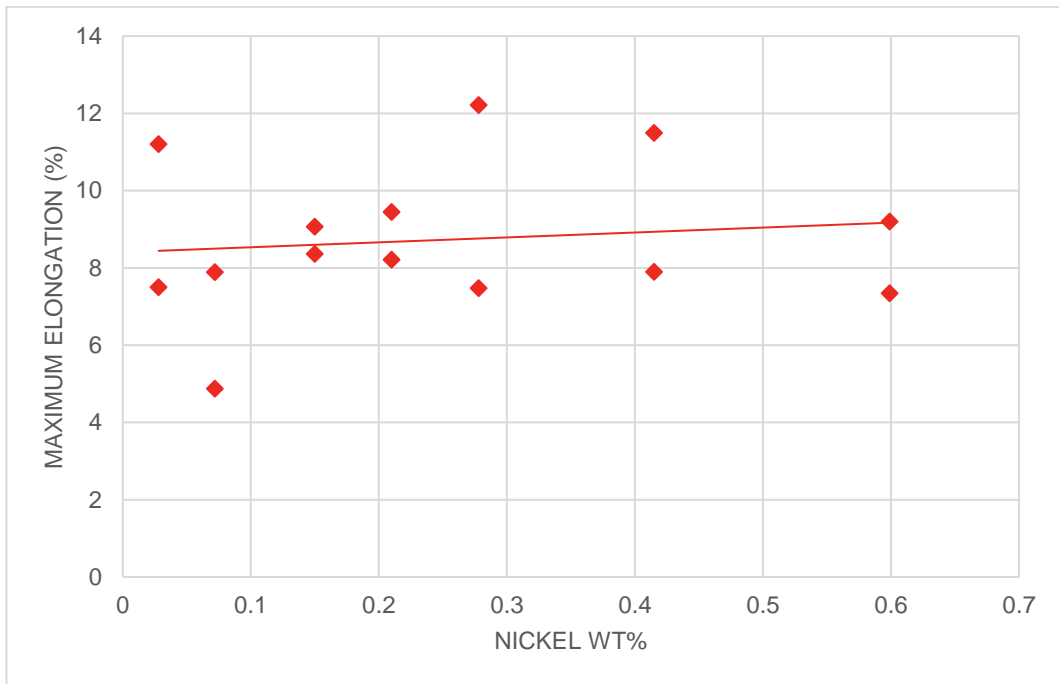
Figure 154 Break elongation of RAP40G_MA_SOL_Ni samples
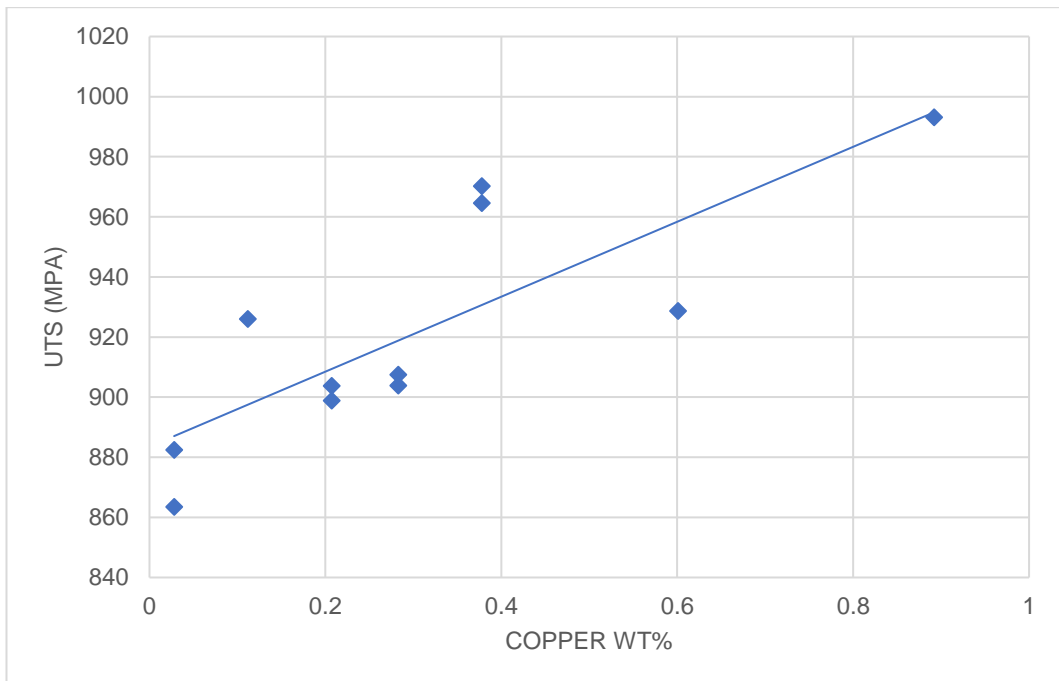
Figure 155 UTS of RAP40G_MA_SOL_Cu samples
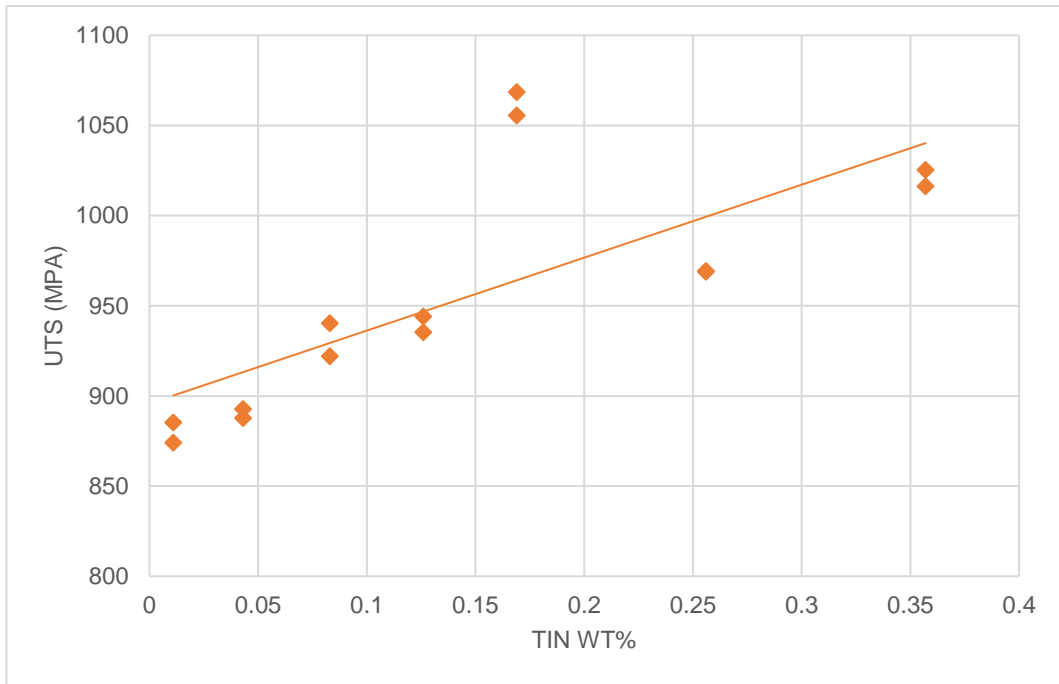
Figure 156 UTS of RAP40G_MA_SOL_Sn samples
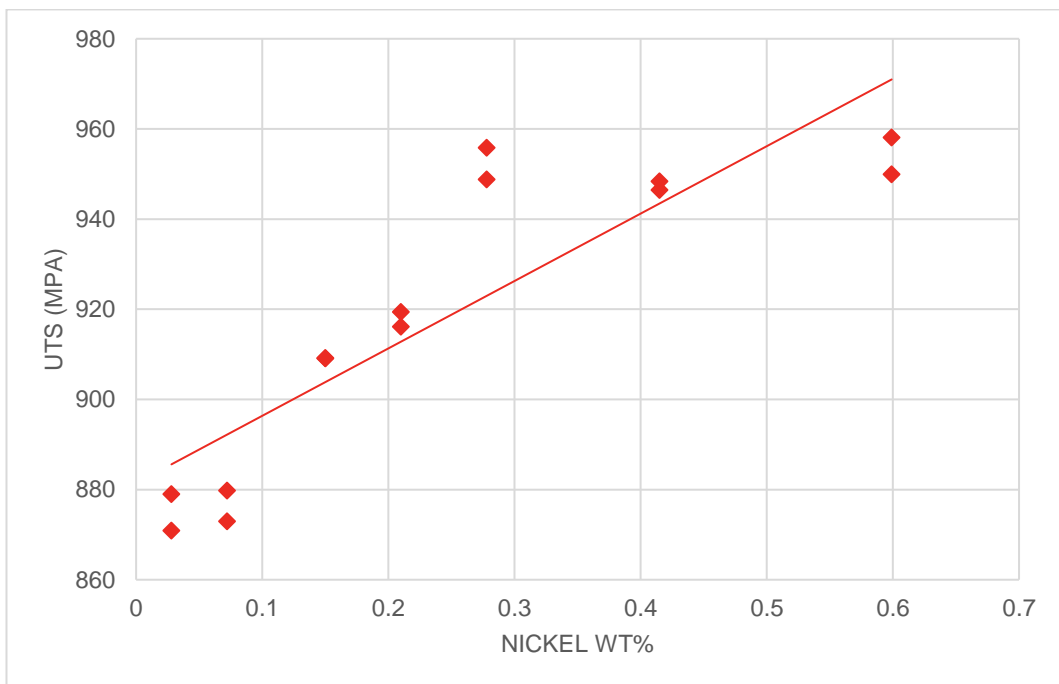
Figure 157 UTS of RAP40G_MA_SOL_Ni samples
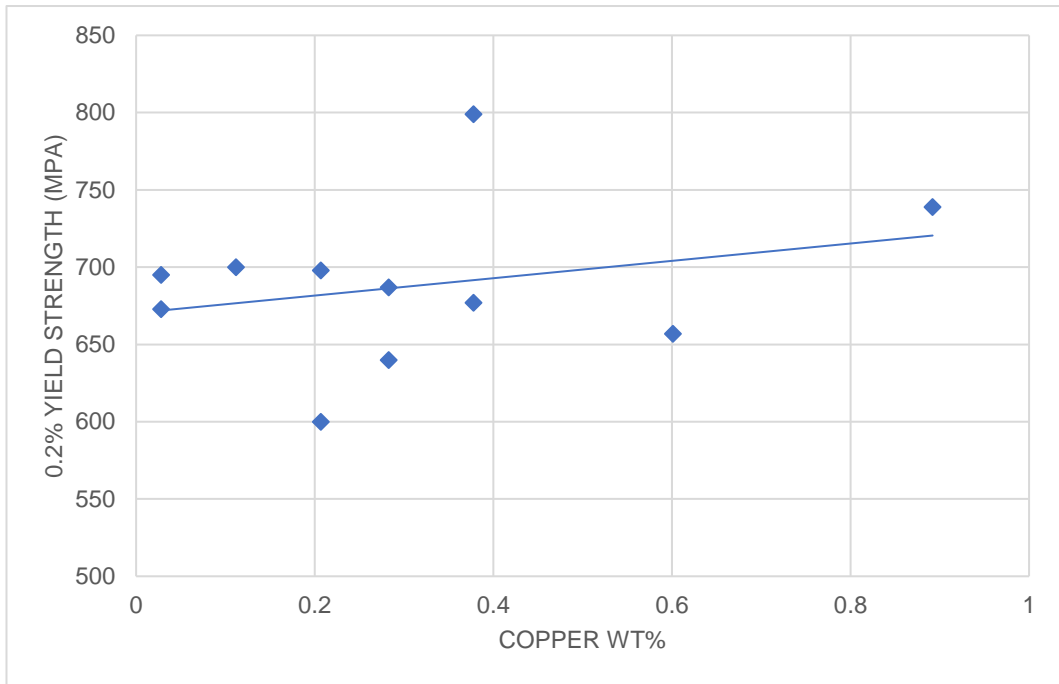
Figure 158 0.2% yield strength of RAP40G_MA_SOL_Cu samples
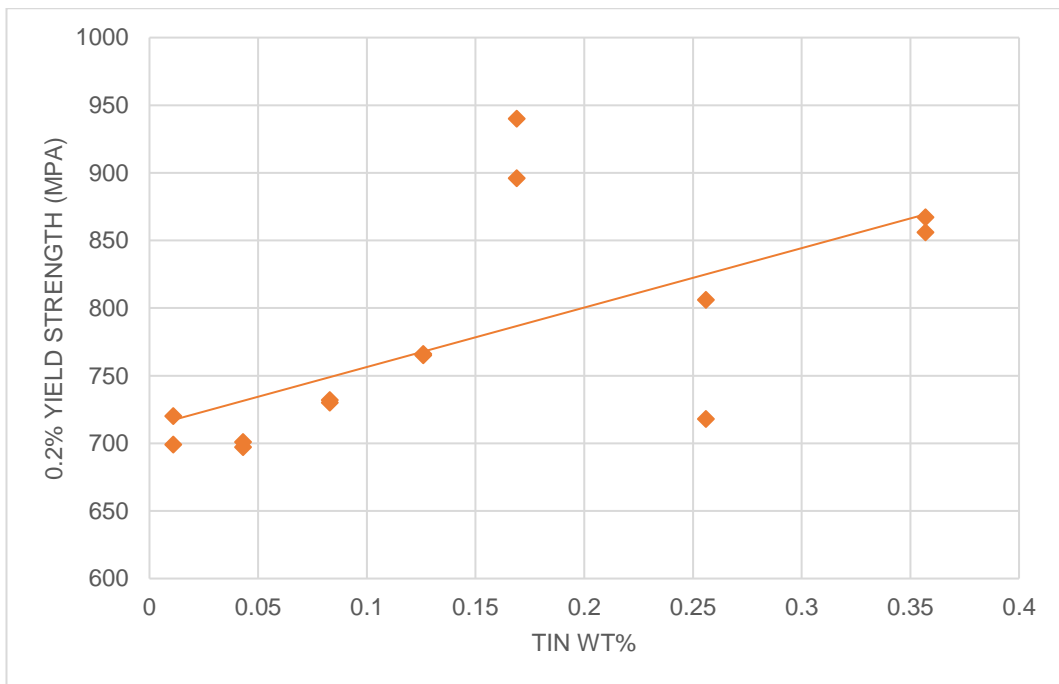
Figure 159 0.2% yield strength of RAP40G_MA_SOL_Sn samples
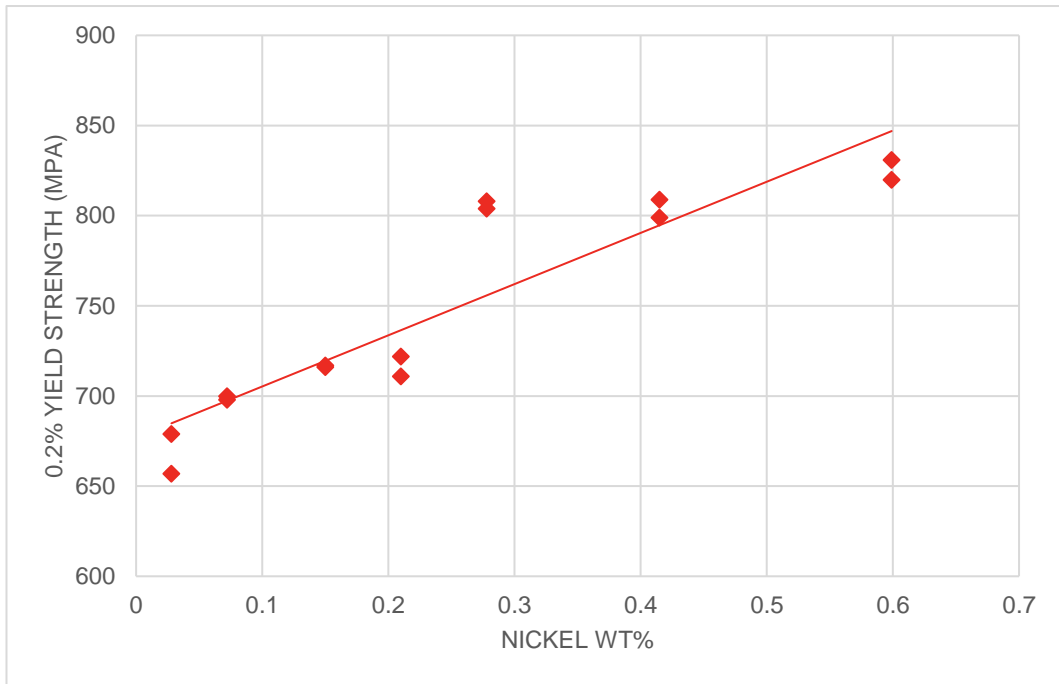
Figure 160 0.2% yield strength of RAP40G_MA_SOL_Ni samples

Figure 152 to Figure 160 show the tensile properties of every test specimen plotted individually. Increasing copper levels decrease the break elongation of the samples, and copper, tin and nickel all increased both the UTS and the 0.2& yield strength.

6.2.5 HARDNESS
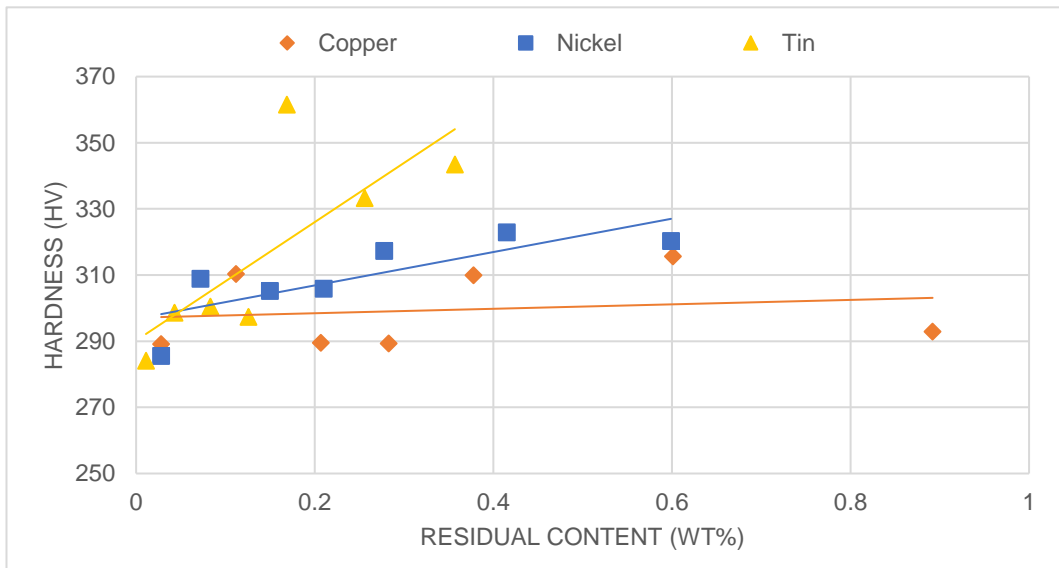
Figure 161 Hardness of synthetic RAP40G_MA_SOL samples

Figure 161 shows the hardness results for the RAP40G_MA_SOL samples. Tin and nickel both increase the sample hardness, while increasing levels of copper appears to have no overall effect.

6.2.6   REGRESSION ANALYSIS

Regression analysis is a way to consider several measurable variables when looking at a set of data. The analyses here considered all the intentionally added elements and is discussed further in 7.7.5.
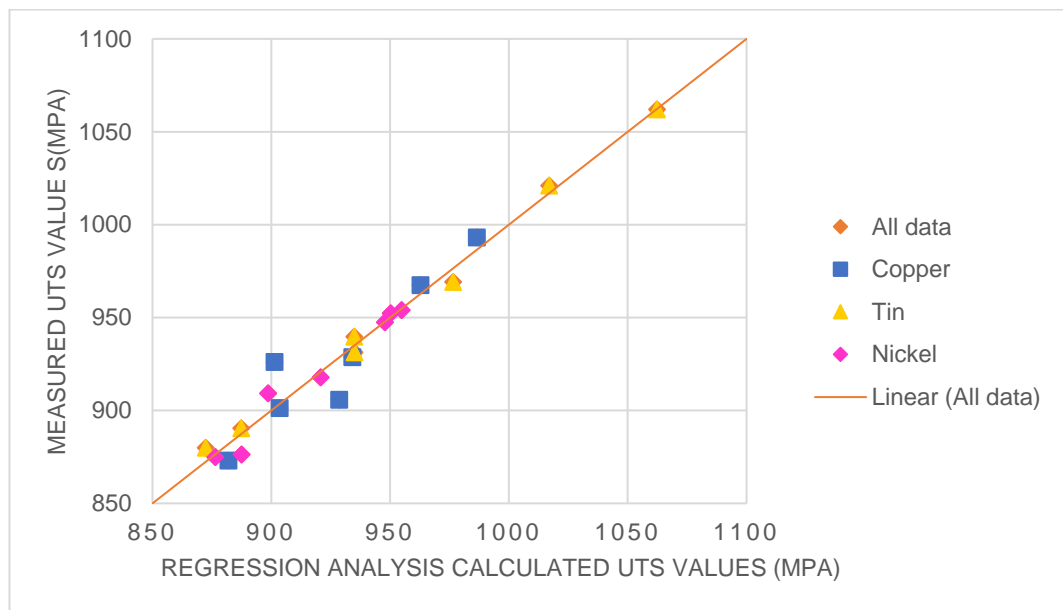
Figure 162 Regression analysis of the average UTS of synthetic DP800 samples made using the 40g master alloy route with various residual additions – R2=0.965

The UTS regression analysis shown in Figure 162 produced the following equation;
UTS(MPa)=35-138C+435Si+690Mn-1130Cr+77   Ni+670Al+144Cu-2585Nb+408Sn+5347Ti
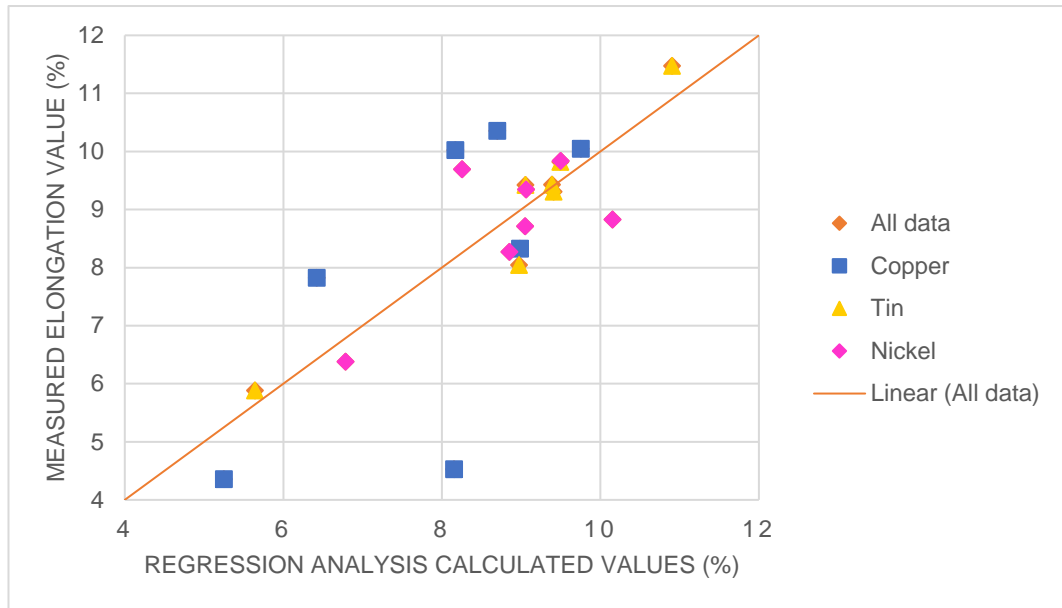
Figure 163 Regression analysis of the average elongation of synthetic DP800 samples made using the 40g master alloy route with various residual additions – R2=0.590

The elongation regression analysis shown in Figure 163 produced the following equation;

$$\text{Elong\_max}(\%)=175+C+21Si+33Mn-379Cr-3Ni+104AlCu-1289Nb+6Sn+184Ti$$
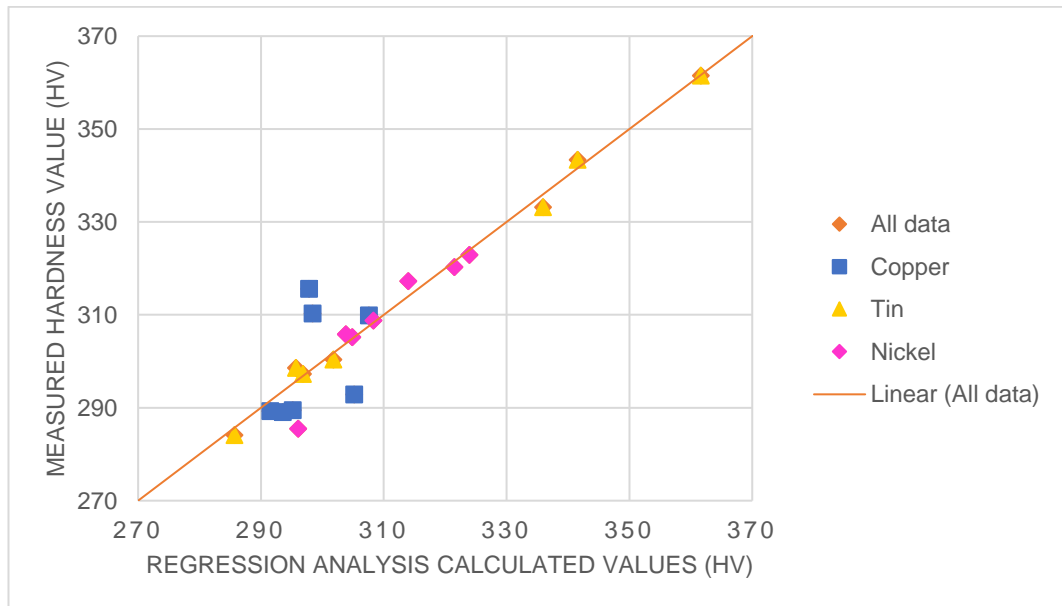
Figure 164 Regression analysis of the average hardness of synthetic DP800 samples made using the 40g master alloy route with various residual additions – R2=0.900

The hardness regression analysis shown in Figure 164 produced the following equation;

Hardness(Hv)=-860-346C+99   Si+39Mn+1348Cr+43Ni-134Al+7Cu+10684Nb+127Sn+2419Ti

Figure 162 to Figure 164 show the results of the regression analysis used to determine the impact of the composition on the mechanical properties. The UTS and hardness show strong a correlation, but the composition has much less impact on the elongation, resulting in a graph with much more scatter.

6.2.7   SUMMARY OF MASTER ALLOY METHOD

The use of the master alloy method produced samples with the most consistent composition when compared to previous trial batches and allowed for two tensile test specimens to be produced per cast. The resulting data showed strong correlations, especially when plotting the UTS values, and when using a regression analysis tool to consider all element additions a series of equations could be plotted unique to the mechanical property.

CHAPTER 7   DISCUSSION

7.1   20G DP800 POWDER ROUTE

7.1.1   SAMPLE PRODUCTION

Table 32 20G DP800 powder route summary

Feedstock	Powder (Fe, C, Mn and Si)
Target grade	DP800
Residual elements considered	Cu, Sn, Ni (powder)
Cast size	20g
Homogenisation temperature	850°C
Homogenisation time	5 hours
Cold rolling reduction	80%
Normalise temperature	900°C
Normalise time	2 minutes

The 20g powder samples, with results shown in Chapter 4 are based on a Tata DP800 steel have residual additions of copper, tin and nickel, as well as carbon, manganese and silicon as shown by Table 16. The compositions as measured by an OES showed a variation between samples with the carbon, manganese and silicon levels outside the target range given by Table 3. All these elements have an influence on the steel, affecting the microstructure and mechanical properties. Despite this, the copper and nickel levels did vary within the samples, giving 15 samples with unique compositions, allowing the different chemistries to be investigated.

These initial samples were made with little understanding for the elements that are gained or lost in the sample production, meaning that no elements were over or under compensated for, even when this would have been necessary. When weighing, small plastic vessels were used to weigh each element, but the powder mass was only measured into the beaker rather than into the mixing vial containing all the powder, meaning that any powder lost by sticking to the side of the plastic container was not

recorded and accounted for. The powder compaction method also led to some powder losses, the elemental content of which was not practically able to be measured.

After the rolling stage the samples were normalised, with the surface temperature of the samples measured throughout the normalisation stage. Figure 34 shows the cooling rate of the samples is variable over the first minute after leaving the furnace. It indicates that the samples cooled by an average of 11°C/s over the first minute after leaving the furnace, but with a range of more than 4°C/s between to fastest and slowest cooling rates. As indicated by Figure 10, the cooling rate of a steel will affect the microstructure present in the final material. The different phases have different properties, so a faster cooling rate, leading to an expected higher level of martensite which as a very hard phase would be expected to increase the strength of the final sample.

7.1.2 CORROSION

The data for the corrosion of the 20g DP800 samples in Figure 35 shows a reduction in resistivity from the samples with higher levels of copper additions but almost no effect of the nickel or tin additions, suggesting that only copper has influenced the corrosion resistance. While it is expected that copper has the most significant effect, based on literature it would also be expected to improve the corrosion properties with increasing tin and nickel levels to some degree [7].

The open circuit potential experiment measures the potential in a system compared to a reference electrode when there is no current applied. This can be used to determine how reactive the surface of the samples are, therefore a more negative potential difference suggests a more reactive sample [108]. The data presented in Figure 35 shows that the increase in tin and nickel levels had no significant impact on how reactive the sample surfaces were. The sample with the highest copper level had a less negative potential difference than the sample with the lowest copper, changing from -0.33V to -0.53V. This suggests that increasing levels of copper in the sample will decrease the reactivity of the sample, a suggestion that the corrosion resistance has improved. These different effects could be due to the corrosion mechanism of each element explained in more detail in 7.2.2.

7.1.3 MICROSTRUCTURE

The microstructure of these samples can be seen in Figure 36 to Figure 41, with the average grain sizes in Figure 42. It can be seen in the optical microscopy images in Figure 36 to Figure 41 that this synthetic DP800 replication does have a microstructure that features two phases, with grains typically below 10µm. As shown in Figure 42, the grain sizes, when averaged, show little in the way of a trend of grain size, especially when taking the levels of scatter into account. It can be seen in images such as Figure 36, the grain sizes can vary between about 5-30µm in the same region of the sample. This variation was observed across most of the samples, leading to such large variation in grain sizes as shown by the error bars in Figure 42.

7.1.4 HARDNESS

From Figure 43 it can be seen that the DP800 samples showed the trend of hardness increasing as residual content increases with tin having a greater effect than copper or nickel. This is as expected from existing literature as shown in Table 2, and indicates that, despite the scatter shown in the data, the RAP method can be a valuable way of identifying the impacts of residual elements on the hardness of the steel.

7.1.5 TENSILE

Figure 44 shows the UTS of the synthetic DP800 made using the powder route and it suggests that increasing tin and nickel levels will increase the UTS, but the copper has little effect. On the other hand, when looking at the individual data points rather than the trendlines it is clear that the data contains a lot of scatter and there is so much variation in the data that it is difficult to confidently quantify the effects of the increased residual levels.

Looking at the results provided by this method, some trends can be identified, such as in Figure 44, where there is a correlation seen within the results of increasing strength in samples with high residual levels, as expected in existing literature [7], [64]. Some of the results, such as Figure 45 showed less of a trend due to large amounts of scatter in the data. This is thought to be due to the uncontrolled variables within the samples. These include the difficulty controlling the composition, the inconsistencies in the

rolling process, and the variations of the heat treatment. These variations may well have introduced more variations between the samples than the different levels of residual additions, making it more challenging to determine any effect from the changing levels of residual elements.

It is widely reported that the inclusion of residual elements increases the steel strength, as shown in Table 2, and the increase in UTS in line with residual element content shown in Figure 44 supports this. The tin and nickel have a particularly significant effect on the strength. The copper appears far less influential which supports the findings of Yamada et al. [64] when compared to tin, but the same study found nickel to have little impact on the strength, but a study by Far et al. [110] found that a combination of copper and nickel did have a strengthening effect on the steel. It would be expected that the samples with the lowest levels of each residual element would have largely similar properties, but the results presented in Figure 44 show that the samples containing the lowest levels of copper have a UTS about 80MPa higher than the samples with similarly low tin and nickel. This suggests that the copper samples may be anomalous and have received a variation during processing that has increased that strength by such a significant amount. The trendline of the samples containing nickel and tin are far more similar to the graph expected from literature in this area [7].

Despite a high degree of accuracy during the weighing out stage, the OES results indicate significant variation between the levels of other elements in the samples. For example, the manganese levels in the samples range from 1.79wt% to 2.00wt% which is likely to have had a more significant effect on the mechanical properties of the samples than the varying residual levels. This means the priority for future work had to either be to investigate the effects of residual elements in a much lower alloy steel where the effects of any residuals will be easier to identify and separate from the other effects of other variations between samples, or to develop a way to produce the samples whilst keeping very close control over the different variables.

It would be expected that the yield strength is proportional to the grain size, as demonstrated by the Hall-Petch relationship, which is as follows:

$$\sigma_y = \sigma_0 + k_y d^{-\frac{1}{2}}$$

As shown in Figure 42 the grain size varies very little, suggesting that the changes to the mechanical properties are not due to a change in grain size.

7.2 DISCUSSION 20G 3190

7.2.1 SAMPLE PRODUCTION

Table 33 3190 powder route summary

Feedstock	Powder (Fe, C, Mn and Si)
Target grade	3190
Residual elements considered	Cu, Sn, Ni, Cr, Mo (powder)
Cast size	20g
Homogenisation temperature	850°C
Homogenisation time	5 hours
Cold rolling reduction	80%
Hot rolling reduction	-
Normalise temperature	900°C
Normalise time	2 minutes

Samples based on a Tata 3190 hot band steel have much lower levels of alloying additions compared to many other steel grades. It is an interim grade steel which has a few potential final grades depending on future processing conditions. The effects of single additions of copper, tin, chromium, molybdenum and nickel are all investigated in this chapter.

As Table 18 shows, the targeted composition is a simplified composition, with fewer element additions than the industrial grade. The intention of this was to decrease the potential variables between the samples, but despite this the measured composition of the samples misses the target by an inconsistent amount. There is also a significant discrepancy in the measured sample composition depending on the measurement method. Part of this will be due to the small levels of alloying additions which are very challenging to measure using most composition measurement methods.

Despite efforts to keep the normalisation stage consistent between samples, the variation in the cooling rate as shown by Figure 42 can lead to differences in phase proportions in the microstructure. This is shown by the CCT diagram in Figure 10, and so can impact the properties of the final steel samples produced.

7.2.2 CORROSION

Alloying elements, especially copper and chromium, are commonly used in industrial alloys to improve corrosion resistance. The OCP experiment aimed to measure the reactivity of the samples, determined by measuring the potential difference in the experimental setup, to compare the corrosion resistance of the samples. A sample with a larger potential difference would be expected to be less resistant to corrosion than a sample with a smaller potential difference, but Figure 49 showing the results of the 3190 samples implies that only the copper is improving the corrosion resistance while the samples with high chromium levels seem to be having the opposite effect. The benefits of copper in corrosion resistance are well documented [7], [12], [111], and the results added here only add to that evidence.

The larger reactivity measured when increasing the chromium level at first glance disagrees with the established literature on the topic which expects chromium to improve the corrosion resistance [7], [50], [112], and studies such as that done by Kim et al. [112] also used a NaCl based solution, but investigated chromium up to 5wt% over nearly two months. The open circuit potential experiment used for the RAP samples only investigated the corrosion effects over the span of one hour. The seeming lack of influence of chromium may be because the method of protection provided by chromium is that the chromium, which is more reactive than iron, oxidises first and produces an impermeable oxide layer, preventing the iron from oxidising.

Whilst these samples may not contain enough chromium to form a complete layer, the levels may be sufficient to provide some protection to the iron in the steel. The initial oxidising of the chromium when forming a protective layer is a reaction which would be measured by an OCP test without distinguishing it from the formation of iron oxide, meaning this may explain why the results do not show that a decrease in reactivity in samples with higher levels of chromium. The samples with chromium additions are

shown to have a higher reactivity from the data collected, but in a longer term test could demonstrate a more protective ability. Copper is more widely cited as benefiting corrosion resistance, while nickel and tin are less commonly associated with corrosion resistance [12], [113].

Corrosion properties are not always considered when discussing residual elements [17] and steel products where corrosion resistance is a priority have a stainless steel composition, or are galvanised, coated, or offered some additional protection, meaning the corrosion protection benefits provided by the residual elements are far less important than the effects on mechanical properties.

7.2.3 HARDNESS

As referenced in Table 2, the hardness of steels is generally increased by the addition of residual elements. Figure 50 presents data that supports this claim, showing that copper, tin, and nickel all increase the hardness of the material, with tin having the most significant effect.

This is likely due to factors other than residual elements varying between samples as discussed in more detail later in 7.3 which explains where some of the uncertainties in the methods may occur.

7.2.4 OPTICAL MICROSCOPY

Figure 51 to Figure 60 show the observed microstructure from some of the samples produced. Whilst there are visual differences between the images, it is likely that this discrepancy originates from the processing of the samples despite efforts to remain consistent, as the normalisation and rolling stages were not able to be kept consistent between samples. Figure 61 indicates that some trends in grain size can be seen in the microscopy work done, but the levels of scatter in the results make it challenging to draw any conclusions.

Chromium would be expected to refine the grains [112], contrary to what is seen from the average grain sizes of each sample measured in Figure 61. The level of variation between samples, and the unexpected nature of some of the trends present suggests that the sample production had not been consistent enough to isolate the effects of the

residual elements, meaning the methodology needed to be developed before reliable information about the microstructure was able to be extracted.

7.2.5   TENSILE

Figure 62 and Figure 63 show some tensile results from these samples. Both graphs show that both the UTS and total elongation appear largely unaffected by the level of residual elements in the samples, but there is a significant amount of scatter in the graphs meaning it is hard to state any confident conclusions about the data gathered. The fact that only one tensile bar was able to be cut from each cast means there are no repeats for the tests, making it difficult to identify any anomalies or produce averages to reduce the scatter seen.

It would be expected that the samples with the lowest levels of residual elements would have very similar properties, but looking at Figure 62 and Figure 63, there is a huge range in properties. This suggests that the differences observed between the samples properties cannot exclusively be attributed to the composition, and the processing has likely had a more significant impact on the tensile properties than the varying residual content.

7.2.6   XRD

The aim of gathering the XRD data and comparing the peak intensity was to be able to see clearly any correlations between the internal structure and orientation of the samples and the residual levels. As can be seen from Figure 64 to Figure 68, there was a trend for some peaks to vary with increasing residual levels for tin and molybdenum in particular but for the copper, nickel and chromium samples there was no conclusive correlation indicating that the samples became more or less orientated as a result of the residual additions [114]. For example, it appears as if increasing the tin and molybdenum content leads to a higher [110] phase fraction as indicated by Figure 65 and Figure 67, which suggests these samples are becoming more oriented in the [110] direction as a results of the higher tin and molybdenum content, but the other crystal structures in the same samples show no evidence of a trend with increasing residual content.

7.3 CAUSES OF UNCERTAINTY IN THE 20G ROUTE

7.3.1 ROLLING

The hand powered cold rolling mill was not possible to regulate and maintain a consistent rolling speed and reduction of sample thickness, introducing a potential for inconsistency in the sample. While attempts were made to roll the samples as similarly as possible, the force needed to reduce the sample thickness was often very high and it was not possible to turn the roll handle at a constant speed throughout. This meant that different sections of the sample were subject to compression from the rolls for different time periods, leading to differing amounts of deformation throughout the sample length and a rolled strip of inconsistent thickness. The number of passes and rolling reduction with each pass was not recorded but is likely to have been slightly different for each sample. The acquisition of a better rolling mill was pursued to improve the consistency of the rolling process in future samples. The difficulties with the rolling process produced many very curved samples that frequently would not lie flat without significant intervention through bending, which will have introduced further stresses into the samples. This introduced an additional challenge when it came to tensile testing because the samples were bent prior to pulling and the sample extension measured included some of the straightening of the sample. This introduced more variation into the results. The time requirements for each sample produced, alongside the fact that it is almost impossible to produce identical sample repeats for each data points due to the many sources of inconsistency, meant that this method was not the most practical approach to produce a large volume of different samples and to try to detect the effects of extremely small variations in residual element levels.

7.3.2 HEAT TREATMENTS

The homogenisation stage of the heat treatment was carried out in a vacuum tube furnace, with the samples lined up on a slab inside the furnace. It was later discovered that the heat distribution within the furnace is not consistent throughout, and only the central section, large enough for approximately four samples, were receiving the

intended heat treatment. This variation means that each specimen would have received a slightly different heat treatment before rolling.

During the post-rolling normalising heat treatment of this batch of samples, the temperatures of the specimens were monitored using thermocouples on the sample surface. The treatment was timed from the moment the samples reached the correct temperature, but in some samples, the point of the thermocouple was not quite touching the sample surface, meaning the temperature reading reflected the air temperature of the furnace rather than the surface temperature, leading to incorrect readings and introducing more variation into the process.

This difference will have mostly affected the microstructure, specifically the grain size because if the sample does not reach the austenitic recrystallisation temperature, the microstructure will not have been able to recrystallise, leaving residual stresses in the microstructures.

7.3.3 COMPOSITION

The composition of the samples is uncertain and the measured element levels after the sample was complete varied significantly from the initial quantities of powder measured out. The casts produced were too small to perform enough repeated tests on an OES machine to give a reputable composition, and the available OES was not able to measure tin. This means that where the independent variable was the tin level, this variable was not able to be measured post-production, and the levels had to be predicted using a wt% calculation from the quantities of powder weighed out.

7.4 DISCUSSION 140G 3190

7.4.1 SAMPLE PRODUCTION

Table 34 140G 3190 remelt route summary

Feedstock	Solids (remelted industrial strip)
Target grade	3190
Residual elements considered	Cu, Cr (solid)
Cast size	140g

Cold rolling reduction	45%
Hot rolling reduction	50%
Hot rolling temperature	200°C
Normalise temperature	900°C
Normalise time	2 minutes

Figure 71 shows linear change in copper and chromium residual levels in 140g centrifugally cast samples made by remelting industrially produced steel strip, with a fuller composition shown in Table 20. The aim of this casting method was to provide samples with a more consistent composition, reducing the variation between the casts. Despite the success in achieving a consistent composition, there were element losses in the melting process leaving the chemistry outside of specification. The centrifugal method also produces larger casts giving more material for repeated tests, which was one of the biggest issues with the 20g route. The larger sample was able to use the inline furnace and the hot rolling mill, in a way that was not possible for the smaller casts meaning the industrial route.

7.4.2 HARDNESS

Despite some differences in composition between samples, it was still possible to identify trends within the data in Figure 72. The residual elements impacted the mechanical properties broadly as expected, with the copper having a more significant effect on the hardness than the chromium. This is due to the difference in the strengthening mechanisms between the elements. Copper has a solid solution strengthening effect on steel, whereas the chromium atoms tended to congregate near inclusions and providing very little solid solution strengthening. The copper, when compared to chromium has less of a preference to join the inclusions, indicating the copper atoms are more likely to be in higher concentrations in the ferrite matrix. Both elements did show in higher concentrations in the regions surrounding inclusions [1].

7.5 DISCUSSION 140G DP800

7.5.1 SAMPLE PRODUCTION

Table 35 140g solid route summary

Feedstock	Solids ((Fe, C, Mn and Si)
Target grade	DP800
Residual elements considered	Cu (solid)
Cast size	140g
Cold rolling reduction	45%
Hot rolling reduction	50%
Hot rolling temperature	200°C
Normalise temperature	900°C
Normalise time	2 minutes

7.5.2 COMPOSITION

As can be seen in Figure 74, many of the elements were still outside of the target range compared to Table 3. The aluminium levels for example were still too low, likely due to the tendency for aluminium to oxidise readily, reacting with any oxygen present in the materials used in the melt to form an oxide which is expected to float to the top. The test only used copper additions and although the copper does increase consistently, the other important additions such as manganese varied enough that it could influence the mechanical properties to a greater extent than the varying residual element levels, making it difficult to determine the effects that are solely due to the residual elements.

7.5.3 OPTICAL MICROSCOPY AND EDX ANALYSIS

The hot rolled microstructure can be seen in Figure 75, Figure 76, and Figure 77 and shows for the first time that a dual phase microstructure has been achieved. The two different coloured grains in the images appear to be ferrite and martensite. As can be seen from Figure 78, there are several large oxide inclusions present in the microstructure which affect the properties of the final product. Using an EDX analysis, it can be seen in Figure 79 and Figure 80 that the inclusions are high in oxygen ,

manganese and silicon and are almost completely free of iron. This indicates that these inclusions were either present in the materials before melting, or a reaction has taken place during the melting process to form the inclusions throughout the microstructure. After investigating the iron bar feedstock, it was realised that the bar purity was approximately 99% pure but included many elements that form oxides in the list of impurities. After this point it was decided that the iron bar, while easy to melt, was not pure enough to continue using and other feedstock approaches were taken to ensure the samples produced were of adequate quality for the residual effects to stand out. This included using electrolytic iron which was 99.99% purity ensuring a high quality melting material.

7.5.4   TENSILE

Despite its toughness, DP800 would be expected to be formable with a ductility allowing an extension of approximately 20% But due to the inclusions in the microstructure that blocked dislocations from spreading through the material and served as crack nucleation sites, the samples were far more brittle than expected meaning the tensile results were more dependent on the frequency and distribution of inclusions in the sample and therefore meaning the effects of the copper variation was overshadowed and difficult to determine. The tensile results are shown in Figure 81 to Figure 85, including example stress-strain curves, can be compared to the previous work on DP800, such as in Figure 44 to Figure 63, which show that these samples appear to be much less ductile than would be expected of a RAP DP800 sample. After some further investigation, it was discovered that the samples all had large inclusions within the microstructure, as seen in Figure 78. It was determined that these inclusions came from the iron bar used as a feedstock material. As the bar was only 99.0% Fe, the other components of the material made up the remaining mass of the feedstock, and then made their way into the cast material. It is thought that these inclusions and pores present in the material are the main reason behind the brittle properties of the samples as seen in Figure 78 and Figure 79.

Some stress-strain curves from the casts can be seen in Figure 84 and Figure 85. These make it easy to see the brittle nature of these samples, with the very low elongation of approximately 5-7% and sudden fracture.

7.5.5 HARDNESS

Despite the prevalence of inclusions in the microstructure, the hardness of the material is less likely to be as seriously affected as the tensile tests, although the results from the hardness testing indicate that there is still a lot of variation between the samples. Figure 86 shows the hardness of a centrifugally cast DP800 made with an iron bar feedstock. It does show a gentle increase in hardness with the increasing copper levels, although the level of scatter in the results mean that claiming this as a trendline would be unreasonable. The feedstock had such a significant impact on the material, it was not feasible to work out where any other sources of error may have occurred, especially in the processing stages. Any inconsistencies that may have occurred were overshadowed by the impact of the oxides from the iron bar.

7.6 DISCUSSION 40G 3190

7.6.1 SAMPLE PRODUCTION

Table 36 40g 3190 powder route summary

Feedstock	Powder (Fe, C, Mn and Si)
Target grade	3190
Residual elements considered	Cu, Cr, Sn, Ni, Mo (powder)
Cast size	40g
Cold rolling reduction	45%
Hot rolling reduction	50%
Hot rolling temperature	900°C
Normalise temperature	900°C
Normalise time	5 minutes
Coiling temperature	600°C

It was found that many elements, especially carbon, experienced significant losses through the production processes. This meant that they had to be accounted for in the weighing out stage to ensure the final composition was close to the target values.

Initial tests with the addition of residual elements included additions of copper and chromium between 1-36X industrial limits of each limits. The target values for the residual content in the samples is shown in Table 24 and the composition of the completed samples is shown in Table 26.

The low-alloy alloy discussed here has an exclusively ferritic microstructure, as seen in Figure 118 to Figure 121 due to the carbon levels of <0.02 wt% which is able to dissolve some residual additions. tends to strengthen the steel via solid solution strengthening due to the atomic size difference between the iron and copper atoms. The chromium strengthens the steel in a similar way, but due to an atomic radius more similar to the radii of an iron atom, the strengthening effect is less for the same wt% of addition. The chromium atoms also had a tendency to be present in oxy-sulphide inclusions at higher concentrations than in the bulk steel microstructure, whereas copper was only detected in the inclusions at approximately the same concentrations as the bulk steel.

A significant amount of experimental time was spend evaluating how to get a consistent composition int the casts. One key aspect of the production process found to have significant effects on the composition of the sample was the material of the weighing pot. Different types of plastic pots retained different amounts of different elements whereas the variation was less noticeable with glass pots and plastic pots that had been previously used and cleaned. The calculations used to determine how much of each element needed to be weighed out to achieve a target composition varied depending of the receptacle that the powder would be weighed in to. The various iterations of this process are shown in Table 7 to Table 9 and in Figure 26. It can be seen that the sample compositions were still fairly inconsistent and difficult to control.

7.6.2 MICROSTRUCTURE

Figure 118 to Figure 121 show the microstructures of samples with copper and chromium additions at high magnification. It is possible to see inclusions within the

microstructure, typically below 1µm in size. Assuming no large pores within the samples, it is likely that inclusions such as these were the initiation sites for cracks as the samples underwent tensile tests. This work was published in [1].

There was no significant variation between the microstructures shown in Figure 122, the grain sizes were very similar, indicating that the copper and chromium had a minimal effect on the microstructure at this scale.

When comparing the microstructures of the samples containing tin, nickel and molybdenum in Figure 123 we see that the grain size varies between the samples, with the molybdenum samples in particular increasing the grain sizes. The visible differences in the microstructure likely originated during the heat treatment stages, where the atoms in the steel have the energy available to move and form larger grains.

7.6.3 TENSILE PROPERTIES

Molybdenum tends to harden steel by a solid solution strengthening mechanism [47], [67], although as can be seen from Figure 92, the tensile tests carried out on the low alloy steel indicated a drop in ultimate tensile strength with increasing levels of molybdenum. This could be due to an error such as an inconsistency in the processing of the samples, or it could be that the molybdenum levels measured were not extreme enough to indicate the expected results. The industrial level of molybdenum is low with a maximum level of 0.02wt%, much lower than the other residual elements considered in this work, meaning that the upper limit investigated here was also significantly lower than the other residual elements. The tight industrial restrictions may be due to its preference to form carbides which would severely affect the ductility of the steel, a vital property for this steel grade.

As with previously discussed residual elements, nickel also strengthens steels via the solid solution method, but unlike molybdenum, it does not form carbides which may explain why it is permitted in much higher quantities. Nickel has the effect of suppressing pearlite formation and promoting the formation of martensite, which would also harden the steel. Figure 91 shows that the UTS increases with higher levels of nickel, as expected from the strengthening effects of more martensite in the

microstructure, although this is not visible in the microstructures presented in Figure 123.

Tin and copper are commonly discussed in similar ways [7], [12], [64], [115] although tin has a much more pronounced effect due to the larger atoms having a more significant impact on an atomic level. Tin is often limited due to the impact on cold working, for example being limited to 0.02 wt% in deep drawing applications [68], [77]. 3190 requires ductility shown by Figure 95 and Figure 97 despite Figure 98 showing that tin has a dramatic strengthening effect on the RAP 3190 samples.

When comparing to [64] we can see that despite Yamada, Oda and Akisue's relatively low levels of residual elements in a low alloy steel, their results largely reinforce the findings from the results presented in 6.1. This paper [64] investigated both copper and chromium up to about 0.2wt%, finding that at these low levels the copper had a clear strengthening effect, along with a decrease in ductility, mirroring the results presented in Figure 89 and Figure 90. When it comes to the effects of chromium, Figure 89 and Figure 90 show little effect at the low levels investigated, similar to the minimal effect on strength and only slight decrease in elongation shown in Yamada's work [64].

Yamada's work only investigated the effects of tin up to 0.085% and found "increased tensile strength and decreased total elongation", and in Figure 91 and Figure 95, with an upper tin level of at least 0.33wt% the same trendlines are easy to see.

Yamada also investigated nickel up to about 0.15wt%, lower than is investigated here, but when comparing to the results in Figure 91 and Figure 95, both agree with the minimal effect of nickel on both UTS and elongation up to a nickel level of approximately 0.15wt%.[64]

In an attempt to better compare the samples, a carbon equivalent was used. The original carbon equivalent calculation did not take tin into consideration, so this was included in the calculation as shown in Equation 4 based on a comparison between the trendline gradients of the Cu and Sn UTS data, shown in Figure 89 and Figure 91. This investigation did not indicate a reduction in the scatter of data, suggesting that the variation of the other alloying elements is not the only influencing factor in the discrepancies between samples.

A comparison of each bar was plotted, shown in Figure 104 to Figure 113 to identify any trend between the mechanical properties and the section of the rolled strip that the tensile bar was cut from. There was no significant identifiable trend between the section of the rolled strip that a tensile specimen was cut, and either the stresses in the sample, or the elongation values achieved meaning that the results from all three samples can be treated as representative of the sample. Although there was some variation for some residual addition batches, there was no trend across all the samples produced, implying that the differences between tensile bars was due to anomalies on a sample level, rather than due to the origin location.

Due to the scatter in the results and the slight inconsistencies between the compositions of each sample, aside from the intended changing levels residual elements, the samples contained multiple variations. To investigate this further, the regression analysis function was used in Microsoft Excel to consider the effects of multiple elements on the properties of the samples. This was done by carrying out a multivariate regression analysis comparing the sample properties to the levels of carbon, silicon, manganese, chromium, molybdenum, nickel, aluminium, tin and copper. The resulting plots are shown in Figure 114 to Figure 117 and indicate a good correlation for the UTS values of the samples, with some success also present when using the yield stress data. The elongation data on the other hand had a large amount of scatter, which is easy to see even when looking at the raw data. Figure 95 to Figure 98 all show large error bars for the majority of samples. This means it is little surprise that when put through the same regression analysis method, the scatter in the data makes it challenging to predict the elongation properties of future samples of a similar composition, as shown in Figure 116 and Figure 117.

7.6.4   HARDNESS

The range of hardness values in each sample mean that both a positive and negative trendline could be plotted within the upper and lower bounds. The increase in hardness could be due to the solid solution strengthening within the samples.

When examining at the hardness trendlines present in Figure 124, it is easy to see how the hardening effect of each element varies based on the gradient of the trendline. The

copper trendline had a gradient of 15.4, whilst the tin trendline had a gradient of 67.8. This indicates that the tin had more than four times the effect on the hardness compared to copper. Comparing this to Equation 2, that suggests that tin is five times as influential as copper, it would seem that the hardness results measured in the RAP samples follow a similar trend to the proposed copper equivalent. Also suggested by Equation 2 is that nickel has a similar impact on material as copper. The gradient of the nickel trendline in Figure 124 is 20.0, also indicated that in the measured samples that the nickel and copper residual additions have a very similar strength.

Comparing Figure 124 with the initial test work shown in Figure 50, it is clear that the development of the RAP method has been able to produce samples of increasing consistency, which in turn adds validity to the results.

The hardness values for the 3190 samples was also investigated using the regression method. Initially, all the average hardness values of the samples were plotted, resulting in Figure 125, although as the hardness testing method carried out 10 indents, it was possible to identify a few indents with unusual values which may have affected the hardness average, as indicated by Figure 126 where one indent was about 20Hv larger than the other hardness values. The full set of hardness data for all samples was investigated, with the most anomalous results removed and a new average hardness value calculated for the affected tests. The resulting graph is shown by Figure 127 which indicated very little change from the initial regression analysis, with the R-squared value only improving slightly from 0.7644 to 0.7697.

7.7 DISCUSSION 40G DP800

7.7.1 SAMPLE PRODUCTION

Table 37 40G DP800 master alloy route summary

Feedstock	Solids (master alloy – Fe-Mn-C, Fe-Si, Fe-Cr, Fe-Ti, Fe-Nb, Fe-Al)
Target grade	DP800
Residual elements considered	Cu, Sn, Ni (solids)
Cast size	40g

Cold rolling reduction	45%
Hot rolling reduction	63%
Hot rolling temperature	900°C
Intercritical annealing temperature	800°C
Intercritical annealing time	2 minutes
Overaging temperature	325°C
Overaging time	15 minutes

During the production of these samples, the master alloy method was developed in chapter 3.8.1, and more attention than ever was paid to achieving a consistent composition, as catalogued in 6.2.2. The final samples had a composition almost entirely within the sample range, except for the aluminium level which was consistently a little high, as can be seen in Table 31.

7.7.2 MICROSTRUCTURE

Microstructure is important to get representative properties, but the industrial process is challenging to replicate on a lab scale. On an industrial scale, the steel slab can be sent through the entire process of casting and rolling in a very tightly controlled and closely monitored way. It also enables the steel to go through the entire rolling process without cooling to room temperature. This is unachievable on a laboratory scale with the facilities available, meaning it is not possible to perfectly replicate the industrial process. Instead it becomes necessary to develop a hot rolling process that replicates the final product, even where the rolling process cannot replicate the industrial equivalent. This approach adapts to the equipment available and prioritises a close monitoring of the RAP sample microstructure at different points in the lab scale process to compare and contrast the result with the target product. The key microstructure features to replicate are the shape and proportion of the constituent phases within the sample. Especially in a product with a strong reliance on the properties, the microstructure is a vital metric to monitor, as it is a major influence on the mechanical performance of the material.

The expected phases present in a dual phase steel would be ferrite and martensite, although it is possible that some austenite would be retained at this stage in the process.

The cooling rate of the synthetic sample when it is cast will undoubtedly affect the microstructure and the proportion of phases present.

The as cast microstructure is shown in Figure 135 and Figure 136, which has what appears to be a mostly bainitic microstructure. Some centre line porosity can be seen which may cause some loss of strength in the material as it can be a nucleus for crack propagation. Some oxides were also found in the microstructure, imaged in Figure 137 and Figure 138 which may also be a cause of weakness in the samples.

Figure 142 to Figure 150 show the microstructure of the final samples with the distinctive banded dual phase microstructure. Although the industrially produced material typically has a ferrite level of 70% [116] the samples produced here typically have a ferrite level of 50%, shown by Figure 151. The rest of the microstructure is martensitic, with the higher martensitic levels than the industrial material, which typically contains about 30% martensite and 70% ferrite, leading to the expectation that the samples will be stronger and harder, but more brittle than the industrial equivalents. The phase volume fraction was calculated using ImageJ software to measure to volume of each phase present in an SEM image.

7.7.3 TENSILE PROPERTIES

When pulling the tensile bars for the synthetic DP800 made using the master alloy method, the specimens with copper additions were pulled in a tensile machine with old grips, meaning some samples slipped in the grips and the data contains errors. New tensile grips were acquired for the other samples which were able to be pulled without issue,

We can see from the tensile results in Figure 152 to Figure 157 that the samples still displayed a lot of variation in the total elongation values, but the UTS data show a strong correlation between increasing residual levels and an increased UTS value. An industrial DP800 would typically have a UTS value a little over 800MPa, but the samples here show UTS values higher than this even in the samples with the lowest levels of residual elements. This is likely due to the higher martensite volume in the material. Each sample was able to produce two tensile bars and the graphs indicate that the two tensile bars from each sample have similar strength properties. The variation

in the elongation values suggest that even though the UTS can be well demonstrated using the synthetic samples, repeatable elongation properties is less repeatable on the small scale.

7.7.4 HARDNESS

The 40g DP800 samples made using the master alloy process indicated that the residual element additions increase the hardness of the material as shown in Figure 161. Whilst there are significant levels of scatter in the results, it is possible to identify some trends in the data. Figure 161 below shows not only the expected trend of increasing hardness with higher levels of residual elements, but there is a greater impact of tin than there is of copper, as expected by the difference in solid solution strengthening caused by the differing grain sizes. This batch of test samples also displayed similar hardness values of approximately 300Hv in the samples with the lowest levels of residual additions, indicating that these samples were very similar. This couples with the similar tensile results also shown in these samples, where RAP40G_MA_SOL_CuX1, RAP40G_MA_SOL_SnX1, and RAP40G_MA_SOL_NiX1 had an average elongation averaging about 10%, a UTS about 880MPa, and a 0.2% yield strength of about 680MPa.

7.7.5 REGRESSION ANALYSIS

A regression analysis approach was used to look at the effect of composition on the mechanical properties, as shown by Figure 162 to Figure 164. This showed that UTS in particular was heavily influenced by the composition, although the elongation had a far less close fit. Sample hardness was also closely influenced by the microstructure and these results show that tin in particular is very influential, raising the UTS and hardness a long way above the samples with lower residual content.
These equations are unique to the DP800 RAP samples and to the mechanical property being measured, but implemented on a wider scale have the potential to predict the impacts of varying levels of residual elements in a more intelligent way that can allow for the replacement of some of the more expensive elements such as manganese with the residual elements that will be introduced into the steel via scrap anyway.

CHAPTER 8   CONCLUSIONS AND FUTURE WORK

8.1   CONCLUSIONS

Two different bench mark alloys were investigated, a low-alloy steel (3190), and a dual phase steel with much higher alloy content (DP800). Over the span of this work, various RAP routes were developed and assessed to determine ways to simulate the industrial scale production of these steels on a laboratory scale. These routes were developed to produce samples with enough material to compare microstructures, hardness, tensile properties, and corrosion. The final tests of each grade show samples of similar production where the effects of residual element additions can be seen and compared.

The routes developed aimed to replicate the industrial process as much as possible. The casts underwent heat treatments and both hot and cold rolling with the aim of producing a microstructure representative of the industrial material.

Throughout the development, several methods were trialled, looking initially at pure elemental powders, then moving on to pure solid material, which developed into a master alloy method which produced a series of master alloys of iron and various alloying elements. The compositional accuracy and consistency has been a consistent challenge throughout the different methods, but the development of the master alloy method allowed for the closest control of the cast composition. The material properties were also affected by the cast processing beyond the composition, and an improvement in equipment availability, and understanding of the possibilities and limitations for the small scale samples in collaboration with other researchers produced a method that is getting ever closer to an industrial replication. More detail on this progress is listed below in 8.2.

The results presented in this thesis demonstrate the applicability of small-scale rapid alloy prototyping in the research of residual elements in steel.

As predicted by the existing literature, the work undertaken shows that higher levels of residual elements generally increases hardness and toughness of samples. The

impacts of these residual elements is different in steel grades with higher and lower alloy contents as the residuals interact differently with other elements present.

A key target outcome was to determine if increasing the levels of scrap in steelmaking is possible without significantly affecting the quality of the final product. Whilst the results presented in this thesis cannot fully predict the effects that increased scrap levels would have on steel products, extensive evidence has been presented that demonstrate that many other factors in the production of samples will affect the properties as well as the residual content. The significant levels of variation within results indicate that many factors affect the properties of a steel, and the levels of residual elements are only a small part of this. It is possible that the effects of increasing the relatively small levels of residual elements to several times the current levels will be obscured by the differences that are introduced at other stages in the process, such as variation in the temperature profile of heat treatments, during or rolling stages.

Throughout this work, several experimental approaches were taken, with samples of two different alloys ranging from 20-140g in size and using a selection of feedstocks including powder, high purity solids, and remelted industrial steel to varying degrees of success.

The samples were subject to a range of heat treatments with the target of replicating the microstructure of the industrially produced steel. The 3190 grade was an intermediate grade of steel, meaning there was no final microstructure to aim for, but the DP800 is a widely researched and commonly used automotive steel and therefore had more precise constraints to aim for.

Errors and inconsistencies between samples in both the 3190 and DP800 investigations were inevitably introduced throughout the process despite efforts to minimise these. Some of the variations were reduced throughout the timespan of the project due to improved equipment, such as new rolling mills with a roll gap which was easier to control than the initial rolling mill used. Other issues were more difficult to reduce, especially when the source of the errors were not easy to isolate and required a series of tests to reduce the issue. One of the greatest challenges was achieving a controlled and consistent composition. The work aimed to produce samples which were near

identical, only varying by the level of residual elements. Every other element should be very close to a target value to isolate the impact of the residual element levels on the material. This was tackled by a series of tests to understand the effects of different weighing pots and the extent of different element losses arising from the powder method. The issue was also reduced by gaining a better understanding of the way elements, especially aluminium, are lost through oxidising and other routes, carefully evaluating the benefits of the powder method used, before moving on to solid additions and master alloys.

Despite the errors, the process was refined over the course of the experimental work, eventually leading to a series each of 3190 and DP800 with a composition that was consistent and very close to the industrially defined limits.

The final 3190 samples looked at copper, chromium, nickel, tin, and molybdenum. These copper, tin, and nickel all increased the UTS whereas chromium and molybdenum indicated little influence on the material strength over the residual range considered, which investigated up to approximately 36 times higher than the current industrially set limits on these residual elements. With the exception of chromium, all these elements indicated a decrease in the sample ductility at increased residual levels, expected to be due to the strengthening effects of the additions. The 40g RAP samples were able to produce three tensile bars per cast, and the bar location in the cast was considered, but there appeared to be no influence on the properties coming from the sample location in the strip. Copper, nickel, and tin increased the hardness of the samples, with tin having the most significant effect.

The final DP800 samples were where the master alloy method was developed, leading to a batch of samples with good consistency and only significantly out of range with the aluminium value which ranged from 0.099-0.114wt% for a target range of 0.02-0.08wt%. Whilst the composition was close to the industrial aim, the microstructure, which in an industrial DP800 typically contains about 70% ferrite, these RAP samples only contained 50% ferrite, with the rest of the microstructure composed of the much harder martensite.

These samples looked at the effects of copper, tin, and nickel which indicated that copper and tin lead to a more brittle material while the samples containing nickel had

very little effect. All the residual elements showed a significant strengthening effect, increasing the strength from about 880MPa to 990MPa for the highest copper level of 0.982wt%, 1110MPa for the highest tin level of 0.357wt%, and 960MPa for the highest nickel level of 0.599wt%. Although the copper samples suggested no impact on the sample hardness, the nickel and tin both hardened the samples with high residual levels. The samples were stronger than their industrial equivalents due to the higher levels of martensite in the microstructure.

8.2 FUTURE WORK

The test specimens investigated in this work only considered samples with one residual element addition. While this made it easier to isolate the effects of each variation by only allowing one variable, it meant the results were limited in their applicability to industry. In reality, scrap steel used in the production of new steel will never just have one residual element and it is important to also understand the ways that different elements will interact in a way that is more reflective of a steel composition that would be produced in an industry setting.

Every element intentionally added to steel is there for a purpose, but many of these elements can be costly. Elements such as manganese and silicon are added to tailor the material properties to a customer's preference, but the properties that these elements lend to the steel are properties that can also be provided by other elements, including residual elements. The drawbacks of residual elements are many and have been discussed in an earlier section of this work, 2.1.2.2, but they can also improve strength, hardness, and corrosion resistance. Future work could investigate a more intelligent way of using high residual scrap that values the elements that contribute properties required in the steel. Techniques including big data and neural networks would allow links to be drawn between the differences not just between compositions, but also processing conditions. The rolling reductions, and the temperatures and heating times used in heat treatments all impact the mechanical properties of the final products. While these parameters have not been researched in this thesis, future work using both a RAP route and industrial scale trials, data can be collected that provide a more holistic understanding of the compositional and processing impacts on the properties.

A better awareness of this would allow the processing conditions to be adjusted to compensate for increased levels of residual elements, potentially allowing more scrap to be use, reducing both the environmental impact and the costs. As an example, a composition with a high level of residual elements would be expected to be stronger than a similar composition with lower residual levels if processed in the same way. Increasing the processing temperatures may have a softening effect on the steel and could be used on the high residual steel to bring the mechanical properties to a level that is similar to the baseline steel with the lower residual element levels.

Providing some strength addition using residual tin or improving corrosion resistance with high copper scrap may allow for financial benefits from the scrap, rather than just a problem to be solved. This relies heavily on good scrap sorting, so the scrap that is used in the manufacture of new steel can be specifically selected to minimise the requirements of other costly additions. The change in mindset from viewing residual elements as an issue to be tolerated to a valuable addition to the scrap could be useful as future steel grades are developed that utilise the unavoidable inclusions in the steel chemistry.

The effects of residual elements will vary on every steel grade as it will be impacted by other element present and by the processing conditions. This means that creating samples to recreate every possibility would be time consuming and unnecessary. The use of tools such as big data and regression analysis can be used alongside the laboratory work to develop a better understanding of the effects of all the different variables.

The demand for RAP methods, especially to research residual elements has recently become an urgent area of research for Tata Steel as it has recently been announced that an electric arc furnace will be built on the Port Talbot site [117]. An electric arc furnace can use up to 100% scrap steel feedstock, which comes with an increased potential for the inclusion of residual elements. It is vital that the effects of these elements on steel products is understood before these products begin production, meaning the work presented in this thesis has provided the groundwork for gaining a rapid understanding of the types of steel that will be produced in Port Talbot in just a few years.

8.2.1 THE PROSPERITY PROJECT

The work in this thesis was undertaken alongside complimentary work by two post-doctoral researchers, Dr Mazher Yar and Dr Shahin Mehraban, as a part of the Prosperity Project. Their work focused on producing a lab scale route for DP800 as a replica of the industrial product and much of their finding has informed this thesis. Whilst this isn't future work as it has already happened, it is relevant to include because there is a lot of work presented in this thesis which also informed their work, improving and accelerating the results produced. A summary of this is presented below, taken from the final report of the Prosperity Project Challenge 5.
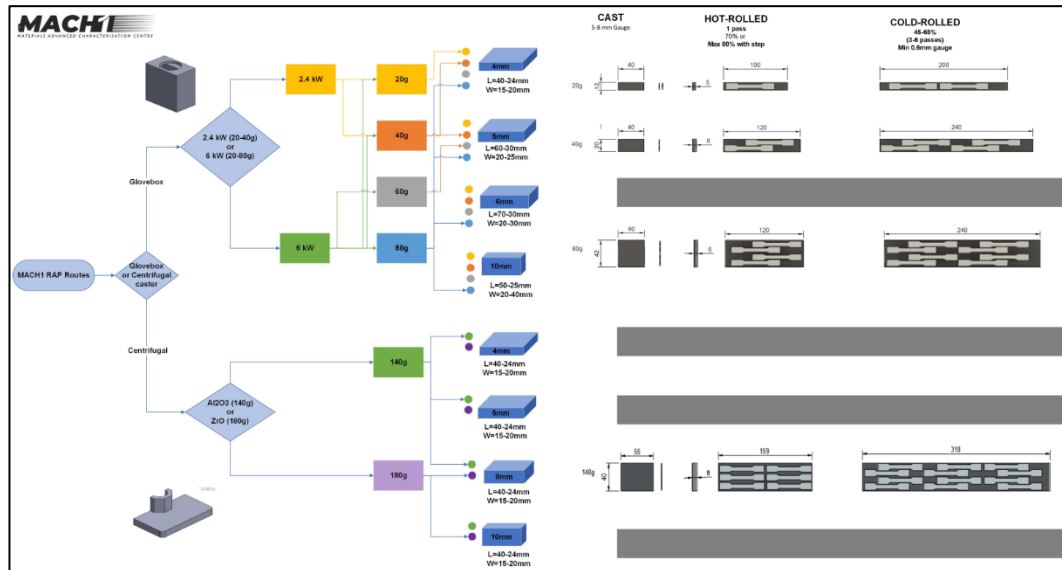
Figure 165 Summary of RAP routes available at MACH1 including cast dimensions, rolling reductions, and tensile bars (ASTM E8)

Table 38 Overview of Rolling schedule and tensile properties of DP800 samples produced with the master alloy method

Sample	Hot Rolled reduction	Cold rolled reduction	Soak Temp (C)	Average UTS	Average break Elongation (%)
RM1	57%	57%	810	754	17
RM2	62%	52%	810	766	16.7

RM3	69%	40%	810	723	15.7
RM4	69%	40%	810	713	16.1
RM5	69%	40%	750	750	17.65

RM1			RM2			RM3			RM4			RM5			Final Product		
GS (um)	BS (um)	F/M (%)	GS (um)	BS (um)	F/M (%)	GS (um)	BS (um)	F/M (%)	GS (um)	BS (um)	F/M (%)	GS (um)	BS (um)	F/M (%)	GS (um)	BS (um)	F/M (%)
6.5 ± 0.8	N/A	72.1/ 27.9	5.03 ± 1.1	10.6 ±1.8	67.3/ 32.7	5.14 ±0.5	10.0± 0.8	74.9/ 25.1	5.75 ± 0.8	10.3± 1.4	77.4/ 22.6	8.67 ± 0.9	21.6± 1.7	79.7/ 20.3	4.46 ± 1.2	5.6±0. 3	69.9/ 30.1

Figure 166 Grain size, band spacing, and ferrite/martensite percentages achieved by altering the rolling schedule of DP800 samples produced with the master alloy method, wher GS refers to the grain size, BS refers to band spacing, and F/M refers to the ferrite/martensite ratio

Five rolling schedules, listed in Table 38, were tested and resulted in a schedule that was able to achieve a microstructure very similar to that of the industrial material, as shown by Figure 166. The series of samples were produced and subjected to the rolling schedules listed, then analysed using an SEM to measure some characteristics of the microstructure. The 40g method developed throughout this thesis has since been expanded into 80g samples which provide more material for testing, and the work has provided validation that a laboratory scale RAP process can closely replicate the industrial grades. The next stage of this research is to use the 80g method to identify the impact of residual elements now that the method inconsistencies have been reduced. This will be key to determining how Tata Steel's product orderbook may look in a just a few years after the installation of the electric arc furnace.

CHAPTER 9   REFERENCES

[1]   M. A. Yar *et al.*, "Small-Scale Rapid Alloy Prototyping of Extra-Low Carbon Steel to Investigate the Effects of Cu and Cr Residuals," *Miner. Met. Mater. Ser.*, pp. 1202–1213, 2022.

[2]   B. Davison, G. W. Owens, and Steel Construction Institute (Great Britain), *Steel designers' manual*. Blackwell Science, 2011.

[3]   "Port   Talbot,   Mill   Visit |."   [Online].   Available: http://www.nass.org.uk/Events/event.asp?eid=3247.   [Accessed: 03-Nov-2022].

[4]   G. W. Bright *et al.*, "Variability in the mechanical properties and processing conditions of a High Strength Low Alloy steel," *Procedia Eng.*, vol. 10, pp. 106–111, Jan. 2011.

[5]   C. D. Williams, "The Development of a Secondary Steel Making Alloy Model," Swansea University, 2011.

[6]   A. Spanlang, W. Wukovits, and B. Weiss, "Development of a blast furnace model with thermodynamic process depiction by means of the rist operating diagram," *Chem. Eng. Trans.*, vol. 52, pp. 973–978, 2016.

[7]   O. Rod, C. Becker, and M. Nylén, "Opportunities and dangers of using residual elements insteels: a literature survey," *Jernkontorets Forsk.*, 2006.

[8]   K. El-Akruti, T. Zhang, and R. Dwight, "Developing an optimum maintenance policy by life cycle cost analysis – a case study," *Int. J. Prod. Res.*, vol. 54, no. 19, pp. 5946–5962, Oct. 2016.

[9]   M. Yellishetty, G. M. Mudd, P. G. Ranjith, and A. Tharumarajah, "Environmental life-cycle comparisons of steel production and recycling : sustainability issues , problems and prospects," *Environ. Sci. Policy*, vol. 14, no. 6, pp. 650–663, 2011.

[10]   K.-P. Bernatzki, M. R. Bussieck, T. Lindner, and M. E. Lübbecke, "Optimal scrap combination for steel production," *OR Spektrum*, vol. 20, no. 4, pp. 251–258, 1998.

[11]   O. A. El Hady, A. E. Amer, I. S. El Mahallawi, and Y. S. Shash, "Optimization of residual manganese in molten metal in basic Oxygen furnace (BOF)," *Mater. Sci. Forum*, vol. 561–565, no. PART 1, pp. 85–89, 2007.

[12]   L. Savov, E. Volkova, and D. Janke, "Copper and Tin in Steel Scrap Recycling," *RMZ - Mater. Geoenvironment*, vol. 50, no. 3, pp. 627–640, 2003.

[13]   R. V. Williams, *Control and Analysis in Iron and Steelmaking*, 1st ed. Bodmin: Butterworth Scientific Ltd., 1983.

[14]   H. Ohno, K. Matsubae, K. Nakajima, and S. Nakamura, "Unintentional Flow of Alloying Elements in Steel during Recycling of End-of-Life," *J. ofIndustrial Ecol.*, vol. 18, no. 2, 2014.

[15]   EFR, "EU-27 Steel Scrap Specification," no. May, p. 9, 2007.

[16]   K. E. Daehn, A. C. Serrenho, and J. M. Allwood, "How Will Copper Contamination Constrain Future Global Steel Recycling ?," *Environ. Sci. Technol.*, vol. 51, pp. 6599–6606, 2017.

[17]   V. Leroy, D. D'Haeyer, J. Defourny, and T. Hoogendoorn, "Mechanical working (Rolling mills): Effects of tramp elements in flat and long products,"

1995.

[18] Y. Igarashi, I. Daigo, Y. Matsuno, and Y. Adachi, "Estimation of the Change in Quality of Domestic Steel Production Affected by Steel Scrap Exports," vol. 47, no. 5, pp. 753–757, 2007.

[19] J. M. Allwood, "A bright future for UK steel: A strategy for innovation and leadership through up-cycling and integration," *Univ. Cambridge*, pp. 1–16, 2016.

[20] C. A. Tuck, "Mineral Commodity Summaries," 2018.

[21] M. Yellishetty, P. G. Ranjith, and A. Tharumarajah, "Iron ore and steel production trends and material flows in the world: Is this really sustainable?," *Resour. Conserv. Recycl.*, vol. 54, no. 12, pp. 1084–1094, 2010.

[22] K. E. Daehn, A. Cabrera Serrenho, and J. M. Allwood, "How Will Copper Contamination Constrain Future Global Steel Recycling?," *Environ. Sci. Technol.*, vol. 51, no. 11, pp. 6599–6606, Jun. 2017.

[23] T. U. of T. Hatayama, Hiroki (Department of Materials Engineering, I. Daigo, Y. Matsuno, and Y. Adachi, "Outlook of the World Steel Cycle Based on the Stock and Flow Dynamics," *Environ. Sci. Technol.*, vol. 44, no. 16, pp. 6457–6463, 2010.

[24] Welsh Assembly Government, "The overarching waste strategy document for wales: Towards zero waste," 2010.

[25] I. S. EL-MAHALLAWI, A. Y. SHASH, A. RAMADAN, and Mattar, "The Challenge between Energy Saving and Steel Quality : Effect of Scrap / Total Charge Ratio," 2014.

[26] S. Grimes, J. Donaldson, and G. Cebrian Gomez, "Report on the Environmental Benefits of Recycling," 2008.

[27] H. Muslemani, X. Liang, K. Kaesehage, F. Ascui, and J. Wilson, "Opportunities and challenges for decarbonizing steel production by creating markets for 'green steel' products," *J. Clean. Prod.*, vol. 315, p. 128127, Sep. 2021.

[28] "GREENSTEEL - LIBERTY Steel Group." [Online]. Available: https://libertysteelgroup.com/delivering-cn30/greensteel/. [Accessed: 27-Aug-2022].

[29] P. W. Griffin and G. P. Hammond, "Industrial energy use and carbon emissions reduction in the iron and steel sector: A UK perspective," *Appl. Energy*, vol. 249, pp. 109–125, Sep. 2019.

[30] P. W. Griffin and G. P. Hammond, "The prospects for 'green steel' making in a net-zero economy: A UK perspective," *Glob. Transitions*, vol. 3, pp. 72–86, Jan. 2021.

[31] P. W. Griffin, G. P. Hammond, and J. B. Norman, "Industrial energy use and carbon emissions reduction: a UK perspective," *Wiley Interdiscip. Rev. Energy Environ.*, vol. 5, no. 6, pp. 684–714, Nov. 2016.

[32] J. Barrett, T. Cooper, G. P. Hammond, and N. Pidgeon, "Industrial energy, materials and products: UK decarbonisation challenges and opportunities," *Appl. Therm. Eng.*, vol. 136, pp. 643–656, May 2018.

[33] S. J. G. Cooper and G. P. Hammond, "'Decarbonising' UK industry: Towards a cleaner economy," *Proc. Inst. Civ. Eng. Energy*, vol. 171, no. 4, pp. 147–157, Nov. 2018.

[34] R. H. Shutt *et al.*, "Exposure to air pollution near a steel plant is associated with reduced heart rate variability: A randomised crossover study," *Environ. Heal. A Glob. Access Sci. Source*, vol. 16, no. 1, pp. 1–10, 2017.

[35] C. Valenti *et al.*, "Respiratory illness and air pollution from the steel industry: the case of Piquiá de Baixo, Brazil (Preliminary report)," *Multidiscip. Respir. Med.*, vol. 11, no. 1, pp. 1–7, 2016.

[36] V. Vogl and M. Åhman, "What is green steel?-Towards a strategic decision tool for decarbonising EU steel Author Names and Affiliation Contact data," in *ESTAD 4th*, 2019.

[37] A. Ramadan, A. Y. Shash, S. Dieter, and T. Mattar, "Studying the Effect of Tramp Elements in Scrap on Industrial Recycled Steel Processing and Quality," *Ind. Acad. Collab.*, 2014.

[38] M. Mujahid, K. Lis, C. Garcia, and A. DeArdo, "Structure – Properties studies of Cu containing HSLA-100 Steels," in *Proceedings of the International Conference on Processing, Microstructure and Properties of Microalloyed and High Strength Low Alloy Steels*, 1991, pp. 345–357.

[39] Y. ping Lang, H. peng Qu, H. tao Chen, and Y. qing Weng, "Research Progress and Development Tendency of Nitrogen-alloyed Austenitic Stainless Steels," *J. Iron Steel Res. Int.*, vol. 22, no. 2, pp. 91–98, 2015.

[40] N. P. Lavery *et al.*, "Combinatorial development and high throughput materials characterisation of steels," *Ironmak. Steelmak.*, vol. 42, no. 10, pp. 727–733, 2015.

[41] "Oak Ridge National Laboratory Intermetallics Program," in *Intermetallic Alloy Development: A Program Evaluation*, Washington D.C.: National Academies Press, 1997, pp. 10–31.

[42] Z. CHANGMING and Z. HUI, "RAPID PROTOTYPING SUBSTITUTE MATERIAL PREPARATION AND APPLICATIONS IN CASTING PROCESS," in *Mechanical and Electronics Engineering - Proceedings of the International Conference on Icmee 2009 : Proceedings of the International Conference on ICMEE*, 2009, pp. 78–82.

[43] Q. Lu, S. Van Der Zwaag, and W. Xu, "High-throughput design of low-activation, high-strength creep-resistant steels for nuclear-reactor applications," *J. Nucl. Mater.*, vol. 469, pp. 217–222, Feb. 2016.

[44] L. Bolzoni, E. Herraiz, E. M. Ruiz-Navas, and E. Gordo, "Study of the properties of low-cost powder metallurgy titanium alloys by 430 stainless steel addition," *Mater. Des.*, vol. 60, pp. 628–636, 2014.

[45] M. O. Bodunrin, L. H. Chown, and J. A. Omotoyinbo, "Development of low-cost titanium alloys: A chronicle of challenges and opportunities," *Mater. Today Proc.*, Mar. 2020.

[46] "Question: The phase diagram of Iron – Carbon: Consider a 94 wt% Fe – 6 wt%." [Online]. Available: http://d2vlcm61l7u1fs.cloudfront.net/media/2ca/2cad2d69-cfaf-4b14-8f4e-19119a4519c9/phpYiY81A.png. [Accessed: 12-Mar-2019].

[47] R. N. Yellakara *et al.*, "Development of Dual-Phase Steel Using Non-Peritectic Carbon Chemistry for Thin-Slab Continuous Casting Compact Strip Production (CSP) Steel Mill," *Iron Steel Technol.*, vol. 14, no. 10, pp. 84–90, 2017.

[48] G. Spanos and W. T. Reynolds, "Microstructure of Metals and Alloys," in *Physical Metallurgy: Fifth Edition*, 5th ed., vol. 1, Elsevier, 2014, pp. 1073–1112.

[49] H. K. D. H. Bhadeshia, "Physical Metallurgy of Steels," in *Physical Metallurgy*, Fifth Edit., Elsevier, 2014, pp. 2157–2214.

[50] R. Rashad, A. Shash, A. E. Amer, and H. Shendy, "Effect of Alloying Elements on Corrosion, Microstructure and Mechanical Properties for Casted Free-Nickel Duplex Stainless Steels," vol. 70, no. June, pp. 0–11, 2015.

[51] William D. Callister, *Materials Science and Engineering: An Introduction*, 6th Editio. John Wiley & Sons, 2002.

[52] R. W. K. Honeycombe and H. K. D. H. Bhadeshia, *Steels Microstructure and Properties*, 2nd ed. London: Edward Arnold, 1995.

[53] H. E. McGannon, Ed., *The making, shaping and treating of steel*, 9th ed. Pittsburgh: United States Steel, 1971.

[54] A. D. Pelton, "Thermodynamics and Phase Diagrams," in *Physical Metallurgy: Fifth Edition*, 1st ed., vol. 1, F. C. Campbell, Ed. Ohio: The MAterials Information Society, 2012, pp. 41–72.

[55] E. W. Hart, *The Nature and Behaviour of Grain Boundaries*, First edit. London: Plenum Press, 1972.

[56] M. Y. Demeri, "Dual-Phase Steels," in *Advanced High-Strength Steels : Science, Technology, and Applications*, A S M International, 2013, pp. 95–106.

[57] I. A. El-Sesy and Z. M. El-Baradie, "Influence carbon and/or iron carbide on the structure and properties of dual-phase steels," *Mater. Lett.*, vol. 57, no. 3, pp. 580–585, Dec. 2002.

[58] J. Ayres, D. Penney, P. Evans, and R. Underhill, "Effect of intercritical annealing on the mechanical properties of dual-phase steel," *Ironmak. Steelmak.*, vol. 49, no. 8, pp. 821–827, 2022.

[59] B. Krebs, L. Germain, A. Hazotte, and M. Gouné, "Banded structure in Dual Phase steels in relation with the austenite-to-ferrite transformation mechanisms," *J. Mater. Sci.*, vol. 46, no. 21, pp. 7026–7038, Nov. 2011.

[60] W. C. Leslie, *The Physical Metallurgy of Steels*, Internatio. Tokyo: McGraw-Hill International Book Company, 1982.

[61] D. Raabe *et al.*, "Alloy Design, Combinatorial Synthesis, and Microstructure–Property Relations for Low-Density Fe-Mn-Al-C Austenitic Steels," *Jom*, vol. 66, no. 9, pp. 1845–1856, 2014.

[62] H. K. D. H. Bhadeshia and R. W. K. Honeycombe, "THE EFFECTS OF ALLOYING ELEMENTS ON IRON – CARBON ALLOYS," in *Steels : Microstructure and Properties*, Oxford: Elsevier Science & Technology, 2006, pp. 71–94.

[63] M. Torkar, "Effect of trace and residual elements on the hot brittleness, hot shortness and properties of 0.15-0.3% C Al-killed steels with a solidification microstructure," *Mater. Tehnol.*, vol. 44, no. 6, pp. 327–333, 2010.

[64] T. Yamada, M. Oda, and O. Akisue, "Effects of Copper,Nickel, Chromium and Tin on Mechanical Extralow-carbon Steel Sheets," *ISIJ Int.*, vol. 35, no. 11, pp. 1422–1429, 1995.

[65] A. Ramadan, A. Y. Shash, I. S. El-Mahallawi, D. Senk, and T. Mattar,

"Identification of copper precipitates in scrap based recycled low carbon rebar steel," *Mater. Des.*, vol. 120, pp. 157–169, 2017.

[66] E. C. Bain, *The Alloying Elements in Steel*. American Society for Metals, 1939.

[67] V. B. Trindade, J. Rezende, and J. Da Cruz Payao, "Effect of different alloying elements on the weld metal properties of C-Mn steels during submerged-arc welding," *Iron Steel Technol.*, vol. 15, no. 10, pp. 106–111, 2018.

[68] P. Kalinowski and T. Minster-Blondeau, "Residuals in Port Talbot DC01 and HX340LA products," Swansea, 2018.

[69] O. A. Zambrano, "A general perspective of Fe–Mn–Al–C steels," *J. Mater. Sci.*, vol. 53, no. 20, pp. 14003–14062, 2018.

[70] I. Chakrabarty, *Alloy Cast Irons and Their Engineering Applications*. Elsevier Ltd., 2018.

[71] A. Ramadan, A. Y. Shash, I. S. El-mahallawi, D. Senk, and T. Mattar, "Effect of Tempcore Processing on Mitigating Problems of Tramp Elements in Low C Steel Produced from Recycled Material," *J. Iron Steel Res. Int.*, vol. 22, no. 7, pp. 582–589, 2015.

[72] G. R. Speich, A. J. Schwoeble, and W. C. Leslie, "Elastic constants of binary iron-base alloys," *Metall. Trans.*, vol. 3, no. 8, pp. 2031–2037, 1972.

[73] Z. Liu, Y. Kobayashi, M. Kuwabara, and K. Nagai, "Interaction between Phosphorus Micro-Segregation and Sulfide Precipitation in Rapidly Solidified Steel—Utilization of Impurity Elements in Scrap Steel," *Mater. Trans.*, vol. 48, no. 12, pp. 3079–3087, 2007.

[74] B. Mishra, K. Kumbhar, K. S. Kumar, K. S. Prasad, and M. Srinivas, "A Effect of copper addition on microstructure and mechanical properties of ultra high strength NiSiCrCoMo steel," *Mater. Sci. Eng. A*, vol. 651, pp. 177–183, 2016.

[75] I. Daigo, "Comparison of Tramp Element Contents of Steel Bars from Japan and China," *ISIJ Int.*, 2016.

[76] K. R. Carpenter, "The influence of microalloying elements on the hot ductility of thin slab cast steel The Influence of Microalloying Elements on the Hot ductility of thin slab cast steel," University of Wollongong, 2004.

[77] B. Björkman and C. Samuelsson, "Recycling of Steel," *Handb. Recycl.*, pp. 65–83, Jan. 2014.

[78] G. Sahoo, B. Singh, and A. Saxena, "Effect of strain rate, soaking time and alloying elements on hot ductility and hot shortness of low alloy steels," *Mater. Sci. Eng. A*, vol. 718, pp. 292–300, Mar. 2018.

[79] K. Abiko, C. M. Liu, and H. Kimura, "Effect of Silicon on the Grain Boundary Segregation of Phosphorus and the Phosphorus Induced Intergranular Fracture in High Purity Fe-Si-P Alloys," in *Strength of Metals and Alloys (ICSMA 8)*, Elsevier, 1989, pp. 1101–1106.

[80] C. S. Li, Z. X. Li, Y. M. Cen, B. Ma, and G. Huo, "Microstructure and mechanical properties of dual phase strip steel in the overaging process of continuous annealing," *Mater. Sci. Eng. A*, vol. 627, pp. 281–289, Mar. 2015.

[81] A. Elsner, *Advanced hot rolling strategies for IF and TRIP steels*. 2005.

[82] H. Springer and D. Raabe, "Rapid alloy prototyping: Compositional and thermo-mechanical high throughput bulk combinatorial design of structural materials based on the example of 30Mn-1.2C-xAl triplex steels," *Acta Mater.*,

vol. 60, no. 12, pp. 4950–4959, 2012.

[83] M. Cristobal, D. San-Martin, C. Capdevila, J. A. Jiménez, and S. Milenkovic, "Rapid fabrication and characterization of AISI 304 stainless steels modified with Cu additions by additive alloy melting (ADAM)," *J. Mater. Res. Technol.*, no. x x, pp. 1–11, 2018.

[84] K. Ratschbacher, U. E. Klotz, and M. Eisenbart, "Diffusion samples as a high-throughput screening method for alloy development," *Mater. Sci. Technol. (United Kingdom)*, vol. 0, no. 0, pp. 1–8, 2018.

[85] G. Mundhra, V. S. Hariharan, and B. S. Murty, "Design of a novel Al–Ti–Zr light-weight alloy: Calphad and experiments," *J. Alloys Compd.*, p. 155304, Apr. 2020.

[86] Z. Wang *et al.*, "High throughput experiment assisted discovery of new Ni-base superalloys," *Scr. Mater.*, vol. 178, pp. 134–138, Mar. 2020.

[87] M. Seifert, S. Siebert, S. Huth, W. Theisen, and H. Berns, "New Developments in Martensitic Stainless Steels Containing C + N," *Steel Res. Int.*, vol. 86, no. 12, pp. 1508–1516, 2015.

[88] J. C. Zhao, "Combinatorial approaches as effective tools in the study of phase diagrams and composition-structure-property relationships," *Prog. Mater. Sci.*, vol. 51, no. 5, pp. 557–631, 2006.

[89] H. Springer, M. Belde, and D. Raabe, "Bulk combinatorial design of ductile martensitic stainless steels through confined martensite-to-austenite reversion," *Mater. Sci. Eng. A*, vol. 582, pp. 235–244, 2013.

[90] A. Deschamps, F. Tancret, I. E. Benrabah, F. De Geuser, and H. P. Van Landeghem, "Combinatorial approaches for the design of metallic alloys," *Comptes Rendus Phys.*, vol. 19, no. 8, pp. 737–754, 2018.

[91] C. Haase, F. Tang, M. B. Wilms, A. Weisheit, and B. Hallstedt, "Combining thermodynamic modeling and 3D printing of elemental powder blends for high-throughput investigation of high-entropy alloys – Towards rapid alloy screening and design," *Mater. Sci. Eng. A*, vol. 688, pp. 180–189, Mar. 2017.

[92] S. Yang, J. Lu, F. Xing, L. Zhang, and Y. Zhong, "Revisit the VEC rule in high entropy alloys (HEAs) with high-throughput CALPHAD approach and its applications for material design-A case study with Al-Co-Cr-Fe-Ni system," *Acta Mater.*, vol. 192, pp. 11–19, Apr. 2020.

[93] X. Zhang and Y. Xiang, "Combinatorial approaches for high-throughput characterization of mechanical properties," *J. Mater.*, vol. 3, no. 3, pp. 209–220, 2017.

[94] G. M. Pharr, E. P. George, and M. L. Santella, "Development of Combinatorial Methods for Alloy Design and Optimization," 2006.

[95] J. Hattrick-Simpers, C. Wen, and J. Lauterbach, "The Materials Super Highway: Integrating High-Throughput Experimentation into Mapping the Catalysis Materials Genome," *Catal. Letters*, vol. 145, no. 1, pp. 290–298, 2015.

[96] R. B. van Dover, L. F. Schneemeyer, and R. M. Fleming, "Discovery of a useful thin-film dielectric using a composition-spread approach," *Nature*, vol. 392, no. 6672, pp. 162–164, Mar. 1998.

[97] J.-C. Zhao, "Reliability of the diffusion-multiple approach for phase diagram

mapping," 2004.

[98] S. S. Lasko *et al.*, "Spectroscopic Imaging in the Mid-Infrared Applied to High-Throughput Studies of Supported Catalyst Libraries," in *High-Throughput Analysis*, Boston, MA: Springer US, 2003, pp. 77–91.

[99] X.-D. Xiang, "COMBINATORIAL MATERIALS SYNTHESIS AND SCREENING: An Integrated Materials Chip Approach to Discovery and Optimization of Functional Materials," *Annu. Rev. Mater. Sci.*, vol. 29, no. 1, pp. 149–171, Aug. 1999.

[100] B. Lu *et al.*, "Direct rapid prototyping of shape memory alloy with linear superelasticity via plasma arc deposition," *Vacuum*, vol. 157, no. August, pp. 65–68, 2018.

[101] K. Kennedy, T. Stefansky, G. Davy, V. F. Zackay, and E. R. Parker, "Rapid method for determining ternary-alloy phase diagrams," *J. Appl. Phys.*, vol. 36, no. 12, pp. 3808–3810, 1965.

[102] N. A. Belov, E. A. Naumova, and D. G. Eskin, "Casting alloys of the Al-Ce-Ni system: Microstructural approach to alloy design," *Mater. Sci. Eng. A*, vol. 271, no. 1–2, pp. 134–142, Nov. 1999.

[103] Y.-Y. Chuang and Y. A. Chang, "A thermodynamic analysis and calculation of the Fe-Ni-Cr phase diagram," *Metall. Mater. Trans. A*, vol. 18, no. 5, pp. 733–745, May 1987.

[104] L. X. Li, M. H. Sun, M. C. Fan, T. S. Yang, and F. S. Du, "New Rapid prototyping technology for the prevention of hydrogen embrittlement of metal strips," *Corros. Sci.*, vol. 164, p. 108341, Mar. 2020.

[105] J. C. T. Cullen, "High Throughput Methodologies and Materials Characterisation for the Optimisation and Discovery of New Alloys," Swansea University, 2019.

[106] L. Zhang, W. Harrison, M. A. Yar, S. G. R. Brown, and N. P. Lavery, "The development of miniature tensile specimens with non-standard aspect and slimness ratios for rapid alloy prototyping processes," *J. Mater. Res. Technol.*, vol. 15, pp. 1830–1843, 2021.

[107] L. Zhang, W. Harrison, S. Mehraban, S. G. R. Brown, and N. P. Lavery, "Size Effect on the Post-Necking Behaviour of Dual-Phase 800 Steel: Modelling and Experiment," *Materials (Basel).*, vol. 16, no. 4, 2023.

[108] S. J. Shin, J. Y. Kim, S. An, and T. D. Chung, "Recent advances in electroanalytical methods for electroorganic synthesis," *Curr. Opin. Electrochem.*, vol. 35, p. 101054, 2022.

[109] "Solutions for Materials Preparation, Testing & Analysis - Buehler United Kingdom - Metallography Equipment & Supplies for Sample Preparation." [Online]. Available: https://www.buehler.com/uk/. [Accessed: 02-Sep-2022].

[110] A. R. H. Far, S. H. M. Anijdan, and S. M. Abbasi, "The effect of increasing Cu and Ni on a significant enhancement of mechanical properties of high strength low alloy, low carbon steels of HSLA-100 type," *Mater. Sci. Eng. A*, vol. 746, pp. 384–393, Feb. 2019.

[111] A. Willman, M. W. And, and U. Solheim, "An evaluation of alloying elements in shredded steel scrap Economic and environmental aspects of the recycling process for the steel scrap category E40," *Degree Proj. Technol.*, 2017.

[112] B. Kim, S. Kim, and H. Kim, "Effects of Alloying Elements (Cr, Mn) on Corrosion Properties of the High-Strength Steel in 3.5% NaCl Solution," *Adv. Mater. Sci. Eng.*, vol. 2018, pp. 1–13, 2018.

[113] K. Shibata *et al.*, "Suppression of surface hot shortness due to Cu in recycled steels," *Mater. Trans.*, vol. 43, no. 3, pp. 292–300, 2002.

[114] C. Slater and C. Davis, "Near Net Shape Casting: Is It Possible to Cast Too Thin?," *Metall. Mater. Trans. B Process Metall. Mater. Process. Sci.*, vol. 51, no. 6, pp. 2532–2541, 2020.

[115] Z. Bůžek, E. Mazancová, Z. Jonšta, and K. Mazanec, "THE INFLUENCE OF SOME RESIDUAL ELEMENTS ON THE SUSCEPTIBILITY TO THE TRANSVERSE CRACKS FORMATION IN CONTINUOUSLY CAST STRUCTURAL STEELS CZ b) NOVÁ HU Ť a . s ., Research and Testing Inst ., Vratimovská , 707 02 , Ostrava , CZ."

[116] L. Zhang, W. Harrison, M. A. Yar, S. Mehraban, S. G. R. Brown, and N. P. Lavery, "Use of miniaturized tensile specimens to evaluate the ductility and formability of dual phased steels for Rapid Alloy Prototyping," *Mater. Sci. Eng. A*, vol. 875, no. December 2022, p. 145075, 2023.

[117] K. Badenoch, D. T. Davies, and J. Hunt, "Welsh steel's future secured as UK Government and Tata Steel announce Port Talbot green transition proposal - GOV.UK," 2023.

CHAPTER 10 APPENDIX

TMS2022 RAP paper.pdf

[1]

Small-Scale Rapid Alloy Prototyping of Extra-Low Carbon Steel to Investigate the Effects of Cu and Cr Residuals

Check for updates

Mazher Ahmed Yar, Caroline Norrish, Jonathan C. T. Cullen, Lintao Zhang, Stephen Brown, Richard Underhill, and Nicholas Lavery

Abstract A small-scale, rapid alloy prototyping (RAP) route is presented for accelerated lab-scale development of an array of steels across many applications in which alloys can be tailored with individual or combined elements to a compositional precision down to 0.1%. At the level of 40 g, over twenty unique compositions can be manufactured and validated in a week, with the process including compacting and melting raw materials, casting into a bar, followed by rolling and heat treatment. A specific application of RAP is presented whereby incremental additions of residual elements, in this instance Cu and Cr, are added to an extra-low carbon steel with the aim of understanding the effects of increased scrap recycling on the final product properties. ASTM tensile test results are discussed reflecting the effects of seven levels of Cu and Cr, up to 36 times the current industrial limits, showing the versatility of this RAP route.

Keywords Iron and steel · Rapid alloy prototyping · Mechanical properties

M. A. Yar (B) · C. Norrish · J. C. T. Cullen · L. Zhang · S. Brown · N. Lavery
Swansea University, Bay Campus, Fabian Way, Swansea S1 8EN, Wales, UK e-mail:
█████████████

C. Norrish e-mail: ████████████████

J. C. T. Cullen e-mail: ███████████████████

L. Zhang e-mail: ██████████████████

S. Brown
e-mail: ██████████████████

N. Lavery e-mail: ████████████████████

R. Underhill
Tata Steel, Harbourside Road, Port Talbot, UK e-mail:
█████████████████████

Introduction

Residual elements are the elements in steel that are unintentional or undesirable and are often introduced through the use of scrap in the steel-making process. These elements are being increasingly discussed and researched due to their presence in scrap steel and the ever increasing pressure to increase recycling rates regardless of the manufacturing challenges that may bring. Previous research predicts that the concentration of residual elements in steel will increase in the future as recycling rates also increase [1, 2]. These elements are particularly challenging to remove from the steel melt as they have low oxygen reactivity, if at all, and as a consequence, they remain in the melt rather than oxidizing and being removed with the slag [3]. The use of rapid alloy prototyping (RAP) presents the opportunity to investigate numerous materials and alloy systems with unique compositions. It allows for a wider understanding of the compositional effects on the bulk mechanical properties through testing across many composition points.

Using a form of rapid alloy prototyping to investigate metallurgy is not a new concept and has been widely researched for decades. Since the 1960s, RAP methods have been used to investigate large numbers of alloy compositions. In 1965, Kennedy et al. used a vapour deposition method to determine the phases present in a Fe-Cr-Ni alloy system [4]. Pharr [5] used a similar method to investigate the same alloy system and found that the combinatorial method can be used to both discover new alloys and develop and refine existing ones [5]. Belov [6] developed a method to produce small samples 10 × 20 ×180 mm in size to investigate the microstructure of the Al-Ce-Ni alloy system. This work proved that using a small sample size made it possible to investigate and understand the microstructure of a new alloy produced in a conventional way [6]. In more recent times, accelerated production methods have been developed by Springer and Raabe [7] allowing new alloy samples to be produced and tested within 35 h [7]. These combinatorial methods produce samples that can highlight understandings of the phases present in the alloy systems and allow for material characterization as well as a mapping the hardness values across a phase diagram of compositions.

The accepted industry standard for new alloy development involves vacuum induction melting (VIM) with trial runs of 25–60 kg per composition, which is time-consuming, expensive, and wasteful [8]. It is difficult to investigate a range of compositions using such large volumes of material, so the introduction of small RAP methodology into the alloy development stage can effectively improve efficiency [9].

The extra-low carbon grade of steel investigated here has lower alloying additions than many other steel grades, and it is predicted that the effects of residual elements can be more amplified in alloys with fewer other additions. If the effects of residual additions can be quantified, it can allow an increase in the amount of scrap steel used in steelmaking, leading to environmental and economic benefits. Such steel grades are

produced in very large volumes for various applications, so even a slight increase in the scrap content in each steel batch can have a very significant benefit.

The residual elements studied in this research work include copper (Cu) and chromium(Cr);however,itcanbeextendedtotheotherresidualelementsaswell,for example, tin, molybdenum, and nickel. Whilst these elements are sometimes added to many steel grades intentionally, in the grade studied here, they are undesirable due to the detrimental effects on mechanical properties. Copper is arguably the most widely researched residual element in steel, and the future predictions expect that by 2050 the copper content in steel will exceed what is acceptable for the steel quality [1]. This can be introduced into the scrap through wires attached to electronic scrap amongst other routes. One of the biggest issues with copper is hot shortness which occurs during hot rolling and has been widely researched [2]. As hot shortness is a factor affecting processability rather than mechanical properties, the steel chosen for this study was an interim grade that would not yet have been cold rolled.

Chromium is intentionally added to some steels, especially stainless steels, to enhance properties such as corrosion resistance, but this can lead to high chromium levels in some scrap. Chromium can be partially removed from a steel melt due to how easily it oxidizes and forms a slag product, but much of it will also remain in the bath where it becomes a residual element in the new steel being produced [3]. Both copper and chromium, along with many other elements commonly regarded as residual elements such as tin, nickel, and molybdenum, increase the hardness and tensile strength of a steel whilst decreasing the ductility [3, 10–12].

The levels of residual elements will vary depending upon the source of scrap used. The obsolete scrap from 'end of life' products may have fairly unknown and unpredictable residuals. However, home scrap originating from other steel processes within the industrial facility usually has known and relatively lower residual levels. [3, 13, 14].

Experimental

Raw Materials, Melting, and Casting

The feedstock for the RAP ingot melting can be materials in various forms, ranging from mixtures of powders and/or solid elements/metals of ≥99% purity available fromcommercialsuppliers.FortheRAProuteinthiswork,eachof40-gsampleswere melted from elemental powders. Corresponding to the specific steel composition, calculated powder amounts of individual elements were weighed and mixed in a container followed by compacting the mixed powders into a green pellet using a hydraulic press. The compacted pellets were transferred into glove box via a vacuum port into a scrubbed argon filled chamber (oxygen ≤30 ppm) and melted using induction melting coil. The molten metal was gravity cast into a rectangular bar sample of approximately $6 \times 12 \times 60$ mm size (Fig. 1).

Spark optical emission spectroscopy (OES) and combustion analysis (C/S) were conducted to determine the steel compositions. The chemistries with the added
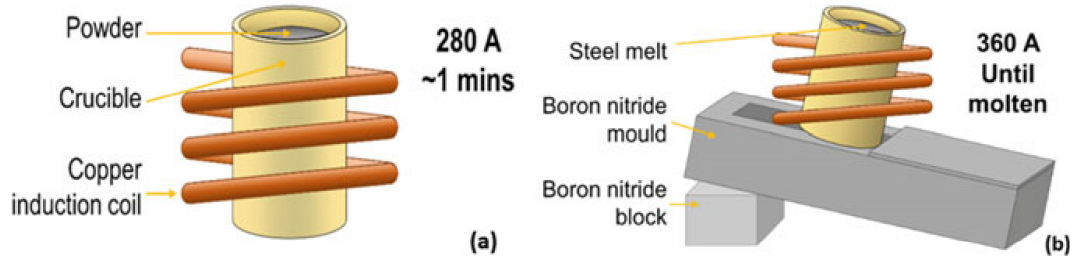

Fig. 1 Schematic of induction melting (**a**) and casting into a bar (**b**)

Table 1 Target baseline composition of extra-low C steel without residual additions

Fe	C	Si	Mn	Cr	Cu	P	S
Bal	0.02 max	0.02 max	0.13–0.14	0.02 max	0.001	0.003	0.01

Table 2 Target amount of residual element additions

Added residual	×1	×4	×8	×12	×16	×24	×36
Cr wt.%	0.025	0.1	0.2	0.3	0.4	0.6	0.9
Cu wt.%	0.03	0.12	0.24	0.36	0.48	0.72	1.08

residual elements selected for investigation are given in Tables 1 and 2. Table 1 represents the target composition of respective baseline steel. Table 2 shows the incremental wt.%ages of Cr and Cu residual elements added to the baseline steel to produce samples for this study. The added levels are increments of 1 to 36 times the current residual limits in a similar industrial steel grade.

Processing

As-cast samples were homogenized in a tube furnace under vacuum at 900 °C for 5 h and then furnace cooled to room temperature overnight. Sample surfaces were ground down or machined to remove surface scale and then cold rolled using a motor-powered lab-scale rolling mill. Each bar (≈ 6 mm thick and 12 mm wide) was 80% cold reduced with ≈1 mm reduction at each pass until a final thickness of approximately 1.2 mm was achieved. Cold-rolled strip samples were normalized heat-treated in air after soaking at 900 °C for 5 min in a pre-heated box furnace.

Characterization and Mechanical Testing

Figure 2c tensile specimens were machined from processed strips for mechanical evaluation. Three tensile specimens were collected from each sample composition manufactured. The processed strips were subject to microstructural characterization using a Zeiss Axio Observer Z1M inverted optical microscope for imaging and grain size measurement and a JEOL scanning electron microscope (SEM) equipped with energy dispersive X-ray (EDX) spectroscopy system (JSM-6010). The crosssectional samples were prepared in the rolling direction (RD) for metallography and were subjected to standard grinding and polishing procedure with final 1 micron diamondsuspension.HardnessmeasurementwasdoneusingaVickerstester(Bruker Wilson VH3300) at 1 kg loads (HV$_1$).

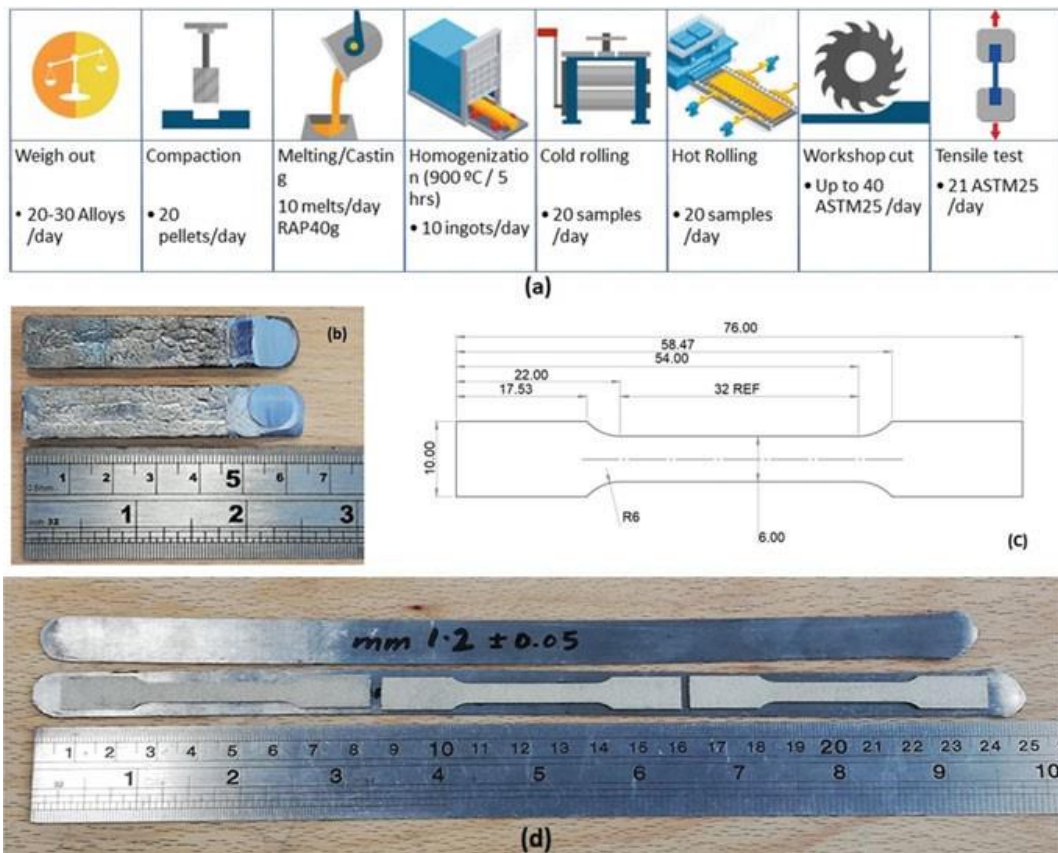Fig. 2 a 40 g RAP-alloy development and testing flow diagram with time for respective steps, b 40 g RAP-alloy cast into bars of approximately 6 × 12 x 65 mm dimension, c dimensions of ASTM-25 tensile specimen, d RAP-alloy material after ≈ 80% cold reduction in the form of strips

(1.2 mm) and representative ASTM-25 tensile specimen size

Results and Discussion

Composition

Compositional analysis by OES was conducted on machined surfaces of as-cast material, while C/S was determined in the final strip material by combustion method. All samples analysed had good composition control as given in Table 3, with average C 0.018% ± 0.005, Mn 0.13–0.14%, Si ≤ 0.02% ± 0.005, and S 0.015%. C/S was determined randomly on some samples to confirm OES results. Supplementary C and Mn were added to compensate the melting losses.

Microstructure and Hardness

The cold-rolled samples were soaked at 900 °C before normalizing. This heat treatment temperature was chosen to allow the steel to be fully in the austenitic region and produce recrystallized microstructure. On cooling, the resultant microstructure was transformed into ferrite. Figure 3 shows microstructures of some of the samples (with 1, 12, 24, and 36 times addition), revealed by optical microscope after etching with 2% Nital solution. The hardness and grain sizes were measured on all samples from the middle of the sheet thickness in RD cross sections and are given in Table 3. It can be observed that Cu and Cr residual additions are not having a significant effect on grain sizes which is also reflected in the hardness results.

SEM investigations of samples revealed fully recrystallized grains and sub-micron sized oxide inclusions in the matrix. EDX elemental analysis showed these oxide inclusions consist of Mn-Si-S with/without Al. Besides, Cu and Cr were also detected in these inclusions in samples made with residual additions. Further, Cu/Cr percentages increase in inclusions with increasing the residual additions in the steel. When compared the inclusions' EDX results in samples with 36 times Cu and 36 times Cr addition, it was found that Cr shows more tendency to be associated with these inclusions than Cu. This indicates that more Cu is present in the ferrite solid solution (Fig. 4).

Copper additions appear to have a stronger effect on the hardness than chromium (Fig. 5), and this may be due to the solid solution strengthening effect of copper [15] and chromium joining the Mn-Si-S inclusion and little solid solution strengthening. The hardness of the steel remains less effective with increasing Cu up to 8 times (0.224 wt.%) which then increases to 121 HV_1 for copper addition of 0.33 to 1.03 wt.%. The chromium from 0.101 to 0.395wt% decreases the hardness of the steel from 108 to 100 HV_1. Further addition of chromium has less effect on hardness.

Table 3 Chemical compositions of RAP samples in wt.% age. measured grain sizes (μm), and hardness values (HV)

Cu	Cr	C	Mn	Si	S	P	Grain size (μm)	Hardness (HV)
0.001	0.017	0.014	0.137	0.028	0.01	0.0037	16.1 ± 1.5	108.6 ± 10
0.0295	0.018	0.022	0.134	0.035	0.015	0.0038	18.2 ± 0.7	106.2 ± 8
0.111	0.017	0.020	0.139	0.020	0.015	0.0038	17.1 ± 0.6	103.9 ± 8
0.224	0.019	0.019	0.144	0.024	0.011	0.0023	15.9 ± 1.4	105.0 ± 4
0.33	0.016	0.016	0.136	0.023	0.015	0.0033	19.2 ± 2.1	116.4 ± 6
0.441	0.017	0.017	0.141	0.023	0.0165	0.003	15.6 ± 0.9	116.1 ± 7
0.676	0.016	0.023	0.138	0.019	0.01	0.0032	19.4 ± 1.2	113.3 ± 7
1.03	0.017	0.022	0.139	0.020	0.016	0.0034	17.2 ± 0.9	120.7 ± 9
N/A	0.017 / 0.001	0.02 / 0.003	0.14 / 0.003	0.024 / 0.006	0.014 / 0.003	0.0033 / 0.0005	N/A	N/A
-	0.026	0.030	0.145	0.022	0.0133	0.004	17.5 ± 0.9	96 ± 3
-	0.101	0.013	0.139	0.019	0.016	0.0032	21.9 ± 0.7	108.9 ± 10
-	0.201	0.021	0.143	0.038	0.015	0.003	15.6 ± 0.8	97 ± 4
-	0.294	0.016	0.131	0.014	0.016	0.0033	23.4 ± 1.7	108.8 ± 12
-	0.395	0.036	0.134	0.016	0.012	0.0023	14.9 ± 1.6	100 ± 6
-	0.578	0.015	0.129	0.012	0.016	0.0033	21.9 ± 1.1	95.8 ± 6
-	0.867	0.022	0.126	0.012	0.011	0.0033	16.3 ± 0.5	100.9 ± 7
N/A	N/A	0.022 / 0.008	0.134 / 0.006	0.0185 / 0.01	0.014 / 0.002	0.003 / 0.0004	N/A	N/A

*C/S results from OES analysis

251

Ref.ID
Baseline*
Cu × 1
Cu × 4
Cu × 8*
Cu × 12
Cu × 16
Cu × 24*
Cu × 36
Average
StandardDeviation
Cr × 1
Cr × 4
Cr × 8
Cr × 12
Cr × 16*
Cr × 24
Cr × 36*
Average
StandardDeviation
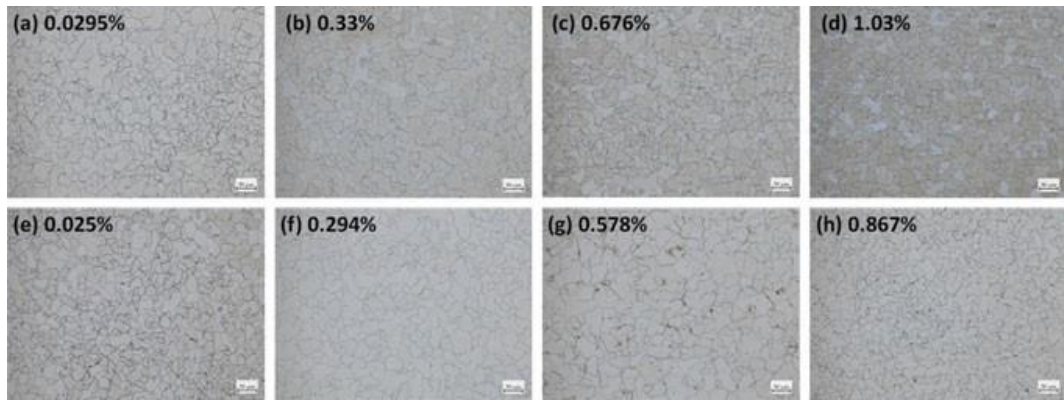
Fig. 3 Microstructure of steels with × 1, × 12, × 24, and × 36 residual additions of Cu (**a**–**d**) in increasing order and Cr (**e**–**h**), as revealed by optical microscope after 2% Nital etching
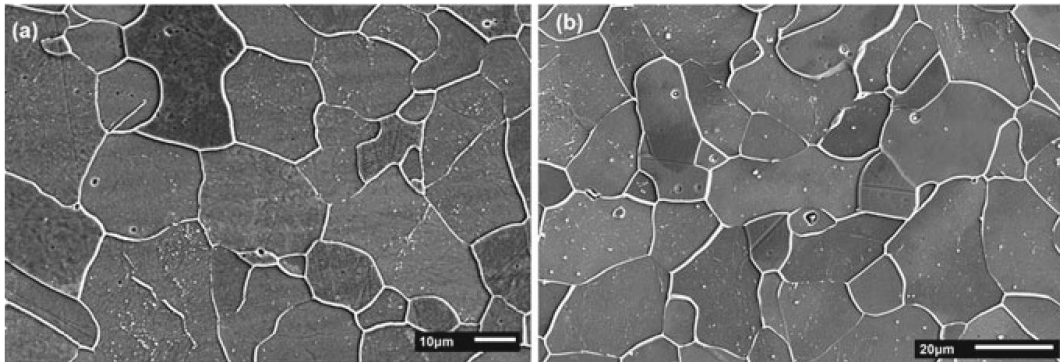

Fig. 4 SEM images of samples prepared from rolling-direction cross section, etched with 2% Nital solution. **a** steel with 36 times Cu addition, **b** 36 times Cr addition
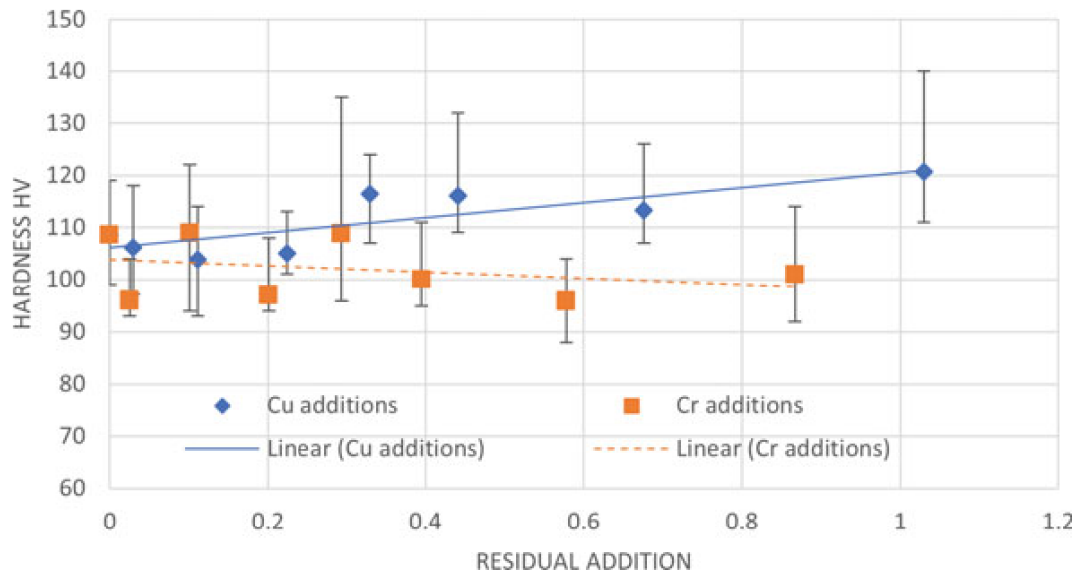

Fig. 5 Vickers hardness results measured on RD cross-sectional samples. The error bars show the maximum and minimum HV1 values

253

Tensile Testing/Mechanical Properties

Three ASTM-25 standard (gauge length 25 mm) tensile bars were machined from each 40 g RAP composition as shown in Fig. 2c. These bars were pulled at a speed of 1 mm/min on a Tinius Olsen H25KS tensile machine until failure and the strain data was gathered using a Xsight-One Video Extensometer.

From the tensile data, it was possible to determine the ultimate tensile strength (UTS) and the uniform elongation at this maximum point. The UTS values were taken from the highest stress recorded over the duration of the test, and then, an average of the three test results of each composition was plotted. To calculate the uniform elongation, the strain rates at all the points that recorded a stress equal to the UTS were averaged for each sample, before averaging the three uniform elongation values to achieve an overall average for each composition. Both properties have been presented with error bars to indicate the range of values recorded for each composition.

The only variation from this method is in the sample with 0.578 wt.% Cr (× 24) which produced an anomalous result due to a surface defect and so has been discounted, and only two usable test samples were available for that composition.

The tensile data produced (Fig. 6) shows that the samples with increased copper levels have a higher UTS, also correlating with reduced uniform elongation. On the other hand, the samples with increasing chromium show very little overall trend in theUTSvaluesdespitetheslightincreaseintheuniformelongationofthespecimens.

Thesteelunderdiscussionhascarbonlevelsof≤0.02%andconsistsofexclusively ferritic microstructure. The addition of copper in such steel will result in a Cuenrichedferriteleadingtoanincreasedsolidsolutionstrengthening.However,copper seems to show more strengthening effect compared to chromium for similar level of additions in this steel. There could be two explanations, (i)the atomic radii difference of Fe (solvent) and the solute atom being added and (ii) the number of solute atoms dissolved in the solid solution, which are further discussed here. The atomic radius of Cu (128 pm) is larger than that of Fe (124 pm) [16]. On the other hand, Cr atomic
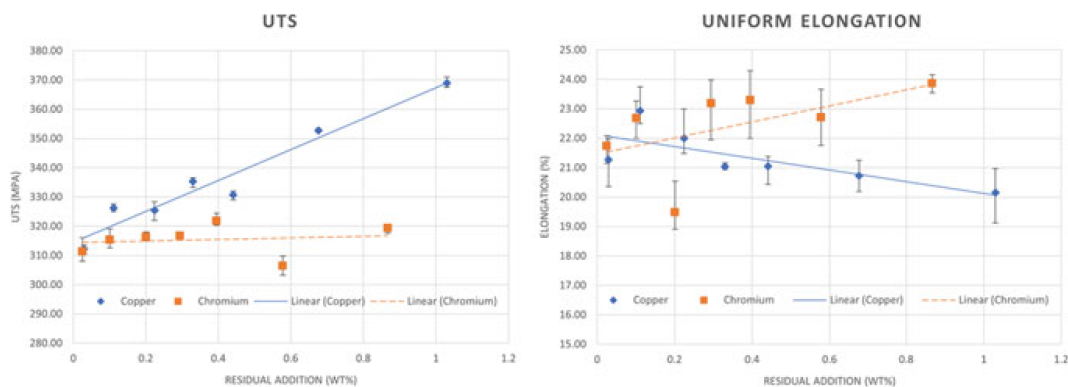

Fig. 6 Ultimate tensile strength (left) and Uniform elongation (right) results with different residual additions

radius (125 pm) is much close to that of Fe and hence a smaller radii difference comparedtothedifferencebetweenCuandFe[16].Thus,Cuhasmorestrengthening effect on solid solution than that of Cr for similar wt. % additions. Besides, EDX analysis revealed that higher chromium was detected in the oxy-sulphide inclusions, than the copper quantified in inclusions present in the steel with similar level of Cu additions. This indicates that lesser chromium was dissolved in the solid solution resulting in lower increase in strength. Although chromium is widely accepted for having strengthening and hardening effects when micro-alloyed in steels, however, a previous study also found very little difference in hardness between samples with Cr levels of <0.01 and 0.51 wt.% in an extra-low carbon steel [17].

Conclusions

From this work, the following results can be drawn as follows:

- The compositions achieved using the rapid alloy prototyping were very close to the target compositions, and the control was exceptionally good considering the 40 g mass of the samples.
- Ultimate tensile strength (UTS) increases for both Cu and Cr residual elements in the investigated ranges, with a large increase of 55 MPa for Cu up to a 1wt.% addition, but with a much smaller increase for the Cr additions. For both residual elements, these trends were as expected.
- Uniform elongation decreases by about 3% for the Cu additions, which is as expected,butfortheCradditions,theelongationincreasesbyupto2%.Elongation to failure shows an increase in scatter with increasing residual content which may be evidence of a residual level limitation.
- Hardness increases from about 106 HV to 120 HV with the increasing Cu additions, again an expected trend. However, there is no clear trend with the Cr additions.
- Microstructures/grain sizes were consistent with little variations between compositions,andnoestablishedrelationwasfoundbetweengrainsizeswitheitherhardness, UTS, or elongation. A solid solution strengthening mechanism is suggested as opposed to precipitation or grain refinement.

Further progress in defining an upper limit to Cu or Cr will depend on additional small-scale tests, which may be based on processability, corrosion, or some other factor. The rapid alloy prototyping has shown itself to be fast and accurate and will be extended to other relevant residual elements over the coming 4–5 weeks. Of interest will be an investigation into the combined effects of more than one residual interacting at the same time at high levels.

References

1. Daehn KE, Serrenho AC, Allwood JM (2017) How will copper contamination constrain futureglobal steel recycling? Environ Sci Technol 51:6599–6606. https://doi.org/10.1021/acs.est.7b0 0997

2. Shibata K et al (2002) Suppression of surface hot shortness due to Cu in recycled steels. MaterTrans 43(3):292–300. https://doi.org/10.2320/matertrans.43.292

3. Rod O, Becker C, Nylén M (2006) Opportunities and dangers of using residual elementsin steels: a literature survey. Open Report, Jernkontorets Forskning, D 819, IM-2006-124, Stockholm

4. Kennedy K, Stefansky T, Davy G, Zackay VF, Parker ER (1965) Rapid method for determiningternary-alloy phase diagrams. J Appl Phys 36(12):3808–3810. https://doi.org/10.1063/1.171 3952

5. Pharr GM., George EP, Santella ML (2006) Development of combinatorial methods for alloydesign and optimization. https://doi.org/10.2172/842122

6. Belov NA, Naumova EA, Eskin DG (1999) Casting alloys of the Al-Ce-Ni system: microstructural approach to alloy design. Mater Sci Eng A 271 (1–2): 134–142, Nov. https://doi.org/10. 1016/s0921-5093(99)00343-3

7. Springer H, Raabe D (2012) Rapid alloy prototyping: compositional and thermo-mechanicalhigh throughput bulk combinatorial design of structural materials based on the example of 30Mn-1.2C-xAl triplex steels. Acta Mater 60(12):4950–4959. https://doi.org/10.1016/j.act amat.2012.05.017

8. Farrugia D, Brown S, Lavery NP, Pleydell-Pearce C, Davis C (2020) Rapid alloy prototypingfor a range of strip related advanced steel grades. Procedia Manuf 50:784–790. https://doi.org/ 10.1016/J.PROMFG.2020.08.141

9. Lavery NP et al (2015) Combinatorial development and high throughput materials characterization of steels. Ironmak Steelmak 42(10):727–733. https://doi.org/10.1179/0301923315Z. 000000000419

10. El-Mahallawi IS, Shash AY, Ramadan A, Mattar (2014) The challenge between energy savingand steel quality: effect of scrap/Total charge ratio. European Steel Environment & Energy Congress (ESEC 2014). At: The Institute of Materials, Minerals and Mining, England

11. Ramadan A, Shash AY, El-Mahallawi IS, Senk D, Mattar T (2017) Identification of copperprecipitates in scrap based recycled low carbon rebar steel. Mater Des 120:157–169. https:// doi.org/10.1016/j.matdes.2017.02.015

12. Torkar M (2010) Effect of trace and residual elements on the hot brittleness, hot shortness andproperties of 0.15-0.3% C Al-killed steels with a solidification microstructure. Mater Tehnol 44(6):327–333

13. Björkman B, Samuelsson C (2014) Recycling of steel. Handb Recycl 65–83, Jan. https://doi. org/10.1016/B978-0-12-396459-5.00006-4

14. Yellishetty M, Mudd GM, Ranjith PG, Tharumarajah A (2011) Environmental life-cyclecomparisons of steel production and recycling: sustainability issues, problems and prospects. Environ Sci Policy 14(6):650–663. https://doi.org/10.1016/j.envsci.2011.04.008

15. Jackson M (2015) Periodic table advanced: atomic, physical, chemical properties & naturalisotopes. BarChart Inc, Boca Raton, Florida

16. LedermuellerC,PratiwiHI,WebsterRF,EizadjouM,RingerSP,PrimigS(2020)Microalloyingeffects of Mo versus Cr in HSLA steels with ultrafine-grained ferrite microstructures. Mater Des 185: 108278, Jan. https://doi.org/10.1016/J.MATDES.2019.108278

17. Yamada T, Oda M, Akisue O (1995) Effects of copper, nickel, chromium and tin on mechanicalproperties of titanium-bearing extralow-carbon steel sheets. ISIJ Int 35(11):1422–1429. https:// doi.org/10.2355/isijinternational.35.1422